Hydrodenitrogenation Kinetics According to Single-Event Methodology

De kinetiek van de stikstofverwijdering volgens de single-event methodologie

Chetan Shreedhar Raghuveer

Promotoren: Prof. Dr. Ir. J. W. Thybaut, Prof. Dr. Ir. G. B. Marin
Proefschrift ingediend tot het behalen van de graad van
Doctor in de Ingenieurswetenschappen: Chemische Technologie

Vakgroep Chemische Proceskunde en Technische Chemie
Voorzitter: Prof. Dr. Ir. G. B. Marin
Faculteit Ingenieurswetenschappen en Architectuur
Academiejaar 2015 – 2016

UNIVERSITEIT GENT

Examination committee

Promoters:

Prof. Dr. Ir. Joris Thybaut	Ghent University, Belgium
Prof. Dr. Ir. Guy Marin	Ghent University, Belgium

Other members of the examination committee:

Dr. Les Bolton	BP plc, UK
Dr. Isabelle Pitault*	Laboratoire de Génie des Procédés Catalytiques, FR
Prof. Dr. Ir. Wolter Prins*	Ghent University, Belgium
Prof. Dr. Ir. Jeriffa De Clercq*	Ghent University, Belgium
Prof. Dr. Ir. Geraldine Heynderickx	Ghent University, Belgium (Secretary)
Prof. Dr. Ir. Gert De Cooman	Ghent University, Belgium (Chairman)

*Reading committee

The research leading to these results has received funding from the European Union Seventh Framework Programme FP7/2007-2013 under grant agreement n° 238013 'MultiMod'. It has also been supported by the CAPITA ERANET programme via the IWT project n° 30900 'WAVES'.

Laboratory for Chemical Technology
Department of Chemical Engineering and Technical Chemistry
Ghent University
Technologiepark 914, B-9052 Ghent, Belgium.

UNIVERSITEIT GENT

Dedicated to my parents…

Acknowledgements

This Ph.D. journey which started about six years ago has been an enthralling one. On the one hand, it has exposed me to the rigours of science and technology, and on the other it has been a great learning about myself. This experience has allowed me to realise my strengths and has allowed to work on my weaknesses. Though it is only my name that appears on the thesis, there have been quite a lot of people who have been responsible for my success. I would like to take this opportunity to thank all of them and express my sincere gratitude towards them.

Firstly, I would like to express my sincere gratitude to my promoters Prof. Guy B. Marin, Prof. Joris W. Thybaut and Dr. Les Bolton (BP plc) for allowing me to perform research on this very interesting topic, in their group and under their supervision.

Prof. Marin, your knowledge in chemical engineering and experience within the field of reactor and reaction engineering has provided great insights into my work. Your technical advice was the key factor in addressing technical challenges and greatly helped me to be on the right track during my research. Your decision making capabilities, dedication towards research and never ending determination are a source of inspiration to me.

Joris, I have the greatest amount of respect to the knowledge you have in this field and I have learnt a lot from you in this aspect. Your patient approach towards solving technical problems has indeed inspired me to a great extent. Your calm demeanour along with your technical prowess is very reassuring and helped me greatly during the course of my thesis. I am really awestruck by the mountains of patience you have and hope to inculcate this character, at least some of it.

Dr. Bolton, your knowledge in chemical engineering is vast and the experiences you have shared with me are invaluable. Your trouble shooting skills have inspired me to look at solving challenges with different approaches. Your constructive technical suggestions and scientific discussions have provided me with a great deal of knowledge and helped shaping the engineer within me. Your support under stressful situations was really helpful, and I will always be indebted towards your timely help. Our informal discussions on various subjects (cricket leading the charts) was a great way to develop personal bonding and I feel extremely lucky to have had a supervisor like you.

During this dissertation I was fortunate enough to have worked with very knowledgeable and friendly technical staff at the LCT. Marcel, your suggestions during the construction of the Rob2 set-up was really great and has helped me improve my technical knowledge. Georges, many thanks for all the suggestions on the IT related things and keeping my laptop in good condition for so long. Brecht, thanks for sharing your knowledge on PLC systems and off course your insights on football. Michael your help on making the GC work at Sterre campus was truly great and I will always remember this. Finally, many thanks to Hans, Tim, Jaimy, Wim, Lambert and Tom for the overall construction of the set-up and providing expertise in dealing with technical issues on the Rob2 set-up.

Petra, Sarah, Kim and Kevin many thanks for all the administrative help, it would have been very difficult to manage everything without you. Petra and Sarah, thanks for all the talk during the breaks, it was a good way to know about the Belgian culture.

I would like to thank everyone from the CaRE group for their technical insights and their suggestions. Jeroen your help during the finishing stages of this thesis was great. The working atmosphere within the CaRE group was comfortable, amongst others, the CaRE events also allowed me to interact with everyone at a personal level.

My master thesis students, Ruben, Roeland and Steven, guiding you guys through your thesis was a very good experience and I enjoyed it completely. I did learn a lot about mentorship and science in return from you guys as well.

I was fortunate to have a fantastic group of office mates Mathias, Dharani, Alexandra and Rakesh, guys thank you so much for the dark, intellectual and insane jokes. I am sure we have all had fun while working, thanks for maintaining a very light working atmosphere.

As a part of the Ph.D. I had an opportunity to work at the petroleum and petrochemical major BP plc. Not only did it allow me to interact with industry experts, it also gave me a different perspective towards research and life. I would like to thank Jane, Laura and Bridget for the administrative help, Matt for making me comfortable in an “Industrial” environment, Dave, Simon, Nick, Mike, Steven and Haitao for technical discussions. Akshai, Josevi and Tolu thank you guys for the informal discussions and various lunch sessions.

During my first stint at Gent, Panos, Maria, Tapan, Madhumita Pravesh, Neeti, Ark, Vatsala, Suku, KD, Carolina, Ionel, Pieter, Unmesh, Gonza, Mike and Marko helped me settle into a comfortable life. This was the time I was getting used to the local beer, fritjes and the culture around. I fell in love with Gent for its lively atmosphere and student friendly culture. It gave be a very good perspective about life and kept me motivated towards my research. On my return to Gent from London it really felt like a sweet homecoming and I had

the opportunity to interact with more people around. Rakesh many thanks for the help in finding a comfortable place to live. VK and Santosh thank you so much guys for all the hospitality and affection. Sandu your dry humour was always gut-wrenching, but I thoroughly enjoyed your friendship. Sunita and Tapas thanks a ton guys for making me one among your family, bhai thanks for agreeing to disagree with me most of the times. Karthik and Aishwarya for the Kannada touch, Macchi thanks for the coffee sessions and listening to all my weird ideas. Angie thank you for your great insights on technical issues and Chanu for all the PoMMs. Manan and Nammi, I know you guys will be grateful to me for ever, but this is my chance to be grateful for your friendship. Kaustav, Shars, Nandini, Divya, Anil, Hasan, Akanksha, Pallavi and Sadhu Saheb (Shailesh) thanks a ton people for bearing my 'over the board insanity'.

Daria, Marita, Roxy, JP, Stavre, Lukas, Martino, Gilly boy, Gijja, Nagmeh, Evgeniy and Malli thanks a ton for your friendship, you guys are great !!!. Along with this Ph.D. I also have bumped into something that I will always cherish for the rest of my life. Gent is and will always be the second most favourite place of mine, after Bangalore that is.

London was awesome, a typical metro which gave me an opportunity to see the world from a different perspective. Meera and Manoj, you guys not only gave me a place to stay but also helped me settle into London. You guys were also my emotional support when I needed it the most. I know words cannot really express the gratitude I have towards you but thank you for everything.

Jan and Iro, thank you for the friendship, our weekend outings really kept me going in my research. TCC V was an amazing experience as well, the cricket not only helped me be a bit fit, but also helped me get away from the stress related to work. Hinay, Uzzi and Nihal thank you guys for your friendship.

Kaushik, Ravi, Bhorgrins and Pintu thank you guys for your time and unconditional friendship. I know I can depend on you guys whenever I want. Thank you for accepting all my idiocy.

Some of my childhood friends have been an important part of shaping me the person I am. BP thanks for the support whenever I needed it the most, I have found myself a *'soul brother'* in you. Chandru, KD, Adi, Arjun, Katu thank you guys for all the help and support. Vate, bob thanks for all the super awesome knowledge on scoring and cooking (*adige maadodu !!!*).

SVYSS boys, Sunil Anna, Ganeshu, Moni, Tumpi, Chini, Sada, Nacchy, Manja, Darshu, Ritu and Devu, Thank you for your unconditional friendship.

DVN sir, thank you for being a great teacher, you have not only taught me science but also have instilled important lessons of life in me. I will always be indebted towards you.

Nanda uncle for being a great mentor and ‘idea bouncing board’, you are an inspiration to me.

Vinu, my *‘brother from another mother’*, thank you for patiently listening to all my crazy ideas.

Pawan, you are more than an elder brother to me and my “one stop solution” for all my problems, be it math, science or life. Thank you for setting high standards for me to match, hope I have lived up to them. Kruthika, you are awesome and my sharing board, thank you for listening to all my stories and being there for emotional support when I needed it the most. Finally, Aaru, you are too you young to read this now, but when you read it I want you to know you are an awesome kid and have filled our lives with a lot of happiness.

Amma, you are my most valuable possession and a source of power. Thank you for being the pillar of strength in all my endeavours. From those early morning kannada teaching sessions to this Ph.D. I guess we have come a long way. Amma, thank you for everything that you have done for me. Dad, I didn’t have to look too far for inspiration and a real life hero. Thank you for sharing your lessons on morals and ethics, trouble shooting and teachings on life. Your motivation when I was really down was very assuring and invaluable. Amma and Dad, I am what I am today because of you both !!!

Chetan

Table of Contents

This page intentionally left blank

List of Figures

This page left intentionally blank

List of Tables

This page intentionally left blank

Nomenclature

Roman symbols

$*$	Coordinatively unsaturated metal sites (CUS) of sulphided catalyst
$'$	Electron location on carbon atom of aromatic ring
$-S^{2-}$	Sulfur anion sites
A	Pre-exponential factor (mol $kg^{-1})^{n-1}$ s^{-1}
A_i	Chromatogram peak surface area for component *i*
a	Specific gas-liquid interface area (m^2 m^{-3})
b	Model parameter vector containing the estimated parameter values
C	Concentration (mol m^{-3})
C_f	Final concentration (mol m^{-3})
C_o	Initial concentration (mol m^{-3})
C_j	Surface concentration of component j (mol kg_{cat}^{-1})
$C_{*,t}$	Total concentration of active centers (mol kg_{cat}^{-1})
C_p	Specific heat capacity (J kg^{-1} K^{-1})
$CF_{i,D}$	Calibration factor of component *i* in detector D
C_5	Pentane and pentene
d_p	Darticle diameter (m_p)
E_a	Activation energy (J mol^{-1})
F	Molar flow rate (mol s^{-1})
F_V	Volumetric flow rate (m^3 s^{-1})
F value	F value for the significance of the regression
f^F	Fugacity in aggregation state *F* (Pa/MPa)
g	Gravitational constant (9.8 $m.s^{-2}$)
$\Delta H°_r$	Standard enthalpy of reaction (kJ mol^{-1})
h	Planck constant (6.63 10^{-34} J s)
H	Henry coefficient (Pa^{-1})
H	Enthalpy (J mol^{-1})
Hydrogen	

k	Rate coefficient of elementary step (s^{-1}, $Pa^{-1}s^{-1}$)
K_{eq}	Reaction equilibrium coefficient
K_i	Chemisorption equilibrium coefficient for species $_i$ (Pa^{-1}/MPa^{-1})
k_B	Boltzmann constant (1.38 10^{-23} J K^{-1})
k_La	Volumetric gas-liquid mass transfer coefficient (s^{-1})
m	Number of unsaturated carbon atoms adjacent to reacting carbon atom (-)
$N_{agitator}$	Number of agitator rotations (rps)
N_{Fr}	Froude Number (-)
n	Degree of branching of reacting carbon atom
n_e	Number of single events
nob	Number of observation
npar	Number of parameters
nresp	Number of responses
p	Pressure (MPa)
p_o	Initial pressure of the degassed liquid (MPa)
p_m	Pressure of the system after it is pressurised (MPa)
p_f	Final pressure of the system after the experimental run (MPa)
P	Pyridine
PP	Piperidine
n-PPP	*n*-pentylpiperidine/ *1*-pentylpiperidine
p_t	Total pressure (Pa/MPa)
p_i	Partial pressure of component i (Pa/MPa)
Q	Volumetric flow rate (m^3 s^{-1})
r	Reaction rate (mol kg_{cat}^{-1} s^{-1})
s	Secondary
R	Universal gas constant (8.314 J mol^{-1} K^{-1})
R_i	Net production rate of component i (mol kg_{cat}^{-1} s^{-1})
S	Entropy (J mol^{-1} K^{-1})
S	Selectivity
SSQ	Sum of squared residual between the experimental and model calculated

	outlet molar flow rates ($mol^2\ s^{-2}$)
T	Temperature (K)
t-value	Student t value for the significance of an individual parameter (-)
t	time (s)
$t_{sampling}$	Time at which the data point was extracted (s)
t_{lag}	Lag time of reactor set-up (s)
V	Volume (m^3)
V_m	Molar volume ($m^3\ mol^{-1}$)
V_L	Liquid volume (m^3)
V_R	Reactor volume (m^3)
$V(b)_{ij}$	Element at row i and column j of the covariance matrix of the parameter matrix
W	Catalyst mass (kg)
wt%	Weight percent of compound i
X	Conversion (mol mol^{-1})
x_i	Liquid phase mole fraction of component *i*
y_i	Gas phase mole fraction of component *i*

Greek symbols

β	Model parameter vector containing the estimated parameter values
ε_L	Liquid hold-up ($m^3\ m^{-3}$)
ε_G	Gas hold-up ($m^3\ m^{-3}$)
ε_b	Void fraction in catalyst bed ($m_f^3\ m_p^{-3}$)
ϕ	Contribution factor
Φ	Fugacity coefficient
Φ	Weisz modulus
Δ	Difference
λ	Thermal conductivity ($W\ m^{-1}\ K^{-1}$)
η_j	Effectiveness factor for reaction *j*
$\gamma_{H2/A}$	Molar hydrogen to aromatics ratio (-)

θ_i	Coverage of the catalyst surface with component i
σ	Symmetry number
τ_L	Liquid residence time (s)
μ^{F}_{i}	Chemical potential of component i (in aggregation state *F*) (J mol^{-1})
ρ_F	Density of phase *F* (kg m^{-3})

Superscripts

^	Model calculated
~	Intrinsic, single-event
‡	Activated complex
g	Gas
o	Reactor inlet value
o	Standard
hyd/deh	via hydrogenation and dehydrogenation
L/l	Liquid
lg	Flashed gas
ll	Flashed liquid
r	Reactant
s	Solid

Subscripts

cat	Catalyst
deh	Dehydrogenation
ext	External
f	Final value
g	Gas phase
glob	Global
hyd	Hydrogenation
I	Initial value
i→j	component/intermediate i to component/intermediate j
int	internal

j	experimental observation index
l	Liquid
m	Instantaneous value
R	Reactor
ref	Reference
regres	Regression
rot	Rotation
trans	Translation
vib	Vibration

Abbreviations

DFT	Density Functional Theory
FID	Flame Ionization Detector
GC	Gas Chromatograph
HPLC	High Pressure Liquid Chromatograph
RDS	Rate-Determining Step
SEMK	Single-Event Micro Kinetics
TCD	Thermal Conductivity Detector

This page intentionally left blank

Glossary of terms

Activation energy	For an elementary-step, it is the difference in internal energy between transition state and reactants. A measure for the temperature dependence of the rate coefficient $k=A \exp(E_a/RT)$ with R is the universal gas constant, T the temperature, A the pre-exponential factor and E_a the activation energy.
Active site	Also called active centre. Those sites for adsorption which are responsible for adsorption and subsequent reaction.
Adsorbate	The adsorbed species.
Adsorbent	Surface on which adsorption is occurring.
Adsorption	The preferential concentration of a species at the interface between two phases. Adherence of the atoms, ions or molecules of a gas or liquid to the surface of another substance.
Adsorption isotherm	The function, for a single gaseous adsorptive on a solid, which relates at constant temperature the amount of substance adsorbed at equilibrium to the pressure (or concentration) of the adsorptive in the gas phase.
Aggregation state	A physically distinctive form of a substance, such as solid, liquid and gaseous state. 'Aggregation state' term is preferred over 'phase' because in the case of two immiscible liquids, two distinct phases are present having the same aggregation state.
Ambient conditions	Referring to conditions of atmospheric pressure *i.e.,* 0.1 MPa and room temperature *i.e.,* 298K. Used to define the conditions at which the experimental data are acquired.
Arrhenius relation	Expresses the dependence of a rate coefficient, k corresponding with a chemical reaction on the temperature T and activation energy, E_a : $k=A \exp(E_a/RT)$ with R is the universal gas constant, T the temperature, A the pre-exponential factor and E_a the activation energy.
Catalyst	A source of active sites, which augments the rate of a chemical reaction and is regenerated at the end of a closed reaction sequence.

Calcination	Heating in air or oxygen (most likely to be applied to a step in the preparation of a catalyst).
Chemisorption	Also known as chemical adsorption. Adsorption in which the forces involved are valence forces of the same kind as those operating in the formation of chemical compounds. Chemisorption strongly depends on the surface and the sorptive, and only one layer of chemisorbed molecules is formed. Its energy of adsorption is the same order of magnitude as in chemical reactions, and the adsorption may be activated.
Chiral	A chiral molecule is a type of molecule that lacks an internal plane of symmetry and thus has a non-super imposable mirror image. Achiral (not chiral) objects are objects that are identical to their mirror image. Human hands are perhaps the most universally recognized example of chirality.
Collision theory	Theory to calculate the rate of a elementary chemical reaction by using the hard sphere model of kinetic theory.
Continuous Stirred Tank Reactor (CSTR)	A steady-state tank reactor which is continuously supplied with feed and at the same time an equal volume of reactor content is discharged in order to maintain a constant level in the tank. The fluid in the tank is agitated such that the composition is uniform throughout the reactor and equal to the effluent composition.
Conversion	Measure for the amount of a reactant that has been transformed into products as a result of a chemical reaction.
Coordinatively Unsaturated Site	Coordinatively Unsaturated Site (CUS) is an active site at the catalyst surface containing empty orbitals.
Deactivation	The decrease in conversion in a catalytic reaction with time of run under constant reaction conditions.
Dissociative chemisorption	Adsorption of a molecule with dissociation into two or more fragments, both or all of which are bound to the surface of adsorbent.
Elementary step	The irreducible act of reaction in which reactants are transformed into products directly, i.e. without passing through an intermediate that is susceptible to isolation.
Effectiveness	Ratio of actual reaction rate for a porous catalyst to reaction rate that

factor	would be observed if the total surface area throughout the catalyst interior were exposed to a fluid of the same composition and temperature as that found at the outside of the particle.
External diffusion	Also called interphase diffusion. Diffusion from the fluid phase to the external surface of catalyst.
Fugacity	Thermodynamic activity in a non-ideal phase with the ideal gas state as the reference state.
Gas Chromatography (GC)	The process in which the components of a mixture are separated from one another by injecting the sample into a carrier gas which is passing through a column or over a bed of packing with different affinities for adsorptive of the components to be separated.
Group contribution method	A technique to estimate and predict thermodynamic and other properties from molecular structures, i.e. atoms, atomic groups, bond type etc.
Halpasol™	A mixture of linear alkanes (*n*-C_9 to *n*-C_{14}).
Heterolytic dissociation	Breaking a chemical bond to produce two oppositely charged fragments, e.g. H_2 into H^+ and H^-.
Homolytic dissociation	Dissociative chemisorption resulting in same species, e.g., H_2 into H.
Intermediate	Is formed from a reactant and transforms into a product during a chemical reaction. The intermediate is often a short-lived and unstable species that cannot directly be detected during a reaction.
Inhibition	Decrease in rate occasioned by a substance (inhibitor, poison) which may be produced during reaction itself or may be a foreign substance.
Internal diffusion	Also called intra-particle diffusion. Motion of atoms within the particles of a solid phase that has a sufficiently large porosity to allow this motion.
Intraparticle diffusion	Motion of atoms or molecules in between particles of a solid phase.
Langmuir adsorption	Adsorption of a gas on a uniform surface in which there is no interaction between adsorbed species. Langmuir isotherm for non-dissociative adsorption has the form $\theta = \frac{k\,p}{1+k\,p}$ where θ = surface coverage,

	p = gas phase pressure of adsoptive, k = Langmuir adsorption equilibrium constant.
Langmuir-Hinshelwood-Hougen-Watson (LHHW) mechanism	It is assumed that both reactants must be adsorbed on the catalyst in order to react in Langmuir-Hinshelwood-Hougen-Watson (LHHW) mechanism. Normally adsorption-desorption steps are essentially at equilibrium and a surface step is rate-determining. Adsorption steps can also be rate-determining.
Liquid hold-up	Ratio of liquid inside the reactor to the total volume of the reactor.
Knudsen diffusion	Type of mass transfer which is dominated by molecule-pore wall collisions, as a result of a large mean free path between collisions compared to the pore diameter. Prevails at low pressures and/or small pore diameters.
Mechanism	A sequence of elementary steps in which reactants are converted into products, through the formation of intermediates.
Most abundant surface intermediate (MASI)	Reaction intermediate on a catalyst surface whose concentration is much greater than that all of the other intermediates.
Network	When several single reactions take place in a system, these parallel and consecutive reactions constitute a network.
Objective function	It is a function used during optimization problems which have to be minimized or maximized by choosing the best set of variables which determines the values of this function.
Pseudo-steady state	Its mathematical expression is that the time rate of change of the concentration of all active centres in a reaction sequence is equal to zero.
Parameter estimation	Process of estimating the parameters of a relation between independent and dependent variables as to describe a chemical reaction as good as possible.
Parity diagram	Diagram representing the model calculated values as a function of the experimentally observed values. The better the correspondence with the first bissectrice, the better the model.
Physisorption	Also known as physical adsorption. Adsorption in which the forces

	involved are inter-molecular forces (van der Waals forces) of the same kind as those responsible for deviation from ideal gas behavior or real gases at the condensation of vapours, and which do not involve a significant change in the electronic orbital patterns of the species involved. Physisorption usually occurs at temperatures near the boiling point of adsorbate, and multilayer can occur. The heat of adsorption is usually significantly less than 10 kcal/mol.
Porosity	A measure of the void spaces in a material, expressed as the ratio of the volume of voids to the total volume of the material.
Pre-exponential factor	The temperature-independent factor of a rate coefficient $k=A \exp(E_a/RT)$ also called the frequency factor.
Reaction family	Classification of elementary reaction steps on the basis of same features.
Reaction rate	The number of moles of a component created by a chemical reaction per unit of time, volume or catalyst weight.
Rate-determining step	If, in a reaction sequence, consisting of *n* steps, *(n-1)* steps are reversible and if the rate of each of these *(n-1)* steps potentially larger in either direction than the rate of the *n*th step, the latter is said to be rate-determining. The rate-determining step need not be reversible.
Reversible	A process or reaction that can be reversed by an infinitesimally small change in conditions.
Residual plot	Plot showing the difference between model calculated and experimentally observed values as a function of an operating condition such as the temperature, pressure, inlet concentration.
Residence time	Amount of time that the components spend inside the reactor.
Sorption	Assimilation of molecules of one substance by a material in a different phase. Adsorption (sorption on a surface) and absorption (sorption into bulk material) are two types of sorption phenomena.
Sorptive	A molecule which is going for sorption on the surface of catalyst.
Steady state	A system in steady-state has certain properties that are time-independent.
Sulphided	Catalysts that contain the sulphided phase as the active phase and

catalysts	promote hydrogenation reactions. These are usually used in the hydrotreating industry for chemical upgradation of fuels.
Surface coverage	Ratio of the amount of adsorbed substance to the monolayer capacity (also, sometimes defined for metals as the ratio of the number of adsorbed atoms or groups to the number of metal surface atoms).
Support	Also called carrier. Material, usually of high surface area, on which the active catalytic material, present as the minor component, is dispersed. The support may be catalytically inert, but it may contribute to the overall catalytic activity.
Surface coverage	Ratio of the amount of adsorbed substance to the monolayer capacity.
Steady-state	A system in steady-state has certain properties that are time-independent.
Tortuosity	Tortuosity of a catalyst expresses that transport through a porous catalyst particle does not occur long the radius of the particle, but occurs through the pores of the solid material. For pores with a uniform diameter, the tortuosity is then defined as the square of the ratio of the average distance between two points and the shortest distance between them.
Transition state	Also called activated complex. The configuration of highest potential energy along the path of lowest energy between reactants and products.
Transition state theory	Theory to calculate the rate of an elementary reaction from knowledge of the properties of the reacting components and their concentrations. Differs from collision theory in that it takes into account the internal structure of reactant components.

Summary

Today's modern industrial world depends on hydrocarbon fuels originating from various geographic locations. While alternative energy sources, such as solar, wind and hydropower seem promising, hydrocarbon based fuels still remain the first choice as an energy carriers. Sulphur, nitrogen and oxygen containing components, which are inherently present in the naturally extracted crude, are transformed into harmful SO_X and NO_X in an automobile internal combustion engine in case they have not been eliminated from the fuel. Therefore, growing environmental issues and stringent laws on fuel qualities have enforced engineers to find solutions for cleaning these 'dirty' feedstocks, *i.e.,* significantly decreasing the sulphur, nitrogen and oxygen content. Hydrotreating is employed to upgrade the crude oil and its derived fractions and is considered to be one of the most important processes during oil refining. Hydrotreating not only removes the above discussed, undesired hetero-atoms and catalyst poisons, it simultaneously upgrades the fuel quality by saturating carcinogenic components such as benzene. Hydrodesulphurisation has been a topic of a large number of publications and the reaction has been understood rather well. Interest in hydrodenitrogenation, however, has only increased recently due to the evermore strict environmental regulations as well as the increasing amounts of nitrogen in the crude oil.

Experimental data obtained at gas phase conditions preferentially constitute the basis of modelling work. In order to develop an adequate kinetic model, experimental data free from any form of hydrodynamic, thermal and transport effects are necessary, *i.e.,* so-called *intrinsic* kinetics data. Gas phase experimentation is often more straightforward compared to liquid phase experimentation since the stabilisation time is fast and the analysis of a single effluent stream allows accurate measuring of the responses. The industrial process implementation being operated at three-phase conditions, experimental data acquired at 'liquid phase' conditions are generally considered more relevant for hydrotreating, since realistic feedstocks and industrially relevant conditions can be maintained during the experimental programmes. Studying a single reaction at gas as well as at liquid phase conditions allows a thorough assessment of these phase effects. Starting from a model constructed at gas phase conditions, it can be extended to liquid phase reactions by considering the non-idealities induced by the presence of the liquid phase [1].

The obtained gas and liquid phase data can then be used for constructing mathematical models describing the investigated reactions. Model construction aiming at the simulation of a particular process typically depends on the simulation purposes for which the model will be used, e.g. a power law model may be sufficient to simulate the reaction behaviour around a stable operating point. Such models are predominantly used in an industrial or control engineering environment where the effects of the operating conditions on the molecular level, *i.e.*, at the catalyst surface are less relevant. Models based on elementary reactions have become powerful tools in chemical engineering because of the unique insights they provide [2]. During the construction of such models, reaction mechanisms which are derived from a critical evaluation of experimental results and literature are employed. Such models conveniently connect the operating conditions to the elementary reaction rates and, hence, allow a fundamental explanation of the products formation. In addition, models based on elementary reactions capture the phenomena occurring on the catalyst surface and the internal pore structure. These models quantify the active site properties in terms of descriptors. After a critical evaluation of model simulations as a function of these descriptor values, synthesis procedure modification can be proposed in order to optimise the catalyst in conjunction with the operating conditions at which it is used.

In this thesis hydrodenitrogenation is investigated from both an experimental as well as a modelling perspective. In accordance to the global theme of the thesis topic, the first objective was studying the reactor performance of a three-phase bench-scale Robinson-Mahoney reactor [3]. The liquid hold-up, ϵ_L, and volumetric gas-liquid mass transfer coefficient, k_La, are important parameters in the framework of reactor design and process intensification. While ϵ_L provides insight in the actual phase distribution within the reactor, k_La gives an indication of the extent of mass transfer between the gas and the liquid phase. Liquid hold-up measurements conducted at industrially relevant as well as ambient conditions showed that the reactor volume always contains at least 50% of liquid even at high inlet volumetric gas to liquid flow ratios. The liquid hold-up is strongly affected by the inlet volumetric gas to liquid ratio and liquid physical properties, such as surface tension. Based on experimental observations it was concluded that the continuous phase within the reactor consists of a liquid containing gas bubbles of various sizes. k_La was found to be affected mainly by the agitator rotation speed. It was observed that k_La increased from 1.22 10^{-2} s^{-1} to 2.14 10^{-2} s^{-1} between agitator rotation speeds of 8.33 and 25 rps. Hence, higher rotations of the agitator enhance the mass transfer

between the gas and the liquid phase. It is suggested that the agitator rotation of 25rps is maintained when acquiring *intrinsic* data.

The second objective of this dissertation was to construct a model for pyridine hydrodenitrogenation reaction using previously acquired gas phase data [4]. The pyridine hydrodenitrogenation reaction mechanism is illustrated in Figures 1 and 2. According to this reaction mechanism pyridine is first hydrogenated into piperidine. Subsequently, piperidine ring opening yields a primary amine, which further reacts to C_5 hydrocarbons. Both the ring opening and the further reaction occur via a H_2S assisted substitution reaction. Langmuir Hinshelwood reaction mechanisms accounting for two types of sites, *i.e.*, coordinatively unsaturated sites (*) and sulphur anions ($-S^{2-}$), were proposed and corresponding kinetic models were derived to assess the experimentally measured kinetics. The novelty of this work lies in explicitly accounting for pyridine hydrogenation through protons and hydride available through heterolytic or homolytic chemisorbed hydrogen and hydrogen sulphide. Another novelty of this work was to account for the elementary reaction steps occurring during the substitution mechanism of the C-N bond scission. The number of parameters to be estimated was reduced by calculating chemisorption entropies *a priori*. The kinetic parameters and chemisorption enthalpies were estimated by regression. The third hydrogen addition and the naphthenic C-N bond breaking were found to be rate determining in pyridine hydrogenation and piperidine denitrogenation, with activation energies amounting to 41 kJ mol^{-1} and 185 kJ mol^{-1}. This model successfully captures all phenomena occurring during the reaction at gas phase conditions and provides the basis for an extension towards liquid phase conditions which is the third objective of this dissertation.

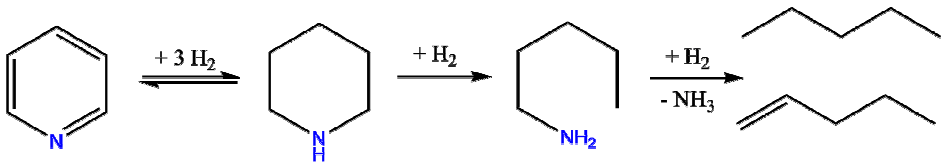

Figure 1. Pyridine hydrodenitrogenation network as observed at gas phase conditions over an industrial NiMo/γ-Al_2O_3 catalyst.

At both gas and liquid phase conditions, the reaction temperature and H_2S inlet partial pressure were found to be most significantly affecting the selectivity to intermediates and final products. At liquid phase conditions, also *n*-pentylpiperidine was observed along with the previously observed products, *i.e.*, piperidine and C_5 hydrocarbons. This additional reaction product, *n*-pentylpiperidine, was formed from a bimolecular reaction between surface piperidine and *n*-pentylamine species, see Figure 2. This could be ascribed to the differences

in density of the phases present during kinetics measurements as well as to the differences in molar H_2 and H_2S to pyridine inlet ratios used. The kinetic model constructed using gas phase data was extended to liquid phase conditions by accounting for liquid phase non-ideality, solvent adsorption effects and the additionally observed product, *i.e.*, *n*-pentylpiperidine.

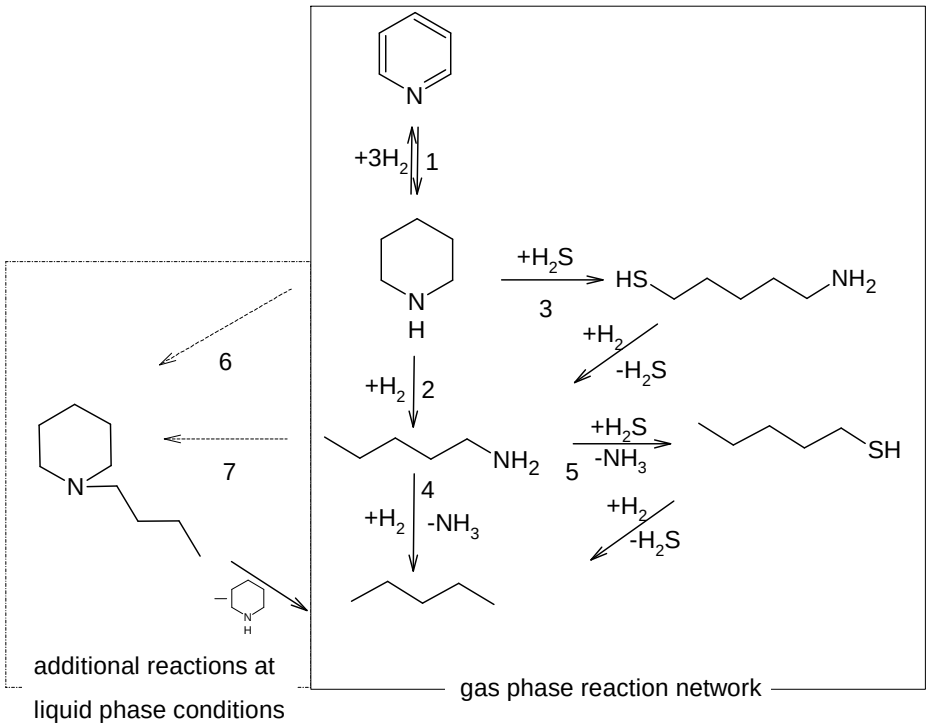

Figure 2. Pyridine hydrodenitrogenation network as observed at liquid phase conditions over an industrial NiMo/γ-Al_2O_3 catalyst.

The final objective of this dissertation was to provide a proof of concept for the extension of the Single Event Micro Kinetic (SEMK) methodology towards components with hetero atoms on one hand and sulphided catalysts on the other hand. According to this methodology, a detailed network incorporating all possible elementary reaction steps occurring during the pyridine hydrodenitrogenation was generated using the in-house software tool 'ReNGeP'. A total number of 33 intermediates were formed during the network generation procedure. This includes 19 partially hydrogenated hetero naphthenic species in addition to 14 acyclic and condensed species. For the complete conversion of pyridine to piperidine and C_5 hydrocarbons, a total number of 70 elementary reactions were encountered. Based on the reactions occurring on the catalyst surface, a comprehensive SEMK model for pyridine hydrodenitrogenation was constructed by defining nine reaction families. The model requires a total number of 48 parameters comprising both kinetic and catalyst descriptors. A parameter reduction was

achieved by maintaining catalyst descriptors at their values determined in previous chapters and by a priori calculating pre-exponential factors for the rate coefficients, based on the assumptions of varying degree of surface mobility. The extended SEMK model was able to satisfactorily describe the effects of the experimental conditions on the pyridine hydrodenitrogenation reaction.

References

1. Thybaut, J.W., C.S. Laxmi Narasimhan, and G.B. Marin, **Catalysis Today**, 2006. 111(1-2): p. 94-102.

2. Thybaut, J.W. and G.B. Marin, **Journal of Catalysis**, 2013. 308: p. 352-362.

3. Mahoney, J.A., K.K. Robinson, and E.C. Myers, **Chemtech**, 1978. 8(12): p. 758-763.

4. Pille, R. and G.F. Froment, **Hydrotreatment and Hydrocracking of Oil Fractions**, 1997. 106: p. 403-413.

This page intentionally left blank

Samenvatting

De huidige industriële wereld is afhankelijk van koolwaterstoffen afkomstig van alle uithoeken van de wereld. Hoewel alternatieve energiebronnen, zoals zonne- en windenergie alsook waterkracht, veelbelovend lijken, zijn traditionele koolwaterstofgebaseerde brandstoffen nog steeds de eerste keuze als energiedragers. Zwavel-, stikstof- en zuurstofbevattende componenten, die inherent aanwezig zijn in de geëxtraheerde ruwe olie, worden, indien ze niet verwijderd worden uit de brandstof, in een autoverbrandingsmotor omgezet in schadelijke SOx en NOx . De groeiende milieuproblematiek en de steeds strengere wetgeving aangaande de hoeveelheid hetero-atomen dwingt ingenieurs tot het zoeken naar oplossingen voor het reinigen van deze 'vuile' grondstoffen, d.i. het fors verlagen van de zwavel-, stikstof- en zuurstofhoeveelheid. Waterstofbehandelingen worden beschouwd als één van de belangrijkste processen tijdens de raffinage. Het wordt toegepast voor het opwaarderen van de ruwe olie en de afgeleide fracties. Tijdens een waterstofbehandeling worden niet alleen de ongewenste hetero-atomen en katalysatorgiffen verwijderd, maar tegelijkertijd wordt de kwaliteit van de brandstof verbeterd door het verzadigen van kankerverwekkende componenten zoals benzeen. Aangezien zwavel het meest voorkomende hetero-atoom is in aardolie, besteedde de academische en industriële wereld de meeste aandacht aan ontzwaveling (HDS). De belangstelling voor stikstofverwijdering (HDN) is pas recent toegenomen als gevolg van de steeds strenger wordende milieuregels en de toenemende hoeveelheden stikstof in de ruwe olie.

Experimentele gegevens die bij voorkeur bij gasfase condities verkregen zijn, vormen de basis van het modeleren. Om een adequate kinetisch model te ontwikkelen, moeten de experimentele gegevens onafhankelijk zijn van eventuele hydrodynamische effecten of massa- en warmteoverdracht, d.i. zogenaamde intrinsiek kinetische data. Gasfase experimenten zijn minder gecompliceerd in vergelijking met experimenten in de vloeibare fase gezien de snellere stabilisatietijd en de nauwkeurige meting van de waarnemingen door middel van de analyse van de effluentstroom. De industriële reactoren worden typisch bedreven bij driefase condities. Experimenteel verworven data in de vloeistoffase wordt doorgaans als meer relevant beschouwd, omdat realistische voedingen en industrieel relevante condities kunnen worden gehandhaafd. Het bestuderen van een enkele reactie in zowel de gas- als de vloeibarefase kan een diepgaand inzicht bieden in de fase-effecten. Vertrekkende van een model voor gasfase

condities, dat wil zeggen waarbij het ideale gas als de standaardtoestand wordt gebruikt, kan, door het introduceren van de niet-idealiteit van de vloeistof, het model worden uitgebreid naar vloeistoffase condities [1].

De verkregen data uit de gas en vloeistoffase kan vervolgens gebruikt worden voor het construeren van wiskundige modellen voor het beschrijven van te onderzoeken reacties. De constructie van een model voor een bepaald proces is typisch afhankelijk van de simulatie doeleinden, zo kan bijvoorbeeld een machtswet model voldoende zijn om het reactiegedrag rond een welbepaald stabiel werkingspunt te simuleren. Dergelijke modellen worden voornamelijk gebruikt in een industriële of regeltechniek omgeving waar de effecten van de reactiecondities om moleculair niveau, d.w.z. op het katalysatoroppervlak, minder relevant zijn. Modellen op basis van elementaire reacties zijn krachtige middelen geworden in de chemische technologie vanwege de unieke inzichten die zij bieden. Tijdens de constructie van dergelijke modellen worden reactiemechanismen, die afgeleid zijn van een kritische evaluatie van de experimentele resultaten en de literatuur, gebruikt [2]. Deze modellen leggen de link tussen de reactiecondities enerzijds en de elementaire reactiesnelheden anderzijds, en bieden derhalve een fundamentele verklaring voor de productvorming. Bovendien, beschrijven de modellen gebaseerd op elementaire reacties de verschijnselen die optreden op het katalysatoroppervlak en de interne poriestructuur. Deze modellen kwantificeren de eigenschappen in termen van modelparameters, zogenaamde katalysatordiscriptoren. Na een kritische evaluatie van de simulaties als functie van deze descriptoren, kunnen deze modellen geïmplementeerd worden voor katalysatorontwerp in combinatie met de optimale procescondities.

In het kader van dit doctoraat werd de stikstofverwijdering onderzocht zowel op experimenteel als modelleringsvlak. In overeenstemming met het globale thema van dit doctoraat, was de eerste doelstelling van dit proefschrift het bestuderen van de reactorprestaties van een driefasige Robinson-Mahoney reactor op laboratorium schaal [3]. De vloeistof hold-up, ϵ_L, en de volumetrische gasvloeistof massa-overdrachtscoëfficiënt, k_La, zijn belangrijke parameters in het kader van het reactorontwerp en de procesintensificatie. Het inzicht in de feitelijke fasespreiding wordt gegeven door ϵ_L, terwijl k_La een indicatie geeft van de omvang van de massa-overdracht tussen de gas en de vloeibare fase. Uit de uitgevoerde vloeistof hold-up metingen, op zowel industrieel relevante procescondities als op omgevingscondities, is gebleken dat het reactorvolume altijd ten minste 50% vloeistof bevat, zelfs bij hoge verhoudingen van de volumetrische inlaat van gasstromen tot vloeistofstromen. Gebaseerd op de experimentele waarnemingen werd geconcludeerd dat de continue fase in de reactor bestaat

uit een vloeistof, die gasbellen bevat van verschillende grootte. k_La bleek voornamelijk beïnvloed door de rotatiesnelheid van de roerder. Er werd waargenomen dat k_La steeg van 1.22 10^{-2} s^{-1} tot 2.14 10^{-2} s^{-1} bij een stijgende rotatiesnelheid van 8.33 tot 25 tps. Hoge rotatiesnelheden verbeteren de massaoverdracht tussen de gas en de vloeibare fase. Er wordt voorgesteld dat de rotatiesnelheid van 25 tps wordt gehandhaafd bij het verkrijgen van de intrinsieke data.

De tweede doelstelling van dit doctoraatswerk was het construeren van een model voor de stikstofverwijdering van pyridine met behulp van eerder verkregen gasfase data set [4]. Het mechanisme van de stikstofverwijdering wordt weergegeven in Figuur 1 en 2. Volgens deze reactiemechanismen wordt pyridine eerst gehydrogeneerd in piperidine. Vervolgens zorgt de ringopening van de piperidine voor de vorming van een primair amine, dat verder reageert tot C_5 koolwaterstoffen. Zowel de ringopening als de verdere reactie vinden plaats via een substitutiereactie, waarbij H_2S een bevorderend effect heeft op de breking van de C-N binding. Een Langmuir-Hinselwood reactiemechanisme met twee actieve sites werd voorgesteld en de bijhorende kinetische modellen werden afgeleid om de experimenteel opgemeten kinetiek te beoordelen. In dit werk worden de twee sites vermeld als coördinatief ongesatureerde sites (*) en zwavel anion sites ($-S^{2-}$). De vernieuwing van dit werk ligt in het expliciet in rekening brengen van de hydrogenatie van pyridine door protonen en de beschikbaarheid van de hydride via heterolytische of homolytische gechemisorbeerd waterstof en waterstofsulfide. Een andere vernieuwing van dit werk is het in rekening brengen van de elementaire reactiestappen tijdens de substitutiestap van de breking van de C-N binding. Het aantal te schatten parameters werd verminderd door het a priori berekenen van de chemisorptie entropie. De kinetische parameters en chemisorptie enthalpiën werden geschat door regressie naar de experimentele data. De derde waterstof additiestap en de breking van de naftenische C-N binding werden als snelheidsbepalend gevonden bij de hydrogenering van pyridine en stikstofverwijdering van piperidine, met respectievelijke activatie-energieën van 41 kJ mol^{-1} en 185 kJ mol^{-1}. Het model is in staat om succesvol alle verschijnselen die tijdens de gasfase reactie optreden, te beschrijven. Het legt tevens de basis voor een extensie naar de beschrijving in de vloeistoffase, wat het derde doel was van dit doctoraatswerk.

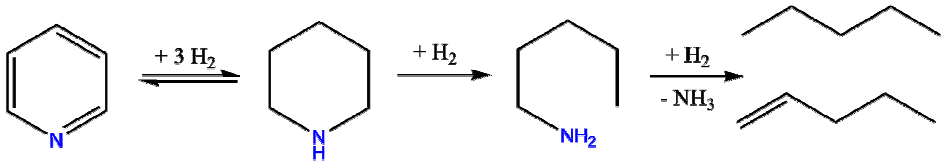

Figuur 1. Reactienetwerk van stikstofverwijdering van pyridine geobserveerd in gasfase experimenten op een industriële NiMo/γ-Al_2O_3 katalysator.

Voor zowel gas als vloeistoffase condities, bleken de reactietemperatuur en de inlaat partiële druk van H_2S de belangrijkste procesparameters te zijn voor de selectiviteit naar de tusssen- en eindproducten. In de vloeistoffase, werd naast de eerder waargenomen producten, piperidine en C_5 koolwaterstoofen, ook n-pentylpiperidine waargenomen. Dit bijkomend reactieproduct, n-pentylpiperidine, wordt gevormd uit een bimoculaire reactie tussen het geadsorbeerd piperidine en n-pentylamine, zie Figuur 2. Deze reactie kan worden toegeschreven aan de verschillen in dichtheid van de aanwezige fasen tijdens de kinetische metingen, alsook aan de verschillen in de inlaat mol verhoudingen van H_2 en H_2S. Het kinetische model voor gasfase fase werd uitgebreid naar de vloeistof fase door het inrekening brengen van de niet-idealiteit van de vloeistof, de adsorptie-effecten van het oplosmiddel en het bijkomend waargenomen product, n-pentylpiperidine.

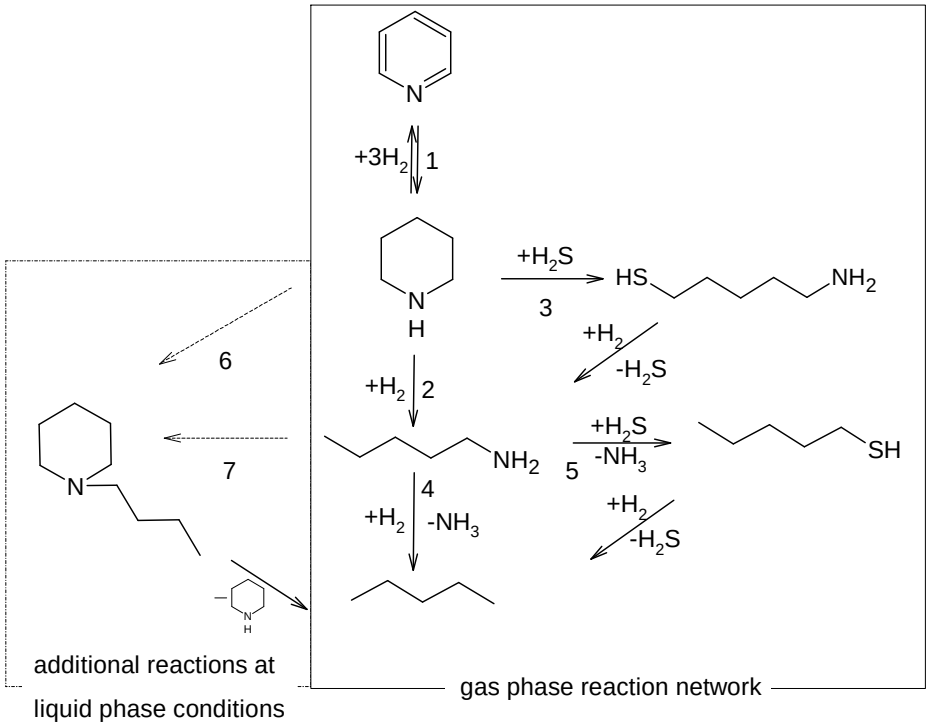

Figuur 2. Reactienetwerk van stikstofverwijdering van pyridine geobserveerd in vloeistof fase experimenten op een industriële NiMo/ γ-Al_2O_3 katalysator.

Het uiteindelijke doel van dit doctoraatswerk was om een proof-of-concept voor de uitbreiding van de Single Event Micro Kinetic (SEMK) methodologie naar enerzijds

componenten met hetero-atomen en anderzijds gesulfideerde katalysatoren te bieden. In deze methodologie wordt een gedetailleerd netwerk, waarin alle mogelijk elementaire reactiestappen die tijdens de stikstofverwijdering van pyridine plaatsvinden, gegenereerd met behulp van de in-house softwaretool “ReNGeP”. Een totaal van 33 tussenproducten werd gevormd tijden de netwerkgeneratie procedure. Hiervan zijn 19 hetero-naftenische componenten gedeeltelijk gehydrogeneerd en 14 acyclische componenten gecondenseerd. Voor de volledige omzetting van pyridine naar piperidine en C_5 koolwaterstoffen, zijn in het totaal 70 elementair reacties waargenomen. Gebaseerd op de waargenomen reacties op het katalysatoroppervlak, werd een uitgebreid SEMK model voor stikstofverwijdering van pyridine geconstrueerd door het definiëren van negen reactiefamilies. Het model vereist zowel kinetische als katalysator descriptoren met een totaal 48 parameters. Een parameter vermindering werd bereikt door het vastzetten van katalysator descriptoren op de eerder bepaalde waarden en het a priori berekenen van pre-exponentiële factoren voor de snelheidscoëfficiënten, gebaseerd op de aannames van verschillende mobiliteit op het oppervlak. Het uitgebreide SEMK model is in staat om de effecten van de experimentele omstandigheden van de stikstofverwijdering van pyridine te beschrijven.

Referenties

1. Thybaut, J.W., C.S.L. Narasimhan, and G.B. Marin, **Catalysis Today**, 2006. 111(1-2): p. 94-102.

2. Thybaut, J.W. and G.B. Marin, **Journal of Catalysis**, 2013. 308: p. 352-362.

3. Mahoney, J.A., K.K. Robinson, and E.C. Myers, **Chemtech**, 1978. 8(12): p. 758-763.

4. Pille, R. and G.F. Froment, **Hydrotreatment and Hydrocracking of Oil Fractions**, 1997. 106: p. 403-413.

This page intentionally left blank

1 Introduction

Dependency of mankind on energy has been well documented [1, 2]. Since the discovery of crude oil, various technical advancements have resulted in higher production of crude oil through deeper subsurface extraction and better fuel quality by advanced refining techniques. Upgrading the technology used in both upstream and downstream vectors of the hydrocarbon industry have been a part of added interest to industry and academia. On the one hand, novel techniques have been proposed and used for increasing production capacity of various sources, while on the other hand, cutting edge research has helped the production of fuels that comply with the stringent rules on the quality of commercial fuel set by various governments across the globe. The current global energy demands are satiated by various sources such as crude oil (to a major extent), coal, natural gas and bio-based feedstock, and according to reports from BP plc, the energy demand will be increasing in the coming years [2]. However, the usage of hydrocarbon based fuels has increased and will continue to increase the stress on the environment due to the emission of harmful SO_x and NO_x along with CO_x, both carbon dioxide and monoxide, resulting from oxidation of these fuels within an internal combustion engine [1, 3, 4]. These gases, amongst others such as CH_4 are known as the most important causes for the global warming and related issues of environmental imbalance.

These concerns raised by government agencies have been dealt with, among others, by improving refining technologies. Refining constitutes one of the most important activities in the chemical upgradation of crude oil. Refining in the general sense is used to refer to the processes that are employed in the petroleum industry to convert the naturally extracted or synthetic crude oil to commercially viable fuels and petrochemicals for direct or indirect use. Typical refinery configurations depend on the type of crude that needs to be processed and the typical product range(s) that are required for the local markets, see *e.g.*, Figure 1-1, After the desalting and the initial distillation of the crude oil, intermediate processes such as hydrocracking, reforming and hydrotreating are employed to produce various products of commercial interest. Each of these processes has been studied carefully in order to optimise the production and overall yield of the products. The focus of this thesis is an important aspect of the hydrotreating reaction, *i.e.*, hydrodenitrogenation, which is more elaborately introduced in section 1.3.

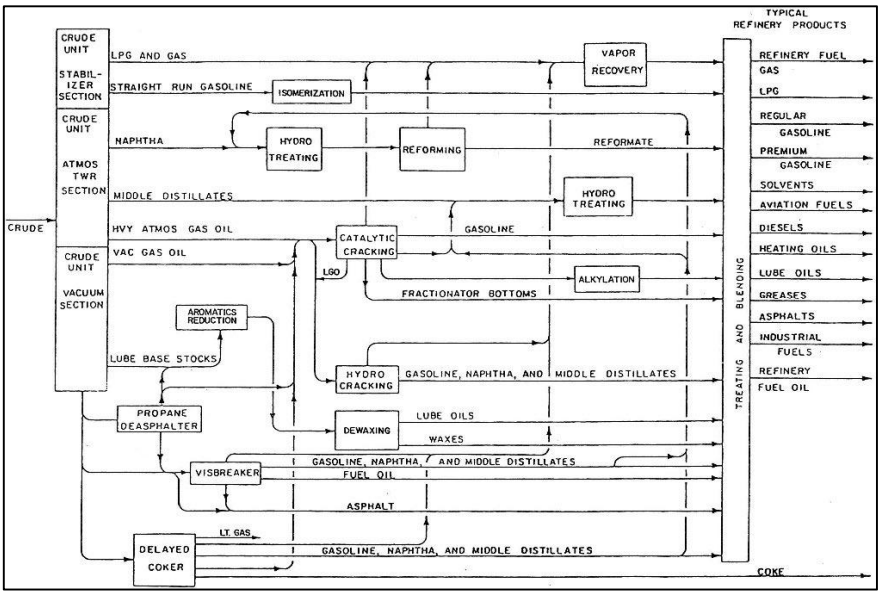

Figure 1-1. Process flow diagram of a typical refining unit [5].

Hydrotreating is the process in which, particularly, heavy oils or bottom products of atmospheric or even vacuum distillation are treated with hydrogen at high pressure in the presence of a bimetallic catalyst in its sulphided state supported by alumina. Hydrotreating is employed for the removal of contaminants/impurities such as sulphur, nitrogen and oxygen through specific reactions called hydrodesulphurisation, hydrodenitrogenation, and hydrodeoxidation. Hydrotreating also improves the quality of the fuel by the saturation of aromatics, which is referred to as hydrodearomatization. All reactions mentioned above are of paramount importance in present day refineries and, hence, these processes are drawing a lot of attention from academia as well as from industry from all over the globe.

1.1 Importance of hydrotreating

Modern refineries add significant value to the local economy not only by providing fuels fit for commercial consumption, but also by providing chemicals for further processing and final products. However, with time, new challenges have been presented to refiners in terms of production volumes and stringent environmental protection laws. Fuel quality has been the foremost driver for production of low sulphur and nitrogen fuels. As can be seen from Table 1-1, the maximum allowed sulphur limit in commercial fuels is continuously decreasing and can be expected to approach even closer to zero in the time to come. The sulphur and nitrogen content in the fuels has a significant impact on the corresponding emissions, *i.e.*, the particulate matter depends on the sulphur and the nitrogen content in fuel, see Figure 1-2.

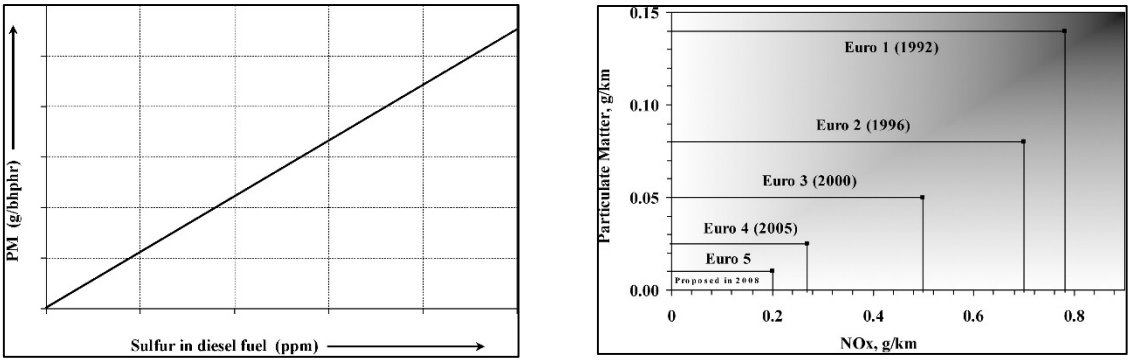

Figure 1-2. Particulate matter as a function of sulphur in diesel fuel (left) and particulate matter and NO_x emission as a function of diesel fuel specification (right) [1].

1.2 Industrial hydrotreating

In addition to the removal of undesired hetero-elements such as nitrogen, sulphur, and oxygen, industrial hydrotreating results in the production of low boiling point products, stabilisation of the olefins to their subsequent paraffins and iso-paraffins. Hydrotreating also is performed prior to processes such as hydrocracking, *e.g.*, to avoid poisoning of the acid sites by the nitrogen components. Various layouts for hydrotreating processes can be found in standard textbooks, highlighting their corresponding advantages and drawbacks [5, 6]. A typical hydrotreating reactor and process design depends on the feedstock that is employed and the desired product spectrum. The catalyst, (Ni/Co)Mo/γ-Al_2O_3, operating conditions (temperature, pressure, H_2/oil, LHSV), configuration (single or multi stage) constitute the set of variables that can be tuned to optimise the whole process.

Industrial hydrotreating process implementations are rather similar to each other, with the major changes being situated in the operating conditions and the general operation of the units, see Table 1-2. Various licensors such as Chevron Lummus [7], UOP Honeywell [8], Axens [9] and KBR [10] provide hydrotreating technology and may have a slightly different flow scheme, mostly for reasons of energy integration or raw material recycling. An example configuration of a typical hydrotreating unit is shown in Figure 1-3.

In the Chevron Lummus process, the feed is mixed with hydrogen-rich treat gas and exchanges heat with the reactor effluent after which it is sent to a heater where the temperature is elevated to the required reactor operating temperature. The mixed feed is then sent to the reactor (1), which is operated as a trickle (multi) bed reactor and contains a typical hydrotreating (NiMo/CoMo over γ-Al_2O_3) catalyst in sulphided state.

Table 1-1. Target for sulphur content in commercial vehicles proposed by various countries [1].

Region	Country	Sulphur (ppmw)	Year of implementation
South America	Argentina	50	2008[a]
	Brazil	500	2008[a]
		50	2009[b]
	Chile	350	2007
		50	2010
	Mexico	500	2005
		15	2009[a]
	Peru	50	2010[a]
	Uruguay	50	2009
Asia Pacific	China	2000	2000
		500	2005[a]
		50	2012[b]
	Hong Kong	50	2007
	India	350	2005[a]
		350	2010[b]
		50	2010[a]
	Singapore	50	2005
	Taiwan	50	2007
	Australia	500	2002
		10	2009
Middle East	Kuwait	2000	2008
		50	2010[b]
	Saudi Arabia	800	2008[a]
		10	2013[b]
	Bahrain, Lebnon, Oman, Qatar, UAE	50	2008
	Qatar, UAE	10	2010
	Bahrain	10	2013
	Iran	50	2008[a]
	Jordon	10000	2008
		350	2012
	Russia	500	2008[a]
		50	2010[b]
EU	Germany, France, Denmark, Sweden	<10	Pushing hard for Euro 5/6

a - Majority of city (selected cities), b - Expected to limit (nation-wide)

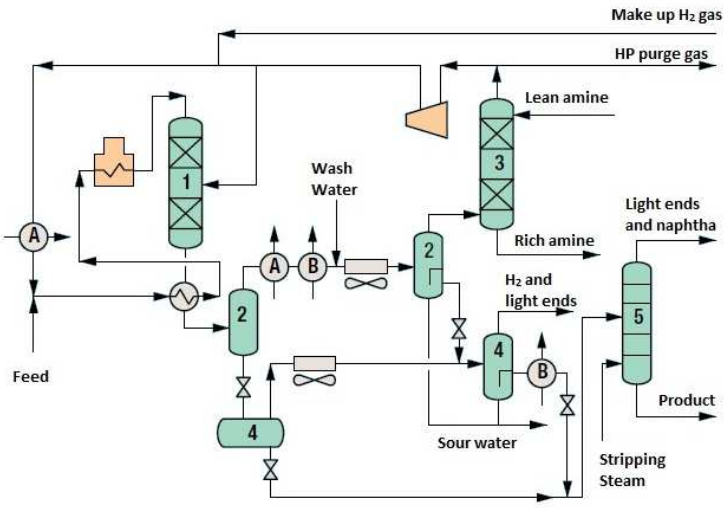

Figure 1-3 Flow sheet of the Chevron Lummus Global LLC ISOTREATING process [11].

Hydrotreating which is an exothermic reaction is quenched with hydrogen as quench gas for controlling the temperature between different catalyst beds. The reactor effluent is cooled and sent to the high-pressure flash (2). In the high-pressure flash the light gases formed during hydrotreating, mostly H_2S and NH_3, and hydrogen are sent over the top. The H_2S is removed in an amine absorber (3), the residual gas is mixed with make-up hydrogen and recompressed before being used as treat gas.

The bottom product of the high-pressure flash goes to a low-pressure flash (4) where additional hydrogen and some light ends are removed. The bottom stream is sent to a stripper and/or fractionator (5) to remove light ends and naphtha-boiling range material and/or to fractionate the higher boiling range materials in product fractions.

Table 1-2. Industrial hydrotreating conditions for different feedstocks [6].

Feedstock	Naphtha	Kerosene	Gas oil	Vacuum gas oil	Residue
Boiling Range [K]	343-453	433-513	503-623	623-823	>823
Operating temperature [K]	543-573	573-613	593-623	633-653	633-653
Hydrogen pressure [MPa]	0.5-1.0	1.5-3.0	1.5-4.0	4.0-7.0	12.0-16.0
Hydrogen consumption [wt.%]	0.05-0.1	0.1-0.2	0.3-0.5	0.4-0.7	1.5-2.0
Liquid Hour Space Velocity (LHSV) [h^{-1}]	4-10	2-4	1-3	1-2	0.15-0.3
H_2/HC ratio [Nm^3 m^{-3}]	36-48	36-48	36-48	36-48	12-24

1.3 Hydrodenitrogenation

Hydrodenitrogenation has not been a major concern in the past because the amount of nitrogen present in the feed to be hydrotreated was much lower than the sulphur content. However, in recent times, because of lower quality crude oils, the scientific world has recognized the importance of concentrating on this aspect of refining. Along with the earlier mentioned environmental and legislative reasons, nitrogen removal is also necessary since the presence of nitrogen components strongly affects other hydrotreating processes such as hydrodearomatisation and hydrodesulphurisation which are often carried out simultaneously with hydrodenitrogenation. It is well accepted in the literature that the nitrogen components competitively adsorb on the active sites of the sulphided catalyst thereby reducing the hydrotreating potential of the catalyst. This reduction in the catalytic activity tends to lower the hydrocarbon conversion which, in turn, requires potentially demanding operating conditions in terms of temperatures, hydrogen partial pressures and total pressures to achieve similar conversions, thereby increasing operating costs.

Hydrodenitrogenation in general refers to the process of selectively removing the nitrogen from the hydrocarbons during crude oil hydrotreating. This is a reduction step carried out in the presence of catalyst and hydrogen at elevated pressures and temperature. The operating conditions vary with different refining units, feed and resulting product range required. Hydrodenitrogenation is different from hydrodesulphurisation chemically since there is no direct removal of the hetero atom from the component [12]. Figure 1-4, shows the scheme of pyridine hydrodenitrogenation, the first step in the removal of the nitrogen from aromatic hetero components is the saturation of the ring followed by the C-N bond cleavage.

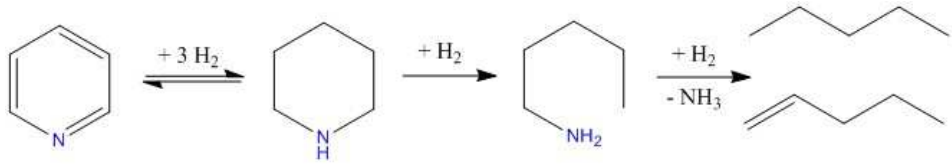

Figure 1-4. Reaction network of pyridine hydrodenitrogenation.

1.4 State of the art in hydrodenitrogenation

Previous sections were dedicated to provide a brief introduction to the topic of this thesis. The sections that follow are aimed at introducing the current state of the art in the various aspects of this thesis.

1.4.1 Experimental Robinson-Mahoney reactor

Experimental studies relating to vapour phase and three phase reactions have been performed in plug flow reactors (PFRs) and continuous, stirred tank reactors (CSTRs). These studies in PFRs have been useful for the acquisition of data for scale-up purposes but issues related to complete catalyst bed wetting and hydrodynamics at the reactor scale remain unclear. Continuous, Stirred Tank Reactors (CSTRs) are used to study three phase reactions and offer better mixing and catalyst wetting in comparison to the PFRs. A special type of fixed basket type three phase reactor has been proposed by Mahoney *et al.*, [13], see Figure 1-5. These reactors, typically denoted as Robinson-Mahoney (RM) reactors are claimed not to exhibit concentration or temperature gradients. They offer better mixing of the involved phases and can be operated in a wide range of operating conditions. While RM reactors have been used for acquiring intrinsic kinetics data [14, 15], also specific research on the reactor hydrodynamics has been performed [16-18].

The proper acquisition of intrinsic kinetics data is essential for satisfactorily explaining the reaction network and to construct a valid kinetic model [13-15]. Hence, estimation of reactor characteristics such as gas and liquid hold-up and volumetric gas-liquid mass transfer coefficient are important to assess the proper regime that exists in the reactor. Assessment of these phenomena provides guidelines for operating in intrinsic kinetic regime and helps in providing data which results in a broader knowledge in terms of reactor design.

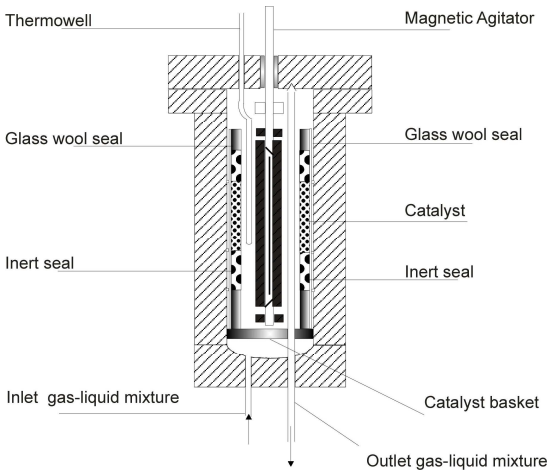

Figure 1-5. Schematic of a three-phase bench-scale Robinson-Mahoney reactor showing the reactor internals [14].

1.4.2 Hydrodenitrogenation - experimental and modelling studies

Experimental studies on hydrodenitrogenation have been performed with various objectives:

a) understanding reaction mechanism and network elucidation for basic and non-basic nitrogen components,
b) effect of various operating conditions on the model component conversion and product distributions and their subsequent optimisation,
c) catalyst characterisation and development, and
d) effect of simultaneous hydrotreating reactions.

Modelling efforts on hydrodenitrogenation have focused on estimating kinetic and catalyst descriptors. In the present section, some particular studies available in the literature which are related to this thesis are discussed and the important results are highlighted.

The first established experimental studies on hydrodenitrogenation, particularly of pyridine, were presented by McIlvried [19], Sonneman *et al.* [20-23] and Satterfield and Cocchetto [24] in the 1970's. McIlvried [19] performed experiments on NiCoMo/Al_2O_3 in a fixed bed tubular reactor and subsequently simulated the reactions using a simple Langmuir-Hinshelwood model to obtain a good fit of the experimental data. The proposed mechanism involved the complete saturation of pyridine to piperidine followed by rapid removal of ammonia through a less stable amine intermediate, see Figure 1-4. Sonneman *et al.* [20-23], in a series of four articles, focused on the various aspects of pyridine hydrodenitrogenation including catalyst preparation, reaction network elucidation and, to some extent, on kinetic modelling and estimation of rate coefficients and activation energies. Sonneman *et al.* [20-23] performed experiments over a Mo/Al_2O_3 and CoMo/Al_2O_3 in a U tube reactor, and studied various aspects by systematically varying all relevant operating conditions to assess their effects on the reaction kinetics. They constructed models based on a top-down methodology by starting from a power law model and, subsequently, extending these findings to a more established Langmuir-Hinshelwood model. Sonneman *et al.* were the first to report the formation of the *n*-pentylpiperidine through disproportionation of two piperidine molecules or condensation between pentylamine and piperidine. They also systematically reported the activation energies for the various (elementary) reactions obtained through regression of the experimental data with the proposed model. Along with the earlier mentioned works, Satterfield and Cocchetto [24] studied the pyridine-piperidine hydrogenation equilibrium over

$NiMo/Al_2O_3$ catalyst and provided important guidelines for performing experiments at conditions where this reaction is not equilibrium-limited.

In the 1980's, research efforts in the framework of hydrodenitrogenation were significantly enhanced, indicating its importance in the context of downstream processing. Although much of the focus was on testing heavier components such as quinoline [25-29], preparation of better catalysts [30-36] and simultaneous hydrodesulphurisation and hydrodenitrogenation [12, 37], some work on pyridine hydrodenitrogenation was still published in this time period [38-41]. Ledoux *et al.* [38, 42], studied the pyridine and piperidine hydrodenitrogenation over different Mo based catalysts promoted by Ni and proposed different kind of sites to be involved in the hydrodenitrogenation of pyridine and piperidine model components. LaVopa and Satterfield [40] studied the poisoning by nitrogen components and correlated the basicity of these nitrogen components to their adsorption strength. These results were helpful in predicting the poisoning effect exhibited by these components on the considered catalysts.

During the 1990's the most pronounced interest in hydrodenitrogenation is evident from the literature. Distinguished groups such as the Prins group at ETH, Zurich [43-53], Kasztelan group at IFP, France [54, 55] Ho and colleagues at Exxon Research, USA [41, 56] were involved in the development of and contributed to the field of hydrodenitrogenation. Reaction network elucidation of various model nitrogen components resulted in a very detailed understanding of the hydrodenitrogenation reaction and provided a basis for kinetic modelling. At the same time, gas phase pyridine hydrodenitrogenation was performed at the Laboratorium voor Petrochemische Techniek, the present Laboratory for Chemical Technology at Ghent University [57]. These data obtained over $NiMo/Al_2O_3$ catalyst are also employed in the present work to develop a two site model accounting for the most recent understanding of the catalytically active phase based on advanced experimental and modelling techniques, see Figure 1-6.

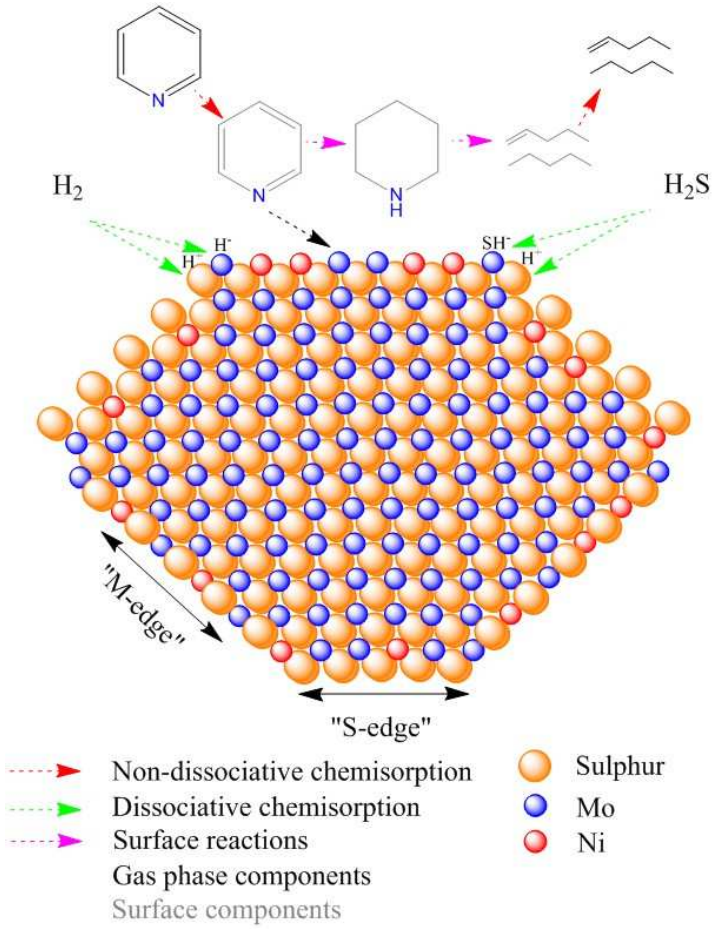

Figure 1-6. Methodology and assumptions adopted for the development of two site gas phase hydrodenitrogenation model.

In the early years of the new millennium the work on hydrodenitrogenation continued [3, 53, 58-64]. Through advanced characterisation techniques and advancements in computer technology and ab-initio based DFT calculations [65-85] the scientific world could better understand the reaction mechanisms and catalyst properties. Models for the description of the experimental data on different catalysts and different assumptions of the active phases and sites were proposed by Kopyscinski *et al.* [86, 87].

Pyridine hydrodenitrogenation kinetics have been simulated using models with two types of sites [14, 88] or in some cases even three types of sites [87]. Pille and Froment [88] considered two types of sites, *i.e.*, Coordinatively Unsaturated Sites (*) and Sulphur Anion (S^{2-}) sites, in their kinetic model, which sufficed to avoid any significant or systematic deviations between the experimental observations and the model simulations. Romero *et al.* [89] also have successfully described naphthalene hydrogenation over an industrial NiMo catalyst by assuming two types of sites. In this work, a model considering * and S^{2-} is further elaborated. The sites are believed to be situated at or at least near the edges of the promoted sulphided

catalysts [89]. This two types of site assumption along with that of homolytic or heterolytic dissociative H_2 and H_2S chemisorption on the catalyst surface is expected to provide the model with the necessary flexibility to adequately simulate both the hydrogenation and denitrogenation reaction via appropriate sulphur and hydrogen surface concentrations.

1.4.3 Hydrotreating catalysts

Industrial hydrotreating catalysts are high surface area materials made up of an active component, a promoter and in few cases co-promoters which are impregnated on supports such as γ-Al_2O_3. These catalysts contain molybdenum sulphide as the active component and cobalt or nickel as promoters. Usually, co-promoters such as phosphorous or tungsten are incorporated as well in small amounts during the impregnation procedure to fine-tune the catalyst performance in terms of activity, selectivity and/or stability. A few other co-promoters used on the catalysts are boron, fluorine and chlorine which influence the catalytic or the mechanical properties of the catalysts. The commercially available catalysts have varying amounts of active components, promoters and co-promoters depending on the application and the feed quality. Generally hydrotreating catalysts contain up to 25 % of active component and 10 to 25 % of promoter. Catalysts are manufactured and pelletized into different shapes according to the reaction and process demands.

Active phase structures for sulphided hydrotreating catalyst have been presented by Topsøe *et al.* [84, 90]. The crucial role of Ni or Co promoted MoS_2 nanocrystallites for the hydrogenation and bond breaking activity has been demonstrated [90]. The promotional effect by Ni or Co on MoS_2 is related to the formation of a Ni-Mo-S or Co-Mo-S phase [90, 91]. The alumina support normally used for hydrotreating catalysts, allows a high dispersion of the stable, unpromoted MoS_2 nano crystals. When a promoter such as Co or Ni is added during the synthesis, the edge sites of the MoS_2 structures are further stabilised by the incorporation of Ni/Co, instead of Mo [84]. Depending on the interaction of these modified nanocrystallites with the catalyst support TYPE I and TYPE II phases are reported to be formed [75], the TYPE II being much more active corresponding to their lower interaction with the support. The presence of a co-promoter such as phosphorus may further enhance the hydrodenitrogenation activity by increasing the number of TYPE II sites as proposed by Eijsbouts *et al.* [52]. The presence of Ni and P in the catalyst under consideration will certainly result in the formation of the aforementioned phases, and minimise TYPE I phase formation. Morphology variations of the modified nano crystallite during various sulpho-reductive conditions are discussed by

Schweiger *et al.* [81, 82], but can be generally considered not to occur to a significant extent, unless a significant change in the reductive conditions would be enforced by varying the feed sulphur concentration.

A huge number of publications has focused on the catalytically active sites in hydrotreating in terms of their location, electronic properties, number and nature. Properties of promoted MoS_2 nanocrystallites have been investigated experimentally [76, 83, 92-94], *i.e.*, by EXAFS, STM, FTIR, as well as theoretically calculated *i.e.*, by DFT [67-70, 74, 75, 95]. The sites exhibit either a Lewis nature, corresponding with sulphur vacancies associated with Mo or the NiMo or a Brønsted nature under the form of –SH groups [96, 97]. More recently the presence of brim sites on MoS_2 active phase has been reported by Topsøe *et al.*[98], as depicted in Figure 1-7. This brim is understood to contain regions of high electron density and is located on the basal plane of the active phase, rather than on the edges. Components that are adsorbed, interact strongly with the brim sites and, hence, exhibit a possibly strong positive effect on relevant reactions such as hydrodesulphurisation and hydrodenitrogenation. This positive effect is attributed to the strong interaction with hetero aromatic components and the vicinity of hydrogen and sulphydril groups which are formed on the edge planes of the active phase Topsøe *et al.* [98].

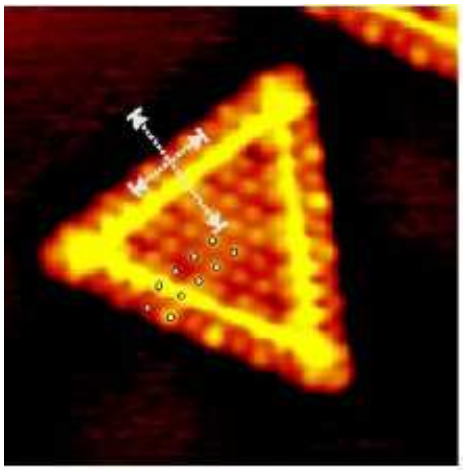

Figure 1-7. Atom-resolved STM image of a single layer MoS_2 nanocluster (light region = brim) [98].

1.4.4 Application of gas phase models to liquid phase reactions

Industrially, hydrotreating is carried out in multiphase reactors, *i.e.*, gas-liquid-solid, in which the catalyst is the solid phase, hydrogen and lighter hydrocarbons are present in the gas phase and the heavier hydrocarbons along with the hetero components are in the liquid phase.

Quite often, at the laboratory scale, reaction kinetics are investigated in a gas-solid reactor in which, again, the catalyst represents the solid phase but in which all reactants are in the gas phase. While the former is typically denoted as 'liquid phase kinetics', the latter is conventionally termed as 'gas phase kinetics'. Liquid phase kinetics tend to be more frequently disguised by phenomena such as hydrodynamic non-idealities, diffusion limitations, heat effects, physical adsorption and thermodynamic non-idealities compared to gas phase kinetics. Extraction of kinetic data can, hence, generally be more readily achieved from gas-phase data, since fewer phenomena occur that potentially obscure these kinetics [99]. A few studies addressing the application of gas phase derived models to liquid phase conditions taking into account various phase related aspects have been published [99-104], however, studies related to hydrodenitrogenation are not explicitly found in the literature.

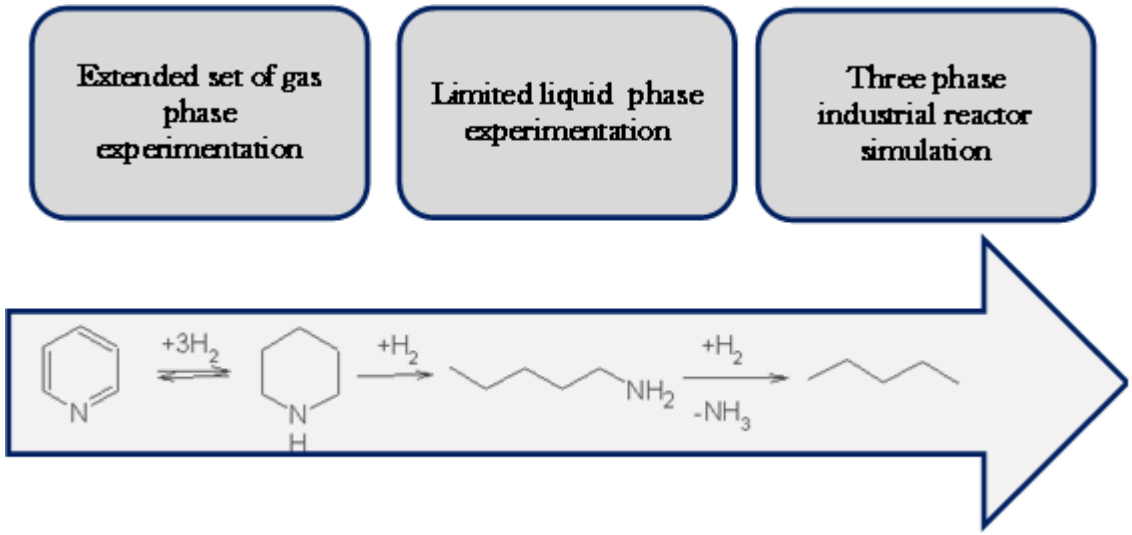

Figure 1-8. Methodology used for the translation of models developed at gas phase conditions to liquid phase reactions.

Madon and Iglesia [105] have given a comprehensive overview on rates of chemical reactions in terms of thermodynamic activities or fugacities of reactants and products. Transition state theory was used to rigorously describe the effects of non-ideal behavior on reaction rates. Rates of catalytic reactions were found to depend on the presence of a solvent only when it affects the activated complex(es) involved in kinetically significant steps in a catalytic cycle. Reinhoudt *et al.* [106] in their discussion on the so called 'gas-liquid-phase controversy', propose that the morphology of the active phase of a sulphided catalyst favours the interaction with a condensed liquid phase. This could be a generic phenomenon for the hydrotreating reactions. Guevera *et al.* [100, 103, 104] have more recently investigated solvent effects on the various reactions occurring during hydrotreatment. Rautanen *et al.* [107] studied liquid phase hydrogenation of toluene. Based on the estimated adsorption equilibrium

coefficients, they observed that hydrogenation rates obtained with the different solvents were different. They explained the difference in rates by differences in the hydrogen solubility, which followed the same trend as the reaction rate. They also verified gas-liquid, liquid-solid and intraparticle mass transport resistance and only found the latter to be significant. At our laboratory research related to application of gas phase models to liquid phase reactions has been done in the area of hydrocracking by Narasimhan *et al.* [108] and Thybaut *et al.* [109], *i.e.*, making use of nano-porous catalysts. Narasimhan *et al.* [108] developed a unified model for the description of gas and liquid phase hydroconversion on a USY zeolite accounting for (i) liquid phase thermodynamic non-ideality, (ii) destabilization of the physisorbed state in the catalyst micropore by compression of the adsorbate by the bulk fluid and (iii) carbenium ion stabilization by sorbent solvation by the bulk fluid. Accounting for these three features allowed adequately describing liquid phase *n*-C_7/*n*-C_9 hydrocracking data starting from a kinetic model obtained from gas phase data. Thybaut *et al.* [109] successfully applied the same methodology in the modelling of gas and liquid phase hydroconversion of Halpasol™ on a USY zeolite. Narasimhan *et al.* [110] extended this model for shape selective catalysts such as Pt/H-ZSM-22.

1.4.5 Single-Event MicroKinetic (SEMK) models

Classical modelling is usually performed using conventional concepts and reaction schemes, such as proposed by Langmuir and Hinshelwood or Eley and Rideal. In this kind of modelling, various possible mechanisms are proposed and rival rate equations are derived considering different elementary steps as rate determining. The models are subsequently regressed to experimental data and after model discrimination, the model exhibiting the best agreement with the experimental data along with good statistical and physical significance of the parameters is selected. As opposed to classical modelling, SEMK provides a more fundamental approach, by considering all the elementary reactions occurring in the bulk and/or on the catalyst surface. In the modelling based on the SEMK methodology, the construction of the model is based on considering all the elementary reaction steps occurring in a specific reaction. During the application of the SEMK methodology for a specific reaction or set of reactions no specific rate determining step is assumed. While constructing models based on the SEMK methodology, reactions are classified based on reaction families such as protonation, hydrogen addition etc. thus reducing the number of parameters that needs to be determined to perform the model simulations. This concept constitutes a sound basis which also helps in

better extension of the model to more complex feedstocks and reaction conditions, with very little or no changes to the model.

The SEMK methodology for modelling transformations in complex reaction mixtures was first proposed by Froment [111] and applied to thermal cracking by Clymans *et al.* [112, 113]. This was subsequently extended to catalytic reactions such as hydrocracking by Baltanas *et al.* [114, 115] and Svoboda *et al.* [116]. Feng *et al.* [117] extended the SEMK methodology to catalytic cracking. Fundamental models for Fischer-Tropsch synthesis were constructed based on the carbene polymerization mechanism by Klinke and Broadbelt [118] and were interpreted according to the SEMK methodology by Lozano *et al.* [119]. Very recently aromatic hydrogenation over metal catalysts was proposed by Bera *et al.* for benzene, toluene and xylene as model components [120-122]. Other reactions that have been comprehensively proposed and extended are xylene isomerization/ethylbenzene dealkylation by Toch *et al.* [123] and methanol to olefins by Kumar *et al.* [124, 125].

The SEMK methodology involves a detailed understanding of underlying elementary steps and implementing them in an adequate mathematical manner in a computer program capable of rendering the complete reaction network and calculating the entropic, *c.q.* symmetry effects. This reaction network can then be used for model construction and regression with the experimental data to estimate the kinetic and catalyst descriptors, see Figure 1-9.

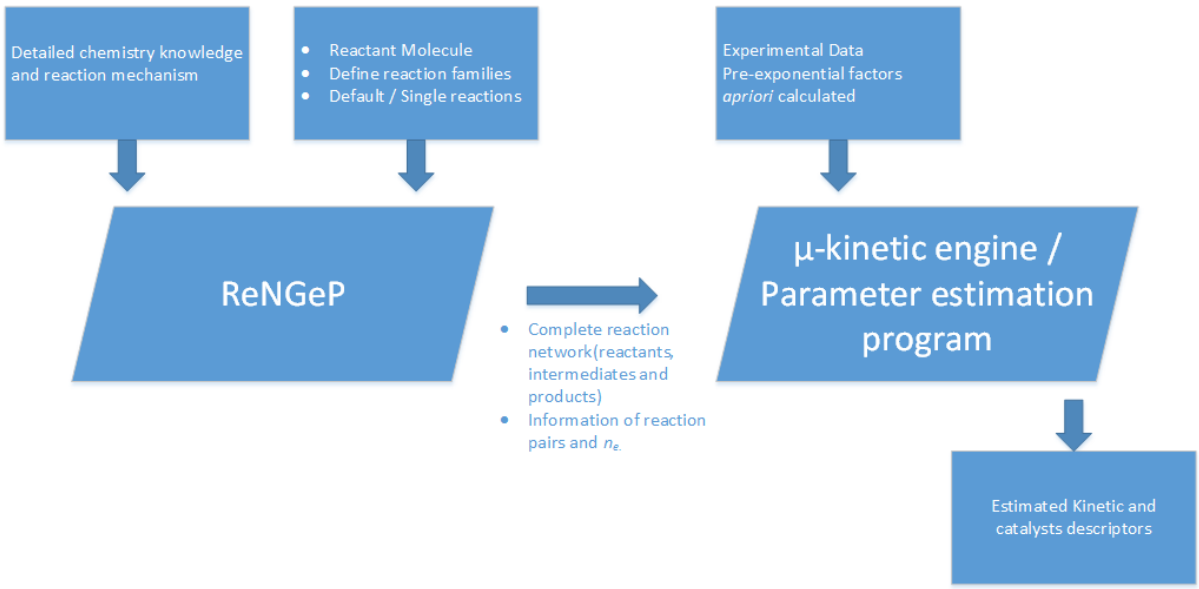

Figure 1-9. Graphical representation of the SEMK methodology.

1.5 Scope of the thesis

In this thesis, hydrodenitrogenation is studied in detail with the help of a model component pyridine. The dissertation is divided into four prominent subtopics:

- Studies dedicated to understanding the performance of three-phase, continuous, stirred tank reactors and their hydrodynamics have already been done before [16-18, 126, 127], however, a study specifically dedicated to the Robinson-Mahoney reactor at industrial conditions is not available yet in the open literature. One of the objectives of this work is, hence, to study parameters such as volumetric gas-liquid mass transfer coefficients and gas/liquid holdup in the reactor which are important to understand the exact reaction conditions from a hydrodynamic and thermodynamic point of view. In this work the aim is to experimentally measure these parameters and compare them with the data available at cold flow conditions and other gas-liquid systems. Equations to correlate the experimentally obtained volumetric gas-liquid mass transfer coefficients have been proposed in the past and verified at cold flow conditions. In this work their applicability for experiments conducted at relevant operating conditions will be assessed. The experimental details and the procedures will allow the experimentalist to verify and validate the reactor before starting the kinetic data acquisition. These parameter values will also provide guidelines for scale-up and/or scale down of reactor if necessary. Finally the data on the liquid hold-up obtained under these conditions can very well be used in the description of the thermodynamic conditions within the reactor. This work forms the third chapter of this thesis.
- Hydrodenitrogenation of various model components has been studied on different catalysts at gas and liquid phase conditions [45, 47, 52, 86-88, 128, 129]. Although an adequate understanding of the hydrodenitrogenation kinetics has already been pursued, specific features such as explaining the H_2S promotional effect on C-N bond scission in terms of elementary steps, accounting for the type of hydrogen and hydrogen sulphide dissociation and correlations between components' chemisorption properties and their proton affinity [76, 83] still remain to be explored and better quantified. Recent developments in catalyst technology and understanding, DFT calculations, modelling methodologies, advances in computer technology and the current state of the art allow to develop an advanced kinetic model accounting for this better understanding. Pyridine hydrodenitrogenation data originally acquired by Pille and Froment [88] are used for model construction, regression and selection purposes, adapting the model

assumptions to the results of more recent work by our group *i.e.*, naphthalene hydrogenation over NiMo/γ-Al_2O_3 by Romero *et al.* [89] as well as to the broader literature [80, 83, 86, 87, 89, 130-132]. As indicated above, the most important distinctions in comparison to the previous work lie in the consideration of heterolytically and homolytically chemisorbing H_2 and H_2S, atomic and molecular addition of H_2 to the aromatic ring and a theoretical explanation on the effect of H_2S on the hydrodenitrogenation reaction. This forms the fourth chapter of this thesis.

- Pyridine hydrodenitrogenation is employed to demonstrate the applicability of the methodology for applying gas phase models to three-phase conditions beyond acid catalysis in hydrocracking [99]. In this case a pyridine hydrodenitrogenation kinetics model based on elementary steps resulting from an extensive gas phase kinetic experimentation [88] has been used for the assessment of liquid phase kinetics data. A limited number of liquid phase experiments have been performed to determine liquid phase thermodynamic non-ideality and other gas versus liquid phase related effects on the pyridine hydrodenitrogenation behaviour. The ability to adequately describe liquid phase chemical kinetics making use of a rate expression derived from gas phase kinetics, provides a sound and efficient route towards the assessment of the kinetics of a variety of industrial reactions at operating conditions focused on intrinsic kinetics determination without having to mimic the industrial operating conditions. This aspect is presented in the fifth chapter of this thesis.
- Finally, another important aspect of this dissertation is to provide a proof-of-concept for the application of the SEMK methodology towards hydrodenitrogenation with pyridine as model component. This extension towards HDN will be the first step towards extension of the methodology to heteroatoms on one hand and towards sulphided catalysts on the other. The extension of the SEMK methodology to pyridine hydrodenitrogenation consists of expanding the capabilities of ReNGeP, more particularly to include hetero atoms, *c.q.* nitrogen, and to implement the relevant, new reaction families, including the calculation of symmetry effects, in the framework of hydrodenitrogenation. A detailed state of the art on the ReNGeP and its improvements forms the sixth chapter of the thesis. Construction of the model and its subsequent assessment against experimental data forms the seventh chapter of this thesis.

1.6 References

1. Stanislaus, A., A. Marafi, and M.S. Rana, **Catalysis Today**, 2010. 153(1-2): p. 1-68.
2. BP.plc, *BP Energy Outlook 2035*. 2014, BP plc.
3. Egorova, M. and R. Prins, **Journal of Catalysis**, 2004. 221(1): p. 11-19.
4. Lewandowski, M. and Z. Sarbak, **Applied Catalysis B: Environmental**, 2008. 79(4): p. 313-322.
5. Gary, J.H. and G.E. Handwerk, *Petroleum refining: technology and economics*. 4th ed. 2001, New York. p. 441.
6. Fahim, M.A., T.A. Asahhaf, and A. Elkilani, *Fundamentals of Petroleum Refining*. 2010: Elsevier B.V.
7. CB&I. *www.cbi.com* 2015.
8. UOP-Honeywell. *www.uop.com*. 2015.
9. Axens. *www.axens.com*. 2015.
10. KBR. *www.kbr.com*. 2015.
11. *Hydrocarbon Processing: 2008 Refining Processes Handbook*. 2008. p. 198.
12. Zeuthen, P., P. Stolze, and U.B. Pedersen, **Bulletin Des Societes Chimiques Belges**, 1987. 96(11-12): p. 985-995.
13. Mahoney, J.A., K.K. Robinson, and E.C. Myers, **Chemtech**, 1978. 8(12): p. 758-763.
14. Raghuveer, C.S., J.W. Thybaut, R. De Bruycker, K. Metaxas, T. Bera, and G.B. Marin, **Fuel**, 2014. 125(0): p. 206-218.
15. Craciun, I., M.F. Reyniers, and G.B. Marin, **Journal of Molecular Catalysis A: Chemical**, 2007. 277(1-2): p. 1-14.
16. Pitault, I., P. Fongarland, D. Koepke, M. Mitrovic, D. Ronze, and M. Forissier, **Chemical Engineering Science**, 2005. 60(22): p. 6240-6253.
17. Mitrovic, M., I. Pitault, M. Forissier, S. Simoens, and D. Ronze, **AIChE Journal**, 2005. 51(6): p. 1747-1757.
18. Magnico, P. and P. Fongarland, **Chemical Engineering Science**, 2006. 61(4): p. 1217-1236.
19. McIlvried, H.G., **Industrial & Engineering Chemistry Process Design and Development**, 1971. 10(1): p. 125-130.
20. Sonneman, J. and P. Mars, **Journal of Catalysis**, 1973. 31(2): p. 209-219.

21. Sonneman, J., G.H. Van den Berg, and P. Mars, **Journal of Catalysis**, 1973. 31(2): p. 220-230.

22. Sonneman, J. and P. Mars, **Journal of Catalysis**, 1974. 34(2): p. 215-229.

23. Sonneman, J., W.J. Neyens, and P. Mars, **Journal of Catalysis**, 1974. 34(2): p. 230-241.

24. Satterfield, C.N. and J.F. Cocchetto, **AIChE Journal**, 1975. 21(6): p. 1107-1111.

25. Cocchetto, J.F. and C.N. Satterfield, **Industrial & Engineering Chemistry Process Design and Development**, 1981. 20(1): p. 49-53.

26. Satterfield, C.N. and J.F. Cocchetto, **Industrial & Engineering Chemistry Process Design and Development**, 1981. 20(1): p. 53-62.

27. Satterfield, C.N. and S.H. Yang, **Industrial & Engineering Chemistry Process Design and Development**, 1984. 23(1): p. 11-19.

28. Yang, S.H. and C.N. Satterfield, **Industrial & Engineering Chemistry Process Design and Development**, 1984. 23(1): p. 20-25.

29. Yang, S.H. and C.N. Satterfield, **Journal of Catalysis**, 1983. 81(1): p. 168-178.

30. Menon, P.G. and G.F. Froment, **Applied Catalysis**, 1981. 1(1-2): p. 31-48.

31. Menon, P.G., G.B. Marin, and G.F. Froment, **Industrial & Engineering Chemistry Product Research and Development**, 1982. 21(1): p. 52-56.

32. Stanislaus, A., M. Absihalabi, and K. Aldolama, **Applied Catalysis**, 1989. 50(3): p. 237-245.

33. Stanislaus, A., M. Absihalabi, K. Aldolama, A. Katrib, and M. Ismail, **Applied Catalysis**, 1988. 41(1-2): p. 109-119.

34. Stanislaus, A. and K. Aldolama, **Journal of Catalysis**, 1986. 101(2): p. 536-539.

35. Stanislaus, A., M.A. Halabi, and K. Aldolama, **Applied Catalysis**, 1988. 39(1-2): p. 239-253.

36. Topsoe, H., N.Y. Topsoe, O. Sorensen, R. Candia, B.S. Clausen, S. Kallesoe, E. Pedersen, and R. Nevald, **ACS Symposium Series**, 1985. 279: p. 235-246.

37. Satterfield, C.N. and S.H. Yang, **Journal of Catalysis**, 1983. 81(2): p. 335-346.

38. Ledoux, M.J., A. Bouassida, and R. Benazouz, **Applied Catalysis**, 1984. 9(1): p. 41-52.

39. Lavopa, V. and C.N. Satterfield, **Chemical Engineering Communications**, 1988. 70: p. 171-176.

40. LaVopa, V. and C.N. Satterfield, **Journal of Catalysis**, 1988. 110(2): p. 375-387.

41. Ho, T.C., A.R. Katritzky, and S.J. Cato, **Industrial & Engineering Chemistry Research**, 1992. 31(7): p. 1589-1597.

42. Ledoux, M.J. and B. Djellouli, **Applied Catalysis**, 1990. 67(1): p. 81-92.

43. Prins, R., M. Jian, and M. Flechsenhar, **Polyhedron**, 1997. 16(18): p. 3235-3246.

44. Prins, R., M. Egorova, A. Röthlisberger, Y. Zhao, N. Sivasankar, and P. Kukula, **Catalysis Today**, 2006. 111(1-2): p. 84-93.

45. Jian, M. and R. Prins, **Journal of Catalysis**, 1998. 179(1): p. 18-27.

46. Jian, M. and R. Prins, **Industrial & Engineering Chemistry Research**, 1998. 37(3): p. 834-840.

47. Jian, M. and R. Prins, **Recent Advances in Basic and Applied Aspects of Industrial Catalysis**, 1998. 113: p. 111-123.

48. Jian, M. and R. Prins, **Hydrotreatment and Hydrocracking of Oil Fractions**, 1997. 106: p. 415-420.

49. Jian, M. and R. Prins, **Catalysis Today**, 1996. 30(1-3): p. 127-134.

50. Jian, M. and R. Prins, **11th International Congress on Catalysis - 40th Anniversary, Pts A and B**, 1996. 101: p. 87-96.

51. Jian, M., F. Kapteijn, and R. Prins, **Journal of Catalysis**, 1997. 168(2): p. 491-500.

52. Eijsbouts, S., J.N.M. Vangestel, J.A.R. Vanveen, V.H.J. Debeer, and R. Prins, **Journal of Catalysis**, 1991. 131(2): p. 412-432.

53. Egorova, M. and R. Prins, **Catalysis Letters**, 2004. 92(3-4): p. 87-91.

54. Kasztelan, S., T. des Courieres, and M. Breysse, **Catalysis Today**, 1991. 10(4): p. 433-445.

55. Vivier, L., V. Dominguez, G. Perot, and S. Kasztelan, **Journal of Molecular Catalysis**, 1991. 67(2): p. 267-275.

56. Ho, T.C., H.T. Lee, and J.R. Hopper, **AIChE Journal**, 1986. 32(10): p. 1754-1759.

57. Pille, R., *Sleutelcomponenten bij de hydrodenitrogenering en hydrodesulfurisering van aardoliefracties*. 1997, Universiteit Gent.

58. Schwartz, V., V.T. da Silva, and S.T. Oyama, **Journal of Molecular Catalysis A: Chemical**, 2000. 163(1-2): p. 251-268.

59. Schwartz, V. and S.T. Oyama, **Journal of Molecular Catalysis A: Chemical**, 2000. 163(1-2): p. 269-282.

60. Schwartz, V., S.T. Oyama, and J.G.G. Chen, **Journal of Physical Chemistry B**, 2000. 104(37): p. 8800-8806.

61. Egorova, M. and R. Prins, **Journal of Catalysis**, 2006. 241(1): p. 162-172.

62. Egorova, M. and R. Prins, **Journal of Catalysis**, 2004. 225(2): p. 417-427.

63. Egorova, M. and R. Prins, **Journal of Catalysis**, 2004. 224(2): p. 278-287.

64. Egorova, M., Y. Zhao, P. Kukula, and R. Prins, **Journal of Catalysis**, 2002. 206(2): p. 263-271.

65. Sun, M., A.E. Nelson, and J. Adjaye, **Journal of Molecular Catalysis A: Chemical**, 2004. 222(1-2): p. 243-251.

66. Sun, M.Y., J. Adjaye, and A.E. Nelson, **Applied Catalysis A: General**, 2004. 263(2): p. 131-143.

67. Sun, M.Y., A.E. Nelson, and J. Adjaye, **Catalysis Letters**, 2006. 109(3-4): p. 133-138.

68. Sun, M.Y., A.E. Nelson, and J. Adjaye, **Catalysis Today**, 2005. 109(1-4): p. 49-53.

69. Sun, M.Y., A.E. Nelson, and J. Adjaye, **Journal of Catalysis**, 2005. 233(2): p. 411-421.

70. Sun, M.Y., A.E. Nelson, and J. Adjaye, **Catalysis Today**, 2005. 105(1): p. 36-43.

71. Sun, M.Y., A.E. Nelson, and J. Adjaye, **Journal of Catalysis**, 2005. 231(1): p. 223-231.

72. Sun, M.Y., A.E. Nelson, and J. Adjaye, **Journal of Catalysis**, 2004. 226(1): p. 32-40.

73. Sun, M.Y., A.E. Nelson, and J. Adjaye, **Journal of Catalysis**, 2004. 226(1): p. 41-53.

74. Byskov, L.S., J.K. Norskov, B.S. Clausen, and H. Topsoe, **Journal of Catalysis**, 1999. 187(1): p. 109-122.

75. Hinnemann, B., P.G. Moses, and J.K. Norskov, **Journal of Physics-Condensed Matter**, 2008. 20(6).

76. Lauritsen, J.V., M.V. Bollinger, E. Laegsgaard, K.W. Jacobsen, J.K. Norskov, B.S. Clausen, H. Topsoe, and F. Besenbacher, **Journal of Catalysis**, 2004. 221(2): p. 510-522.

77. Logadottir, A., P.G. Moses, B. Hinnemann, N.Y. Topsoe, K.G. Knudsen, H. Topsoe, and J.K. Norskov, **Catalysis Today**, 2006. 111(1-2): p. 44-51.

78. Moses, P.G., B. Hinnemann, H. Topsoe, and J.K. Norskov, **Journal of Catalysis**, 2009. 268(2): p. 201-208.

79. Moses, P.G., B. Hinnemann, H. Topsoe, and J.K. Norskov, **Journal of Catalysis**, 2007. 248(2): p. 188-203.

80. Raybaud, P., **Applied Catalysis A: General**, 2007. 322: p. 76-91.

81. Schweiger, H., P. Raybaud, G. Kresse, and H. Toulhoat, **Journal of Catalysis**, 2002. 207(1): p. 76-87.

82. Schweiger, H., P. Raybaud, and H. Toulhoat, **Journal of Catalysis**, 2002. 212(1): p. 33-38.

83. Temel, B., A.K. Tuxen, J. Kibsgaard, N.Y. Topsoe, B. Hinnemann, K.G. Knudsen, H. Topsoe, J.V. Lauritsen, and F. Besenbacher, **Journal of Catalysis**, 2010. 271(2): p. 280-289.

84. Topsoe, H., **Applied Catalysis A: General**, 2007. 322: p. 3-8.

85. Topsoe, H., B. Hinnemann, J.K. Norskov, J.V. Lauritsen, F. Besenbacher, P.L. Hansen, G. Hytoft, R.G. Egeberg, and K.G. Knudsen, **Catalysis Today**, 2005. 107-08: p. 12-22.

86. Kopyscinski, J., J. Choi, L. Ding, S. Zhang, B. Ibeh, and J.M. Hill, **Catalysis Letters**, 2012. 142(7): p. 845-853.

87. Kopyscinski, J., J. Choi, and J.M. Hill, **Applied Catalysis A: General**, 2012. 445: p. 50-60.

88. Pille, R. and G.F. Froment, **Hydrotreatment and Hydrocracking of Oil Fractions**, 1997. 106: p. 403-413.

89. Romero, C.M.C., J.W. Thybaut, and G.B. Marin, **Catalysis Today**, 2008. 130(1): p. 231-242.

90. Topsoe, H., B.S. Clausen, N.Y. Topsoe, and P. Zeuthen, **Catalysts in Petroleum Refining 1989**, 1990. 53: p. 77-102.

91. Topsoe, H., **Journal of Catalysis**, 2003. 216(1-2): p. 155-164.

92. Bouwens, S.M.A.M., D.C. Koningsberger, V.H.J. Debeer, S.P.A. Louwers, and R. Prins, **Catalysis Letters**, 1990. 5(3): p. 273-284.

93. Louwers, S.P.A. and R. Prins, **Journal of Catalysis**, 1992. 133(1): p. 94-111.

94. Louwers, S.P.A. and R. Prins, **Journal of Catalysis**, 1993. 139(2): p. 525-539.

95. Besenbacher, F., M. Brorson, B.S. Clausen, S. Helveg, B. Hinnemann, J. Kibsgaard, J. Lauritsen, P.G. Moses, J.K. Norskov, and H. Topsoe, **Catalysis Today**, 2008. 130(1): p. 86-96.

96. Satterfield, C.N. and S.H. Yang, **Industrial & Engineering Chemistry Process Design and Development**, 1984. 23: p. 20-25.

97. Sundaramurthy, V., A.K. Dalai, and J. Adjaye, **Applied Catalysis B: Environmental**, 2006. 68(1-2): p. 38-48.

98. Topsøe, H., B. Hinnemann, J.K. Nørskov, J.V. Lauritsen, F. Besenbacher, P.L. Hansen, G. Hytoft, R.G. Egeberg, and K.G. Knudsen, **Catalysis Today**, 2005. 107–108(0): p. 12-22.

99. Thybaut, J.W., C.S. Laxmi Narasimhan, and G.B. Marin, **Catalysis Today**, 2006. 111(1-2): p. 94-102.

100. Guevara, A., R. Bacaud, and M. Vrinat, **Applied Catalysis A: General**, 2003. 253(2): p. 515-526.

101. Reinhoudt, H.R., C.H.M. Boons, A.D. van Langeveld, J.A.R. van Veen, S.T. Sie, and J.A. Moulijn, **Applied Catalysis A: General**, 2001. 207(1-2): p. 25-36.

102. Madon, R.J. and E. Iglesia, **Journal of Molecular Catalysis A: Chemical**, 2000. 163(1-2): p. 189-204.

103. Contreras-Valdez, Z., J.C. Mogica-Betancourt, A. Alvarez-Hernandez, and A. Guevara-Lara, **Fuel**, 2013. 106: p. 519-527.

104. Mogica-Betancourt, J.C., Z. Contreras-Valdez, and A. Guevara-Lara, **Revista Mexicana De Ingenieria Quimica**, 2012. 11(3): p. 447-453.

105. Madon, R.J. and E. Iglesia, **Journal of Molecular Catalysis a-Chemical**, 2000. 163(1-2): p. 189-204.

106. Reinhoudt, H.R., C.H.M. Boons, A.D. van Langeveld, J.A.R. van Veen, S.T. Sie, and J.A. Moulijn, **Applied Catalysis A: General**, 2001. 207(1-2): p. 25-36.

107. Rautanen, P.A., J.R. Aittamaa, and K.O.I. Krause, **Industrial & Engineering Chemistry Research**, 2000. 39(11): p. 4032-4039.

108. Narasimhan, C.S.L., J.W. Thybaut, J.A. Martens, P.A. Jacobs, J.F. Denayer, and G.B. Marin, **Journal of Physical Chemistry B**, 2006. 110(13): p. 6750-6758.

109. Thybaut, J.W., C.S.L. Narasimhan, and G.B. Marin, **Catalysis Today**, 2006. 111(1-2): p. 94-102.

110. Narasimhan, C.S.L., J.W. Thybaut, J.F. Denayer, G.V. Baron, P.A. Jacobs, J.A. Martens, and G.B. Marin, **Industrial & Engineering Chemistry Research**, 2007. 46(25): p. 8710-8721.

111. Froment, G.F., **Catalysis Reviews-Science and Engineering**, 2005. 47(1): p. 83-124.

112. Clymans, P.J. and G.F. Froment, **Computers & Chemical Engineering**, 1984. 8(2): p. 137-142.

113. Clymans, P.J., G.F. Froment, M. Berthelin, and P. Trambouze, **AIChE Journal**, 1984. 30(6): p. 904-915.

114. Baltanas, M.A. and G.F. Froment, **Computers & Chemical Engineering**, 1985. 9(1): p. 71-81.

115. Baltanas, M.A., K.K. Vanraemdonck, G.F. Froment, and S.R. Mohedas, **Industrial & Engineering Chemistry Research**, 1989. 28(7): p. 899-910.

116. Svoboda, G.D., E. Vynckier, B. Debrabandere, and G.F. Froment, **Industrial & Engineering Chemistry Research**, 1995. 34(11): p. 3793-3800.

117. Feng, W., E. Vynckier, and G.F. Froment, **Industrial & Engineering Chemistry Research**, 1993. 32(12): p. 2997-3005.

118. Klinke, D.J. and L.J. Broadbelt, **Chemical Engineering Science**, 1999. 54(15-16): p. 3379-3389.

119. Lozano-Blanco, G., J.W. Thybaut, K. Surla, P. Galtier, and G.B. Marin, **Oil & Gas Science and Technology-Revue D Ifp Energies Nouvelles**, 2006. 61(4): p. 489-496.

120. Bera, T., J.W. Thybaut, and G.B. Marin, **Industrial & Engineering Chemistry Research**, 2011. 50(23): p. 12933-12945.

121. Bera, T., J.W. Thybaut, and G.B. Marin, **ACS Catalysis**, 2012. 2(7): p. 1305-1318.

122. Bera, T., *Hydrogenation of aromatics: single-event microkinetic (SEMK) methodology and scale-up*, in *Laboratory for Chemical Technology*. 2012, Ghent University: Ghent.

123. Toch, K., J.W. Thybaut, B.D. Vandegehuchte, C.S.L. Narasimhan, L. Domokos, and G.B. Marin, **Applied Catalysis A: General**, 2012. 425: p. 130-144.

124. Kumar, P., J.W. Thybaut, S. Svelle, U. Olsbye, and G.B. Marin, **Industrial & Engineering Chemistry Research**, 2013. 52(4): p. 1491-1507.

125. Kumar, P., J.W. Thybaut, S. Teketel, S. Svelle, P. Beato, U. Olsbye, and G.B. Marin, **Catalysis Today**, 2013. 215: p. 224-232.

126. Pitault, I., P. Fongarland, M. Mitrovic, D. Ronze, and M. Forissier, **Catalysis Today**, 2004. 98(1-2): p. 31-42.

127. Dietrich, E., C. Mathieu, H. Delmas, and J. Jenck, **Chemical Engineering Science**, 1992. 47(13-14): p. 3597-3604.

128. Deepa, G., T.M. Sankaranarayanan, K. Shanthi, and B. Viswanathan, **Catalysis Today**, 2012. 198(1): p. 252-262.

129. Hrabar, A., J. Hein, O.Y. Gutierrez, and J.A. Lercher, **Journal of Catalysis**, 2011. 281(2): p. 325-338.

130. Kasztelan, S. and D. Guillaume, **Industrial & Engineering Chemistry Research**, 1994. 33(2): p. 203-210.

131. Vanrysselberghe, V. and G.F. Froment, **Industrial & Engineering Chemistry Research**, 1996. 35(10): p. 3311-3318.

132. Guernalec, N., T. Cseri, P. Raybaud, C. Geantet, and M. Vrinat, **Catalysis Today**, 2004. 98(1-2): p. 61-66.

2 Procedures

This chapter discusses the procedures adopted in this thesis to acquire the experimental data, the techniques used for data analysis and treatment as well as the theoretical background for parameter estimation and model selection. Pyridine hydrodenitrogenation over a commercial, sulphided NiMo/γ-Al_2O_3 catalyst was performed in two types of Continuous Stirred Tank Reactors, CSTRs, both located at Laboratory for Chemical Technology, LCT, Ghent University. Kinetic data for the gas phase pyridine hydrodenitrogenation have been acquired using a Berty reactor as part of previous work by Pille and Froment [1], while kinetic data at three-phase conditions were acquired using a bench scale Robinson-Mahoney reactor set-up [2] as part of the present thesis. The gas and the liquid phase experimental data that have been acquired using these set-ups and used in model construction in this thesis are reported in Appendix A. The interpretation of the experimental results at varying operating conditions, the data available from literature with respect to the reaction chemistry and data together with ab-initio based DFT studies provide guidelines for rival kinetic model construction. Via regression of those models to the experimental data, values for the kinetic parameters in these models can be estimated.

The procedures section is divided into two sub-sections, *i.e.*, experimental and modelling. First, the materials and methods used during the experimental investigations at gas and liquid phase conditions are presented. The analysis and calculation procedures for the same have also been explained. The second part of this chapter introduces the procedures used during the modelling including the mathematical treatment of these data and computer tools required for model construction and parameter estimation.

2.1 Experimental

2.1.1 Catalyst

A commercially available NiMo catalyst supported on γ-Al_2O_3 (Procatalyse EC/22/216/91) was employed to study both the gas and liquid phase hydrodenitrogenation. The catalyst composition by weight is 9.3% Mo, 2.5% Ni and 103 ppm P. Other physical characteristics of the catalyst are reported in Table 2-1. The BET surface area was measured by N_2 adsorption [3]. Catalyst pellets as received were crushed and sieved to obtain a particle

size between 540 and 600 μm which was sufficiently low to avoid internal mass transfer limitations. During the gas phase experiments 0.715 10^{-3} kg of catalyst was used while 2.5 10^{-3} kg of catalyst was used during the liquid phase investigation, as the difference in operating conditions required correspondingly adapted space times. During the gas phase experimentation catalyst pre-sulphiding was done by first drying the catalyst in argon atmosphere at 0.6 MPa and 423 K for 2 hours, and subsequently using 15 mol% H_2S in H_2 at 0.6 MPa and 663 K for 4 hours. At liquid phase conditions, the catalyst was dried in a nitrogen atmosphere at 3.0 MPa and 423 K for 1 hour and was subsequently pre-sulphided with a 1 wt.% mixture of DMDS in halpasol at 573K for 4 hours. Once the catalyst is pre-sulphided, it is stabilised with the reaction feed for 12 hours before kinetic data are recorded.

Table 2-1. Characteristics of the NiMo/γ-Al_2O_3 catalyst used in the gas and liquid phase experimental program

Property		Units
Specific surface area	190 10^3	m^2/kg
Pore volume	4.94 10^{-4}	m^3/kg
Density	1297	kg/m^3
Porosity	0.66	-
Pore diameter	0.01	μm

2.1.2 Reactor set-ups

2.1.2.1 Gas-phase continuous stirred tank reactor (Berty type) set-up

Pyridine hydrodenitrogenation experiments were performed at gas phase conditions in a set-up comprising a Berty type continuous stirred tank reactor. A schematic representation of the set-up is given in Figure 2-2, along with the symbols used. The Berty set-up is divided in four sections, *i.e.,* (i) the feed section, (ii) the reaction section, (iii) the effluent section and (iv) the analysis section, see Figure 2-2.

(i) Feed section

Pyridine and/or piperidine as liquid feed is mixed with *n*-C_6 and *n*-C_7 as solvent in a glass feed bottle which is maintained under a slight nitrogen over-pressure of 0.02 MPa. The liquid feed (1) is pumped to the reaction section using an High Pressure Liquid Chromatography, HPLC, pump (2). Liquid flow rates can be adjusted between 1 and 10 ml min^{-1}. Heat tracing, HABIA, coils are wrapped around the inlet lines to facilitate the flow of heavy components.

The possible gases which can be fed to the reactor are H_2, N_2 and H_2S in H_2. The internal standard CH_4 is mixed with the reactor effluent before analysis. The flow rates of these gases

are controlled by thermal mass flow controllers (3) and (4) in the range of 1 and 500 Nl h^{-1}. H_2 and 5 mol% H_2S in H_2 are mixed and the majority of the mixture is sent to the reaction section via a mixer/evaporator/preheater (6) where it is mixed with the evaporating hydrocarbons and preheated to a typical temperature of 473 K. The remaining part of the H_2/N_2 mixture enters the reaction section via the shaft of the magnetic drive assembly to cool it internally and to prevent hydrocarbon condensation in that shaft.

(ii) Reactor section

The Berty type high pressure reactor (8) is constructed by Autoclave Engineers. A magnetically driven impeller (11) induces an internal recycle flow pattern in the reactor going upwards between the catalyst basket (9) and the reactor wall and going down through the catalyst basket, see Figure 2-1. The gaseous hydrogen/hydrocarbon mixture enters the reactor just above the blades of the impeller, while the effluent leaves the reactor at the bottom under the impeller. The Berty reactor can be modelled as an ideal continuous stirred tank or an perfectly mixed flow reactor [4]. Typically the impeller is set to revolve at a speed of 25 rps. The temperature in the reactor is maintained by a heating cap (12) containing three heating elements of 500 W each controlled by two PID controllers (13) and (14) connected to two thermocouples measuring the temperature just on top of and below the catalyst basket. A third thermocouple is used as a safety control to measure the external wall temperature of the reactor. It is connected to an on-off switch ensuring that the temperature will not rise above the safe operation level. The sealing between the reactor body and cover is ensured by the use of a ductile aluminium gasket.

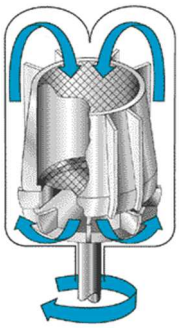

Figure 2-1. Cross sectional image showing the internal circulation in a Berty gas phase high pressure reactor.

(iii) Effluent section

The reactor effluent passes through a filter (15) before being mixed with the internal standard methane. The molar methane (99.95 vol.%, Air Liquide) flow rate is controlled with

a Brooks thermal mass flow controller (5) in the range of 2 and 10 Nl h^{-1}. The mixture of the reactor effluent and the internal standard is split into two flows. The majority of this flow is directly sent to a condenser (17), while a minor fraction passes through a six-way sampling valve (16) before being sent to this condenser. In the condenser the major part of the hydrocarbons condenses and is kept in a collector. The uncondensed part of the reactor effluent flows through the back pressure regulator (18) which is used to keep the installation under the desired pressure and is sent to the vent afterwards (20).

(iv) Analysis section

With the six-way valve, a 20 µl sample is sent towards a gas chromatograph (GC – Hewlett Packard Series II) (19) via a heated line. This GC is equipped with an Flame Ionization Detector, FID. Separation of the gases occurs in a capillary column with a polydimethylsiloxane film of 0.25 $x10^{-6}$ m. Cryogenic cooling of the column is possible with liquid nitrogen (21) to enhance the separation of the lighter components. The capillary column is 50 m long, has an internal diameter of 0.32 $x10^{-3}$ m and uses H_2 as carrier gas. The FID flame requires both hydrogen and air, and is stabilized by use of a nitrogen make-up flow. The flame transforms incoming hydrocarbons to ions which generate a small electronic current in a collector electrode placed above the flame. The electronic signal is related to the number of atoms that reached the detector, the latter being especially sensitive to carbon atoms. The signal is enhanced and processed by the software package Atlas.

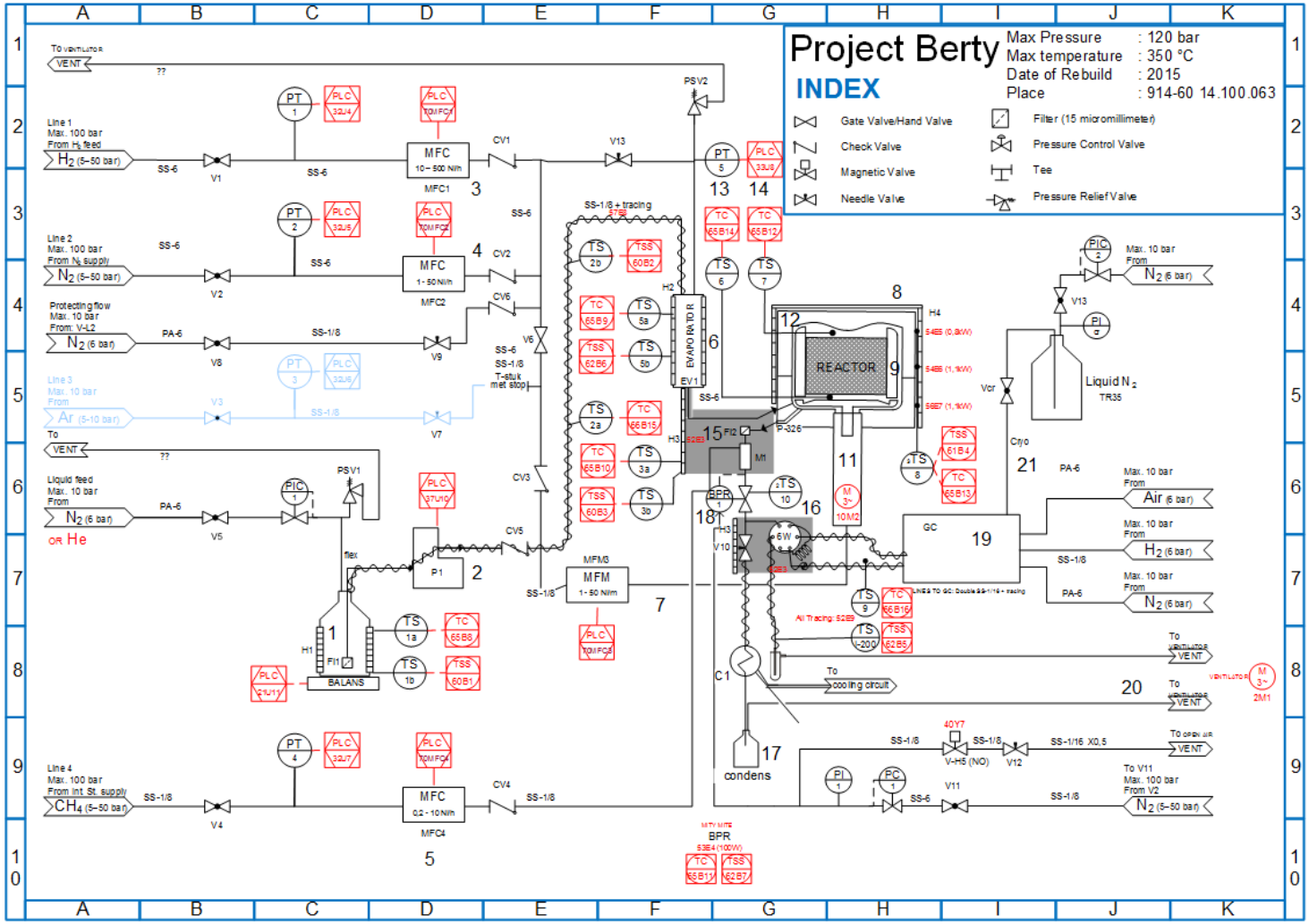

Figure 2-2. Schematic representation of the vapour-phase Berty CSTR set-up [5]

2.1.2.2 Three-phase continuous stirred tank reactor (Robinson-Mahoney type) set-up

A schematic representation of the liquid-phase Robinson-Mahoney CSTR set-up at Ghent University used for pyridine hydrodenitrogenation study is shown in Figure 2-3 along with the symbols used [6]. Again, four different sections can be distinguished, i.e. (i) the feed section, (ii) the reaction section, (iii) the effluent section and (iv) the analysis section.

(i) Feed Section

A total of four gas feed lines are available for feeding gases to the reactor directly. While two of them are used for N_2 and H_2, the others are used to feed gases such as H_2S in H_2 or CH_4. The flow rates are controlled by four thermal mass flow controllers in the range of 3 to 400 Nl h^{-1} (1) and (2) of various calibrated gases. The gas flows are preheated separately allowing more flexibility (3) and (4), before they are mixed (8) and sent to the reaction section. The liquid feed, *i.e.*, a pyridine and Halpasol™ mixture (5) is fed by an HPLC pump (6). Before entering the reaction section, the liquid feed is also preheated (7) and mixed with the gas flows (8). In this mixer, the gases are dispersed in the liquid phase by means of a sintered stainless steel filter.

(ii) Reactor section

The most important section of the experimental set-up consists of a Robinson-Mahoney reactor, which is of the CSTR type, see Figure 2-4, and which is equipped with a fixed cylindrical catalyst basket. The reaction mixture is introduced at the bottom of the reactor. A magnetically driven impeller induces a flow pattern directed to the reactor wall through the catalyst basket and with recirculation above and under the basket, see Figure 2-4. Typically the impeller is set to revolve at a speed of 25 rps, ensuring good mixing of the reaction mixture inside the reactor. The catalyst, mixed with inert material, is located at mid-height of the basket, where the flow through the basket is most uniform. Directly above and under the catalyst/inert mixture, more inert material is present in the catalyst basket, while at the top and the bottom the basket is filled with glass wool. Typically the amount of catalyst used in hydrodenitrogenation experiments was 2.0 $x10^{-3}$ to 3.0 $x10^{-3}$ kg diluted with α-Al_2O_3 to obtain 1.0 cm height in the catalyst basket which corresponds to 20% of the total basket volume.

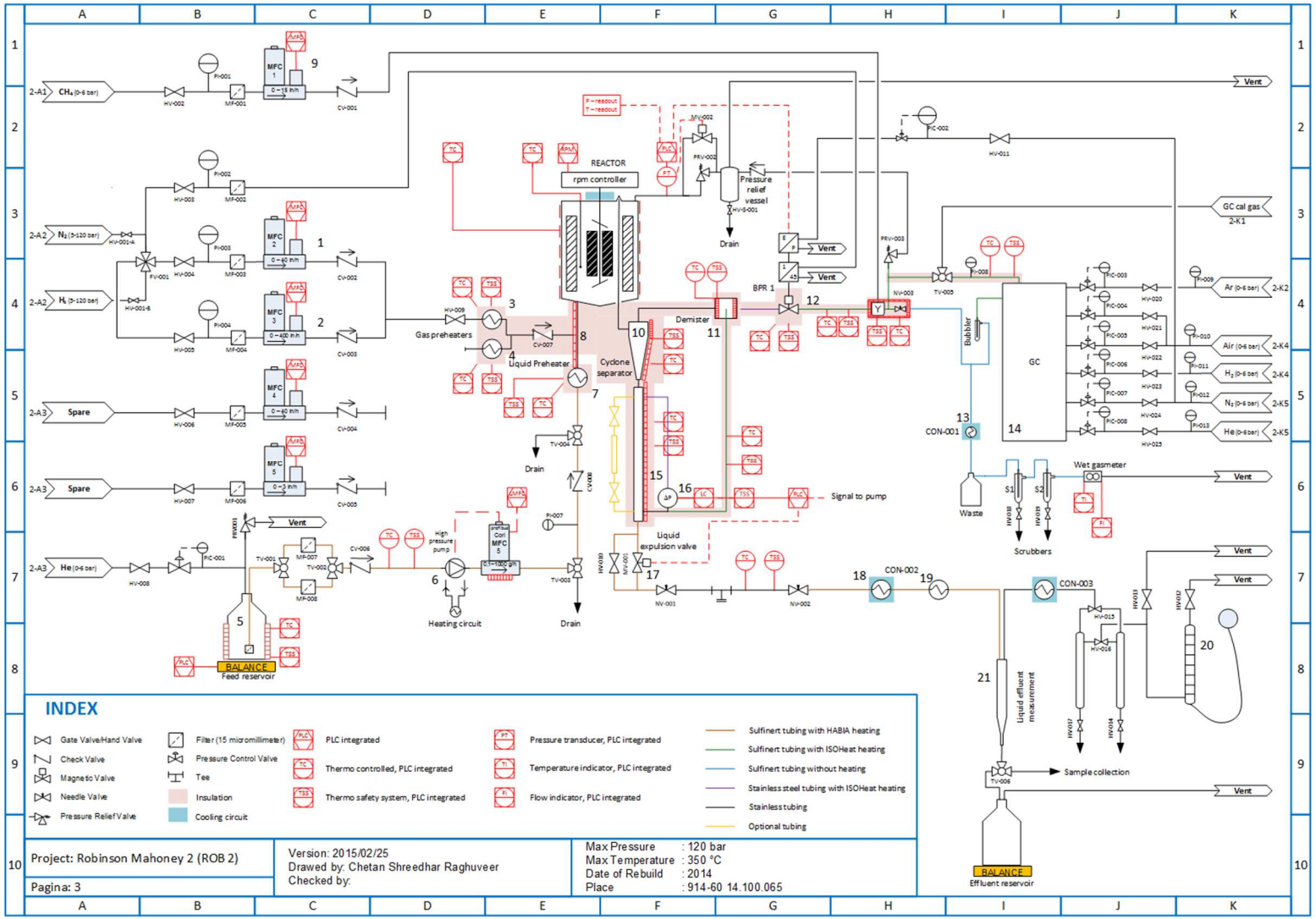

Figure 2-3. Schematic representation of the liquid phase Robinson-Mahoney CSTR set-up at LCT, Ghent University.

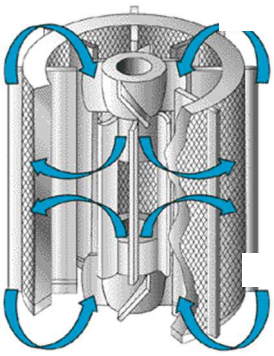

Figure 2-4. Cross sectional view of the Robinson-Mahoney reactor showing the flow pattern inside the reactor[5].

(iii) Effluent section

The gas-liquid mixture leaves the Robinson-Mahoney reactor via a down-comer, which extends into a small indent drilled in the upper flange of the reactor, and is subsequently separated in a cyclone (10) mounted downstream of the reactor. Because some small droplets may still be entrained with the gas flow, it is passed through a demister (11). The potentially entrained droplets are retained on a gauze in this demister and collected in a tube connected to the liquid effluent outlet of the cyclone. The 'dry' gas leaves the demister at the top and flows to a back pressure regulator (12) with which the set-up is kept under the working pressure. After the back pressure regulator the gas flow is mixed with the internal standard CH_4, which is controlled by MFC (9). This mixture is split into a main stream which is sent directly to a condenser (13) and into a smaller stream which is sent to a GC (14) for online analysis.

The liquid effluent of the cyclone enters a tubular reservoir (15). The liquid level in this tube is governed by an automatic level controller (16), which periodically discharges the liquid from the reservoir by means of a magnetic valve (17). The time interval for the periodic discharge can be adjusted via a needle valve which is placed in parallel with the magnetic valve. Downstream of the level control system the liquid flow is cooled (18) and flashed (19). Upon flashing the gas dissolved in the liquid is liberated and captured in a gas burette (20) connected with a vessel open to the air. This allows to measure the flow rate of the gas that was dissolved in the liquid under reaction conditions, further denoted as 'flashed gas'. The 'flashed liquid' falls down by gravity and is collected in a liquid burette (21) where the flashed liquid flow rate can be measured. Offline samples can be taken from the flashed liquid and flashed gas for analysis on the gas chromatograph (14).

(iv) Analysis Section

The analyses of the various effluent streams are performed with a Thermo scientific TRACE 1310 GC. The resulting chromatograms are processed using the Chromeleon® software package. The layout of the GC is as shown in Appendix A. It comprises an auxiliary oven (isothermal), which contains the Hayesep Q and Molsieve 5A columns coupled with an TCD which is used to analyse H_2 and CH_4 in the sample, and a non iso-thermal oven for the detailed hydrocarbon analysis, DHA, with an FID preceded by a polydimethylsiloxane capillary column and for NH_3, H_2S and H_2O analysis using a Volamine column coupled with a TCD. Argon and Helium are used as carrier gases within these columns. Online gas effluent analyses can be performed with the two TCDs and the FID whereas offline liquid injection of the liquid samples is possible on the split-split less injector (SSL) connected to the FID.

The gas product of the reaction is injected online to the GC through a heated sampling six way valve. A volume of 0.2 to 1.0 µl is injected using a manual syringe via the SSL column injection port. The continuous signals from the various detectors of the GC are sent to a PC where the Chromeleon software package is used for the peak surface integration.

2.1.2.3 Cold flow reactor set-up

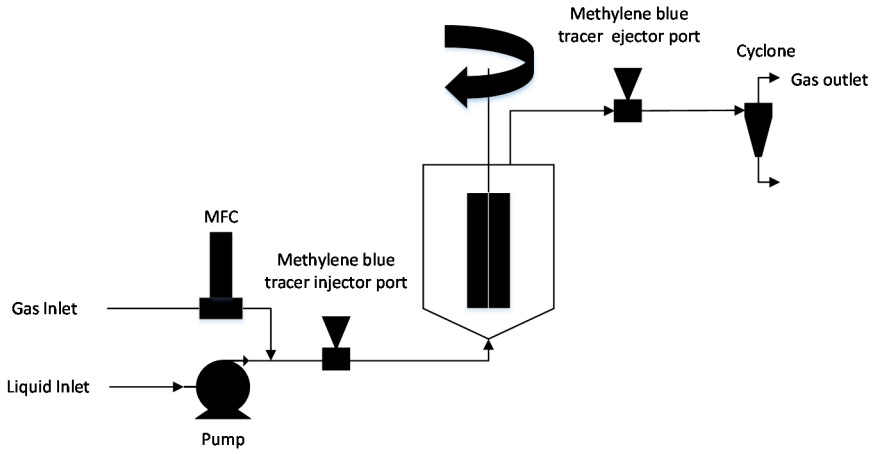

Figure 2-5. Flow diagram of the cold flow set-up constructed for studying the liquid hold-up with impulse flow experiments in a Robinson-Mahoney reactor [7].

Experiments at so-called ‘cold flow’ or ambient conditions have also been performed [7], however, with a glass mock-up model reactor with identical dimensions to those of the high temperature/pressure stainless steel reactor as supplied by autoclave engineers, see Figure 2-5. These experiments were performed by injecting an impulse of tracer to the set-up operating at steady state conditions. The configuration of this glass reactor was slightly different from the one at relevant conditions: instead of the over-flow arrangement for the effluent that is present in the stainless steel reactor, the outlet for the gas-liquid mixture went through the upper flange

of the reactor. Tracer impulse experiments were performed in the absence of the catalyst basket and catalyst pellets. The inlet section consisted of a centrifugal pump delivering continuous flow of liquid to the reactor, the liquid flow is mixed with a steady flow of H_2 which is sent through a highly precise thermal mass flow controller. An injector port is inserted at about $3x10^{-2}$ m from the inlet of the reactor, this port is used for introducing the impulse of the methylene blue tracer. The outlet of the reactor is connected to a sampling port which is used for drawing off a sample of the liquid effluent and subsequent offline measurements of methylene blue tracer concentration using a spectrophotometer. The glass reactor could not be operated at elevated pressures and temperatures, but at ambient pressures and room temperatures provides an opportunity to visually observe the gas-liquid interactions.

2.1.3 Composition of the reactor effluent

The Robinson-Mahoney set-up as explained in section 2.1.2.2 was the re-constructed set-up which was used to acquire data for the results discussed in chapter 3. The data that are discussed in chapter 5, were acquired with a set-up that existed earlier.

2.1.3.1 Liquid effluent

A schematic representation of the different inlet and outlet flows of the setup is given in Figure 2-6. Three effluent streams are identified: the gas phase effluent denoted as F_g, the flashed gas effluent, F_{lg}, and the flashed liquid effluent, F_{ll}. The liquid effluent F_{ll} is analysed offline by the FID connected to the polydimethylsiloxane capillary column. Using *n*-C_9 as an internal standard ($CF_{C9} = 1$), the weight fraction w_i of all compounds can be calculated using calibration factors CF_i, which were calculated with a reference mixture a priori, see Appendix A, and the GC surface areas A_i that originate from the Atlas software as shown in equation 2-1:

$$w_i = CF_i w_{C9} \frac{A_i}{A_{C9}} \qquad 2\text{-}1$$

2.1.3.2 Gas effluent

Typically the gas effluent stream, F_g sample is analysed online by the TCD connected to the Haysep Q packed column while an F_{ll} sample is analysed on the offline FID connected to the polydimethylsiloxane capillary column. However, since the TCD in the GC was unavailable, quantitative analysis of the gas phase was not performed. The main components present in the gas phase effluent, F_g, are NH_3, H_2, H_2S and CH_4. Molar flow rates were determined by using molar balances of the different atomic balances based on the liquid effluent. Care is taken that all relevant hydrocarbons from the flashed gas effluent, F_{lg}, are

completely condensed such that they are measured together with the flashed liquid F_{ll}. Incondensable gases such as H_2, H_2S and CH_4 are typically measured based by the liquid volume displacement by these gases over a period of time, see also Section 2.1.2.2 (iv). The device consists of an open ended flask which is connected to a column which has grading to measure the liquid volume. The flask is placed on a manually adjustable screw shaft which can be used to adjust the liquid height of the column. At steady operation of the set-up the flashed gas flow rate is measured as a function of time. An ejector port situated at the top of a liquid column is used to draw a sample for off-line analysis. It was observed that the flow rate of F_{lg} was very low in comparison to F_g and was neglected during the analysis.

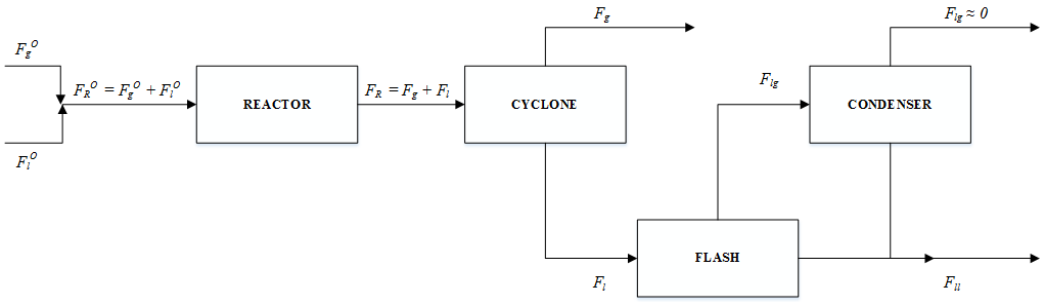

Figure 2-6. Scheme showing the inlet and outlet flows considered in the Robinson-Mahoney bench-scale three-phase CSTR experimental set-up.

2.1.3.3 Elemental balances

The carbon and the nitrogen balance were calculated considering the outlet flowrates of the components in liquid effluent, F_{ll} and the corresponding deviation of the mass balances were calculated. A maximum of ± 5% deviation was observed in the carbon and nitrogen mass balance at all the experimental conditions. A corresponding equal deviation for the hydrogen and sulphur was assumed and subsequently calculated based on the molar balance of consumption or production.

(i) Carbon balance

All the relevant carbon species involved in the reaction can be safely assumed to leave the system in the liquid phase, *i.e.*, the flashed liquid. This is confirmed by verifying the outlet composition of F_{lg}. Additionally, DMDS decomposes into H_2S and CH_4 and needs to be considered while accounting for the total carbon balance in the gas stream. The molar methane flow rate in the gaseous effluent can be calculated using the balance as shown in Eq. 2-2:

$$\sum_i c_i F_i^0 = \sum_i c_i F_i^g + \sum_i c_i F_i^{ll} \qquad 2\text{-}2$$

with c_i the number of carbon atoms in component i.

(ii) Nitrogen balance

Each nitrogen atom that is present in pyridine in the feed is converted into one of the intermediate nitrogen containing compounds eluting via the liquid outlet or in the gaseous effluent as ammonia. Thus, the molar flow rate of ammonia can be calculated from the nitrogen balance as shown in 2-3:

$$\sum_i n_i F_i^0 = \sum_i n_i F_i^g + \sum_i n_i F_i^{ll} \quad 2\text{-}3$$

which leads to:

$$F_{NH_3}^g = F_P^0 - (F_P^{ll} + F_{PP}^{ll} + F_{n-PPP}^{ll}) \quad 2\text{-}4$$

with n_i the number of nitrogen atoms in compound *i* and F_i^g the flow rate of compound *i* in the gaseous effluent, F_i^0 the feed flow rate of compound *i* and F_i^{ll} the flow rate of compound *i* in the liquid effluent.

(iii) Hydrogen balance

The inlet hydrogen is consumed in the C-N bond scission and hydrogenation reactions, including saturation of the aromatic ring. The hydrogen that is not consumed in the reaction will leave the reactor mainly through the gas phase, the amount leaving the set-up via the flashed gas being negligible. Thus the molar flow rate of hydrogen in the gaseous effluent can be written as 2-5:

$$\sum_i h_i F_i^0 = \sum_i h_i F_i^g + \sum_i h_i F_i^{ll} \quad 2\text{-}5$$

with h_i the number hydrogen atoms in compound *i*. This can be written as:

$$F_{H_2}^g = F_{H_2}^0 - (3\, F_{PP}^{ll} + 5\, F_{C5}^{ll} + 7\, F_{n-PPP}^{ll}) \quad 2\text{-}6$$

(iv) Sulphur balance

Since the sulphydril intermediates are not considered to be stable enough to elute from the reactor, the only sulphur containing compound which needs to be considered is the H_2S generated by the complete decomposition of DMDS which is co-fed with the pyridine and the solvent. The H_2S generated from the DMDS is in the gas phase and the molar flow rate of H_2S can thus be calculated as shown in equations 2-7 and 2-8:

$$\sum_i s_i F_i^0 = \sum_i s_i F_i^g + \sum_i s_i F_i^{ll} \quad 2\text{-}7$$

$$F_{H_2S}^g = 2\, F_{DMDS}^0 \quad 2\text{-}8$$

with s_i the number of sulphur atoms in compound *i*.

2.1.4 Conversion, selectivity, yield

The conversion X_i of feed component *i* on a molar basis is defined as equation 2-9:

$$X_i = \frac{F_i^0 - F_i}{F_i^0} \qquad 2\text{-}9$$

F_i^0 and F_i represent the molar inlet flow rate and molar outlet flow rate of compound *i*, respectively.

The selectivity for product *j* originating from feed component *i*, $S_{j,i}$, can be calculated as equation 2-10 (c_i and c_j represent the carbon number of the feed component *i* and product *j* respectively) :

$$S_{j,i} = \frac{c_j(F_j - F_j^0)}{c_i(F_i^0 - F_i)} \qquad 2\text{-}10$$

Using the above defined quantities, the yield of product *j* can be calculated as equation 2-11:

$$Y_j = \frac{c_j(F_j - F_j^0)}{c_i F_i^0} = S_{j,i} X_i \qquad 2\text{-}11$$

2.2 Modelling

2.2.1 Parameter estimation

A kinetic model, described as a set of mathematical equations for the *n* experimental output variables $\underline{y}$, *i.e.*, the outlet flow rates of the different products, also denoted as responses, needs to be derived to setup a parameter estimation case. Such non-linear multi-response models are a function of *m* independent variables $\underline{x}$, *e.g.*, temperature, pressure, molar inlet flow rates, etc. and *p* model parameters $\underline{\beta}$, *e.g.*, activation energies and chemisorption enthalpies and can be represented as shown in equation 2-12.

$$\underline{y} = \underline{f}\left(\underline{x}, \underline{\beta}\right) + \underline{\varepsilon} \qquad 2\text{-}12$$

with $\underline{f}$ the model function and $\underline{\varepsilon}$ the experimental error. This can be represented in matrix notation as shown in 2-13:

$$\begin{bmatrix} y_1 \\ y_2 \\ \vdots \\ y_n \end{bmatrix} = \begin{bmatrix} f_1(x_1, x_2, \dots, x_m\,;\, \beta_1, \beta_2, \dots, \beta_p) \\ f_2(x_1, x_2, \dots, x_m\,;\, \beta_1, \beta_2, \dots, \beta_p) \\ \cdot \\ \vdots \\ f_n(x_1, x_2, \dots, x_m\,;\, \beta_1, \beta_2, \dots, \beta_p) \end{bmatrix} + \begin{bmatrix} \varepsilon_1 \\ \varepsilon_2 \\ \vdots \\ \varepsilon_n \end{bmatrix} \qquad 2\text{-}13$$

Parameter estimation is based on the minimization of the weighted sum of squares (SSQ) of the residuals between the experimental outlet flow rates and the model determined outlet flow rates $\hat{F}$:

$$SSQ = \sum_{i=1}^{nob} \sum_{j=1}^{nresp} w_j \left(F_{i,j} - \hat{F}_{i,j}\right)^2 \xrightarrow{\underline{b}} Min \qquad 2\text{-}14$$

This is done by varying the estimates $\underline{b}$ for the parameter values $\underline{\beta}$ which are expected to approach the real parameter value when the global minimum of the SSQ is reached. $F_{i,j}$ stands for the experimentally observed outlet flow of response *j* in experiment *i*, $\hat{F}_{i,j}$ stands for the model simulated value of that same response in experiment *i* and w_j for a weight that can be assigned to a response (w_j = 1 during parameter estimation).

2.2.2 Regression and statistical tests

Model regression results can be evaluated by a multitude of tests. In this work the *F* test and *t* test are used to validate the global significance of the regression and the individual significance of the parameters.

2.2.2.1 Significance of the regression, F test

If the *F* value for the global significance of the regression, F_c, exceeds the tabulated $F(0.95)$-value, the regression is deemed to be statistically significant. The *F* value of a regression is defined as the ratio of the sum of squares of the regression and the residual sum of squares, divided by their respective degrees of freedom, see equation 2-15:

$$F_c = \frac{\frac{\sum_{i=1}^{q}\sum_{j=1}^{n} w_j \hat{F}_{i,j}^2}{p}}{\frac{\sum_{i=1}^{q}\sum_{j=1}^{n} w_j (F_{i,j} - \hat{F}_{i,j})^2}{q(n-p)}} \qquad 2\text{-}15$$

2.2.2.2 Significance of individual parameters, t test

The significance of a parameter estimate b_i is based on its *t* value, which should exceed the corresponding, tabulated *t* value, see equation 2-16:

$$t_i = \frac{b_i}{\sqrt{V(b)_{i,i}}} > t_{q,q(n-p)}(0.95) \qquad 2\text{-}16$$

$V(b)_{i,i}$ corresponds to the diagonal element on row *i* of the covariance matrix *V(b)* of the regression. This implies a high sensitivity of the model towards the parameter and a narrow 95% confidence interval, defined as below, see equation 2-17:

$$b_i - t_{q,q(n-p)}(0.95)\sqrt{V(b)_{i,i}} \leq \beta \leq b_i + t_{q,q(n-p)}(0.95)\sqrt{V(b)_{i,i}} \quad 2\text{-}17$$

2.2.3 Regression routine

In this thesis, regression, c.q., parameter estimation, was performed using the nonlinear least-squares technique by applying a combination of a Rosenbrock [8] and a Levenberg-Marquardt [9] algorithm for minimization of the objective function. Since the Rosenbrock method has a smaller chance to diverge when the parameter values are remote from the optimum, this method is applied first to find an appropriate direction leading to a possible optimum. In order to prevent the combined Rosenbrock Marquardt search from arriving in a local optimum, a few Rosenbrock Marquardt searches were performed starting from different initial parameter estimates to verify the global character of the optimum that was reached. An in-house written code is used for the Rosenbrock method, while the Marquardt algorithm is implemented by selecting the Ordinary Least Squares (OLS) option within ODRPACK-package version 2.01 [10, 11]. Some additional source code was added to ODRPACK in order to retrieve additional statistical information, in particular, variance analysis, by Thybaut et al [5].

2.2.4 Calculation of outlet flow rates and reactor model

The net rate of formation of the j^{th} component for the i^{th} experiment for a given set of kinetic parameters is a function of the reaction temperature, T_i; the total pressure, $p_{t,i}$ and the mole fraction of the reaction mixture, $z_{i,j}$. and is formulated using the appropriate kinetic equations developed further in this thesis. This kinetic model equation is independent of the reactor model equation.

$$R_{i,j} = f(T_i, p_{t,i}, z_{i,1}, \ldots, z_{i,nresp}) \quad 2\text{-}18$$

The composition of the reaction mixture was obtained in a straightforward way from these outlet flow rates.

$$z_{i,j} = \frac{F_{i,j}}{\sum_{j=1}^{nresp} F_{i,j}} \quad 2\text{-}19$$

The calculation of the composition of an individual phase, *i.e.*, liquid phase, is addressed in more detail in chapter 5.

2.2.5 Continuous stirred tank reactor (CSTR) model

At the investigated operating conditions, a Berty reactor as mentioned in section 2.1.2.1 and a Robinson-Mahoney reactor as mentioned in section 2.1.2.2 conform to a perfectly mixed CSTR. Vapour-liquid equilibrium verifications in liquid phase experimentations have been performed using the Peng-Robinson equation of state [5]. The system is assumed to be isothermal and isobaric. The molar outlet flow rate of a component *j* in experiment *i* is obtained from the solution of the set of *nresp* algebraic equations in the *nresp* unknown molar outlet flow rates $F_{i,j}$:

$$F_{i.j} - F_{i,j}^{o} - R_{i,j} W_{cat,i} = 0 \qquad \text{2-20}$$

The set of non-linear algebraic equations is solved using the DNSQE routine available at the Netlib software library [12]. The purpose of DNSQE is to find the solution of a set of *n* nonlinear algebraic equations in *n* variables by a modification of the Powell hybrid method [13, 14].

2.3 References

1. Pille, R. and G.F. Froment, **Hydrotreatment and Hydrocracking of Oil Fractions**, 1997. 106: p. 403-413.

2. Raghuveer, C.S., J.W. Thybaut, R. De Bruycker, K. Metaxas, T. Bera, and G.B. Marin, **Fuel**, 2014. 125(0): p. 206-218.

3. Pille, R., *Sleutelcomponenten bij de hydrodenitrogenering en hydrodesulfurisering van aardoliefracties*. 1997, Universiteit Gent.

4. Berty, J.M., **Chemical Engineering Progress**, 1974. 70(5): p. 78-85.

5. Thybaut, J.W., *Production of low-aromate fuels: kinetics and industrial application of hydrocracking*. 2003, Universiteit Gent.

6. Mahoney, J.A., K.K. Robinson, and E.C. Myers, **Chemtech**, 1978. 8(12): p. 758-763.

7. Hoernaert, J., *Hydrodesulfurisatie op een CoMo/γ-Al_2O_3 katalysator in tubulaire en gradientloze reaktoren*. 1988, Rijksuniverseteit Gent.

8. Rosenbrock, H.H., **Computer Journal**, 1960. 3(3): p. 175-184.

9. Marquardt, D.W., **Journal of the Society for Industrial and Applied Mathematics**, 1963. 11(2): p. 431-441.

10. Boggs, P.T., J.R. Donaldson, R.H. Byrd, and R.B. Schnabel, **ACM Transactions on Mathematical Software**, 1989. 15(4): p. 348-364.

11. Boggs, P.T., R.H. Byrd, J.E. Rogers, and R.B. Schnabel, **NISTIR**, 1992: p. **92**-4834.

12. Netlib, **http://www.netlib.org**.

13. Powell, M.J.D., **Computer Journal**, 1964. 7(2): p. 155.

14. Powell, M.J.D., *A hybrid method for nonlinear equations in numerical methods for nonlinear algebraic equations*. 1988: Ed. P Rabinowitz, Gordon and Breach.

This page intentionally left blank

3 Gas-liquid hold-up and volumetric mass transfer coefficient in a three-phase bench-scale Robinson-Mahoney reactor at industrially relevant operating conditions

The liquid hold-up, ε_L, as well as the volumetric gas-liquid mass transfer coefficient, k_La, have been measured in a bench-scale, gradientless, three-phase Robinson-Mahoney reactor at industrially relevant operating conditions with realistic feeds. k_La has been determined via the so called 'dynamic gas absorption technique' where a total pressure decrease is monitored as a function of the time. k_La was found to increase from 1.22 10^{-2} s^{-1} to 2.14 10^{-2} s^{-1} with the agitator rotation speeds, $N_{agitator}$, from 8.33 to 25 rps according to the relationship $k_La = 1.77\ 10^{-7} * N_{agitator}{}^{3.4} + 1.21\ 10^{-2}$.

The liquid hold-up was investigated by imposing a step change or injecting an impulse of tracer in the liquid phase fed to the reactor. At industrially relevant operating conditions, *i.e.*, between 523 to 583 K and 2.5 to 5.5 MPa and volumetric inlet H_2/Halpasol™ ratio in the range of 5 to 250 $m^3\ m^{-3}$, the C_{10} content in Halpasol™ – an *n*-paraffin mixture in the range C_9 to C_{14} – was varied. For a H_2/water mixture, at ambient conditions, *i.e.*, 298 K, 0.1 MPa and a volumetric inlet H_2/water ratio in the range of 0 to 580 $m^3\ m^{-3}$, a methylene blue tracer impulse was employed. At industrially relevant conditions, the temperature and total pressure were

found to only exert a minimal impact on the liquid hold-up, *i.e.*, it remained constant at about 70%. In contrast, a decrease to a liquid hold-up of about 50% was observed by changing the volumetric inlet gas-liquid ratio from 5 to 250 $m^3\,m^{-3}$. At ambient conditions, for H_2-water mixture a more pronounced change in the volumetric inlet gas-liquid ratio, *i.e.*, from 0 to 580 $m^3\,m^{-3}$, was necessary to achieve a similar reduction in liquid hold-up. This could be attributed to differences in surface tension rather than in operating conditions. The experimentally measured liquid hold-up always exceeded the one obtained from vapour-liquid equilibrium calculations based on the volumetric inlet gas liquid ratio. It is indicative of a reactor in which the liquid constitutes the continuous phase, while the gas is present as the disperse phase, although at the highest volumetric inlet gas-liquid ratio the gas phase may start adopting a continuous character.

3.1 Introduction

Three-phase reactions are among the most encountered in the chemical and process industry. Such reactions are especially prevalent in petroleum refining with processes such as hydrotreating and hydrocracking [1-4]. Typically, these three-phase reactions comprise a solid catalyst which is contacted by the hydrocarbon liquid to be converted under a high hydrogen pressure. Other light gases, such as hydrogen sulphide, ammonia, methane and ethane tend to end up in the gas phase as well.

Reactions involving three phases have been studied extensively in the past to unravel several of the many aspects involved. On the one hand research dedicated to understanding the intrinsic kinetics of the reactions has been pursued to optimise the operating conditions to be employed [4-7], while on the other hand research dedicated to the hydrodynamics as well as mass and heat transfer phenomena has provided a basis for reactor design and process intensification [8-13]. The latter research, as reported by a variety of publications has contributed to the development of comprehensive reactor models, taking into consideration all relevant physical phenomena encountered in an industrial reactor in addition to the chemical kinetics [7, 14, 15].

Many three-phase reactions have been experimentally investigated in plug flow reactors (PFRs) operating in the trickle flow regime [1, 16]. Such studies have been useful in data acquisition for scale-up purposes. Nevertheless, issues with respect to complete catalyst wetting and reactor hydrodynamics remained unclear. Continuous Stirred Tank Reactors (CSTRs) are believed to provide better mixing and catalyst wetting in comparison to PFRs, explaining their advantages in catalyst performance evaluation in general and intrinsic kinetics

determination, particularly for three-phase reactions. A special type of fixed-basket, three-phase reactor was proposed by Mahoney *et al.* [17]. These reactors, also denoted as Robinson-Mahoney (RM) reactors, are gradientless in concentration and temperature and, hence, can be considered to approximate an ideal CSTR. Additionally, these reactors can be operated in a wide range of operating conditions thereby providing flexibility to study reactions at industrially relevant conditions.

The presence of three phases and the design of the RM reactor internals result in a seemingly complex lay-out and hydrodynamics, see Figure 3-1. The gas liquid mixture enters the reactor from the bottom and reaches the centre of the annular basket by the action of the agitator's bottom blades. The vertical, centrally located blades on the high speed rotating agitator push the gas-liquid mixture through the catalyst basket to the reactor wall, where part of it moves upwards and another part downwards. An intense internal recirculation is achieved in the reactor thanks to the blades tilted over 45° and -45° above and below the central, vertical blades of the agitator. This recirculation largely exceeds the inlet flow at the bottom of the reactor as well as the outlet flow in the down comer situated at the top of the reactor. This flow pattern, which dominates at high turbulence, is necessary to achieve uniform concentrations throughout the reactor, hence, approximating the ideal CSTR flow pattern and turning the RM reactor into a potent tool in the acquisition of intrinsic kinetic data [4-6, 18-21].

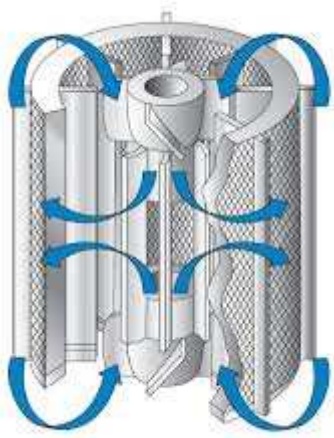

Figure 3-1 3D representation of the Robinson-Mahoney reactor internals and flow pattern at high agitator rotation speeds (source: Autoclave Engineers [22])

The interest in RM reactors has motivated research to assess the various effects of the reactor internals on the fluid hydrodynamics inside the reactor by theoretical, CFD studies [23] as well as by experimental investigations [24-26].

Some of the important parameters for assessing the reactor performance are the volumetric gas-liquid mass transfer coefficient, k_La, along with the gas and liquid hold-up, ε_G and ε_L. Appropriate changes in the reactor geometry can be made in order to attain very high values for k_La, which are generally desired. Gas or liquid hold-up are defined as the percentage or fraction, by volume, of the gas or liquid in the total reactor volume. These are important since they constitute essential information for drawing an adequate picture of the actual phase distribution within the reactor.

The performance of three-phase CSTRs and their hydrodynamics have already been the subject of a considerable number of investigations [24-31]. Nevertheless, a study dedicated to the RM reactor at industrially relevant operating conditions has not been reported yet. The main objectives of this work are, hence, to evaluate crucial parameters such as k_La, ε_G and ε_L in three-phase operation in a CSTR at such industrially relevant conditions. A correlation that is able to capture the effect of agitator rotation speed, $N_{agitator}$, on the k_La is proposed and compared to a literature reported correlation constructed for H_2-gasoil/water mixture at atmospheric pressure i.e., 0.1 MPa and room temperature i.e., 298 K [24]. Data on ε_G and ε_L are used to propose an adequate image of the phase distribution in the reactor volume compared to the one calculated based on the feed composition.

3.2 Procedures

The experimental set-ups used during the estimation of the volumetric gas-liquid mass transfer coefficient and hold-up are described in detail in Chapter 2.

3.2.1 Volumetric gas-liquid mass transfer coefficient

The experimental methodology reported by Dietrich *et al.* [30] and Pitault *et al.* [24], for studying k_La in a batch configuration has been adopted in the present work. Since the set-up used comprises a continuous reactor, see Chapter 2, the outlet gas and liquid flow were closed in order to perform these experiments. k_La was quantified from experimental data by using Eq. 3-1 as described by Dietrich *et al.* [30] and Pitault *et al.* [24]. The k_La measurement procedure involved filling the reactor with Halpasol™, degassing the solution by agitating the mixture at high speeds in the absence of gas and noting the resulting pressure, p_o. Subsequently, the agitator was stopped and H_2 was admitted until the desired pressure, p_m , was attained. The agitator was re-started and the pressure decrease as a function of time due to H_2 absorption in the Halpasol™, as a result of this agitation, was carefully tracked and logged till the final

pressure, p_f ,was attained. Data acquired at different agitation speeds resulted in an understanding of the variation in the k_La for a particular gas-liquid system.

$$\frac{p_m - p_f}{p - p_f} = \exp\left(\frac{p_m - p_o}{p_f - p_o}\, k_L a \,.\, t\right) \qquad 3\text{-}1$$

3.2.2 Gas and Liquid Holdup

As described in Chapter 2 and also evident from the P&ID, the auxiliary components such as cyclone, demister and level tube, incorporated in the Robinson Mahoney set-up impact on the actual time at which concentration changes are measured at the liquid outlet. The set-up can, hence, be considered to comprise two different types of zones, a completely mixed one, also denoted as the 'reactive' zone and two tubular ones upstream and downstream of the reactor, also denoted as the 'non-reactive' zones, through which the mixture is assumed to move in plug flow. In the reactive section ideal CSTR behaviour is assumed for the gas-liquid mixture in contact with the catalyst. During continuous operation and kinetic data acquisition at steady state conditions, the zones in which plug flow is established will not interfere with these kinetics measurements. However, during the determination of liquid hold up in the reactive zone with the help of a tracer, the observation of the concentration changes with time will be delayed because of these non-reactive, plug flow zones. The corresponding '*lag time*' of the set-up varies with the inlet liquid flow rate in an inversely proportional manner. Further details are provided in Section 3.4.1. Experiments are performed with the chemicals and materials as shown in Table 3-1, the components in the experiments are used as supplied without further purification.

Table 3-1. Materials and chemicals used during the experimental study of the Robinson-Mahoney three phase bench scale reactor hydrodynamics.

Chemical	Phase	Supplier	Code
Decane	Liquid	Sigma Aldrich	30570
Halpasol™	Liquid	Haltermann	190-240
H_2	Gas	Airliquide	N40
Alumina balls	Solid	Gimex	(-)

Liquid hold-up is an aspect of reactor design that is typically investigated in trickle bed reactor configurations using various techniques [16, 32]. Publications on liquid hold-up in CSTRs are scarce to non-existent, especially at industrially relevant operating conditions. Measuring a step response to a change in the liquid feed concentration of the tracer component constitutes an ideal method to characterize the behaviour of an existing set-up at industrially relevant operating conditions, without having to implement major modifications. In addition to

the step response experiments at relevant conditions, also pulse response experimentation has been performed for the analysis of the reactor behaviour with a H_2/water mixture at atmospheric pressure, 0.1 MPa, and room temperature, 298K. Apart from the actual comparison of the gas and liquid-phase hold-up behaviour at different operating conditions, the latter experimentation also provides an opportunity to visually observe the investigated phenomena

3.2.2.1 Step response to a change in the liquid phase concentration

Step response experiments were performed by implementing an abrupt change in the liquid phase *n*-decane concentration within a Halpasol™ solvent. The original liquid feed and gas flow rates to the reactor were started and the desired temperature and pressure were set. Once steady state conditions were achieved, an amount of *n*-decane was added to the Halpasol™ solvent in the liquid feed recipient at time zero. The *n*-decane outlet concentration was monitored over the period of time, $t_{sampling,}$ in which its concentration evolved from the original one to the new one. This *n*-decane concentration profile as a function of time allowed calculating the corresponding gas and liquid holdup in the reactor as well as the lag time, t_{lag}, corresponding with the plug flow zones in the set-up upstream and downstream of the completely mixed reactive zone. During typical experiments, t_{lag} amounted to about 1080 s for the combination of set-up and operating conditions used.

In order not to complicate the data treatment, the liquids used, *i.e.,* Halpasol™ and *n*-decane, exhibited sufficiently low vapour pressures at the investigated operating conditions such that any vaporization can be safely neglected. As a result, the transient mass balance for the *n*-decane concentration can be written as follows, see Eq.3-2:

$$V_L \frac{dC}{dt} = F_{V,f} C_f - F_V . C \qquad 3\text{-}2$$

Where, V_L, is the liquid volume in the reactor, C and C_f, are the tracer concentration in the reactor and the feed respectively, and $F_{V,f}$ and F_V are the liquid inlet and outlet volumetric flow rates. Since, vaporization of the liquid in the reactor can be assumed to be negligible, the liquid inlet and outlet volumetric flow rates are identical. The unambiguous definitions of the residence time, τ_L, and liquid hold-up, ϵ_L, are presented in Eqs. 3-3 and 3-4.

$$\tau_L = \frac{V_L}{F_V} \qquad 3\text{-}3$$

$$\epsilon_L = \frac{V_L}{V_R} = \frac{\tau_L . F_V}{V_R} \qquad 3\text{-}4$$

The outlet tracer concentration profile as a function of the time can be obtained by integrating Eq. 3-2, see Eq. 3-5, where C_0 represents the tracer concentration in the reactor at the start of the experiment and C_f. represents the final concentration of tracer at steady

$$C = C_f + (C_0 - C_f).exp\left(-\frac{t}{\tau_L}\right) \quad 3\text{-}5$$

As a consequence of the non-reactive plug flow zones in the reactor set-up, *i.e.*, between the injector and the reactor inlet and between the reactor outlet and the liquid collection burette, the lag time, t_{lag}, should be taken into account. Hence, the experimental observations should be assessed using equation 3-6:

$$\frac{C - C_f}{C_0 - C_f} = exp\left(-\frac{(t_{sampling} - t_{lag})}{\frac{\varepsilon_L * V_R}{F_V}}\right) \quad 3\text{-}6$$

As evident from Eq. 3-6, a non-linear parameter estimation procedure should be employed to estimate the parameter, ε_L. The expression on the left hand side of the equation contains quantities that have served as input or have been observed as a function of the measured sampling time, $t_{sampling}$. An estimate of the lag time is also inherently present in the equation and can easily be compared with the experimentally observed data.

3.2.2.2 Response to an impulse of tracer

Liquid hold-up with a H_2/water mixture at atmospheric pressure, 0.1 MPa, and room temperature, 298K was assessed by injecting 0.7 10^{-6} m^3 of methylene blue tracer impulse into a continuous liquid feed (water) of 0.13 10^{-6} m^3 s^{-1} upstream of the reactor with an injector port [33]. The subsequent outlet methylene blue concentration was determined off-line with spectrophotometric equipment. The time of the injection determines the starting time of the experiment and the outlet methylene blue concentration is measured with respect to time to calculate the liquid hold-up. To investigate the effect of the inlet gas-liquid ratio on the liquid hold-up, H_2 at 100 and 280 Nl h^{-1} was introduced into the liquid feed using a thermal MFC.

A similar data treatment methodology as proposed for the step-input of a tracer is used for experiments conducted at atmospheric pressure, 0.1 MPa, and room temperature, 298K, as well, see section 3.2.2.1. However, since, an injection of the impulse of a tracer rather than a step change in concentration is implemented, the equation is slightly different, see Eq. 3-7. The terms on the left hand side of Eq. 3-7, serve as the input for the parameter estimation problem with t_{lag} and ε_L as the model parameters. As in the cold flow reactor set-up, the injector and the liquid collection ports are located close to the reactor inlet and outlet, t_{lag} will be practically negligible.

$$\frac{C}{C_o} = exp\left(-\frac{(t_{sampling} - t_{lag})}{\frac{\varepsilon_L * V_R}{F_V}}\right) \quad 3\text{-}7$$

3.2.3 Regression analysis

Athena visual studio [34] was used to estimate the model parameters, *i.e.*, k_La, ε_L and t_{lag}. The model parameters were estimated by the minimisation of the objective function Eq. 3-8, by employing a non-linear least squares algorithm.

$$SSQ = \sum_{i=1}^{nob} \sum_{j=1}^{nresp} \left(Y_{i,j} - \hat{Y}_{i,j}\right)^2 \overset{b}{\rightarrow} Min \quad 3\text{-}8$$

The model parameters were assessed for their physical and statistical significance [35]. The global significance of regression was confirmed by the resulting *F* value for the global significance of the regression, while the student *t*-test was used to assess the statistical significance of the individual parameters.

3.3 Results and Discussion

3.3.1.1 Volumetric Gas-Liquid Mass Transfer coefficient

Berger *et al.* [36] specifically elaborate on the potentially limiting phenomena that may arise within gas-liquid-solid reactors in addition to those occurring in the gas or liquid phase only. Apart from the adequate mixing of a single phase in the entire reactor volume, also the dispersion of the occurring phases needs to be guaranteed by the reactor hydrodynamics. Not only the 'conventional' external and the internal mass (and heat) transfer phenomena at the catalyst pellet scale need to be assessed, but also the mass and heat transfer between the fluid phases present in the reactor needs to be considered. Many empirical correlations have already been developed in this respect, nevertheless, an experimental validation particularly at industrially relevant operating conditions remains desired. In order to acquire intrinsic kinetics, the volumetric gas-liquid mass transfer coefficient must be well above the necessary limits. In what follows the evolution of k_La as a function of the agitator rotation speed in a gas-liquid CSTR at industrially relevant conditions has been investigated

Thermodynamics as well as hydrodynamics play a crucial role in the dominant phenomena. While thermodynamics are related to phenomena such as gas dissolution and liquid vaporisation, which essentially occur at the molecular level, hydrodynamics account for the mixing and dispersion phenomena, occurring at the macroscopic level.

The hydrodynamics which predominantly govern phase mixing constitute an important aspect during agitation of fluid phases. The dispersion of gas bubbles in the liquid phase is the result of inertial forces acting on the mixture induced by the agitator. The fluid flowing through the catalyst basket and around the catalyst and diluent particles is believed to provide the necessary shear for the creation of bubbles of variable sizes. This force increases with the agitator rotation speed as quantified by the Froude Number, N_{Fr}, see Eq. 3-9. This dimensionless group quantifies the ratio of the inertial to the gravitational forces and allows identifying the dominating forces at various agitator speeds.

$$N_{Fr} = \frac{N^2 D}{g} \qquad 3\text{-}9$$

The creation of bubbles in a continuous liquid phase increases the mass transfer rate between this gas and liquid by increasing the interfacial area. The agitator rotation speed affects the dynamic coalescence and breaking of bubbles and, consequently, changes $k_L a$. As long as the physical properties of the considered fluids such as density and viscosity are not changing drastically, static forces such as surface tension do not critically determine the gas liquid mass transfer coefficient [16, 37-39].

The volumetric gas-liquid mass transfer coefficient is estimated using Eq. 3-1 . The obtained F values for the global significance of the regression were exceeding the tabulated value of 3.84 at all agitator speeds, see Table 3-2. The evolution of $k_L a$ as a function of agitator speed is visualised in Figure 3-2. While initially the increase is only moderate, it increases more rapidly once a certain threshold agitator speed has been reached. This evolution can be regarded as having to overcome an initial, minimum resistance induced by the reactor internals, such as the catalyst basket consisting of concentric metal gauzes with a very fine mesh filled with inert alumina material. Once this initial resistance has been overcome, a high turbulence regime is entered wherein $k_L a$ increases more rapidly with the agitator speed. These results show that higher agitation speeds are best to attain maximum transfer within the phases involved.

Table 3-2. Estimated values of the volumetric gas-liquid mass transfer coefficient, k_La, along with their 95% confidence intervals, in a three phase bench-scale Robinson-Mahoney reactor for a H_2-Halpasol™ mixture. Eq. 3-1 was used for the estimation procedure. The tabulated F value was 3.84 for all the experimental conditions.

$N_{agitator}$ (rps)	k_La (s^{-1})			F Value
8.33	$1.26\ 10^{-2}$	±	$2.36\ 10^{-4}$	$2.50\ 10^{3}$
8.33	$1.23\ 10^{-2}$	±	$1.95\ 10^{-4}$	$3.47\ 10^{3}$
12.50	$1.36\ 10^{-2}$	±	$3.42\ 10^{-4}$	$1.39\ 10^{3}$
16.67	$1.39\ 10^{-2}$	±	$2.53\ 10^{-4}$	$2.62\ 10^{3}$
20.83	$1.74\ 10^{-2}$	±	$4.65\ 10^{-4}$	$1.21\ 10^{3}$
25.00	$2.23\ 10^{-2}$	±	$8.62\ 10^{-4}$	$5.64\ 10^{2}$

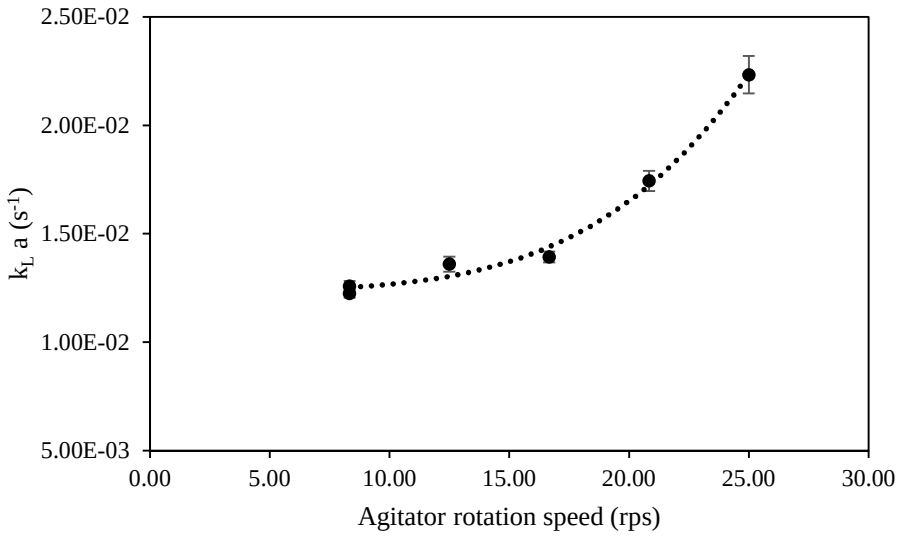

Figure 3-2. Evolution of the volumetric gas-liquid mass transfer coefficient, k_La, as a function of the agitator rotation speed in a three-phase bench-scale Robinson-Mahoney reactor for a H_2-Halpasol™ mixture. (●) parameter values obtained by regression of experimental data with Eq. 3-1, the error bars represent the 95% confidence intervals, (line) model simulated values using Eq. 3-10 and parameter values shown in Table 3-5 Other experimental conditions: T = 523 K, p = 3.0 MPa.

Table 3-3. Comparison of three-phase mixed flow reactors as encountered in the literature.

Reactor characteristics		Dietrich *et al.* [30]*	Pitault *et al.* [24]	This work
Volume	m^3	$500\ 10^{-06}$	$1100\ 10^{-06}$	$250\ 10^{-06}$
Inner diameter	m	$7.00\ 10^{-02}$	$8.00\ 10^{-02}$	$5.00\ 10^{-02}$
Inner height	m	-	$22.00\ 10^{-02}$	$13.50\ 10^{-02}$
Length of straight blades	m	-	$7.00\ 10^{-02}$	$6.30\ 10^{-02}$
Turbine diameter	m	$3.20\ 10^{-02}$	$3.00\ 10^{-02}$	$1.84\ 10^{-02}$
bottom shape	-	-	Curved	Curved

* The reactor used by Dietrich *et al*. [30] does not have a catalyst basket and is of slurry type CSTR.

Table 3-4. Experimental conditions maintained during the experimental determination of the G-L liquid volumetric mass transfer coefficient.

Experimental variable		Dietrich *et al*. [30]*	Pitault *et al*. [24]	This work
Liquid phase		Water, pure ethanol, and mixture obtained by hydrogenation of adiponitrile.	Water, gasoil	Halpasol™, Water
Gas phase		H_2	Air, H_2	H_2
Temperature range	(K)	293, 353	298	523
Pressure	(MPa)	0.01325	0.01325	3.0

* The reactor was operated in slurry mode

The mixing quality increases with the agitator speed since the Froude number, N_{Fr}, exhibits a second order dependency on this agitator rotation speed, see Eq. 3-9. The experimental measurements performed as part of this work are in agreement with what has already been published for alternative completely mixed reactor configurations, typically at (slightly) different operating conditions, see Table 3-3 and Table 3-4 respectively [24, 30].

Pitault *et al.* [24] performed experiments in two different three-phase CSTRs acquired from two suppliers, a first one from Autoclave Engineers (AE) and a second one from Parr instrument company. While the AE reactor was used for air-water mixtures, the Parr reactor was used for H_2-gasoil mixtures. All experimentation was performed at 298K and atmospheric pressure. At the investigated operating conditions k_La varied from 2.65 $x10^{-3}$ to 7.91 10^{-2} s^{-1}

with agitator speeds from 8.33 to 25 rps for the AE reactor at high inlet gas flow rates, *i.e.,* 18 Nl h^{-1} while it varied from 2.93 10^{-3} to 6.41 10^{-2} s^{-1} for agitator speeds from 8.33 to 29.16 rps at low inlet gas flow rates *i.e.,* 3.6 Nl h^{-1} [24]. On the other hand, k_La as measured in the Parr reactor varied between 1.29 10^{-3} to 4.28 10^{-2} for agitator speeds of 8.33 to 29.16 rps. Our results are in in the same order of magnitude as those reported by Pitault *et al.* [24], albeit that the variation with the agitator speed is less pronounced in our case. In addition to a difference in temperature, also the use of a gas inducing impeller in the Parr reactor may have led to a more pronounced dependence of the gas-liquid mass transfer coefficient on the agitator speed. Nevertheless, the sufficiently high k_La already achieved at low agitator speeds in our work eliminates the need for a more advanced impeller design.

Dietrich *et al.* [30] report k_La values between 0.2 to 2.4 s^{-1} for a 500 10^{-6} m^3 slurry reactor operated with agitator speeds amounting from 15 to 37.5 rps The results were obtained for a H_2-water mixture with a non-pyrophoric Ni catalyst dispersed in water. Their gas-liquid mass transfer coefficients are exceeding the ones reported by Pitault *et al.* [24] and those found in our work by at least one order of magnitude. Their higher value can be attributed to the catalyst being present as a slurry of finely dispersed particles. The movement of the catalyst particles along with the fluid mixture induces stretching, break-up and coalescence of the bubbles and, hence, result in an increased interfacial area and, correspondingly, enhanced mass transfer. Another effect that potentially contributes to the higher k_La as observed by Dietrich *et al.* [30] is the so-called 'shuttle mechanism' according to which gas adsorbed on the catalyst particles at the gas-liquid interface is transported and released in the bulk liquid phase. Additionally the catalyst particle size used by Dietrich *et al.* [30] was much lower compared to that used in our work, *i.e.,* 10 to 15 µm compared to 500 µm, which could also induce additional surface area between the gas and the liquid phase.

In order to describe the variation of the k_La with agitator rotation speed an equation consisting of three parameters is proposed, see Eq. 3-10.

$$k_l a = C_1 N_{agitator}{}^{C_2} + C_3 \qquad 3\text{-}10$$

The parameters C_1 and C_2 can be denoted as the 'agitator parameters' which potentially depend on the agitator type used, while parameter C_3 corresponds to the volumetric gas-liquid mass transfer coefficient in the absence of stirring. For a the H_2-gasoil mixture in the Parr reactor Pitault et al. [24], propose the dependency of volumetric gas-liquid mass transfer according to the following correlation $k_La \propto N_{agitator}{}^{3.4}$. Because preliminary regressions indicated that it was impossible to estimate C_1 and C_2 simultaneously, the latter was fixed at

the value as determined by Pitault *et al.* [24], *i.e.*, 3.4, and the remaining two model parameters were estimated by regression, see Table 3-5. The global regression was significant, as evident from a calculated *F*-value exceeding the tabulated one. The volumetric gas-liquid mass transfer coefficient in the absence of stirring, *i.e.*, C_3 amounts to $1.21\ 10^{-2} \pm 0.07\ 10^{-2}\ s^{-1}$ which is close to the mass transfer coefficient experimentally observed at an agitator speed of 8.33 rps. This means that stirring at low agitator rotation speeds does not significantly increase the mass transfer, as evident indeed from the rather low value of the agitator dependent scaling parameter C_1.

Table 3-5. Agitator parameters along with their 95% confidence intervals for a Robinson-Mahoney three-phase bench-scale reactor, calculated with a H_2-Halpasol™ mixture. The *F* value of the regression amounted to 332 while the tabulated *F* value amounted to 7.7. The binary correlation coefficient amounted to 0.7.

Constant	Parameter estimates		
C_1	$1.77\ 10^{-7}$	±	$0.27\ 10^{-7}$
C_2*		3.4	
C_3	$1.21\ 10^{-2}$	±	$0.07\ 10^{-2}$

* Value proposed by Pitault *et al.* [24]

3.4 Liquid hold up

The gas and liquid in the reactor are assumed to be in thermodynamic equilibrium and, hence, in principle, the gas dissolution and liquid vaporisation equilibrium can be calculated by making use of a conventional simulation package, such as AspenPlus. In such calculations the thermodynamic equilibrium is assessed as the one established in a closed system comprising amounts of gas and liquid that are proportional to the feed flow rates. While these thermodynamic models satisfactorily reproduce the internal composition of the individual gas and liquid, their accountability on the gas liquid distribution within the reactor is not established. In practice, unrealistically low liquid hold-ups are calculated [4]. Hence, complementary experimental evidence is pursued to determine the actual volumes in the reactor occupied by gas and liquid.

As explained in Section 3.2.2, the liquid hold-up was determined from step and impulse response measurements of a tracer input at with a H_2-Halpasol™ at industrially relevant as well as with H_2-water mixture at atmospheric pressure and room temperature. The industrially

'relevant' conditions varied in the following ranges, *i.e.*, temperatures between 523 and 583 K, total pressures between 2.5 and 5.5 MPa and inlet volumetric H_2-Halpasol™ ratios between 5 and 250 $m^3 m^{-3}$. A potential impact of the agitator speed on the gas and liquid hold-up [24] was not specifically assessed as the guidelines used for kinetics measurements indicate a single value amounting to 25 rps, see below. The quantification of the gas and liquid hold-up will provide a clear view on which of both phases can be considered as the continuous one, respectively the dispersed one. The comparison of the data acquired at ambient and industrially relevant conditions will provide a basis for the extrapolation potential starting from the data acquired at ambient conditions to those at the more relevant conditions.

3.4.1 Step input of C_{10} tracer at industrially relevant condition

As explained in section 3.2.2.1, the response at the set-up outlet for an abrupt step increase of the tracer concentration at the reactor inlet was monitored. A typical evolution in the relative tracer concentration at the set-up outlet is shown in Figure 3-3. The exponential decrease of the relative tracer concentration is characteristic for ideal CSTR behavior. Parameter estimation making use of Eq. 3-6 to determine the liquid hold-up and the lag time resulted in the model parameters shown in Table 3-6. Since a constant liquid volumetric flow rate of 0.04 $x10^{-6}$ m^3 s^{-1} was used, a single lag time is considered to describe all experiments. The experimentally observed lag time, t_{lag}, of the set-up, *i.e.*, 1080 s was fixed during the estimation of the liquid hold-up at different experimental conditions.

Table 3-6. Estimated hold-up *i.e.*, ε_L, see Eq. 3-6, along with their 95% confidence intervals for the three-phase bench-scale Robinson-Mahoney reactor set-up with H_2-Halpasol™ mixture at industrially relevant conditions. Experiments were performed by introducing a step change of a tracer *i.e.*, *n*-C_{10} to a reactor operating at steady state conditions. t_{lag} of the set-up amounted to 1080 s. The *F* value for the total regression amounted to 274 and a corresponding tabulated *F* value of 4.

Experimental condition			ε_L
Pressure MPa	Temperature K	Volumetric inlet H_2-Halpasol™ ratio $m^3\ m^{-3}$	
2.5	523	18.75	0.72 ± 0.11
4	523	18.75	0.72 ± 0.12
5.5	523	18.75	0.66 ± 0.11
4	523	18.75	0.66 ± 0.12
4	553	18.75	0.67 ± 0.11
4	583	18.75	0.65 ± 0.11
4	523	6.75	1.00 ± 0.07
4	523	62.5	0.72 ± 0.12
4	523	250	0.49 ± 0.10

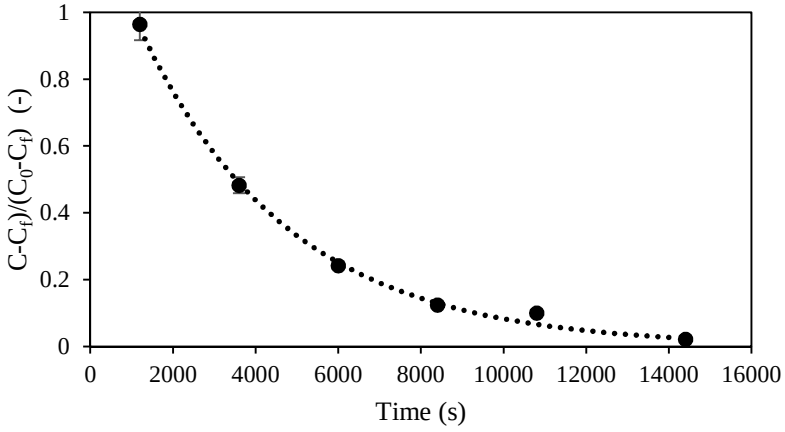

Figure 3-3. Evolution of the tracer concentration as a function of the sampling time, $t_{sampling}$, as observed in a three-phase bench-scale Robinson-Mahoney reactor. Operating conditions: T: 583 K, P: 4.0 MPa, Volumetric inlet H_2-Halpasol™ ratio: 18.75 $m^3\ m^{-3}$. (●) Experimentally obtained values (line) model simulated values by using Eq. 3-6 and parameters shown in Table 3-6. t_{lag} of the set-up amounted to 1080 s.

3.4.1.1 Temperature effect

Experiments to measure the liquid hold-up at different temperatures were performed between 523 and 583K. The total pressure and inlet H_2-Halpasol™ ratio were fixed at 4.0 MPa and 18.75 m^3/m^3 respectively. No significant change in liquid hold-up was observed with varying temperature, see Figure 3-4. This is attributed to the minor change in vapour pressure, c.q., volatility, of the liquid used in this temperature range.

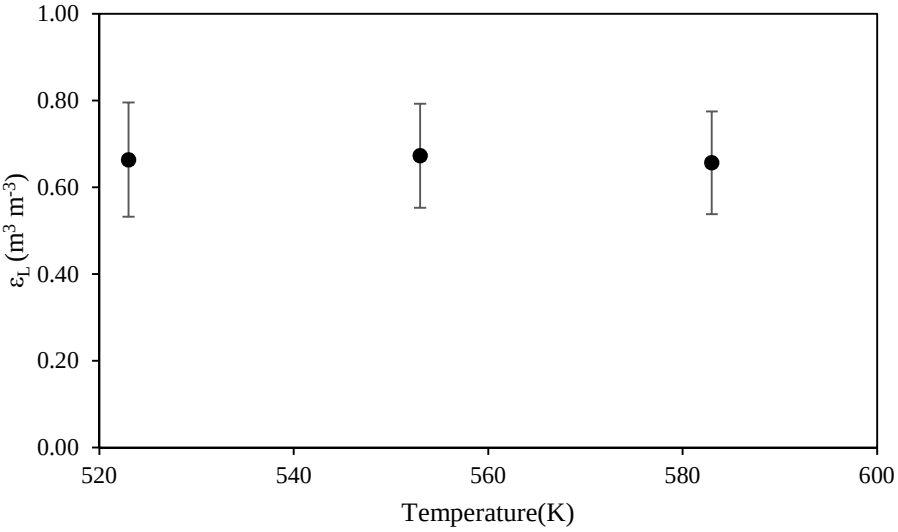

Figure 3-4 Liquid hold-up, ε_L, as a function of the temperature in a RM reactor at 4.0 MPa and volumetric inlet H_2-Halpasol™ ratio: 18.75 m^3 m^{-3}. Values of liquid hold-up estimated by the regression of experimental data along with the model equation 3-6. t_{lag} of the set-up amounted to 1080 s. Error bars represent 95% confidence interval values.

3.4.1.2 Total pressure effect

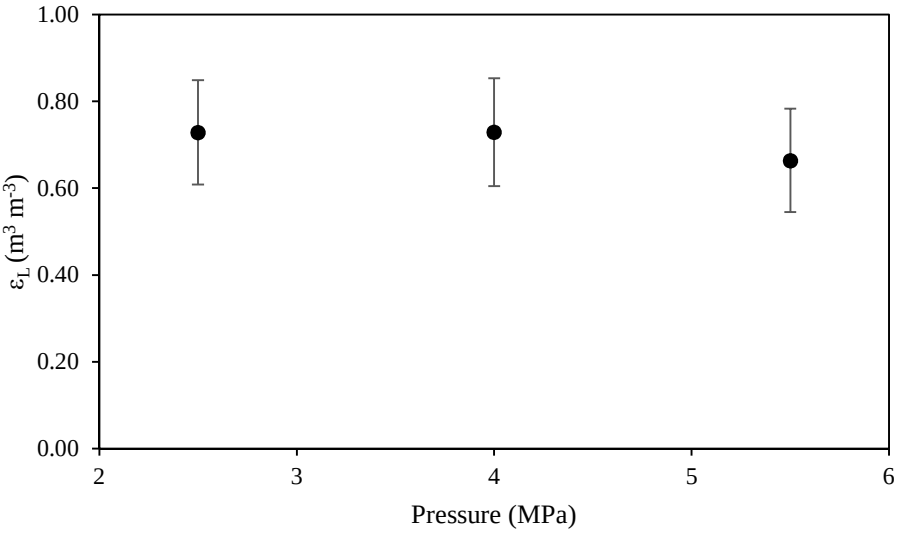

Figure 3-5 Liquid hold-up, ε_L, as a function of the total pressure in a RM reactor at 523 K and volumetric inlet H_2-Halpasol™ ratio:18.75 m^3/m^3. Values of liquid hold-up estimated by the regression of experimental data along with the model equation 3-6. t_{lag} of the set-up amounted to 1080 s. Error bars represent 95% confidence interval values.

Experiments were performed at varying total pressure between 2.5 and 5.5 MPa. The temperature and inlet H_2-Halpasol™ ratio were fixed at 523K and 18.75 $m^3\,m^{-3}$ respectively No significant change in the liquid hold-up was observed, showing that the liquid was non compressible and that the gas phase density had no significant impact on the results in the investigated range of total pressures.

3.4.1.3 Inlet H_2/Halpasol™ effect

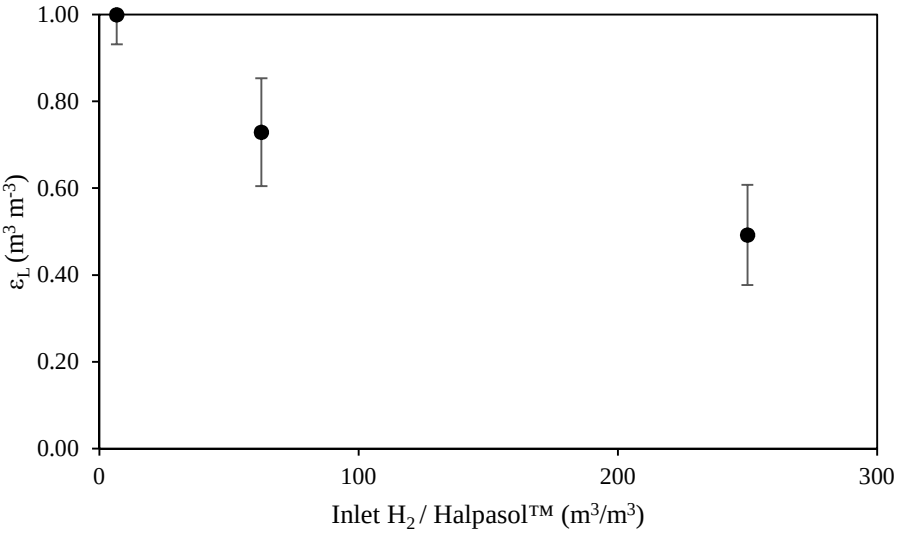

Figure 3-6. Liquid hold-up, ε_L, dependency in a H_2-Halpasol™ mixture for a RM reactor. Other experimental conditions: Pressure = 4.0 MPa and Temperature = 553 K. Values of liquid hold-up estimated by the regression of experimental data along with the model equation 3-6. t_{lag} of the set-up amounted to 1080 s. Error bars represent 95% confidence interval values.

At varying inlet H_2/Halpasol ratio from 5 to 280 m^3 m^{-3}, by systematically increasing the gas flow rate, while keeping the liquid flow rate constant, the liquid hold-up was observed to decrease by about 50 %. At very low inlet H_2/Halpasol™ ratio, *i.e.*, about 5 m^3 m^{-3} the liquid hold-up in the reactor is close to unity showing that the reactor is completely filled with liquid. As this inlet ratio increases the liquid hold-up in the reactor decreases. Initially being more pronounced, the decrease in liquid hold-up in the reactor levels of at higher values of the volumetric inlet H_2-Halpasol™ ratio. The evolution of the phase distribution in the reactor with increasing inlet H_2-Halpasol™ ratio can be envisaged as a transition from a reactor which is completely filled with liquid over one with dispersed gas bubbles in a continuous liquid to a reactor in which both gas and liquid comprise significant fractions of the volume. This experimentally determined liquid hold-up in the reactor is clearly distinct from the one obtained using gas-liquid equilibrium calculations with the gas and liquid feed flow rates as input, *i.e.*, about 70% compared to practically 0, at typical relevant experimental conditions, see Figure 3-4 and Figure 3-5. Given the limited volatility of the liquid that is considered and the gas solubility reaching its saturation, a limited impact on the internal phase composition can be understood, however, to adequately simulate the gas and liquid hold-up in the reactor, the liquid accumulation needs to be accounted for.

3.4.2 Impulse input of methylene blue at ambient conditions

Impulse input experiments with methylene blue and water were performed to assess the liquid hold-up at ambient conditions. As explained in Section 3.2.2.2, a similar data treatment as in the step response measurements was performed. Model Eq. 3-7 was subjected to regression analysis against the experimental data to estimate the lag time and liquid hold-up at different inlet volumetric H_2-water ratios. The liquid hold-up evolution with the volumetric inlet H_2-water ratio and the corresponding 95 % confidence intervals is presented in Figure 3-7. The lag time of the set-up was not significantly different from 0 s which is in line with the experimental observations. It confirms that, in the cold flow set-up with the use of high water flow rates and the injection and sampling port being situated close to the reactor inlet and outlet, respectively, the non-reactive plug flow zones could be safely ignored in the impulse response experiments.

Table 3-7. Estimated liquid hold-up , ε_L, along with their 95% confidence intervals for the three-phase bench-scale Robinson-Mahoney reactor set-up with H_2 and water mixture at ambient conditions. Experiments were conducted by injecting an impulse of tracer *i.e.*, methylene blue to a reactor operating at steady state conditions. The *F* value for the total regression amounted to 562 and a corresponding tabulated *F* value of 4.75.

Inlet volumetric H_2-water ratio ($m^3\ m^{-3}$)	ε_L		
0	1.00	±	0.15
280	0.80	±	0.17
580	0.62	±	0.19

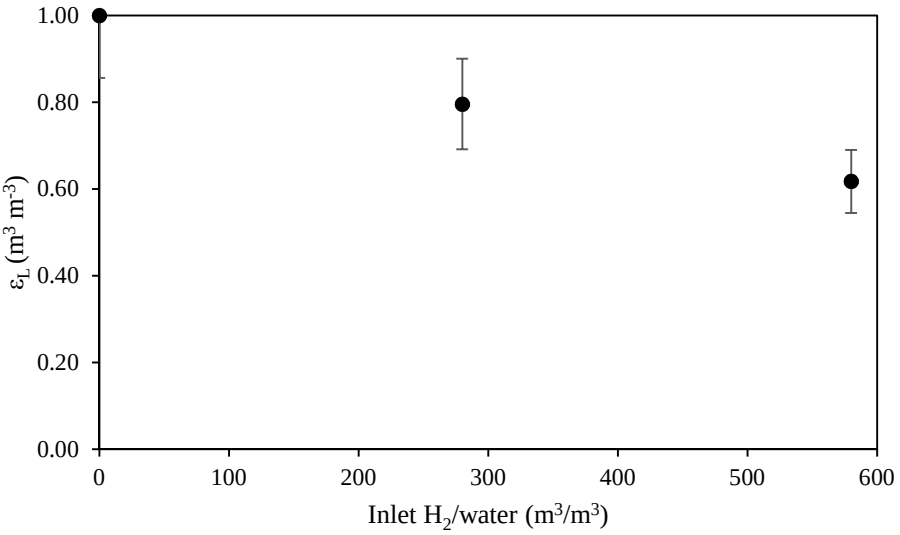

Figure 3-7. Liquid hold-up, ε_L, dependency with volumetric inlet gas-liquid ratio in a H_2-water mixture for a Robinson-Mahoney reactor at ambient conditions *i.e.*, T=298K and P=0.101 MPa. The liquid hold-up estimated as parameters by using Eq. 3-7. Error bars showing 95% confidence intervals of the parameters.

Similar to the liquid hold-up measured at industrially relevant operating conditions using the step response technique, experiments with the injection of a tracer impulse at ambient conditions exhibit a decrease in the liquid hold-up with increasing volumetric inlet H_2-water ratio. For the H_2-water mixture at ambient conditions, the inlet gas-water ratio required to achieve a similar reduction of in the liquid hold-up amounted to about 580 m^3 m^{-3}, *i.e.*, more than the double of the ratio required at industrially relevant operating conditions with a H_2-Halpasol™ mixture, see also Section 3.4.3. At ambient conditions it was visually observed that the number and the size of the gas bubbles increased with increasing inlet gas flow rates.

Very few data are available in the literature with respect to liquid hold-up in three phase CSTRs. Moreover, most of what is reported, if not all, refers to results acquired at ambient conditions [24, 27-29]. Pitault *et al.* [24] reported liquid hold-ups in the range of 90% at an air –water mixture for volumetric gas flow rates of 10^{-6} to 5 10^{-6} m^3 s^{-1}. The liquid hold-up was found to decrease with the agitator speed, as could be expected because of the better gas dispersion within the liquid. Also the use of a gas inducing impeller reduced the liquid hold-up in the reactor. Total gas hold-up of less than 10% was reported for both Autoclave Engineers manufactured Robinson-Mahoney reactor and Parr company manufactured Robinson-Mahoney reactor. For an air-water mixture, Yawalkar *et al.* [27] reported a liquid hold-up in the range of 80% for a CSTR with inlet volumetric gas flow rate of 1 10^{-3} to 4 10^{-3} m^3 s^{-1}.

Yawalkar *et al.* [27] also suggest that the turbulence generated by the agitator and the inlet gas flow rates assist in increasing the gas hold-up within the reactor.

3.4.3 Industrially relevant versus ambient conditions and determination of dispersed phase

While an inlet volumetric ratio 250 $m^3\ m^{-3}$ of gas to liquid was sufficient to decrease the liquid hold-up by 50% for H_2-Halpasol™ mixtures at relevant operating conditions, a volumetric ratio amounting to 580 $m^3\ m^{-3}$ was necessary to reduce the liquid hold-up to a similar extent for the H_2-water mixture at ambient conditions. Since it was observed that the pressure and the temperature did not have any significant effect on the liquid hold-up, an explanation for this difference was sought in the liquid phase physical properties. Additionally, the absence of the catalyst basket in the cold flow reactor may have impacted on the internal reactor hydrodynamics and potentially be responsible for the observed changes, *i.e.,* the presence of a filled catalyst basket may cause additional gas bubble coalescence and break-up, resulting in enhanced gas hold-up in the reactor. Differences in gas hold-up and, hence, also liquid hold-up, have also already been interpreted in terms of liquid phase viscosity and surface tension, among others, [16, 39] for both plug flow and mixed flow reactors.

In the present work, the differences in liquid phase physical properties along with the presence of reactor internals in the case of the measurements at relevant conditions are indeed believed to explain the observed differences. The lower surface tension of Halpasol™ compared to water, *i.e.,* 23.0 versus 72.5 mN m^{-1}, results in a much more stable gas bubble formation in Halpasol™ and comparatively more bubble coalescence in case of the H_2-water mixture. The higher surface tension in the case of water is, hence, in line with the higher liquid hold-up that was observed when using water and the correspondingly higher required gas to liquid inlet flow rate ratio to attain the same liquid hold up in comparison to the H_2-Halpasol mixture [16]. This difference in liquid surface tension, along with the earlier mentioned presence of reactor internals at industrially relevant conditions results in a comparatively lower liquid hold-up at industrially relevant conditions.

3.5 Conclusions

Experimental studies for calculating the volumetric gas-liquid mass transfer coefficient, k_La, and liquid hold-up, ε_L, for a three-phase bench-scale Robison-Mahoney reactor were performed at industrially relevant as well as at ambient operating conditions. Experiments were performed using H_2 and Halpasol™ at high temperature and pressure for the first time to mimic

the conditions encountered in an industrially relevant environment. Experimental results showed that k_La depends on the agitator speed according to the following correlation $k_La = 1.77\ 10^{-7} * N_{agitator}{}^{3.4} + 1.21\ 10^{-2}$. This correlation is in line with earlier reported correlations based on less relevant gas liquid mixtures and operating conditions.

The liquid hold-up of a low-volatility liquid did not exhibit any variations with temperature and pressure suggesting no significant impact of liquid vaporisation nor gas compression. The most influential factor on the liquid hold-up appeared to be the inlet volumetric gas-liquid ratio. It resulted in a 50 % decrease of the liquid hold-up with the inlet H_2/Halpasol™ ratio increasing from 5 to 250 $m^3\ m^{-3}$ at relevant operating conditions while a volumetric inlet gas-liquid ratio of about 580 $m^3\ m^{-3}$ was required to reduce the liquid hold-up to a similar percentage at ambient conditions with water as the liquid phase. Irrespective of the operating conditions used, including the feed composition, it was observed that with increasing inlet gas-liquid ratio, the phase distribution within the reactor evolves from being completely filled with liquid over a continuous liquid phase with a dispersed gas phase to a practically equal distribution between gas and liquid phase at volumetric inlet gas flow rates exceeding that of the liquid by at least two orders of magnitude.

3.6 References

1. Stanislaus, A., A. Marafi, and M.S. Rana, **Catalysis Today**, 2010. 153(1-2): p. 1-68.

2. Thybaut, J.W., C.S.L. Narasimhan, and G.B. Marin, **Catalysis Today**, 2006. 111(1-2): p. 94-102.

3. Romero, C.M.C., J.W. Thybaut, and G.B. Marin, **Catalysis Today**, 2008. 130(1): p. 231-242.

4. Raghuveer, C.S., J.W. Thybaut, R. De Bruycker, K. Metaxas, T. Bera, and G.B. Marin, **Fuel**, 2014. 125(0): p. 206-218.

5. Craciun, I., M.F. Reyniers, and G.B. Marin, **Journal of Catalysis**, 2012. 294: p. 136-150.

6. Craciun, I., M.F. Reyniers, and G.B. Marin, **Journal of Molecular Catalysis A: Chemical**, 2007. 277(1-2): p. 1-14.

7. Froment, G.F., L.C. Castaneda-Lopez, and C. Marin-Rosas, **Catalysis Today**, 2008. 130(2-4): p. 446-454.

8. Shah, Y.T., *Gas-liquid-solid reactor design*. 1979, New York: McGraw-Hill International Book Co. x, 373 p.

9. Ramachandran, P.A. and R.V. Chaudhari, *Three-phase catalytic reactors*. Topics in chemical engineering,. 1983, New York: Gordon and Breach Science Publishers. xii, 427 p.

10. Dudukovic, M.P., F. Larachi, and P.L. Mills, **Chemical Engineering Science**, 1999. 54(13-14): p. 1975-1995.

11. Meeuwse, M., E. Hamming, J. van der Schaaf, and J.C. Schouten, **Chemical Engineering and Processing**, 2011. 50(10): p. 1095-1107.

12. Meeuwse, M., J. van der Schaaf, B.F.M. Kuster, and J.C. Schouten, **Chemical Engineering Science**, 2010. 65(1): p. 466-471.

13. van Eeten, K.M.P., R. Verzicco, J. van der Schaaf, G.J.F. van Heijst, and J.C. Schouten, **Chemical Engineering Science**, 2015. 129: p. 14-24.

14. Froment, G.F., **Applied Catalysis**, 1986. 22(1): p. 3-20.

15. Froment, G.F., **Chemie Ingenieur Technik**, 1974. 46(9): p. 374-386.

16. Pangarkar, V.G., *Design of multiphase reactors*. 2014, Wiley,: Hoboken, New Jersey. p. 1 online resource.

17. Mahoney, J.A., K.K. Robinson, and E.C. Myers, **Chemtech**, 1978. 8(12): p. 758-763.

18. Lopez-Salinas, E., J.G. Espinosa, J.G. Hernandez-Cortez, J. Sanchez-Valente, and J. Nagira, **Catalysis Today**, 2005. 109(1-4): p. 69-75.

19. Bunch, A., L. Zhang, G. Karakas, and U.S. Ozkan, **Applied Catalysis A: General**, 2000. 190(1-2): p. 51-60.

20. Froment, G.F., **Catalysis Today**, 2004. 98(1-2): p. 43-54.

21. Santana, A., M.A. Larrayoz, E. Ramirez, J. Nistal, and F. Recasens, **Journal of Supercritical Fluids**, 2007. 41(3): p. 391-403.

22. *http://www.autoclave.com/*. 2015.

23. Magnico, P. and P. Fongarland, **Chemical Engineering Science**, 2006. 61(4): p. 1217-1236.

24. Pitault, I., P. Fongarland, D. Koepke, M. Mitrovic, D. Ronze, and M. Forissier, **Chemical Engineering Science**, 2005. 60(22): p. 6240-6253.

25. Pitault, I., P. Fongarland, M. Mitrovic, D. Ronze, and M. Forissier, **Catalysis Today**, 2004. 98(1-2): p. 31-42.

26. Mitrovic, M., I. Pitault, M. Forissier, S. Simoens, and D. Ronze, **AIChE Journal**, 2005. 51(6): p. 1747-1757.

27. Yawalkar, A.A., V.G. Pangarkar, and A.A.C.M. Beenackers, **Canadian Journal of Chemical Engineering**, 2002. 80(1): p. 158-166.

28. Yawalkar, A.A., A.B.M. Heesink, G.F. Versteeg, and V.G. Pangarkar, **Canadian Journal of Chemical Engineering**, 2002. 80(5): p. 791-799.

29. Yawalkar, A.A., A.B.M. Heesink, G.F. Versteeg, and V.G. Pangarkar, **Canadian Journal of Chemical Engineering**, 2002. 80(5): p. 840-848.

30. Dietrich, E., C. Mathieu, H. Delmas, and J. Jenck, **Chemical Engineering Science**, 1992. 47(13-14): p. 3597-3604.

31. Chaudhari, R.V., R.V. Gholap, G. Emig, and H. Hofmann, **Canadian Journal of Chemical Engineering**, 1987. 65(5): p. 744-751.

32. Al-Dahhan, M. and W. Highfill, **Canadian Journal of Chemical Engineering**, 1999. 77(4): p. 759-765.

33. Hoernaert, J., *Hydrodesulfurisatie op een CoMo/γ-Al_2O_3 katalysator in tubulaire en gradientloze reaktoren*. 1988, Rijksuniverseteit Gent.

34. Stewart, W.E. and M. Caracotsios, *Computer-Aided Modelling of Reactive Systems*. 2008, Hoboken, NJ: Wiley-Interscience.

35. Toch, K., J.W. Thybaut, and G.B. Marin, **AIChE Journal**, 2015. 61(3): p. 880-892.

36. Berger, R.J., E.H. Stitt, G.B. Marin, F. Kapteijn, and J.A. Moulijn, **Cattech**, 2001. 5(1): p. 30-60.

37. Dursun, G., R. Orhan, and C. Akosman, **Journal of Chemical Technology and Biotechnology**, 2003. 78(4): p. 446-451.

38. Dursun, G. and C. Akosman, **Journal of Chemical Technology and Biotechnology**, 2006. 81(12): p. 1859-1865.

39. Akosman, C., R. Orhan, and G. Dursun, **Chemical Engineering and Processing**, 2004. 43(4): p. 503-509.

This page intentionally left blank

4 Pyridine hydrodenitrogenation kinetics over a sulphided NiMo/γ-Al_2O_3 catalyst

Gas phase pyridine hydrodenitrogenation (HDN) kinetics have been determined over a commercial, sulphided NiMo/γ-Al_2O_3 catalyst in a Berty type Continuous Stirred Tank Reactor (CSTR). Temperatures and total pressures varied from 573 to 633 K and from 1.5 to 4.0 MPa, in a space time range from 350 to 1800 kg_{cat} s mol^{-1}_P. Pyridine was first hydrogenated into piperidine. The subsequent denitrogenation went via piperidine ring opening to pentyl amine followed by the actual nitrogen removal, yielding C_5 hydrocarbons and ammonia as end products. The C-N bond scission rate was enhanced by the presence of H_2S, which could be rationalized based on a substitution mechanism. Langmuir Hinshelwood reaction mechanisms accounting for two types of sites, *i.e.*, coordinatively unsaturated sites (*) and sulphur anions (S^{2-}), have been developed to assess the experimentally measured kinetics. These models explicitly accounted for the substitution mechanism in the C-N bond scission in terms of elementary steps. Model discrimination has allowed assessing the importance of hydrogen addition to pyridine through heterolytically or homolytically chemisorbed hydrogen and hydrogen sulphide, as well as of sulphydril or hydrogen assisted C-N bond scission in piperidine denitrogenation. Chemisorption entropies were calculated a priori such that, in addition to the kinetic parameters, only chemisorption enthalpies had to be estimated by regression. The third hydrogen addition and the naphthenic C-N bond breaking were found to be rate determining in pyridine hydrogenation and piperidine denitrogenation, with activation energies amounting to 41 kJ mol^{-1} and 185 kJ mol^{-1}. A distinct linear relationship was

established between the proton affinity of the various nitrogen components and their free energy of chemisorption.

4.1 Introduction

The awareness related to the environmental impact of fossil fuel production and use has continuously risen during last decades [1-5]. This is reflected at present in the evermore stringent regulations that are enforced by governments all around the globe [6]. Academia as well as industry have focused on finding alternative energy vectors while existing process innovation and technology enhancement have also received considerable attention. Hydrodesulphurisation has been of primary interest in this respect, since sulphur is the most abundant heteroatom present in crude oil. With the advent of ultralow sulphur fuels, exhibiting sulphur levels below 10 ppm, as well as of feeds of a renewable origin such as from algae oils, there is an increasing interest in the removal of other heteroatoms, such as nitrogen, and their impact on hydrodesulphurisation. More specifically, the removal of the final sulphur traces has been found to largely depend on the amounts and types of nitrogen components in the feed [4, 7].

The interaction between a nitrogen containing component and the active site depends on its molecular characteristics. Nitrogen containing molecules can be classified in two ways: *structurally*, as 'heterocyclic', in which the nitrogen atom is inside a ring, or 'non heterocyclic' and *chemically*, as 'basic' or 'non-basic' depending on the electronic configuration of the nitrogen atom involved. The nitrogen in pyridine like components is contained in the aromatic ring together with 5 carbon atoms and is bonded to these neighbouring carbon atoms *via* sp^2 orbitals by providing an electron each to the π cloud, the third sp^2 orbital of the carbon atoms in the ring forms a bond with a hydrogen atom whereas the third sp^2 orbital of the nitrogen atom contains a pair of electrons, available for sharing and providing pyridine with its basic character. On the other hand, the 'free' electron pair on the nitrogen in pyrrole is required for establishing the aromatic π cloud via the overlap of two *p* orbitals and, hence, is unavailable for sharing turning pyrrole into a weak base [8, 9].

Over the years advanced analytical techniques enabled the determination of the detailed composition of crude oil and typical hydrotreating feeds originating from different sources [10-13]. Generally the total nitrogen content varied in the range from 500 to 2500 ppm [14, 15]. A more detailed composition analysis such as reported by Adam *et al.* [10, 12] has shown varying amounts of basic and neutral nitrogen components within this total nitrogen content. Due to the inhibiting effect of nitrogen components, particularly of the basic ones, on the

chemisorption and further reaction of sulphur components [3, 16-21], the former can jeopardize the fuel quality that can be achieved by 'conventional' hydrotreatment processes. Moreover, insufficient "basic" nitrogen removal potentially results in a devastating effect on the acid catalyst in subsequent conversion or cracking units [22].

Experimental [23-27], *i.e.*, EXAFS, STM, FTIR, as well as theoretical *i.e.*, DFT [28-35] investigations have significantly improved the understanding of the active sites on hydrotreating catalysts in terms of their location, electronic properties, number and nature of promoted MoS_2 nanocrystallites. Active phase structures for sulphided hydrotreating catalysts have been presented by Topsøe *et al.* [36, 37]. The alumina support normally used for hydrotreating catalysts, allows a high dispersion of the stable, unpromoted MoS_2 nano crystals. When a promoter such as Co or Ni is added during the synthesis, the metal edges of the MoS_2 structures are further stabilised by the incorporation of Ni/Co, instead of Mo only [37]. The active sites are believed to be located at or near the edges of the nano crystallites and exhibit either a Lewis nature, corresponding with sulphur vacancies associated with Mo or the NiMo or a Brønsted nature under the form of –SH groups [29, 38, 39]. Hydrogen activation and changes in the MoS_2 active phase morphology at different sulpho-reductive conditions have been a topic of interest, recently [35, 40-42]. Detailed experimental studies by Schachtl *et al*. [40] and Gutierrez *et al*. [41] have provided insights in the stability of surface species and the corresponding H_2 activation on the edges of the MoS_2 nanostructures. DFT calculations by Prodhomme *et al*. [35] and Raybaud *et al*. [39] revealed that the morphology of the MoS_2 is a function of the temperature and pH_2S/pH_2. The kinetic experiments used in the present work however have been performed at conditions in which the amount of sulphur to which the catalyst has been exposed is changing less significantly. Hence, the time scale of the desired hydrocarbon conversion reactions, c.q., hydrodenitrogenation, is significantly shorter than that of the catalyst structural changes. It allows decoupling of the hydrocarbon conversion kinetics from those of the catalyst structural changes and, hence, justifies the assumption that no interconversion of active sites occurs within the considered experimental data [43].

HDN of various model components has been studied on different catalysts at gas and liquid phase conditions [44-51]. Although an adequate understanding of the HDN kinetics has already been pursued, specific features such as explaining the H_2S promotional effect on C-N bond scission in terms of elementary steps, accounting for the type of hydrogen and hydrogen sulphide dissociation and correlations between components' chemisorption properties and their proton affinity still remain to be explored. Recent developments in catalyst technology and understanding, DFT calculations, modelling methodologies have allowed the construction of a

correspondingly more detailed kinetics model. Pyridine hydrodenitrogenation data obtained by Pille and Froment [46] are used for this purpose. The original model assumptions made by these authors have been assessed against the more recent literature [26, 27, 34, 39, 42, 47, 48, 52-55] and more recent work on naphthalene hydrogenation by our group in particular [43]. Pyridine HDN kinetics have typically been simulated using models with two types of sites [46, 56] or in some cases even three types of sites [47]. Pille and Froment [46] considered two types of sites, *i.e.,* * and S^{2-} sites, in their kinetic model, which sufficed to avoid any significant or systematic deviations between the experimental observations and the model simulations. Also Romero *et al.* [43] have successfully described naphthalene hydrogenation over an industrial NiMo catalyst by assuming two types of sites. In the present work, a model considering * and S^{2-} is further elaborated. This two type of site assumption, along with that of homolytic or heterolytic dissociative H_2 and H_2S chemisorption on the catalyst surface, is expected to provide the model with the necessary flexibility to adequately simulate both the hydrogenation and denitrogenation reaction via appropriate sulphur and hydrogen surface concentrations. As indicated above, the most important distinctions in comparison to the previous work lie in the consideration of heterolytically and homolytically chemisorbing H_2 and H_2S, atomic and molecular addition of H_2 to the aromatic ring and a mechanistic explanation of the HDN enhancement by H_2S.

4.2 Procedures

Gas phase pyridine hydrodenitrogenation was investigated over an industrial NiMo/γ-Al_2O_3 catalyst [46]. The operating conditions comprised temperatures and total pressures ranging from 573 to 633 K and from 1.5 to 4.0 MPa. The molar inlet hydrogen to pyridine and hydrogen sulphide to pyridine ratio was 80 to 600 (mol mol^{-1}) and 1 to 16 (mol mol^{-1}) respectively. The space time was varied between 350 and 1800 kg_{cat} s $mol^{-1}{}_P$. The experiments have been performed in a Berty type CSTR with a fixed catalyst basket and a volumetric capacity of 200ml, excluding the reactor internals. The pyridine dissolved in hexane as solvent is evaporated and mixed with the hydrogen and hydrogen sulphide gases before feeding into the reactor. The product analysis is done online using a Chrompack gas chromatograph equipped with an FID and CP sil5CB column.

4.2.1 Equilibrium and kinetic regime verifications

Pyridine hydrogenation to piperidine, which is the first step of pyridine hydrodenitrogenation is potentially equilibrium limited at the investigated operating conditions

[40]. The affinities of the pyridine hydrogenation reaction can be calculated at various operating conditions to verify the equilibrium limitations by equation 4-1. At the investigated conditions, the reaction affinity (A) was always above 1 10^9 (kJ mol^{-1}) which shows that pyridine hydrogenation is not equilibrium limited.

$$\exp\left(-\frac{A}{RT}\right) = K\left[\frac{p_P p_{H_2}^3}{p_{pp}}\right] \qquad 4\text{-}1$$

The absence of mass and heat transfer limitations was verified, in particular for the experiments where the observed reaction rate was high [41]. The maximum temperature gradient in the catalyst particles was found to be 0.7 K at the highest reaction rate using the Prater criterion [42]. External mass transfer limitations were reduced by having high agitation speeds, typically between 20.83 to 25 rps. Internal diffusion limitations were assessed using the Weisz and Prater criterion [42]. The maximum Weisz modulus was found to be 0.016 which is well below the threshold value of 0.08. It could, hence, be concluded that the acquired data were free from transport limitations and, hence, situated in the intrinsic kinetics regime. The catalyst stability and repeatability of experimental results were verified by repeated experimentation at reference operating conditions. The experimental error amounted to maximum 5%.

4.2.2 Model simulation and parameter estimation procedure

The piperidine (PP) and pentane (C_5) molar outlet flow rates were calculated from a CSTR mass balance, as presented in chapter 2.

Parameter estimation was performed by minimisation of the sum of squared residuals between the experimental and model calculated molar product outlet flow rates of piperidine and pentane. The objective function and the solution routines in the parameter estimation are explained in chapter 2.

The objective function used in this work considers the molar outlet flow rates of piperidine and pentane as responses. This is different from the objective function used by Pille and Froment [28] wherein pyridine conversion and piperidine and pentane yields are used as the responses. Although not the main aim of the present work, the differences in responses considered may result in subtle differences in modelling results since experiments in which high conversions are obtained generally correspond with high space times and, hence, low flow rates. As a result, data points with a more pronounced impact on the sum of squares in the present work might have exerted less impact in the previous work and vice versa. The objective

function as used in the present work allowed determining a higher number of statistically significant parameters with a physical meaning which is not contradicting the previously obtained ones. It hence, allows an enhanced understanding of the reaction mechanism compared to before, see also section 4.5.

The global significance of the regression was assessed *via* the corresponding *F* value whereas the number of significantly estimated parameters was evident from the reported *t* values. A thorough assessment of the physical meaning of the global model as well as of the individual model parameters is performed to validate and discriminate between rival models. The maximum absolute value of the linear binary correlation coefficients between the parameter estimates was always significantly below 0.95 for all models. The product of the rate and (chemisorption) equilibrium coefficients in the kinetic factor of the derived Langmuir-Hinshelwood rate equations was estimated as a single parameter to avoid high correlation between the various coefficients and to limit the non-linearity in the parameters of the model equations.

4.3 Experimental results

The observed pyridine hydrodenitrogenation products were piperidine, pentane, pentene and ammonia. At the investigated operating conditions, the pentene yield was very low in comparison to pentane, *i.e.*, below 5%, and, hence, pentane and pentene were considered as a single C_5 response. The selected range of operating conditions, *i.e.*, high temperatures and high H_2S to pyridine inlet molar ratios resulted in a low piperidine yield, typically below 15%. *n*-pentylpiperidine formation, through condensation or disproportionation reactions involving piperidine, which is often cited in the literature as a side reaction during pyridine hydrodenitrogenation [15, 43-47] could, hence, be suppressed allowing for a more straightforward kinetic analysis.

In Figure 4-1, two typical pyridine conversion and product yield versus space time curves are shown. The rather steady level of the piperidine yield as well as the observed increase in pentane yield with increasing spacetime, are in line with the primary and secondary product nature of these components.

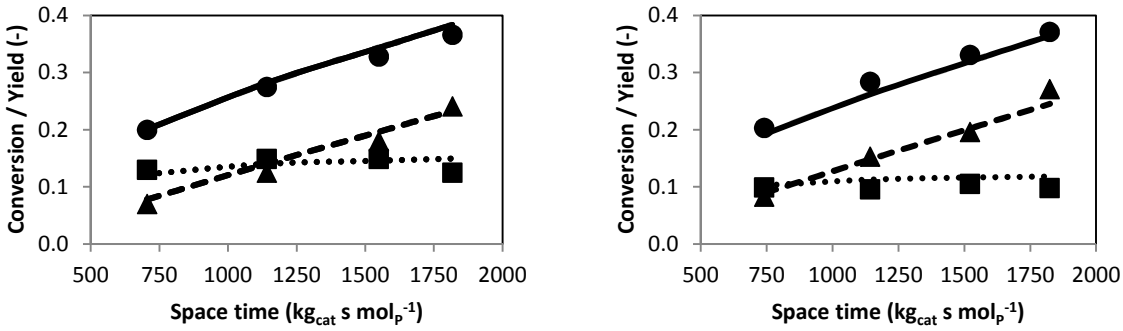

Figure 4-1. Pyridine conversion and product yields as a function of the space time. Operating conditions: T = 573K; p = 3.0 MPa; H_2/Pyridine (mol mol^{-1}) = 500; H_2S/Pyridine (mol mol^{-1}) = 2 (left), H_2S/Pyridine (mol mol^{-1}) = 7.5 (right). Symbols: ● pyridine conversion; ■ yield-piperidine; ▲yield-C_5. Lines: --- pyridine conversion; … yield-piperidine; - - - yield-C_5 model calculated values obtained by solving reactor model equations presented in chapter 2 (Eq. 2-20) and rate equations corresponding to model 6 *i.e.*, heterolytic mechanism, proton addition first, 3rd hydrogenation step and 2nd denitrogenation (ring opening) step as rate determining (as shown in Table 4-3), along with the set of parameter values of kinetic and catalyst descriptors reported in Tables 4-6 and 4-10.

Hydrogen sulphide is known to impact the hydrodenitrogenation activity and selectivity [21, 43, 45, 48, 49]. In the present work the H_2S effect is visualised in Figure 4-1, representing pyridine conversion and product yields as a function of the space time for two different inlet H_2S/pyridine (mol mol^{-1}). Hydrogen sulphide potentially reduces the amount of chemisorbed hydrogen on the catalyst surface due to competitive chemisorption, and, hence, may also decrease the pyridine hydrogenation rate and overall conversion. While the effect on the overall pyridine conversion is limited, the selectivity towards C_5 is about 8% higher at H_2S/pyridine = 7.26 (mol mol^{-1}) than H_2S/pyridine = 1.95 (mol mol^{-1}), see Table 4-1. This can be attributed to a promotional effect on C-N bond breaking by facilitating nitrogen removal *via* a substitution reaction rather than an elimination reaction [5, 50, 51]. Cattenot *et al.* [52], have clearly demonstrated the preferential occurrence of the substitution mechanism. Massoth *et.al.* [5], further propose that the denitrogenation rate promoted by H_2S is directly proportional to the square root of the H_2S partial pressure. However, nitrogen removal can even proceed in the absence of H_2S [29, 30] albeit at reduced pace. It indicated that the slower elimination mechanism is also active in nitrogen removal.

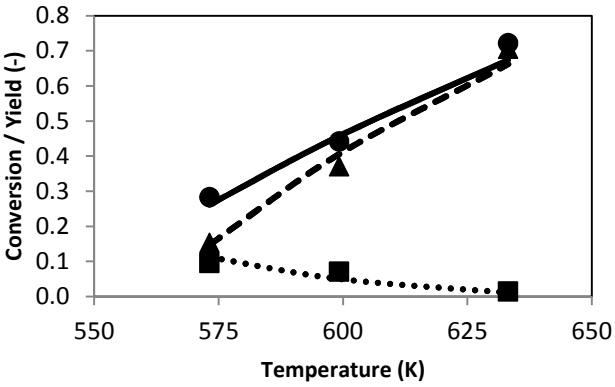

Figure 4-2. Pyridine conversion and product yield as a function of the temperature. Operating conditions: p = 3.0 MPa; Space time = 1080 Kg_{cat} s mol_P^{-1}; H_2/Pyridine (mol mol^{-1}) = 500; H_2S/P (mol mol^{-1}) = 7.6. Symbols: ● pyridine conversion; ■ yield-piperidine; ▲yield-C_5. Lines: --- pyridine conversion; … yield-piperidine; - - - yield-C5, model calculated values obtained by solving reactor model equations provided in chapter 2 (Eq. 2-20) and rate equations corresponding to model 6 *i.e.*, heterolytic mechanism, proton addition first, 3rd hydrogenation step and 2nd denitrogenation (ring opening) step as rate determining (as shown in Table 4-3), along with the set of parameter values of kinetic and catalyst descriptors reported in Tables 4-6 and 4-10.

Within the investigated range of operating conditions, the hydrodenitrogenation conversion was found to increase with the temperature. This indicates that the increase in rate coefficient overcompensates a potential decrease in reactant surface concentrations as opposed to what has been reported for aromatic hydrogenation on noble metals [53]. Higher temperatures may also lead to reduced surface concentrations of potentially inhibiting species, such as hydrogen sulphide or ammonia. The high selectivity for pentane in the range of higher temperatures, see Table 4-1, indicates that C-N bond breaking is more temperature dependent. At an equal conversion amounting to 40% the C_5 selectivity is 20% higher at 599K compared to the one observed at 573K *i.e.*, 79% vs 59%, thus supporting the former. Following the previous statements, a higher (apparent) activation energy for C-N bond breaking is expected than for hydrogenation, see also section 4.5.

Table 4-1. Experimental observations, highlighting the effect of H_2S partial pressure, temperature and total pressure on product selectivity at 40 percent pyridine conversion.

Effect	T	P	Space-time*	F_{H2S}/F_{P°	Selectivity (%)	
	T(K)	P(MPa)	(kg_{cat} s mol_P^{-1})	(mol/mol)	C_5 (-)	PP (-)
H_2S	573	3.0	1820	7.3	74	26
	573	3.0	1820	2.0	66	34
Temp.	573	3.0	1520	7.6	59	41
	599	3.0	720	7.2	79	21
Pressure	614	2.9	740	6.2	90	10
	614	2.1	1080	5.8	96	4

* W_{cat}/F^o_P

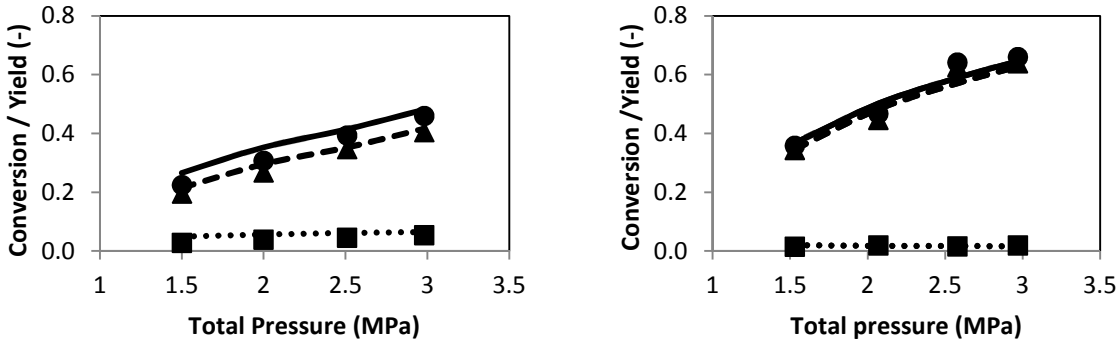

Figure 4-3. Pyridine conversion and product yields as a function of the total pressure; T = 598.15K (left) – 623.15K (right); Space time = 1150 Kg_{cat} s mol_P^{-1}; H_2/Pyridine (mol mol^{-1}) = 200 (left) – 300 (right); H_2S/P (mol mol^{-1}) = 2.1 (left) – 6.3 (right). Symbols: ● pyridine conversion; ■ yield-piperidine; ▲yield-C_5. Lines: --- pyridine conversion; … yield-piperidine; - - - yield-C_5, model equations provided in chapter 2 (Eq. 2-20) and rate equations corresponding to model 6 *i.e.*, heterolytic mechanism, proton addition first, 3rd hydrogenation step and 2nd denitrogenation (ring opening) step as rate determining (as shown in Table 4-3), along with the set of parameter values of kinetic and catalyst descriptors reported in Tables 4-6 and 4-10.

Increasing total pressures exhibited a positive effect on the pyridine conversion in the investigated range of operating conditions, see Figure 4-3. The hydrogenation rate increases at

higher pressures. When the C-N bond scission rate is more moderate, *i.e.*, at lower temperatures and inlet molar H_2S to pyridine ratio, an increasing pressure can result in the accumulation of the piperidine, which is more basic than pyridine molecules and, hence, chemisorbing more strongly on the catalyst surface and resulting in a slight inhibiting effect on the catalyst activity. Figure 4-3 (left) illustrates the pyridine HDN performance at such conditions, *i.e.*, 598.15K and 2.1 H_2S/Pyridine(mol mol^{-1}). It leads to inhibition and a more moderate increase in the overall conversion and a higher piperidine yield. If operating conditions are such that piperidine ring opening is fast, *i.e.*, at high temperatures and higher inlet molar H_2S to pyridine ratios, the formed piperidine molecules react quickly to pentane and, hence, only a minor fraction of the catalyst surface will be covered with piperidine molecules. Figure 4-3 (right), illustrates the pyridine HDN performance at such conditions *i.e.*, 623.15K and 6.3 H_2S/Pyridine (mol mol^{-1}). It also results in correspondingly low piperidine surface concentrations as discussed below in section 4.5. The low amount of inhibiting nitrogen components on the surface leaves more vacant active sites for additional H_2S molecules to chemisorb at higher pressure. This causes a further enhancement of the naphthenic C-N bond scission rate at higher pressures as can be seen on Figure 4-3 (right) exhibiting a correspondingly lower piperidine yield at high pressure.

4.4 Kinetic analysis

4.4.1 Reaction network and mechanism

The global pyridine hydrodenitrogenation reaction network, as evident from the experimental results presented in chapter 1 of this thesis which is in agreement with previous published data [40, 45, 46, 49, 54, 55]. Direct nitrogen removal is generally not encountered. It is well established that the aromatic C-N bond is much stronger than the naphthenic C-N bond, and, hence, that pyridine denitrogenation is only possible after a prior hydrogenation to piperidine. Due to its low activation energy, pyridine hydrogenation is a much more easy reaction than hydrodenitrogenation [56]. Hence the former reaction occurs at a much faster rate compared to the latter. Subsequently, the naphthenic ring can open to form an amine, which further undergoes deamination to form final hydrocarbon products.

4.4.1.1 Pyridine hydrogenation

Pyridine hydrogenation to piperidine is an reversible reaction [40]. Each surface elementary step is considered as an atomic hydrogen addition, similar to, *e.g.*, benzene and naphthalene hydrogenation [36, 57]. During the rate equation derivation, both heterolytic and homolytic hydrogen dissociation was taken into consideration and every single hydrogen

addition was considered potentially rate determining [36, 58]. In the case of heterolytic hydrogen dissociation both proton and hydride addition were considered to, potentially, occur first. The basicity of pyridine would be the reason to have proton addition first, however if the N-Ni bond would cause the electron density to be withdrawn from the ring a possibility would be opened up for hydride addition first [59]. Model construction and its corresponding discrimination can, hence, be performed by considering proton or hydride additions first, after which successive alternating hydride or proton additions are considered in order to restore the electronic neutrality of the hydrocarbon species involved. An example scheme for a proton addition first is shown in Figure 4-4.

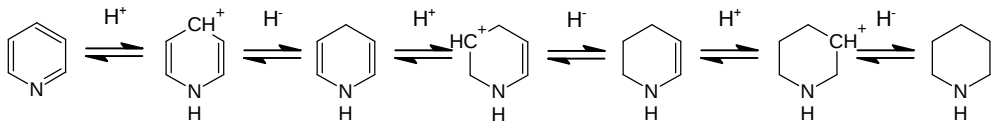

Figure 4-4. Hydrogenation of pyridine in terms of elementary steps assuming heterolytic mechanism and proton addition first

4.4.1.2 Piperidine ring opening

Piperidine undergoes ring opening through hydrogen additions only, see Figure 4-5. During the model construction of piperidine ring opening, only proton addition first is considered, since hydride addition first would not allow the further reaction of -SH substitution to proceed. Proton addition to the nitrogen containing the free electron pair, is much more plausible owing to the basic nature of the piperidine. Hence, during the modelling procedure, the piperidine ring opening is considered to proceed by proton addition first only.

The presence of H_2S at typical hydrotreating conditions has been shown to promote the C-N scission rate, by enabling a comparatively faster substitution pathway [49, 60]. The thiol end group in the intermediate formed is a good leaving group and is rapidly removed as H_2S. The mechanism shown in Figure 4-5 is in line with the mechanism proposed by various researchers [60] which comprises several steps including the formation of the aminethiol species.

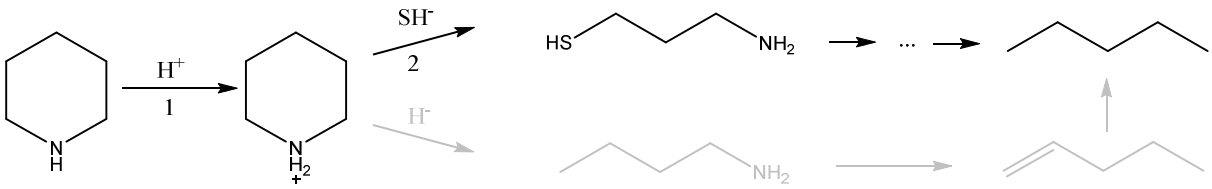

Figure 4-5. Reaction mechanism of the denitrogenation step, considered during modelling of pyridine HDN over NiMo/γ-Al_2O_3. 1 and 2 represent the steps that are considered as potentially rate determining. The kinetic relevance of the other steps is limited at the investigated operating conditions such that they can be assumed to occur instantaneously. Reactions occurring through the direct amine removal (indicated in grey) are less likely to occur under the operating conditions used, particularly because of the higher H_2S partial pressures.

4.4.1.3 Pentylamine denitrogenation

Pentylamine was not observed in the reactor effluent. Being a linear amine, the orbitals of the carbon and nitrogen atoms involved in the bond that needs to be broken aiming at the denitrogenation can orient themselves much more favourably compared to a C-N bond in a cyclic structure. Hence, C-N bond scission in a linear chain is expected to proceed much faster for acyclic alkylamines such as pentylamine compared to cyclic amines such as piperidine. A similar effect is observed for C-C bond scission in linear versus cyclic hydrocarbons [61, 62]. For the modelling purposes in the present work pentylamine denitrogenation can, hence, be assumed to occur instantaneously such that only two rate equations are needed to describe the hydrodenitrogenation of pyridine, *i.e.,* pyridine hydrogenation and piperidine denitrogenation.

4.4.1.4 Active sites on sulphided catalysts

Pyridine hydrodenitrogenation kinetics have been simulated using models with two types of sites [28, 47] or in some cases even three types of sites [29]. Pille and Froment [28] considered two types of sites, *i.e.,* * and S^{2-} sites, in their kinetic model, which sufficed to avoid any significant or systematic deviations between the experimental observations and the model simulations. Romero *et al.* [36] also have successfully described naphthalene hydrogenation over an industrial NiMo catalyst by assuming two types of sites. In the present work, a model considering * and S^{2-} is further elaborated. The sites are believed to be on the edges of the promoted sulphided catalysts [36]. This two type of site assumption along with the assumption of homolytic or heterolytic dissociative H_2 and H_2S chemisorption of on the catalyst surface is expected to provide the model with the necessary flexibility to adequately simulate both the

hydrogenation and denitrogenation reaction *via* appropriate sulphur and hydrogen surface concentrations.

4.4.2 Model construction

The assumptions made during model construction are in agreement with our previously published work on naphthalene hydrogenation [36]. More particularly the site balances as required according to the homolytic and the heterolytic mechanism are constructed along identical lines.

4.4.2.1 Site balances

In accordance with the assumptions made by Romero *et al.*,[36], 2 site balances need to be constructed *i.e.*, one for the coordinatively unsaturated sites, denoted as * as shown in equation 4-2, and one for the sulphur anions, denoted as S^{2-}. While the site balance for the sulphur anions is literally identical as the previously used one, that for the coordinatively unsaturated sites needs to be adapted to the other hydrocarbon compounds that are considered:

$$C_{*,tot} = C_* + C_{C_5H_5N^*} + C_{C_5H_5NH^{+*}} + C_{C_5H_6NH^*} + C_{C_5H_7NH^{+*}} + C_{C_5H_8NH^*} + C_{C_5H_9NH^{+*}} + C_{C_5H_{10}NH^*} + C_{C_5H_{12}{}^*} + C_{NH_3{}^*} + C_{H^{-*}} + C_{SH^{-*}} \quad 4\text{-}2$$

The derivation of the site balances and the relationship between the * and the S^{2-} sites are provided in Appendix B.

Table 4-2. Chemisorption equilibria used for constructing the pyridine HDN models.

Chemisorption/desorption equilibria		Coefficient
Heterolytic	**Homolytic**	
Hydrogen and hydrogen sulphide	Hydrogen and hydrogen sulphide	
$H_2S + * + S^{2-} \rightleftarrows SH^{-*} + S^{2-}H^+$	$H_2S + * + S^{2-} \rightleftarrows SH^* + S^{2-}H$	K_{H2S}
$H_2 + * + S^{2-} \rightleftarrows H^{-*} + S^{2-}H^+$	$H_2 + 2\ * \rightleftarrows 2\ H^*$	K_{H2}
	$H_2 + 2\ S^{2-} \rightleftarrows 2\ S^{2-}H$	$K_{H2,S}{}^{2-}$
Nitrogen components		
$C_5H_5N + * \rightleftarrows C_5H_5N^*$		K_P
$C_5H_{11}N + * \rightleftarrows C_5H_{11}N^*$		K_{PP}
$NH_3 + * \rightleftarrows NH_3{}^*$		K_{NH3}

4.4.2.2 Rate equation derivation

Rival rate equations for pyridine hydrogenation and piperidine denitrogenation are obtained by considering alternative, potentially rate-determining steps. The elementary steps in the reaction mechanism with proton addition first in both hydrogenation and denitrogenation can be written as shown in equations 4-3 to 4-8 and 4-9 and 4-10 and respectively.

$$C_5H_5N^* + S^{2-}H^+ \rightleftarrows C_5H_5NH^{+*} + S^{2-} \qquad K_{P-PH} \qquad 4\text{-}3$$

$$C_5H_5NH^{+*} + H^{-*} \rightleftarrows C_5H_6NH^* + * \qquad K_{PH-PH2} \qquad 4\text{-}4$$

$$C_5H_6NH^* + S^{2-}H^+ \rightleftarrows C_5H_7NH^{+*} + S^{2-} \qquad K_{PH2-PH3} \qquad 4\text{-}5$$

$$C_5H_7NH^{+*} + H^{-*} \rightleftarrows C_5H_8NH^* + * \qquad K_{PH3-PH4} \qquad 4\text{-}6$$

$$C_5H_8NH^* + S^{2-}H^+ \rightleftarrows C_5H_9NH^{+*} + S^{2-} \qquad K_{PH4-PH5} \qquad 4\text{-}7$$

$$C_5H_9NH^{+*} + H^{-*} \rightleftarrows C_5H_{10}NH^* + * \qquad K_{PH5-PP} \qquad 4\text{-}8$$

$$C_5H_{10}NH^* + S^{2-}H^+ \rightleftarrows {C_5H_{10}NH_2}^{+*} + S^{2-} \qquad 4\text{-}9$$

$$\left[{C_5H_{10}NH_2}^{+*} + SH^{-*} \rightarrow NH_2C_5H_{10}SH^* + *\right]^{\neq} \qquad 4\text{-}10$$

≠ Further steps in the reaction are considered to occur instantaneously.

As an example, when the third hydrogen addition is considered to be rate determining, the rate equation can be derived starting from Eq. 4-5, such that the following expression is obtained,

$$R_{P\rightleftarrows PP} = k_{p,+}\left(C_{C_5H_6NH^*}C_{S^{2-}H^+} - \frac{C_{C_5H_7NH^{+*}}\,C_{S^{2-}}}{K_{PH2-PH3}}\right) \qquad 4\text{-}11$$

Similarly, for denitrogenation, when piperidine protonation is considered rate determining, the corresponding rate equation can be derived starting from Eq. 4-9 such that the following expression is obtained,

$$R_{PP} = k_{PP-PPH}\,C_{C_5H_{10}NH^*}\,C_{S^{2-}H^+} = k_{PP-PPH}\,K_{PP}\,\sqrt{\mu\,\delta}\,P_{C_5H_{10}NH}\,{C_*}^2 \qquad 4\text{-}12$$

The surface concentrations can be calculated based on the equilibria of the preceding steps while the surface concentration of hydrogen and of the active sites can be calculated from the site balance presented in Appendix B.

Similar rate equations are developed considering each of the hydrogenation steps as rate determining. An overview of these equations for the heterolytic mechanism, both for proton and hydride addition first are given in Table 4-3.

Table 4-3. Rate equations for pyridine hydrogenation and piperidine denitrogenation assuming heterolytic chemisorption of H_2 and H_2S

	Proton addition first	Hydride addition first
Pyridine hydrogenation		
1	$R_p = k_{p,+} K_P C_*^2 \sqrt{\delta \mu} \left(P_{C_5H_5N} - \frac{1}{K_{Equi}} \frac{P_{C_5H_{10}NH}}{P_{H2}^3} \right)$	$R_p = k_{p,+} K_P K_{H2} C_*^2 \sqrt{\frac{\delta}{\mu}} \left(P_{C_5H_5N} P_{H2} - \frac{P_{C_5H_{10}NH}}{K_{Equi} P_{H2}^2} \right)$
2	$R_p = k_{p,+} K_{P-PH} K_{H2} K_P C_*^2 \left(P_{C_5H_5N} P_{H2} - \frac{1}{K_{Equi}} \frac{P_{C_5H_{10}NH}}{P_{H2}^2} \right)$	$R_p = k_{p,+} K_P K_{H2} K_{P-PH} C_*^2 \delta \left(P_{C_5H_5N} P_{H2} - \frac{P_{C_5H_{10}NH}}{K_{Equi} P_{H2}^2} \right)$
3	$\boldsymbol{R_p = k_{p,+} K_{P-PH2} K_{H2} K_P C_*^2 \sqrt{\delta \mu} \left(P_{H_2} P_{C_5H_5N} - \frac{1}{K_{Equi}} \frac{P_{C_5H_{10}NH}}{P_{H2}^2} \right)}$	$R_p = k_{p,+} K_P K_{H2}^2 K_{P-PH2} C_*^2 \sqrt{\frac{\delta}{\mu}} \left(P_{C_5H_5N} P_{H2}^2 - \frac{P_{C_5H_{10}NH}}{K_{Equi} P_{H2}} \right)$
4	$R_p = k_{p,+} K_{P-PH3} K_{H2}^2 K_P C_*^2 \left(P_{H_2}^2 P_{C_5H_5N} - \frac{1}{K_{Equi}} \frac{P_{C_5H_{10}NH}}{P_{H2}} \right)$	$R_p = k_{p,+} K_P K_{H2}^2 K_{P-PH3} C_*^2 \delta \left(P_{C_5H_5N} P_{H2}^2 - \frac{P_{C_5H_{10}NH}}{K_{Equi} P_{H2}} \right)$
5	$R_p = k_{p,+} K_{P-PH4} K_{H2}^2 K_P C_*^2 \sqrt{\delta \mu} \left(P_{H_2}^2 P_{C_5H_5N} - \frac{1}{K_{Equi}} \frac{P_{C_5H_{10}NH}}{P_{H2}} \right)$	$R_p = k_{p,+} K_P K_{H2}^3 K_{P-PH4} C_*^2 \sqrt{\frac{\delta}{\mu}} \left(P_{C_5H_5N} P_{H2}^3 - \frac{P_{C_5H_{10}NH}}{K_{Equi}} \right)$
6	$R_p = k_{p,+} K_{P-PH5} K_{H2}^3 K_P C_*^2 \left(P_{H_2}^3 P_{C_5H_5N} - \frac{1}{K_{Equi}} P_{C_5H_{10}NH} \right)$	$R_p = k_{p,+} K_P K_{H2}^3 K_{P-PH5} C_*^2 \delta \left(P_{C_5H_5N} P_{H2}^3 - \frac{P_{C_5H_{10}NH}}{K_{Equi}} \right)$
Piperidine denitrogenation		
1	$R_{PP} = k_{PP} C_{C_5H_{10}NH^+} C_{S^{2-}H^+} = k_{PP} K_{PP} \sqrt{\mu \delta} P_{C_5H_{10}NH} C_*^2$	Not considered
2	$\boldsymbol{R_{pp} = k_{PP} K_{PP-PPH} K_{PP} \mu P_{C_5H_{10}NH} C_*^2}$	Not considered

Symbols : $K_{X\text{-}XH}$ = equilibrium coefficient for species X and hydrogen additions to X; K_{equi} = global equilibrium coefficient pyridine and piperidine

In the case of piperidine denitrogenation, as explained earlier two potentially kinetically significant steps are considered, *i.e.*, first protonation followed by sulphydril assisted C-N bond scission in piperidine, see Figure 4-5. The expressions derived for the denitrogenation rate are listed in Table 4-3.

4.4.2.3 Homolytic mechanism

Rate equations for the homolytic mechanisms are based on similar chemisorption equilibria as discussed for the heterolytic mechanism. The differences are situated in the elementary steps involving hydrogen and hydrogen sulphide. A separate hydrogen

chemisorption equilibrium is considered on the * and S^{2-}. Different rate equations can be constructed accounting either for a preferential hydrogen addition from the sulphur anions or from the coordinatively unsaturated sites, *i.e.*, hydrogenation occurring solely through hydrogen atoms from * and S^{2-} sites. The homolytic rate equations are summarised in Table 4-4. Note that the piperidine denitrogenation rate equations depend on the type of site where the hydrogen atom for piperidine hydrogenation originates from.

The enhanced understanding of HDN catalysis, in terms of catalyst active sites, their location, characteristics as well as the assumption of dissociative H_2 and H_2S chemisorption result in rate equations as, listed in Table 4-3 and Table 4-4, that are different from those derived by Pille and Froment [28]. Moreover, in this work the promoting effect of H_2S on "hydrogenolysis" is taken into account by assuming a substitution reaction pathway while in the previous work this was done empirically, *i.e.*, multiplying the rate of piperidine denitrogenation rate by $(1+(K_{H2S}\ P_{H2S})^{0.5})$ based on the results proposed by Massoth *et al.* [5, 63].

Table 4-4. Derived rate equations for pyridine hydrogenation and piperidine denitrogenation assuming homolytic chemisorption of H_2 and H_2S

	Pyridine hydrogenation	
	Hydrogen addition from *	**Hydrogen addition from S^{2-}**
1	$R_P = k_{p,+}\, K_P\, {C_*}^2 \sqrt{K_{H2,*}\, P_{H2}} \left(P_{C_5H_5N} - \frac{1}{K_{Equi}} \frac{P_{C_5H_{10}NH}}{{P_{H2}}^3}\right)$	$R_P = k_{p,+}\, K_P\, C_*\, C_{S^{2-}} \sqrt{K_{H2,S^{2-}}\, P_{H2}} \left(P_{C_5H_5N} - \frac{1}{K_{Equi}} \frac{P_{C_5H_{10}NH}}{{P_{H2}}^3}\right)$
2	$R_P = k_{p,+}\, K_{P-PH}\, K_P\, {C_*}^2\, K_{H2,*}\, P_{H2} \left(P_{C_5H_5N} - \frac{1}{K_{Equi}} \frac{P_{C_5H_{10}NH}}{{P_{H2}}^3}\right)$	$R_P = k_{p,+}\, K_{P-PH}\, K_P\, C_*\, C_{S^{2-}}\, K_{H2,S^{2-}}\, P_{H2} \left(P_{C_5H_5N} - \frac{1}{K_{Equi}} \frac{P_{C_5H_{10}NH}}{{P_{H2}}^3}\right)$
3	$R_p = k_{p,+}\, K_{P-PH2}\, K_P\, {C_*}^2 \left(K_{H2,*}\, P_{H2}\right)^{\frac{3}{2}} \left(P_{C_5H_5N} - \frac{1}{K_{Equi}} \frac{P_{C_5H_{10}NH}}{{P_{H2}}^3}\right)$	$R_p = k_{p,+}\, K_{P-PH2}\, K_P\, C_*\, C_{S^{2-}} \left(K_{H2,S^{2-}}\, P_{H2}\right)^{\frac{3}{2}} \left(P_{C_5H_5N} - \frac{1}{K_{Equi}} \frac{P_{C_5H_{10}NH}}{{P_{H2}}^3}\right)$
4	$R_p = k_{p,+}\, K_{P-PH3}\, K_P\, {C_*}^2 \left(K_{H2,*}\, P_{H2}\right)^2 \left(P_{C_5H_5N} - \frac{1}{K_{Equi}} \frac{P_{C_5H_{10}NH}}{{P_{H2}}^3}\right)$	$R_p = k_{p,+}\, K_{P-PH3}\, K_P\, C_*\, C_{S^{2-}} \left(K_{H2,S^{2-}}\, P_{H2}\right)^2 \left(P_{C_5H_5N} - \frac{1}{K_{Equi}} \frac{P_{C_5H_{10}NH}}{{P_{H2}}^3}\right)$
5	$R_P = k_{p,+}\, K_{P-PH4}\, K_P\, {C_*}^2 \left(K_{H2,*}\, P_{H2}\right)^{\frac{5}{2}} \left(P_{C_5H_5N} - \frac{1}{K_{Equi}} \frac{P_{C_5H_{10}NH}}{{P_{H2}}^3}\right)$	$R_P = k_{p,+}\, K_{P-PH4}\, K_P\, C_*\, C_{S^{2-}} \left(K_{H2,S^{2-}}\, P_{H2}\right)^{\frac{5}{2}} \left(P_{C_5H_5N} - \frac{1}{K_{Equi}} \frac{P_{C_5H_{10}NH}}{{P_{H2}}^3}\right)$
6	$R_P = k_{p,+}\, K_{P-PH5}\, K_P\, {C_*}^2 \left(K_{H2,*}\, P_{H2}\right)^3 \left(P_{C_5H_5N} - \frac{1}{K_{Equi}} \frac{P_{C_5H_{10}NH}}{{P_{H2}}^3}\right)$	$R_P = k_{p,+}\, K_{P-PH5}\, K_P\, C_*\, C_{S^{2-}} \left(K_{H2,S^{2-}}\, P_{H2}\right)^3 \left(P_{C_5H_5N} - \frac{1}{K_{Equi}} \frac{P_{C_5H_{10}NH}}{{P_{H2}}^3}\right)$
	Piperidine denitrogenation	
	Hydrogen addition from *	**Hydrogen addition from S^{2-}**
1	$R_{PP} = k_{PP}\, {C_*}^2\, K_{PP} \sqrt{K_{H2,*}\, P_{H2}}\, P_{C_5H_{10}NH}$ $R_p = k_{PP} K_{PP-PPH} K_{PP}\, P_{C_5H_{10}NH} {C_*}^2$	$R_{PP} = k_{PP}\, C_*\, C_{S^{2-}}\, K_{PP} \sqrt{K_{H2,S^{2-}}\, P_{H2}}\, P_{C_5H_{10}NH}$
2	$\left(\sqrt{\frac{K_{H_2,*}}{K_{H_2,S2-}}} K_{H_2S} P_{H_2S} + K_{H_2,*}\, P_{H_2}\right)$	$R_{pp} = k_{PP}\, K_{PP-PPH}\, K_{PP}\, P_{C_5H_{10}NH}\, C_* \left(C_*\, K_{H_2S} P_{H_2S} + C_{S^{2-}} K_{H_2,S^{2-}} P_{H_2}\right)$

4.5 Results and discussion

In total 48 different models, corresponding to 4 different types of reaction mechanisms with each 6 potentially rate-determining hydrogenation steps and 2 possible rate-determining steps for piperidine denitrogenation, were subject to regression. The number of parameters to be estimated during non-isothermal regression for models based on the heterolytic mechanism amounted to 14, while for those based on the homolytic mechanism this number amounted to 16. In order to keep the number of parameters to be estimated at a reasonable number and simplify the model assessment, chemisorption entropies were determined *a priori*, see section 4.5.1. This allowed reducing the number of adjustable parameters to 9 and 10 in case of models

based on heterolytic and homolytic mechanism, respectively, and typically resulted in a higher number of remaining model parameters that can be estimated significantly. Moreover, it will allow a more thorough comparison with literature reported values.

4.5.1 Chemisorption entropy assessment

Statistical thermodynamics are used to determine an appropriate range for the pre-exponential factor of the chemisorption coefficients and, hence, the corresponding chemisorption entropies [64]. The pre-exponential factor corresponds to the change in the entropy upon chemisorption. The latter was calculated once by assuming retaining a maximum of translational freedom upon chemisorption, *i.e.,* a loss of only a single degree of freedom, and once by assuming a complete loss of all translational entropy. The Sackur-Tetrode equation [65] was used for this purpose. The corresponding ranges can be determined by considering a minimum and a maximum loss of degrees of freedom, see Table 4-5. The discrepancy in the ranges proposed for H_2 and H_2S with respect to the other components stems from the dissociative character of their chemisorption compared to the molecular one for the other components [36].

Table 4-5. Range of chemisorption entropies used for molecular and dissociative chemisorption

Component	$\Delta S^0_{chemisorption}$ (J mol^{-1} K^{-1})	
	Upper bound	Lower bound
Piperidine / Ammonia	-95.7	-191
Hydrogen / Hydrogen sulphide	0	-191

Various regressions have been performed with different combinations of chemisorption entropies. The set giving the best results in terms of number of parameters that could be estimated significantly and of physical meaning of the parameter estimates is listed in Table 4-6. These entropy values indicate that mobility of the different molecules on the surface decreases in the order ammonia – piperidine – hydrogen – hydrogen sulphide.

Table 4-6. Chemisorption entropy values and their corresponding loss in degrees of freedom for reacting components used during fixed entropy regressions.

Component	$\Delta S^0_{chemisorption}$ (J mol^{-1} K^{-1})	Corresponding loss of degrees of freedom*
Ammonia	-98	1
Piperidine	-158	1
Hydrogen	-187	2
Hydrogen sulphide	-190	2

* Approximate value

4.5.2 Initial regression and primary discrimination

Table 4-7. Statistical information of rival models used in the discrimination of models for gas phase HDN of pyridine over sulphided NiMo/γ-Al_2O_3

RDS		Heterolytic (9 par.)						Homolytic (10 par.)					
		Proton		Model	Hydride		Model	*		Model	S^{2-}		Model
P→PP	PP→C5	F	s.p	No	F	s.p	No	F	s.p	No	F	s.p	No
1	1	253	5	1	1603	6	13	1312	7	25	1318	7	37
1	2	22	5	2	952	7	14	1396	7	26	1324	7	38
2	1	2700	9	3	2717	9	15	1968	8	27	2224	7	39
2	2	2334	9	4	2012	9	16	2248	9	28	2356	9	40
3	1	2793	9	5	2071	7	17	2239	8	29	2399	8	41
3	2	2758	9	6	1763	7	18	2734	9	30	2327	5	42
4	1	2210	7	7	2357	8	19	1834	4	31	1935	6	43
4	2	1948	8	8	1562	8	20	1595	6	32	1562	6	44
5	1	2481	8	9	1063	5	21	1264	5	33	1470	3	45
5	2	2354	8	10	353	3	22	1335	7	34	566	3	46
6	1	956	6	11	1058	8	23	910	4	35	N.C		47
6	2	970	7	12	590	4	24	912	5	36	889	4	48

The statistical results of the regression performed for all models are summarised in

Initial regression and primary discrimination

Table 4-7. 18 models, *i.e.*, 11 models based on the heterolytic mechanism and 7 based on the homolytic mechanism exhibited an F value for the global significance of the regression

exceeding 2000. These models were further discriminated based on the physical significance of the estimated parameters as discussed below. The corresponding, comprehensive information comprising all parameter values are provided in Table 4-8 and Table 4-9.

4.5.2.1 Models based on heterolytic mechanism

As mentioned above, 11 models based on the heterolytic mechanism exhibited a high global significance, out of which 5 models *i.e.*, models nr. 7, 9, 10, 17 and 19 did not allow estimating all parameters significantly. Despite their higher F values for the global significance of the regression these models resulted in lower number of significantly estimated parameters, hence, the focus was put on the other 6 models *i.e.*, models nr. 3, 4, 5, 6, 15 and 16 which generally exhibited the higher F values and allowed estimating all parameters significantly.

Since none of the models assuming the first hydrogen addition to be rate determining, *i.e.*, models nr. 1 and 2, had good F values for the global significance of the regression nor a reasonable number of significantly estimated parameters, it can be concluded that, despite the pronounced endothermicity of the first hydrogen addition to pyridine [59], it is not rate determining. The aromatic structure of pyridine is potentially preserved after the first hydrogen addition due to the ionic or the radical character after the first hydrogen addition. The second hydrogen addition is exothermic since it compensates for the charge. However, the lack of physical significance in the parameter estimates indicates that this cannot be the rate-determining step either, *i.e.*, the pyridine chemisorption coefficient in models 3 and 4 is substantially lower than the one reported by La Vopa and Satterfield [18]. In the case of model 3, on top of the low pyridine chemisorption coefficient an activation energy for pyridine hydrogenation amounting to 22 kJ mol^{-1} is obtained, which is much lower than the literature reported values [28], whereas in the case of Model 4, the denitrogenation activation energy is excessively high, amounting to 207 kJ mol^{-1}. For models 15 and 16 considering the second hydrogen addition as rate determining with hydride addition first, the pyridine chemisorption coefficient is estimated relatively high at 8.1 MPa^{-1} and 7.5 MPa^{-1}, with very wide confidence intervals [18]. Additionally model 16 has a quite high denitrogenation activation energy [28].

The lack of physical significance of at least one of the parameters in models nr. 3, 4, 15 and 16 further suggest that these can be discarded from further model discrimination. Models 5 and 6 resulted in the statistically and physically significant parameters and are further discussed below.

Table 4-8. Kinetic and catalytic descriptors estimated during regression of models related to heterolytic mechanism for pyridine HDN over NiMo/Al_2O_3, along with their 95% confidence intervals.

Model number	3			4			5			6			7			9			10		
F Value	2700			2334			2793			2758			2210			2481			2354		
Number of significant parameters	9/9			9/9			9/9			9/9			7/9			8/9			8/9		
$k_{p\rightleftarrows pp}$ A^{*a}	3.10^{-3}	±	4.10^{-4}	3.10^{-3}	±	8.10^{-4}	8.10^{-3}	±	1.10^{-3}	9.10^{-3}	±	2.10^{-3}	6.10^{-4}	±	4.10^{-3}	8.10^{-4}	±	3.10^{-4}	8.10^{-4}	±	3.10^{-4}
$k_{p\rightleftarrows pp}$ Ea	22	±	11.0	16	±	12.0	48	±	11.0	41	±	10.0		NS			NS			NS	
$k_{pp\rightarrow pa}$ A^{*a}	2.10^{0}	±	4.10^{-1}	3.10^{0}	±	2.10^{0}	1.10^{0}	±	2.10^{-1}	1.10^{0}	±	2.10^{-1}	8.10^{-1}	±	1.10^{-1}	2.10^{0}	±	6.10^{-1}	2.10^{0}	±	6.10^{-1}
$k_{pp\rightarrow pa}$ Ea	170	±	14.3	207	±	17.5	126	±	16.0	185	±	19.0	123	±	11.1	51	±	8.6	100	±	11.5
K^{a}_{P}	1.5	±	0.1	1.5	±	0.1	4.6	±	1.4	6.1	±	1.5	2.7	±	0.6	4.3	±	1.7	6.4	±	2.8
$-\Delta H_{PIP}$	113	±	1.7	113	±	2.0	119	±	2.0	117	±	3.0	114	±	3.0	128	±	1.3	127	±	1.6
$-\Delta H_{NH3}$	69	±	1.3	69	±	1.4	75	±	2.0	76	±	2.0	74	±	1.3	78	±	2.3	81	±	2.4
$-\Delta H_{H2,*}$	73	±	4.1	85	±	3.8	99	±	5.0	104	±	3.0	102	±	4.6	102	±	3.0	109	±	2.8
$-\Delta H_{H2S,*}$	103	±	3.8	107	±	4.0	111	±	10.0	129	±	3.0		NS		126	±	5.8	137	±	3.0

Units : k (A*) [mol $s^{-1}kg_{cat}^{-1}$], Ea [kJ mol^{-1}), K [MPa^{-1}] and ΔH [kJ mol^{-1}] [a] Reaction and chemisorption coefficient at the average temperature, *i.e.*, 599 K

15 2717 9/9	16 2012 9/9	17 2071 7/9	19 2357 8/9
3.10^{-3} ± 8.10^{-4}	3.10^{-3} ± 1.10^{-3}	8.10^{-5} ± 8.10^{-5}	6.10^{-4} ± 2.10^{-4}
36 ± 8.7	37 ± 10	NS	NS
6.10^{0} ± 2.10^{0}	2.10^{1} ± 1.10^{1}	1.10^{0} ± 4.10^{-1}	8.10^{0} ± 4.10^{0}
176 ± 18.3	232 ± 24.4	166 ± 13.9	84 ± 11.7
8.1 ± 2.1	7.5 ± 2.3	3.6 ± 0.8	10.1 ± 5.8
119 ± 2.4	116 ± 3.6	110 ± 8.7	129 ± 2.2
76 ± 2.0	76 ± 2.4	74 ± 1.6	82 ± 3.0
74 ± 4.9	85 ± 5.1	89 ± 5.1	86 ± 4.3
106 ± 4.3	109 ± 4.9	NS	115 ± 4.2

Units : k (A*) [mol $s^{-1}kg_{cat}^{-1}$], Ea [kJ mol^{-1}), K [MPa^{-1}] and ΔH [kJ mol^{-1}], [a] Reaction and chemisorption coefficient at the average temperature, *i.e.*, 599 K

Table 4-9. Kinetic and catalytic descriptors estimated during regression of models related to homolytic mechanism for pyridine HDN over NiMo/ γ-Al_2O_3, along with their 95% confidence intervals.

Model number	28	29	30	39	40	41	42
F Value	2248	2239	2734	2224	2356	2399	2327
Number of significant parameters	9/10	8/10	9/10	7/10	9/10	8/10	5/10
$k_{p\rightleftarrows pp}$ A*[a]	2.10^{-3} ± 8.10^{-4}	7.10^{-3} ± 5.10^{-3}	4.10^{-3} ± 3.10^{-3}	3.10^{-3} ± 3.10^{-3}	4.10^{-3} ± 9.10^{-4}	4.10^{-3} ± 3.10^{-3}	NS
$k_{p\rightleftarrows pp}$ Ea	22 ± 11	NS	NS	29 ± 11.9	28 ± 9.5	NS	NS
$k_{pp\rightarrow pa}$ A*[a]	NS	1.10^{0} ± 8.10^{-1}	3.10^{-1} ± 1.10^{-1}	1.10^{-1} ± 9.10^{-2}	4.10^{-0} ± 2.10^{0}	7.10^{-1} ± 5.10^{-3}	NS
$k_{pp\rightarrow pa}$ Ea	200 ± 28.8	83 ± 11.8	208 ± 15.7	112 ± 18.6	219 ± 18.0	80 ± 11.7	179 ± 13.3
K $^{a}_{P}$	1.4 ± 0.2	5.4 ± 2.1	4.0 ± 1.4	8.0 ± 7.0	8.3 ± 2.1	NS	NS
$-\Delta H_{PIP}$	113 ± 1.9	115 ± 2.9	115 ± 3.2	123 ± 4.0	119 ± 2.6	120 ± 5.9	124 ± 6.3
$-\Delta H_{NH3}$	70 ± 1.3	76 ± 2.2	75 ± 1.8	77 ± 3.8	77 ± 2.0	77 ± 5.5	80 ± 6.2
$-\Delta H_{H2,*}$	72 ± 27.1	110 ± 4.7	106 ± 5.6	NS	NS	85 ± 61	NS
$-\Delta H_{H2,S2-}$	190 ± 0	190 ± 0	190 ± 5.6	NS	190 ± 0.0	190 ± 10.1	190 ± 7.7
$-\Delta H_{H2S,*}$	100 ± 2	104 ± 94	134 ± 2.6	NS	84 ± 0.0	112 ± 50.4	97 ± 7.8

Units : k (A*) [mol $s^{-1}kg_{cat}^{-1}$], Ea [kJ mol^{-1}), K [MPa^{-1}] and ΔH [kJ mol^{-1}], [a] Reaction and chemisorption coefficient at the average temperature, *i.e.*, 599 K

4.5.2.2 Models based on homolytic mechanism

At most 9 out of 10 parameters could be estimated significantly in the models considering homolytic H_2 and H_2S dissociation. While the models corresponding to the third hydrogen addition being rate determining exhibited better performance, the models considering the second hydrogen addition as rate determining also showed good global significance of regression. In these models, the kinetic descriptors, *i.e.,* both the hydrogenation and denitrogenation activation energies could not be estimated statistically or physically significantly. *E.g.,* an unrealistically high activation energy amounting to 200 kJ mol^{-1} was obtained for the denitrogenation step with model 28 while with a value of 22 kJ mol^{-1} the hydrogenation activation energy step is extremely low [28]. The pyridine chemisorption coefficient was also estimated as 1.4 ± .2 MPa^{-1} which is much lower than the expected value [18]. While these models corresponding to the homolytic mechanism resulted in rather good F values, none of them was capable to give physically acceptable values for all parameter estimates *i.e.,* activation energies and or chemisorption coefficients. As a result, none of these models was retained for further evaluation.

4.5.3 Final model selection

Overall heterolytic mechanisms considering proton addition first result in higher F values and a higher number of significantly estimated parameters compared to heterolytic mechanisms considering hydride addition first or homolytic mechanisms and, hence, seem to be the preferred reaction mechanism. Romero *et.al.,* [36] also obtained the best regression results in the case of naphthalene hydrogenation with a heterolytic mechanism. However, in their work hydride addition first was found to be more likely than proton addition first. While pyridine and naphthalene are both aromatics, the reason for the different mechanisms regarding both components can be attributed to the presence of nitrogen as hetero atom in pyridine and its corresponding basicity. The higher proton affinity of pyridine compared to naphthalene, *i.e.,* 930 kJ mol^{-1} versus 803 kJ mol^{-1} [66], explains why proton addition first is more logical for pyridine than for naphthalene.

Models 5 and 6, in which the addition of the third hydrogen atom in pyridine hydrogenation was considered rate determining exhibited better global significance of regression, good physical meaning of the parameters and the best overall agreement with the experimental data, see Figure 4-1 to Figure 4-3 . Interestingly models where the third hydrogen addition was shown to be rate determining were also reported for naphthalene hydrogenation [36] in which rate equations were constructed based on similar assumptions. Additionally, this

observation for the hydrogenation mechanism seems also to be independent of the selected piperidine reaction mechanism. The identification of the third hydrogen addition as the rate-determining step similarly to previous work [36], indicates that pyridine's basic properties do not critically interfere with the aromatic hydrogenation.

Table 4-10. Kinetic and catalytic descriptors estimated during regression of models for pyridine HDN over NiMo/γ-Al_2O_3 along with their 95% confidence intervals. Best performing models *i.e.*, model 5 and model 6, see Table 4-7 for statistical information. Models derived based on assuming proton addition first with fixed entropy values shown in Table 4-6.

Parameter	A* / K				Ea / -ΔH			
	Model 5		Model 6		Model 5		Model 6	
$k^a_{p\rightleftarrows pp}$	$8\ 10^{-3}$	± $1\ 10^{-3}$	$9\ 10^{-3}$	± $2\ 10^{-3}$	48	± 11	41	± 10
$k^a_{pp\rightarrow pa}$	1.15	± 2.10^{-1}	1.15	± 2.10^{-1}	126	± 16	185	± 19
$K_p{}^a$	4.6	± 1.4	6.1	± 1.5	10.8[b]		11.0[b]	
K_{pp}	13.5[c]		8.5[c]		119	± 2	117	± 3
K_{NH3}	2.5[c]		3.0[c]		75	± 2	76	± 2
K_{H2}	0.01[c]		0.02[c]		99	± 5	104	± 3
K_{H2S}	0.1[c]		2.1[c]		111	± 10	129	± 3

Units : k (A*) [mol $s^{-1}kg_{cat}^{-1}$], Ea [kJ mol^{-1}), K [MPa^{-1}] and ΔH [kJ mol^{-1}]

[a] Reaction and chemisorption coefficient at the average temperature, *i.e.*, 599 K

[b] Calculated, assuming similar loss of mobility as piperidine

[c] Calculated from estimated chemisorption enthalpy and best fitting chemisorption entropy, Table 4-6

The difference between models 5 and 6 is situated in the rate determining step considered for piperidine denitrogenation. Model 5, considering the protonation of the completely saturated aromatic ring as rate determining step has a slightly higher F value for the global significance, compared to model 6, considering the piperidine C-N bond scission as rate determining step. However, both models allow estimating all the parameters significantly. A comparison of the parameter estimates on physical grounds helps in further discrimination between the models.

As could be expected, both models estimate similar hydrogenation activation energies and similar NH_3 and H_2 chemisorption enthalpies. The major differences in the model parameter estimates are situated in the activation energy of the rate determining step, in the denitrogenation mechanism and the piperidine and H_2S chemisorption enthalpies.

Since a direct comparison of activation energies is unavailable for the piperidine protonation step, ab initio calculations for pyridine are referred to [59]. A pyridine chemisorption enthalpy amounting to 125 $kJmol^{-1}$ through an end-on chemisorption *via* N-Ni bonding was reported. Assuming this energy involves pyridine chemisorption as well as its subsequent protonation to form the pyridinium ion, one would expect a much lower protonation activation energy when a compound with higher basicity such as piperidine is considered. In our case model 5 estimates a protonation activation energy of about 126 kJ mol^{-1} which is rather high. The larger value for chemisorption equilibrium coefficient for piperidine of 13.5 MPa^{-1} related to model 5, shows a much larger deviation from the physical relevance of the parameter. For model 6, the activation energy for piperidine denitrogenation step amounts to 185 kJ mol^{-1}, which is rather well in agreement with literature reported values [28, 29]. The piperidine chemisorption equilibrium coefficient amounts to 8.5 MPa^{-1}, which is also much closer to the expected value [18].

The hydrogenation and denitrogenation activation energies for models 5 and 6 confirm the less pronounced temperature dependence of the hydrogenation rates compared to the denitrogenation rates. The obtained activation energies confirm the experimentally observed higher selectivity towards C_5 hydrocarbons at higher temperatures at 40% pyridine conversion, see Table 4-1. These results are not only in qualitative but also in quantitative agreement with the results of various other authors [28-30]. The difference in the activation energies can be related to the more energy demanding transition state formation in C-N bond breaking compared to hydrogenation through a proton or an hydride.

On top of the physical grounds, a distinct trend can be observed in the residuals for piperidine as a function of the H_2S inlet flow rate obtained with model 5. A clear systematic downward behaviour with the H_2S flow rate of the residuals Figure 4-6 can be observed when considering the proton addition step as rate determining in piperidine denitrogenation. Model 5, hence, seems to fail to account for the changes in piperidine outlet flow rate that arise from varying H_2S partial pressure. The absence of such systematic deviations when using model 6, see Figure 4-7, supports the selection of the substitution/ring opening mechanism with the C-N bond scission as the rate-determining step as an adequate representation of the actual reaction. Performance curves as shown in Figure 4-1 to Figure 4-3 allow a more severe assessment of the model simulation capabilities. No indications for any lack of fit can be observed.
Although model 6 has a slightly lower F value than model 5 on physical grounds, *i.e.,* because the sound physical significance of the model parameters and the performance, model 6 is the preferred one.

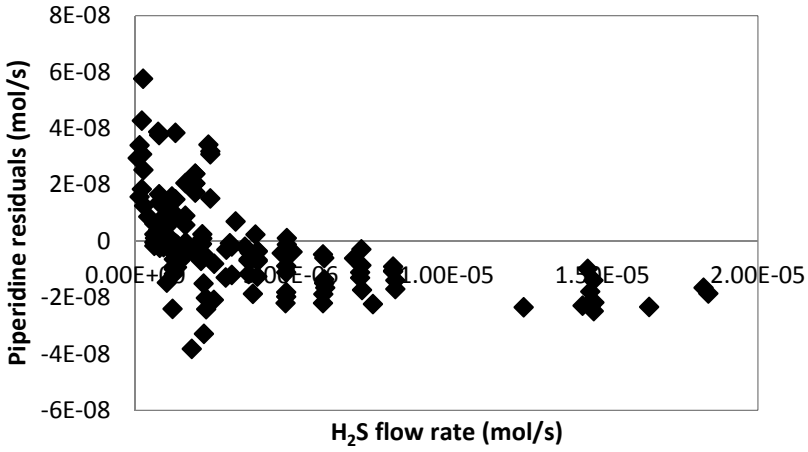

Figure 4-6. Residual figure for the piperidine outlet flow rate at varying inlet H_2S flow rate. Model calculated values obtained by solving reactor model provided in chapter 2 (Eq. 2-20) and rate equations corresponding to model 5 *i.e.*, heterolytic mechanism, proton addition first, 3rd hydrogenation step and 2nd denitrogenation (protonation) step as rate determining (as shown in Table 4-3), along with the set of parameter values of kinetic and catalyst descriptors reported in Tables 4-6 and 4-10.

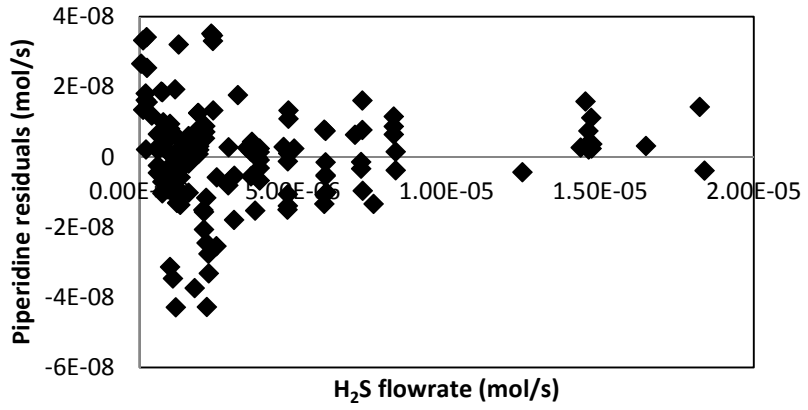

Figure 4-7. Residual figure for the piperidine outlet flow rate at varying inlet H_2S flow rate. Model calculated values obtained by solving reactor model equations provided in chapter 2 (Eq. 2-20) and rate equations corresponding to model 6 *i.e.*, heterolytic mechanism, proton addition first, 3rd hydrogenation step and 2nd denitrogenation (ring opening) step as rate determining (as shown in Table 4-3), along with the set of parameter values of kinetic and catalyst descriptors reported in Tables 4-6 and 4-10.

4.5.4 Chemisorption coefficient assessment in the selected model

4.5.4.1 Hydrogen and hydrogen sulphide chemisorption coefficients

Naphthalene hydrogenation (HDA) over a NiMo catalyst [36] and dibenzothiophene hydrodesulphurisation (HDS) over a CoMo catalyst [37], have been investigated and were modelled according to similar model assumptions. The corresponding hydrogen and hydrogen sulphide chemisorption coefficients are compared with the presently obtained ones in Table 4-11. Both the chemisorption entropy and enthalpy for H_2 are lower in comparison with the HDA study. Even though the investigated operating range is similar in both cases, the catalysts are slightly different. The catalyst used in this study is co-promoted with phosphorus, whereas the one used in HDA of Romero *et al.* [36] study is not co-promoted. The difference with the H_2 chemisorption coefficient obtained in the HDS study is rather high and is attributed to the different promoter, *i.e.,* Co rather than Ni. Nickel as a promoter is known to have better hydrogenation characteristics [67] compared to Co. The H_2S chemisorption enthalpy is similar to the one obtained in the HDA study. The chemisorption entropy of H_2S is higher in the present work compared to the HDA study but considered to be physically more meaningful.

Table 4-11. Reported values of hydrogen and hydrogen sulphide chemisorption equilibrium coefficients, Van‘t Hoff parameters

		Pyridine HDN (NiMo)	Naphtalene HDA[a] (NiMo)	Dibenzothiophene HDS[b] (CoMo)
K_{H2}	$\Delta H°$ (kJ mol^{-1})	-104	-80	-143
	$\Delta S°$ (J mol^{-1} K^{-1})	-187	-156	-142
K_{H2S}	$\Delta H°$ (kJ mol^{-1})	-129	-128	-106
	$\Delta S°$ (J mol^{-1} K^{-1})	-190	-253	-150

[a] Work on Naphthalene hydrogenation [36]

[b] Work on DBT hydrodesulphurisation [37]

4.5.4.2 Pyridine, piperidine and ammonia chemisorption coefficients

The chemisorption of nitrogen components has been investigated quite extensively due to their inhibiting effect on hydrodesulphurisation and hydrodearomatisation [18, 59, 68]. La Vopa and Satterfield [18] have established a relationship between the proton affinity of nitrogen containing components and their chemisorption coefficients. The pyridine chemisorption enthalpy could not be significantly estimated for any of the models and, hence, the corresponding coefficient was treated as temperature independent and estimated as a single parameter at average temperature, *i.e.,* 599 K. This was also reported in the work by Pille and

Froment [28], and typically stems from relatively weak chemisorption in comparison to other components. A higher proton affinity indicates a stronger interaction with the catalyst surface. Our results are in agreement with those results of La Vopa and Satterfield [18], where the chemisorption coefficients of the nitrogen components decrease in the following order: piperidine > pyridine > ammonia. The strong piperidine chemisorption on the * sites is evident from the in more negative chemisorption entropy for piperidine, amounting to -158 J mol^{-1} K^{-1}, in comparison to naphthalene, -129 J mol^{-1} K^{-1}, and tetralin, -97 J mol^{-1} K^{-1}, which were reported by Romero *et al*. [36]. Accordingly, a comparatively less negative chemisorption entropy for ammonia *i.e.*, -98 J mol^{-1} K^{-1}, indicates a higher mobility due to the weaker interaction with * sites which is explained by its lower proton affinity.

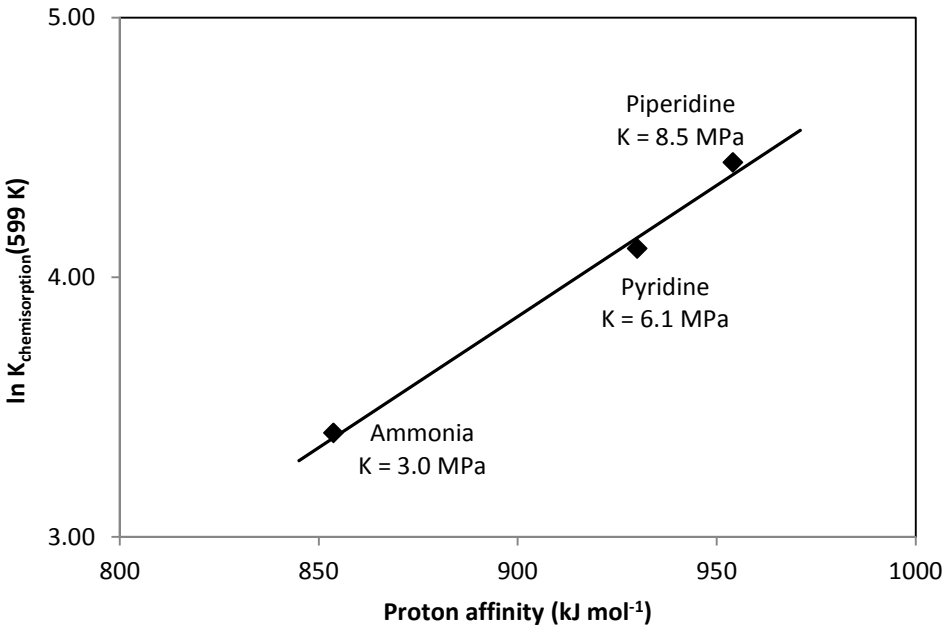

Figure 4-8. Chemisorption coefficient for the different nitrogen molecules at the average temperature (*i.e.*, 599K); plot constructed in a similar way as by La Vopa and Satterfield [18], line: best fitting linear curve

4.5.4.3 Surface coverages

The selected model was further used to simulate the surface coverages of the relevant components at the operating conditions used. Figure 4-9, shows that the model predicts 50% of the * sites to be occupied by H_2S molecules under typical operating conditions. This ensures the availability of surface sulphydril species for the denitrogenation to proceed *via* the substitution pathway. It also indicates the tendency of the catalyst to remain in its sulphided state. The surface coverages by the other species vary from a minimum of 5% to a maximum 20%. The free site concentration is very low indicating the surface to be completely occupied

by the species involved in the reaction. This is mainly a result of the strongly adsorbing nitrogen containing species and H_2S. At higher total pressures only the piperidine surface coverage increases significantly while the hydrogen and hydrogen sulphide surface coverages remain rather constant.

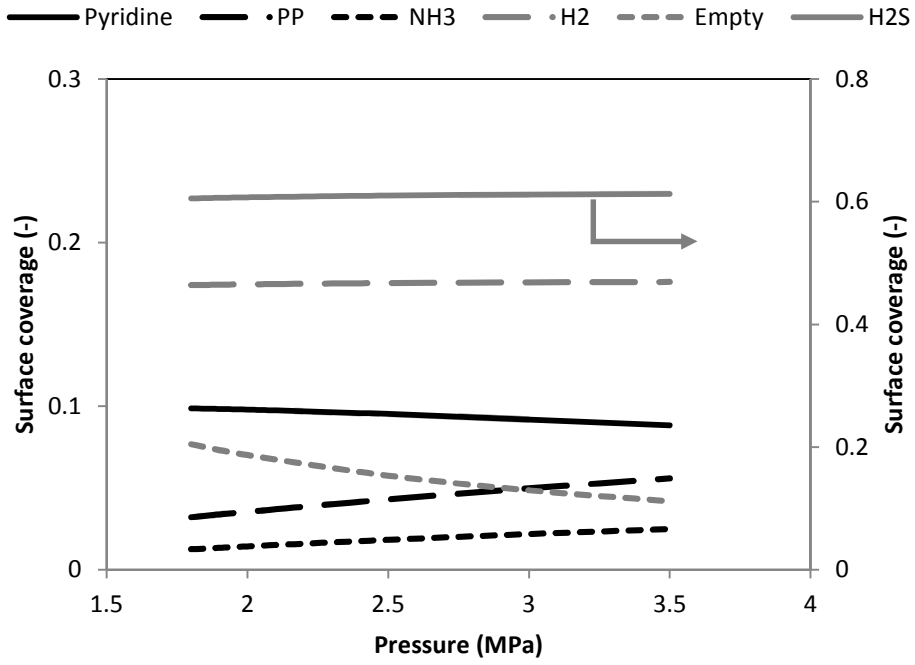

Figure 4-9. Surface coverage of components over the *, corresponding with Figure 4-3 (right), model calculated values obtained by solving reactor model equations provided in chapter 2 (Eq. 2-20) and rate equations corresponding to model 6 *i.e.*, heterolytic mechanism, proton addition first, 3rd hydrogenation step and 2nd denitrogenation (ring opening) step as rate determining (as shown in Table 4-3), along with the set of parameter values of kinetic and catalyst descriptors reported in Tables 4-6 and 4-10.

4.6 Conclusions

Pyridine hydrodenitrogenation occurs as a two-step reaction *i.e.*, hydrogenation of the aromatic ring to form piperidine and subsequent denitrogenation to release ammonia and yield C_5 hydrocarbons. H_2 and H_2S were found to chemisorb heterolytically on the catalyst surface, providing proton, hydride and sulphydril species for the occurring reactions. The aromatic ring undergoes stepwise hydrogenation with proton addition first as a consequence of its basicity. Nitrogen is predominantly eliminated via a H_2S enhanced substitution mechanism which, was the sole denitrogenation mechanism incorporated in the model. For the first time, this

denitrogenation mechanism was modelled in terms of elementary steps. An a priori assessment of the chemisorption entropies based on statistical thermodynamics, allowed the significant estimation of all model parameters, except for the pyridine chemisorption enthalpy, in all models retained after preliminary selection. The higher activation energy for naphthenic C-N bond scission than for hydrogenation, *i.e.*, 185 versus 41 kJ mol^{-1}, quantifies the more pronounced temperature dependence of the former compared to the latter. The addition of the third hydrogen atom being rate determining in the hydrogenation sequence is in line with what is generally observed in aromatic hydrogenation and does not seem to be influenced by pyridine's basic character. Piperidine denitrogenation is enhanced by the presence of H_2S via a sulphydril assisted C-N bond scission, the ring-opening C-N bond scission being more energy demanding than the acyclic one. The proton affinity of the various nitrogen containing components is linearly related with the corresponding chemisorption coefficients. The surface coverage is dominated by the sulphydril species explaining the impact on the C-N bond scission while piperidine is the most strongly chemisorbing basic compound.

4.7 References

1. Ding, L.H., Y. Zheng, Z.S. Zhang, Z. Ring, and J.W. Chen, **Applied Catalysis A: General**, 2007. 319: p. 25-37.

2. Laredo, G.C., P.M. Vega-Merino, F. Trejo-Zárraga, and J. Castillo, **Fuel Processing Technology**, 2013. 106(0): p. 21-32.

3. Furimsky, E. and F.E. Massoth, **Catalysis Today**, 1999. 52(4): p. 381-495.

4. Dong, D., S. Jeong, and F.E. Massoth, **Catalysis Today**, 1997. 37(3): p. 267-275.

5. Massoth, F.E., K. Balusami, and J. Shabtai, **Journal of Catalysis**, 1990. 122(2): p. 256-270.

6. Stanislaus, A., A. Marafi, and M.S. Rana, **Catalysis Today**, 2010. 153(1-2): p. 1-68.

7. Rabarihoela-Rakotovao, V., S. Brunet, G. Berhault, G. Perot, and F. Diehl, **Applied Catalysis A: General**, 2004. 267(1-2): p. 17-25.

8. Garcia-Martinez, J.C., C.O. Castillo-Araiza, J.A.D. Heredia, E. Trejo, and A. Montesinos, **Chemical Engineering Journal**, 2012. 210: p. 53-62.

9. Morrison, R.T., R.N. Boyd, and D.S. Noyce, *Organic chemistry*. 1959 ed. Vol. 10. 1960, Boston Massachusetts: Tetrahedron.

10. Valencia, D., T. Klimova, and I. Garcia-Cruz, **Fuel**, 2012. 100: p. 177-185.

11. Adam, F., F. Bertoncini, N. Brodusch, E. Durand, D. Thiebaut, D. Espinat, and M.C. Hennion, **Journal of Chromatography A**, 2007. 1148(1): p. 55-64.

12. Adam, F., F. Bertoncini, V. Coupard, N. Charon, D. Thiebaut, D. Espinat, and M.C. Hennion, **Journal of Chromatography A**, 2008. 1186(1-2): p. 236-244.

13. Adam, F., F. Bertoncini, C. Dartiguelongue, K. Marchand, D. Thiebaut, and M.C. Hennion, **Fuel**, 2009. 88(5): p. 938-946.

14. Adam, F., C. Vendeuvre, F. Bertoncini, D. Thiebaut, D. Espinat, and M.C. Hennion, **Journal of Chromatography A**, 2008. 1178(1-2): p. 171-177.

15. Park, Y. and H.-K. Rhee, **Korean Journal of Chemical Engineering**, 1998. 15(4): p. 411-416.

16. Flego, C. and C. Zannoni, **Fuel**, 2011. 90(9): p. 2863-2869.

17. Beltramone, A., S. Crossley, D. Resasco, W. Alvarez, and T. Choudhary, **Catalysis Letters**, 2008. 123(3): p. 181-185.

18. La Vopa, V. and C.N. Satterfield, **Journal of Catalysis**, 1988. 110(2): p. 375-387.

19. Kwak, C., J.J. Lee, J.S. Bae, and S.H. Moon, **Applied Catalysis B: Environmental**, 2001. 35(1): p. 59-68.

20. Choi, K.H., Y. Korai, I. Mochida, J.W. Ryu, and W. Min, **Applied Catalysis B: Environmental**, 2004. 50(1): p. 9-16.

21. Farag, H., M. Kishida, and H. Al-Megren, **Applied Catalysis A: General**, 2014. 469(0): p. 173-182.

22. Fu, C.M. and A.M. Schaffer, **Industrial & Engineering Chemistry Product Research and Development**, 1985. 24(1): p. 68-75.

23. Raybaud, P., **Applied Catalysis A: General**, 2007. 322: p. 76-91.

24. Lauritsen, J.V., J. Kibsgaard, G.H. Olesen, P.G. Moses, B. Hinnemann, S. Helveg, J.K. Norskov, B.S. Clausen, H. Topsoe, E. Laegsgaard, and F. Besenbacher, **Journal of Catalysis**, 2007. 249(2): p. 220-233.

25. Kibsgaard, J., J.V. Lauritsen, E. Laegsgaard, B.S. Clausen, H. Topsoe, and F. Besenbacher, **Journal of the American Chemical Society**, 2006. 128(42): p. 13950-13958.

26. Jian, M. and R. Prins, **Recent Advances in Basic and Applied Aspects of Industrial Catalysis**, 1998. 113: p. 111-123.

27. Deepa, G., T.M. Sankaranarayanan, K. Shanthi, and B. Viswanathan, **Catalysis Today**, 2012. 198(1): p. 252-262.

28. Pille, R. and G. Froment, **Hydrotreatment and Hydrocracking of Oil Fractions**, 1997. 106: p. 403-413.

29. Kopyscinski, J., J. Choi, and J.M. Hill, **Applied Catalysis A: General**, 2012. 445: p. 50-60.

30. Kopyscinski, J., J. Choi, L. Ding, S. Zhang, B. Ibeh, and J.M. Hill, **Catalysis Letters**, 2012. 142(7): p. 845-853.

31. Jian, M. and R. Prins, **Journal of Catalysis**, 1998. 179(1): p. 18-27.

32. Eijsbouts, S., J.N.M. Vangestel, J.A.R. Vanveen, V.H.J. Debeer, and R. Prins, **Journal of Catalysis**, 1991. 131(2): p. 412-432.

33. Hrabar, A., J. Hein, O.Y. Gutierrez, and J.A. Lercher, **Journal of Catalysis**, 2011. 281(2): p. 325-338.

34. Temel, B., A.K. Tuxen, J. Kibsgaard, N.Y. Topsoe, B. Hinnemann, K.G. Knudsen, H. Topsoe, J.V. Lauritsen, and F. Besenbacher, **Journal of Catalysis**, 2010. 271(2): p. 280-289.

35. Lauritsen, J.V., M.V. Bollinger, E. Laegsgaard, K.W. Jacobsen, J.K. Norskov, B.S. Clausen, H. Topsoe, and F. Besenbacher, **Journal of Catalysis**, 2004. 221(2): p. 510-522.

36. Romero, C.M.C., J.W. Thybaut, and G.B. Marin, **Catalysis Today**, 2008. 130(1): p. 231-242.

37. Vanrysselberghe, V. and G.F. Froment, **Industrial & Engineering Chemistry Research**, 1996. 35(10): p. 3311-3318.

38. Guernalec, N., T. Cseri, P. Raybaud, C. Geantet, and M. Vrinat, **Catalysis Today**, 2004. 98(1-2): p. 61-66.

39. Kasztelan, S. and D. Guillaume, **Industrial & Engineering Chemistry Research**, 1994. 33(2): p. 203-210.

40. Satterfield, C.N. and J.F. Cocchetto, **AIChE Journal**, 1975. 21(6): p. 1107-1111.

41. Stitt, E.H., R.J. Berger, G.B. Marin, F. Kapteijn, and J.A. Moulijn, **Cattech**, 2001. 5(1): p. 30-60.

42. Froment, G.F. and K.B. Bischoff, *Chemical reactor analysis and design* 1979, New York Wiley.

43. Wang, H. and R. Prins, **Catalysis Letters**, 2008. 126(1): p. 1-9.

44. Sonneman, J. and P. Mars, **Journal of Catalysis**, 1974. 34(2): p. 215-229.

45. Hanlon, R.T., **Energy & Fuels**, 1987. 1(5): p. 424-430.

46. Schwartz, V. and S.T. Oyama, **Journal of Molecular Catalysis A: Chemical**, 2000. 163(1-2): p. 269-282.

47. Raghuveer, C.S., J.W. Thybaut, R. De Bruycker, K. Metaxas, T. Bera, and G.B. Marin, **Fuel**, 2014. 125(0): p. 206-218.

48. Egorova, M., Y. Zhao, P. Kukula, and R. Prins, **Journal of Catalysis**, 2002. 206(2): p. 263-271.

49. Prins, R., A. Egorova, A. Rothlisberger, Y. Zhao, N. Sivasankar, and P. Kukula, **Catalysis Today**, 2006. 111(1-2): p. 84-93.

50. Prins, R., M. Jian, and M. Flechsenhar, **Polyhedron**, 1997. 16(18): p. 3235-3246.

51. Schwartz, V., V.T. da Silva, and S.T. Oyama, **Journal of Molecular Catalysis A: Chemical**, 2000. 163(1-2): p. 251-268.

52. Cattenot, M., J.L. Portefaix, J. Afonso, M. Breysse, M. Lacroix, and G. Perot, **Journal of Catalysis**, 1998. 173(2): p. 366-373.

53. Bera, T., J.W. Thybaut, and G.B. Marin, **Industrial & Engineering Chemistry Research**, 2011. 50(23): p. 12933-12945.

54. Sonneman, J., W.J. Neyens, and P. Mars, **Journal of Catalysis**, 1974. 34(2): p. 230-241.

55. Sonneman, J., G.H. Van den Berg, and P. Mars, **Journal of Catalysis**, 1973. 31(2): p. 220-230.

56. Mcilvried, H.G., **Industrial & Engineering Chemistry Process Design and Development**, 1971. 10(1): p. 125.

57. Saeys, M., J.W. Thybaut, M. Neurock, and G.B. Marin, **Molecular Physics**, 2004. 102(3): p. 267-272.

58. Sun, M., A.E. Nelson, and J. Adjaye, **Catalysis Today**, 2005. 105(1): p. 36-43.

59. Sun, M., A.E. Nelson, and J. Adjaye, **Journal of Catalysis**, 2005. 231(1): p. 223-231.

60. Sivasankar, N. and R. Prins, **Catalysis Today**, 2006. 116(4): p. 542-553.

61. Martens, G.G., J.W. Thybaut, and G.B. Marin, **Industrial & Engineering Chemistry Research**, 2001. 40(8): p. 1832-1844.

62. Jacobs, P.A., M. Tielen, J. Martens, and H.K. Beyer, **Journal of Molecular Catalysis**, 1984. 27(1-2): p. 11-23.

63. Massoth, F.E. and J. Miciukiewicz, **Journal of Catalysis**, 1986. 101(2): p. 505-514.

64. Dumesic, D.A., D.F. Rudd, L.M. Aparicio, J.E. Kekoske, and A.A. Trevino, *The microkinetics of heterogeneous catalysis*. 1993, American Chemical Society: Washington, DC.

65. Moore, W.J., *Physical chemistry*. 3d ed. Prentice-Hall chemistry series. 1962, Englewood Cliffs, N.J.,: Prentice-Hall. 844 p.

66. Hunter, E.P.L. and L. Sharon.G, **Journal of Physical and Chemical Reference Data**, 1998. 27(3).

67. Kim, S.C. and F.E. Massoth, **Journal of Catalysis**, 2000. 189(1): p. 70-78.

68. Sun, M., A.E. Nelson, and J. Adjaye, **Journal of Molecular Catalysis A-Chemical**, 2004. 222(1-2): p. 243-251.

This page intentionally left blank

5 Pyridine hydrodenitrogenation over industrial NiMo/γ-Al_2O_3 catalyst: Application of gas phase kinetic models to liquid phase reactions

A systematic methodology for simulating gas-liquid-solid kinetics starting from a gas-solid kinetics model (presented in chapter 4) and applied to pyridine hydrodenitrogenation over an industrial NiMo/γ-Al_2O_3 catalyst at liquid phase, is developed. Data have been acquired in two independent, dedicated experimental programmes: *i.e.,* an extended set of gas phase experiments that were previously carried out in a Berty type reactor setup at 573-633 K, 1.5 – 4.0 MPa and space times between 0.36 to 1.8 kg_{cat} s $mmol^{-1}_P$ and a more limited set of liquid phase experiments that were performed as part of the present work in a Robinson-Mahoney reactor setup at 543 – 613 K, 6.0 – 8.0 MPa and space times between 0.45 to 3.0 kg_{cat} s $mmol^{-1}_P$. At liquid phase conditions the pyridine conversion ranged from 37 to 80%, while at gas phase conditions the pyridine conversion ranged from 17 to 72%. The reaction temperature and H_2S inlet partial pressure were found to be most significantly affecting the selectivity to

intermediates and products in both experimental programmes. *n*-pentylpiperidine formation, a bimolecular reaction product exclusively observed at liquid phase conditions, could be ascribed to the differences in phases present during the kinetic measurements as well as to the differences in molar H_2 and H_2S to pyridine inlet ratios used and the resulting surface concentrations. A kinetic model constructed using the gas phase data was extended to liquid phase conditions by accounting for (i) liquid phase non-ideality (ii) solvent adsorption effects and (iii) the additionally observed response, *i.e.*, *n*-pentylpiperidine. The latter was found to be produced via condensation between piperidine and pentylamine.

5.1 Introduction

Hydrotreating, which is mainly aiming at the removal of heteroatoms and aromatics from complex hydrocarbon mixtures, is one of the most important processes in petroleum refining [1-3]. The importance of hydrodenitrogenation in the context of crude-oil based feedstocks has been presented in chapter 1.

Industrial hydrotreating catalysts are high surface area materials comprising an active component, a promoter and, potentially, co-promoters which are impregnated on supports such as γ-Al_2O_3, SiO_2 or zeolites. A detailed discussion on the industrial hydrotreating catalysts has been presented in chapter 1. The location, morphology, electronic nature and the acidity of the active sites of these sulphided Ni/Co-Mo catalysts have been a matter of debate [4-7]. Previous modelling efforts have typically considered two types of sites to explain the various reactions involved in hydrodenitrogenation. Although differences exist in the exact interpretation of the nature and function of the active sites considered, a common trend is to propose one type of site, such as coordinatively unsaturated sites (*), with a metallic character, for hydrocarbon and light gas adsorption and another type of site, such as the sulphur anion sites (S^{2-}) exclusively for adsorption of light gases that help catalyse C-N bond breaking by providing the required acidity through protons or sulphydril species, see also chapter 4 [8, 9].

Different types of nitrogen compounds can be found in crude oil [10, 11]. As a result, various nitrogen compounds have been used to study different aspects. In depth reaction network elucidation and kinetic modelling have been performed typically with model compounds with more complex structures [12-16]. Other studies have focused on the interplay between hydrodesulphurisation and hydrodenitrogenation reactions during the deep desulphurisation of crude oil [17] and rather made use of more simple, substituted pyridines and benzothiophenes. The latter, together with nitrogen compounds with six-membered aromatic rings, have been most widely investigated [17-25]. In the present work, which is

aimed at investigating ‘gas versus liquid phase kinetics’, see below, pyridine is used as the model compound. In addition to the wide availability of literature data, it forms relatively few intermediates, which allows focusing on the ‘gas to liquid phase kinetics’ aspect.

In the present work, pyridine hydrodenitrogenation is employed to demonstrate the applicability of the methodology for applying gas phase models to three-phase conditions beyond acid catalysis in hydrocracking [26]. In this case a pyridine hydrodenitrogenation kinetics model based on elementary steps resulting from an extensive gas phase kinetic experimentation [8] has been used for the assessment of liquid phase kinetics data. A limited number of liquid phase experiments have been performed to determine liquid phase thermodynamic non-ideality and other gas versus liquid phase related effects on the pyridine hydrodenitrogenation behaviour. The ability to adequately describe liquid phase chemical kinetics making use of a rate expression derived from gas phase kinetics, provides a sound and efficient route towards the assessment of the kinetics of a variety of industrial reactions at operating conditions focused on intrinsic kinetics determination without having to mimic the industrial operating conditions.

5.2 Procedures

The gas-solid and the gas-liquid-solid phase experimental investigations, denoted shortly as gas-phase and liquid-phase experimentation, have been performed independently in a Berty and a Robinson Mahoney reactor. Details of the reactor set up including the data treatment procedures can be found in chapter 2, while the details of gas phase experiments can be found in chapter 4 and previous work by Pille and Froment [8]. However, Table 5-2 provides a quick look-up into the differences in the operating conditions in the gas and liquid phase experiments.

5.2.1 Catalyst and Chemicals

A commercially available NiMo/γ-Al_2O_3 catalyst (Procatalyse EC/22/216/91) was employed. Properties of the catalyst composition and its physical characteristics are provided in chapter 2. The chemicals, both gases and liquids, used for the liquid phase experimental programme were used as available commercially without further purification. The supplier and codes of the various chemicals used in the experimental program are listed in

Table 5-1.

Table 5-1. Codes and suppliers of the chemical used in the experimental program for liquid phase hydrodenitrogenation studies of pyridine on a NiMo/γ-Al_2O_3 catalyst

Chemical	Phase	Supplier	Code
Pyridine	Liquid	VWR Prolabo	203-809-9
Dimethyl disulphide	Liquid	Acros Organic	624-92-0
Nonane	Liquid	Acros Organic	111-84-2
Halpasol™	Liquid	Haltermann	190-240
H_2	Gas	Airliquide	N40

™ : Product of Haltermann, is a *n*-paraffinic mixture and consequently the mildest in terms of solvent effect and odour.

5.2.2 Set-up and operating conditions

The gas and liquid phase operating conditions are reported in Table 5-2. The major differences are situated in the total pressure and the molar inlet H_2 and H_2S to pyridine ratio as they arise from the phase requirements. Additionally, a heavier solvent, *i.e.*, Halpasol™, which is a mixture comprising *n*-alkanes in the range of *n*-C_9 to *n*-C_{14}, is used in the liquid phase experimentation compared to a light solvent such as *n*-C_6 at gas phase conditions. Thermodynamic vapour liquid equilibrium calculations were performed to ensure the expected phase equilibrium of the reactants.

Table 5-2. Summary of gas and liquid phase pyridine hydrodenitrogenation experimental programme over a sulphided NiMo/γ-Al_2O_3 catalyst

Program	Gas phase [8]	Liquid phase
Reactor type	Berty type	Robinson Mahoney
Temperature range (K)	573 – 633	543 – 613
Total pressure (MPa)	1.5 – 4.0	6.0 – 8.0
Inlet H_2/pyridine ratio (mol mol^{-1})	80 – 600	10 – 15
H_2S/Pyridine(mol/mol^{-1})	0.1–18	0.04 – 0.20
Space time (kg_{cat} s $mmol^{-1}$)	0.36 – 1.8	0.45 – 3.0
Inlet solvent/pyridine (mol mol^{-1})	40	20 – 40
Solvent	*n*-C_6	Halpasol™

5.2.3 Kinetic regime verification

In order to measure intrinsic kinetics, the experimental data had to be free from mass and heat transfer effects. Several criteria for the assessment of these effects have been proposed [27], and have been successfully been employed [28]. Mass transfer at the gas liquid interphase and the liquid solid interphase were assessed by calculating the dimensionless Carberry number at the extremes of the operating conditions, *i.e.*, highest and lowest operating temperatures and

pressures, and were found to be insignificant with Carberry numbers well below the limit value of 0.05. The Weisz - Prater [29] criterion addresses the intraparticle diffusion for the various reactants and products. The most critical value obtained was for hydrogen and amounted to 0.039, which is still below the limit value of 0.08.

The absence of heat transfer was verified by using the criteria reported by Mears [30]. The temperature gradients were compared with the maximum allowed limits between the liquid solid interphase $\Delta T_{L\text{-}S}$ and particle ΔT_{int}. The most critical values of $\Delta T_{L\text{-}S}$ and ΔT_{int} were found to be 0.058 and 0.015 respectively, at the highest operating temperature which is much lower than Mears' criterion of 1.9, confirming the absence of heat transfer limitations.

5.2.4 Thermodynamic non-ideality at liquid phase conditions

Thermodynamic non-ideality is an issue that often needs to be addressed at liquid phase conditions due to the interactions involved between molecules of a different type or nature. In the present case, thermodynamic non-ideality can be expected due to the interaction between the aromatic heterocompounds, the aliphatic hydrocarbons and the light gases, *i.e.*, hydrogen and hydrogen sulphide.

The basis for the calculation of deviations from a standard state can be established with the help of the chemical potential μ_i, which is independent of the assumed standard state and can be expressed as follows:

$$\mu_i = \mu_i^{standard} + RT\ ln\ a_i \qquad 5\text{-}1$$

The chemical potential is expressed with respect to a selected standard state and requires the calculation of a generalised activity, a_i, which depends on this selected standard state. This generalized activity is denoted as an 'activity' in the case the pure liquid is considered as the standard state or a 'fugacity' when the ideal gas is referred to as the standard state. Given the gas to liquid phase aspect of the present kinetics study, the corresponding vapour liquid equilibrium calculations for hydrocarbon mixtures are performed using the ideal gas state at 0.1 MPa as the standard state for both the liquid and the vapour phase [31]. As a consequence, the generalised activity a_i in equation 5-1 represents a fugacity f_i which can be calculated using the Peng-Robinson equation of state. The equality of the chemical potentials of all individual components *i* in a mixture with *n* components as shown in equation 5-2 as a requirement for the phase equilibrium is then reduced to the equality of fugacities as shown in equation 5-3.

$$\mu_i^v = \mu_i^l \qquad i = 1, \dots, n \qquad 5\text{-}2$$

$$f_i^v = f_i^l \qquad i = 1, \dots, n \tag{5-3}$$

The fugacity of a component is related to its partial pressure with the help of the fugacity coefficient 'φ' [32], which is presented in equation 5-4. The partial pressure in this equation can be related to its mole fraction using equation 5-5.

$$f_A = \varphi_A \, p_A \tag{5-4}$$

$$p_A = y_A \, p_t \tag{5-5}$$

The concentration of a species A in the liquid phase, C_A^l, can be related to its mole fraction considering the molar volume of the liquid. The fugacity can be obtained from equation 5-6.

$$f_A^l = \varphi_A^l \, p_t \, V_m^l \, c_A^l \tag{5-6}$$

The interactions between chemisorbed species and the liquid molecules are considered to be insignificant compared to the interaction of the chemisorbed species with the catalyst [31]. The description of the effects of the liquid phase thermodynamic non ideality on the reaction kinetics is then entirely situated in the chemisorption steps, *i.e.,* the transfer of the reactants from the fluid phase to the catalyst surface.

Consider the chemisorption of a component A on a surface with the site '*' as shown in equation 5-7.

$$A + * \rightarrow C_A \tag{5-7}$$

For which the equilibrium relationship can be written as,

$$K_A = \frac{C_A}{f_A^l \, C_*} \tag{5-8}$$

Upon using concentrations for modelling the liquid phase kinetics, the chemisorption coefficient can then be replaced considering equations 5-8 and 5-9

$$K_A^l = K_A \, \varphi_A^l \, P_t \, V_m^l \tag{5-9}$$

Non-idealities due to interaction between the various gases and the hydrocarbons are implemented as suggested by Moysan *et al.* [33]. Estimation of the molar volume of the liquid mixture is performed using the Hankinson-Brobst-Thomson method [32].

5.2.5 Reactor Model

The Robinson-Mahoney reactor used for the liquid phase pyridine hydrodenitrogenation is as continuous stirred tank reactor, hence the reactor model equation is similar to the one presented in chapter 2.

5.2.6 Parameter estimation

The methodology for parameter estimation is based on the minimisation of the weighted sum of squared residuals between the experimental and model calculated outlet molar flow rates. Detailed information on the parameter estimation procedure and the tests performed for assessing the model is provided in chapter 2.

5.3 Qualitative assessment of liquid phase pyridine hydrodenitrogenation

5.3.1 Pyridine hydrodenitrogenation reaction network

Experimental pyridine hydrodenitrogenation investigations at varying operating conditions, *i.e.*, temperatures, total pressures, and inlet molar H_2 and H_2S to pyridine ratios have been performed [8, 21, 23, 34, 35]. The corresponding reaction network has been extensively investigated and was found to comprise a reversible initial saturation of the hetero-aromatic ring followed by irreversible ring opening and nitrogen removal [18-20, 36]. While piperidine has been indicated as an intermediate in all the studies, only a few investigations have reported the observation of pentylamine [9] and *n*-pentylpiperidine [18, 25, 36-38]. The end products of pyridine hydrodenitrogenation were C_5 hydrocarbons, with higher selectivity towards pentane and lower selectivity towards pentene.

The complete reaction network is summarised in Figure 5-1. Pyridine, upon complete hydrogenation (1), is converted into piperidine, which can subsequently undergo ring opening to form pentylamine by a direct route (2) or through a substitution reaction pathway (3) where a thiol amine is formed as an intermediate. Similarly, pentylamine undergoes a Hofmann elimination type (4) or a substitution type (5) reaction [12, 35, 39] to form C_5 hydrocarbons. Reversibility of the initial hydrogenation has been indicated by the corresponding double headed reaction arrows, while all other reactions are considered to be irreversible in the investigated range of operating conditions indicated by the single headed reaction arrows in Figure 5-1. Additionally, in the present work, *i.e.*, at liquid-phase conditions, a significant amount of *n*-pentylpiperidine was formed. This has been considered as the result of a disproportionation reaction between two piperidine molecules (6) or a condensation between piperidine and pentylamine (7) [18, 21, 36, 37] and is further addressed in more detail in this work. Both the disproportionation and the condensation reactions are assumed to occur irreversibly.

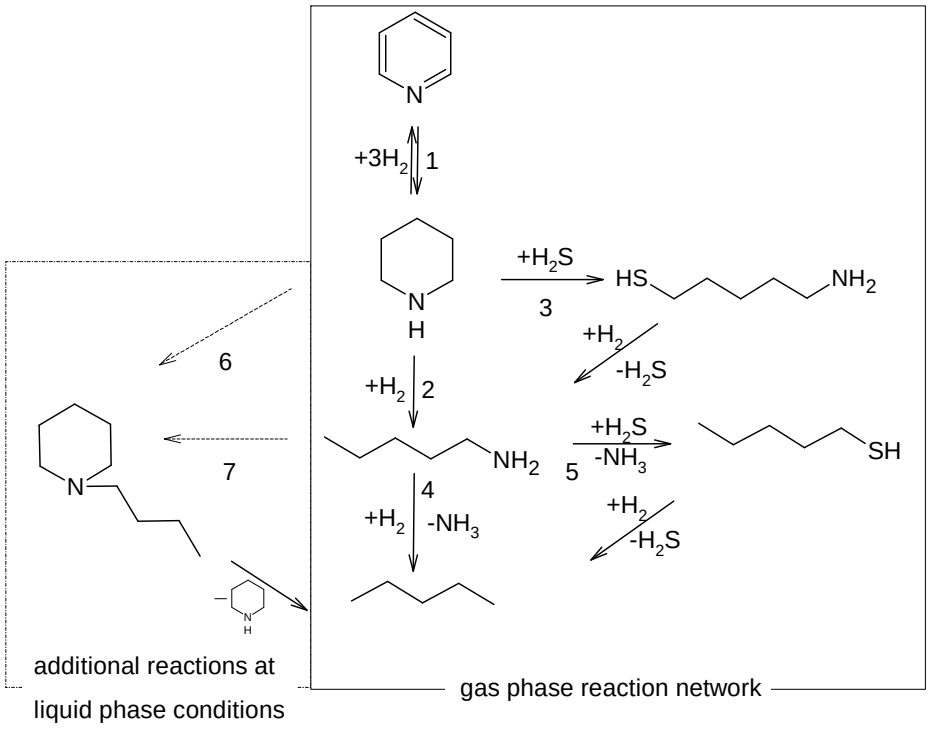

Figure 5-1. Detailed reaction network comprising all intermediates in pyridine hydrodenitrogenation. Explanation of enumerated reactions can be found in section 5.3.1.

5.3.2 Effect of the operating conditions on the liquid phase pyridine hydrodenitrogenation kinetics

The most pertinent operating conditions have systematically been varied to investigate their effect on the reaction kinetics. As could be expected, the pyridine conversion increased with increasing temperature, total pressure, and space time. However, differences in the product distribution were noticed in each of the cases. Increasing space times enhances the consecutive reactions of the intermediate piperidine and, hence, result in higher selectivity towards the end-product pentane. The rather high selectivity towards piperidine at liquid phase conditions observed in the present work compared to the previous gas phase experimentation can be explained by the different molar inlet H_2S to pyridine ratios used. The lower inlet molar H_2S to pyridine ratios at liquid phase conditions result in less pronounced substitution reactions and, hence, lower C-N bond scission compared to hydrogenation rates at these operating conditions. Along with the promotional effect of H_2S on the C-N bond cleavage reaction, this observation suggests that also the removal of ammonia from the primary amine occurs through substitution reactions of the SN_2 type, rather than elimination reactions as suggested by Cattenot *et al.* [40]. This is further in agreement with a recent work by Kopyscinski *et al.* [34]

who did report the presence of pentylamine in their experimental program in the absence of H_2S. This results in a higher concentration of strongly chemisorbing nitrogen components such as piperidine on the catalyst surface, which also provides a potential explanation for the significant occurrence of the aforementioned *n*-pentylpiperidine formation.

5.3.3 Temperature

Higher temperatures were found to enhance the pyridine conversion, despite the typically lower reactant surface concentrations due to the exothermic nature of adsorption. This temperature effect on chemisorption is overcompensated by the increase in the surface reaction rate with the temperature. These are similar observations to those made during gas phase pyridine hydrodenitrogenation experiments [8].

The product selectivity at different temperatures, but similar conversion, are compared to assess the temperature effect on the various reaction types involved in pyridine hydrodenitrogenation, see Table 5-3. A higher selectivity towards C_5 products is observed at 583 K compared to 573 K, The piperidine selectivity is correspondingly lower, while that towards *n*-pentylpiperidine remained similar. These trends which are further confirmed by the data presented in Figure 5-2 at constant space time, indicate that the lowest apparent activation energy is obtained for pyridine hydrogenation towards piperidine, while the C-N bond cleavage reaction is most strongly temperature dependent and, hence, has the highest apparent activation energy. *n*-pentylpiperidine formation has an intermediate apparent activation energy, explaining why its selectivity is rather independent of the temperature, see also Section 5.4.

Table 5-3. Product selectivity as a function of the temperature at a conversion amounting to 0.65 and a total pressure of 6.0 MPa and an inlet molar ratio H_2S/Pyridine of 0.04.

T	**W/Fp°**	**X**	**Selectivity**		
			C_5	**PP**	***n*-PPP**
(K)	(kg_{cat} s mol_P^{-1})	(-)	(-)	(-)	(-)
573	1129	0.64	0.34	0.44	0.22
583	790	0.65	0.45	0.35	0.20

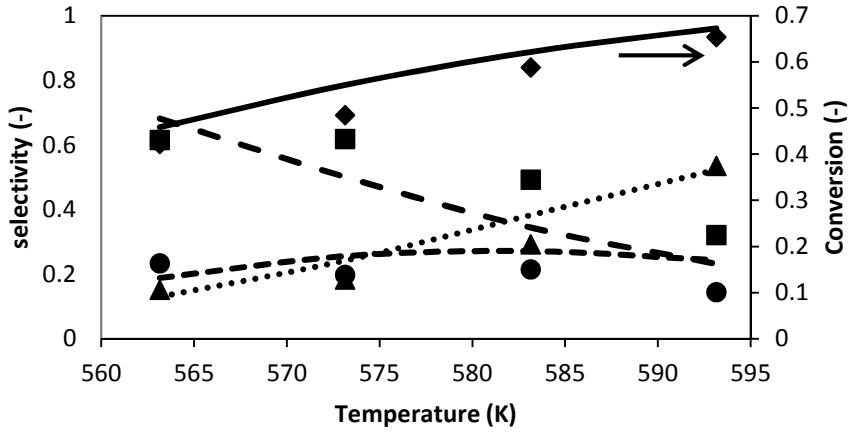

Figure 5-2. Temperature effect on pyridine conversion and product selectivity in liquid phase pyridine hydrodenitrogenation over a sulphided NiMo/γ-Al_2O_3 catalyst. Operating conditions: Total Pressure = 6.0 MPa, space time = 790 kg s mol^{-1}, molar inlet H_2/pyridine = 10 (mol mol^{-1}), molar inlet H_2S/pyridine = 0.04 (mol mol^{-1}), molar inlet solvent/pyridine = 40; Symbols: experimentally obtained values, ♦ : pyridine, ■ : piperidine, •: *n*-pentylpiperidine, ▲: C_5 hydrocarbons; Lines: Calculated using model simulated outlet flow rates from reactor model equation presented in chapter (Eq. 2-20) along with rate equations 5-10, 5-11 and 5-18 to 5-20 and net rates of formation 5-21 to 5-24 and parameters from chapter 4 (Table 4-10) , Tables 5-4 and 5-6, —— : Pyridine, — — : Piperidine, -- : *n*-Pentylpiperidine, ••• : C_5 hydrocarbons.

5.3.4 Molar inlet H_2S to pyridine ratio

Increasing the molar inlet H_2S to pyridine ratio slightly increases the overall pyridine conversion, see Figure 5-3, however, a significant increase in the C_5 product selectivity was observed at a higher molar inlet H_2S to pyridine ratio. The positive effect of H_2S on the C-N bond scission rate by its involvement in the substitution reaction is much more pronounced than the, potentially expected, decrease in hydrogenation rate by competitive chemisorption between H_2S and H_2 on the catalyst surface. As a result, lower surface concentrations of the most strongly binding piperidine are established at a higher molar inlet H_2S/pyridine ratio and the overall pyridine conversion is moderately enhanced. Conversely, at lower molar inlet H_2S/pyridine ratios a higher selectivity towards nitrogen components, such as piperidine, can be observed, which consequently also results in a more prominent occurrence of bimolecular reactions leading to *n*-pentylpiperidine and a reduced C_5 selectivity

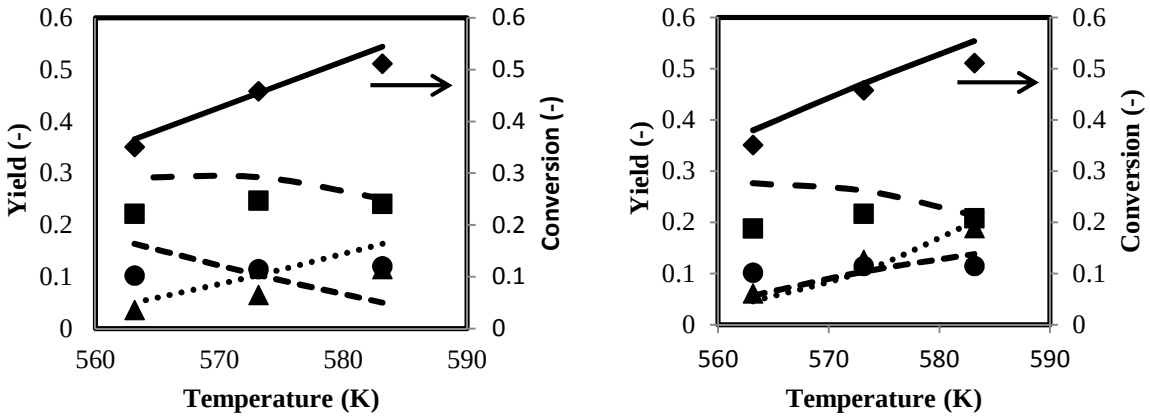

Figure 5-3. Effect of molar inlet H_2S/pyridine ratio on pyridine conversion and product yields as a function of the temperature in liquid phase pyridine hydrodenitrogenation over a sulphided NiMo/γ-Al_2O_3 catalyst. Operating conditions: Total pressure = 6.0 MPa, space time = 439 kg_{cat} s mol_P^{-1}, molar inlet H_2/pyridine = 10 (mol mol^{-1}), molar inlet H_2S/pyridine = 0.04 (mol mol^{-1}) (left) – 0.2 (mol mol^{-1}) (right); solvent/pyridine = 40 (mol mol^{-1}); Symbols: experimentally obtained values, ♦: pyridine, ■: piperidine, •: *n*-pentylpiperidine, ▲: C_5 hydrocarbons; Lines: Calculated using model simulated outlet flow rates from reactor model equation presented in chapter (Eq. 2-20) along with rate equations 5-10, 5-11 and 5-18 to 5-20 and net rates of formation 5-21 to 5-24 and parameters from chapter 4 (Table 4-10) , Tables 5-4 and 5-6; Lines: model simulated values, ——— : Pyridine, — — : Piperidine, -- : *n*-Pentylpiperidine, ••• : C_5 hydrocarbons.

5.3.5 Molar inlet H_2 to pyridine ratio

The molar H_2 inlet flow rate was systematically increased and the liquid feed flow rate was kept constant, see Figure 5-4. Hence, the molar inlet H_2 to pyridine ratio was varied simultaneously with the total pressure. It only resulted in a moderate effect on the overall reaction compared to the other operating conditions, which can be understood from a compensation between the hydrogenation and C-N bond cleavage reaction. A higher molar inlet H_2 to pyridine ratio results in an increase of the H_2 partial pressure and, hence, an enhanced H_2 solubility in the liquid phase. At the same time, the higher H_2 partial pressure results in a decrease of the H_2S partial pressure and, hence, in significantly higher hydrogen concentrations on the catalyst surface at the expense of H_2S. As a result, piperidine surface concentrations

increase because of a decrease in the rate of the substitutions reactions. The resulting accumulation of strongly adsorbing piperidine molecules on the catalyst surface results in a less pronounced increase in pyridine hydrogenation rate than would be expected for a simple aromatic hydrogenation reaction [28].

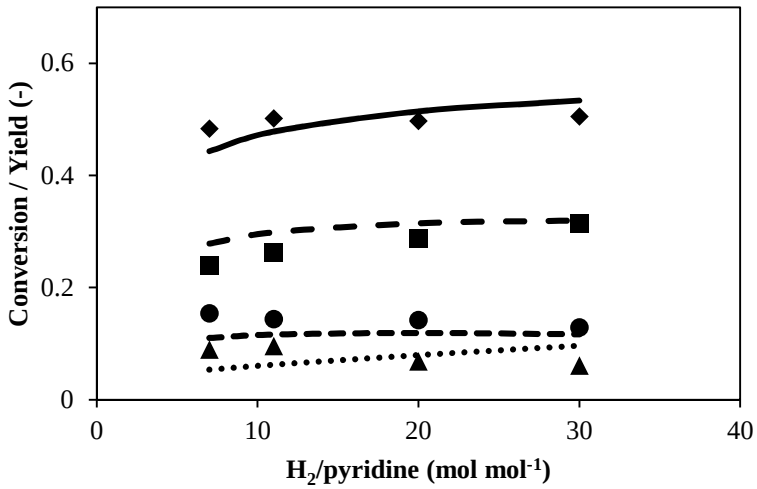

Figure 5-4. Effect of the molar inlet H_2/pyridine ratio on pyridine conversion and product yields observed in liquid phase hydrodenitrogenation of pyridine over a sulphided NiMo/γ-Al_2O_3 catalyst. Operating conditions: Temperature = 573 K, space time = 564 kg s mol^{-1}, molar inlet H_2S/pyridine = 0.04 (mol mol^{-1}); molar inlet solvent/pyridine = 40 (mol mol^{-1}); Symbols: experimentally obtained values, ♦: pyridine, ■: piperidine, •: *n*-pentylpiperidine, ▲: C_5 hydrocarbons; Lines: Calculated using model simulated outlet flow rates from reactor model equation presented in chapter (Eq. 2-20) along with rate equations 5-10, 5-11 and 5-18 to 5-20 and net rates of formation 5-21 to 5-24 and parameters from chapter 4 (Table 4-10) , Tables 5-4 and 5-6; Lines: model simulated values, —— : Pyridine, — —: Piperidine, --: *n*-Pentylpiperidine, •••: C_5 hydrocarbons.

In summary, liquid phase pyridine hydrodenitrogenation was found to comprise three main reaction types: pyridine hydrogenation, piperidine and pentylamine C-N bond cleavage and bimolecular reactions leading to *n*-pentylpiperidine. Piperidine and H_2S were identified as the crucial intermediates in the reaction mechanism. Piperidine chemisorbs more strongly than pyridine and, hence, exerts inhibiting effects when it accumulates on the catalyst surface. The latter particularly occurs when the H_2S availability at the active sites is limited and, hence, when C-N bond cleavage via the substitution mechanism is slowed down. Compared to

previous gas phase experimentation, liquid phase conditions were such that more significant amounts of piperidine were observed, also resulting in a more pronounced occurrence of bimolecular reactions leading to *n*-pentylpiperidine.

5.4 Gas to liquid phase kinetics modelling

5.4.1 Gas phase kinetic model

The kinetic modelling of the presented liquid phase kinetic data started from the model developed based on the gas phase data [41]. The pyridine hydrodenitrogenation kinetic modelling, particularly the accompanying model assumptions, have also taken inspiration from previous efforts to model toluene and naphthalene hydrogenation [28, 42] as well as dibenzothiophene hydrodesulphurisation over a (Co)NiMo/Al_2O_3 catalyst in the presence of H_2S [43]. The corresponding gas phase pyridine hydrodenitrogenation model *i.e.*, model 6 is presented in chapter 4, and is used without further modifications in the present work.

The best performing gas phase kinetics model was based on a heterolytic mechanism with proton addition first and where 3rd hydrogenation step and 2nd denitrogenation step are considered rate determining, see chapter 4, and is used as basis for the liquid phase modelling. The liquid phase operation and, hence, the deviation from ideal gas conditions requires replacing the partial pressures in rate equations, see chapter 4, by the corresponding fugacities, see equations 5-10 and 5-11.

$$r_{P\rightarrow PP} = k_{p,+} K_{P-PH2}\, K_{H2}\, K_P\, C_*^{\,2} \sqrt{\delta\, \mu} \left(f_{H_2} f_{C_5H_5N} - \frac{1}{K_{Equi}} \frac{f_{C_5H_{10}NH}}{f_{H_2}^{\,2}} \right) \qquad 5\text{-}10$$

$$r_{PP\rightarrow PA} = k_{PP}\, K_{PP-PPH}\, K_{PP}\, \mu\, f_{C_5H_{10}NH}\, C_*^{\,2} \qquad 5\text{-}11$$

Accordingly, the auxiliary variable δ has been extended by including terms for the solvent as well as *n*-pentylpiperidine chemisorption on the coordinatively unsaturated sites. See Appendix B for involved site balances.

5.4.2 Extension of gas-phase kinetic model towards liquid phase data

According to the proposed methodology for the extension of gas phase kinetics models to liquid phase reactions, the knowledge obtained in terms of the parameter values from the gas phase modelling is used in the simulation of the same reactions at liquid phase conditions. The model parameters that are relevant to gas phase reactions, namely the rate coefficients for pyridine hydrogenation and piperidine hydrodenitrogenation as well as the chemisorption coefficients of the various compounds involved, see chapter 4, are used without further

adjustment during the determination of the parameters specifically pertaining to the liquid phase operation. As a result, only four additional coefficients need to be introduced into the liquid phase kinetics model, *i.e.*, 2 rate coefficients related to disproportionation/condensation and dealkylation reactions and 2 chemisorption coefficients related to the solvent and *n*-pentylpiperidine, in addition to the parameter values obtained from the gas phase modelling.

The reaction network discussed earlier, see Figure 5-1, indicated already the formation of an additional component, *n*-pentylpiperidine, at liquid compared to gas phase conditions. *n*-pentylpiperidine formation was first reported by Sonnemans *et al.* [25] , who established that the consecutive step in pyridine hydrodenitrogenation after its initial hydrogenation to piperidine was not ring opening to pentylamine but rather disproportionation to *n*-pentylpiperidine and ammonia. Later, Hanlon [36] proposed that *n*-pentylpiperidine formation may be the result of a condensation reaction between pentylamine and piperidine. Similar conclusions with respect to *n*-pentylpiperidine formation have also been drawn by other authors [21, 37]. Accordingly, in this simulation work, model equations corresponding to two alternative reaction mechanisms for describing *n*-pentylpiperidine formation have been derived, one mechanism accounting for piperidine disproportionation and a second one for a condensation reaction between pentylamine and piperidine.

Statistical thermodynamics and transition state theory were used to calculate the chemisorption entropies and pre-exponential factors of chemisorption and rate coefficients *a priori* in order to reduce the number of parameters when accounting for their temperature dependence [44]. Depending on the mobility of the surface species, values for the adsorption entropy ranging between -95.7 J mol^{-1} K^{-1} and -190 J mol^{-1} K^{-1} for a mobile and an immobile surface species have been considered. Different combinations of pre-exponential factor values corresponding with different assumptions about the mobility of the species involved have been assessed while determining the corresponding activation energies and chemisorption enthalpies by regression. The final pre-exponential factor values for the rate coefficients in both models are shown in Table 5-4. The best agreement between experimental data and model simulations was obtained when 1 translational degree of freedom was retained upon adsorption of the solvent and *n*-pentylpiperidine, which is in line with earlier kinetic modelling work [28]. This corresponded to adsorption entropies amounting to -98 J/mol K for the solvent and -130 J/mol K for *n*-pentylpiperidine.

Table 5-4. Calculated pre-exponential factor values for the rate coefficients based on statistical thermodynamics and used during non-isothermal regression of liquid phase pyridine hydrodenitrogenation

piperidine disproportionation model	Pre-exponential factor	Pre-exponential factor value	Units
$r_{PP \rightarrow PentylPP}$	$k_{PP \rightarrow PentylPP}\ K_{PP}{}^{2}$	1 x10^{5}	$s^{-1}\ bar^{-2}$
$r_{PentylPP \rightarrow PP+C5}$	$k_{PentylPP}\ K_{PentylPP-PentylPPH}\ K_{Pentyl}$	5 x10^{2}	$s^{-1}\ bar^{-1}$
piperidine pentylamine condensation model			
$r_{PA \rightarrow C5}$	$k_{PA}\ K_{PA-PAH}\ K_{PA}$	1 x10^{2}	$s^{-1}\ bar^{-1}$
$r_{PA+PP \rightarrow PentylPP}$	$k_{PA+PP}\ K_{PP}\ K_{PA}$	1 x10^{5}	$s^{-1}\ bar^{-2}$
$r_{PentylPP \rightarrow PP+C5}$	$k_{PentylPP}\ K_{PentylPP-PentylPPH}\ K_{Pentyl}$	1 x10^{4}	$s^{-1}\ bar^{-1}$

5.4.3 Piperidine disproportionation

In the first mechanism, further denoted as “piperidine disproportionation”, *n*-pentylpiperidine formation via piperidine disproportionation and the release of ammonia is considered, see Figure 5-5. Via dealkylation, *n*-pentylpiperidine decomposes into a C_5 hydrocarbon fragment and piperidine. The corresponding model equations 5-12 for disproportionation and 5-13 for dealkylation along with the equations 5-10 and 5-11 for pyridine hydrogenation and piperidine ring opening reactions complete the set of kinetic equations for pyridine hydrodenitrogenation accounting for piperidine disproportionation.

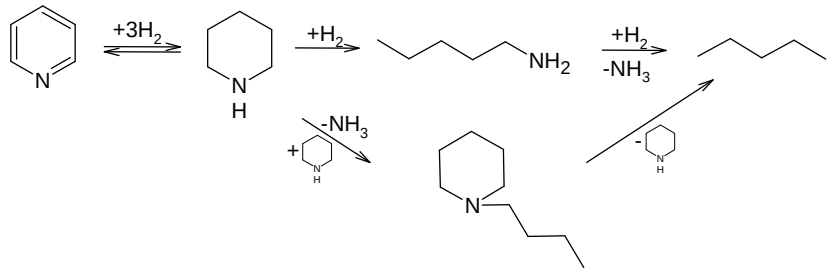

Figure 5-5 . Piperidine disproportionation reaction scheme

Piperidine Disproportionation

$$r_{PP\rightarrow PentylPP} = k_{PP\rightarrow PentylPP}\ {K_{PP}}^2 \sqrt{\frac{\mu}{\delta}}\ {f_{C_5H_{10}NH}}^2\ {C_*}^2 \quad 5\text{-}12$$

Dealkylation of *n*-pentylpiperidine

$$r_{PentylPP\rightarrow PP+C5} = k_{PentylPP}\ K_{PentylPP-PentylPPH}\ K_{PentylPP}\ \mu\ f_{PentylPP}\ {C_*}^2 \quad 5\text{-}13$$

It leads to the following net production rates for the various products according to the piperidine disproportionation model:

$$R_P = -r_{P\rightarrow PP} \quad 5\text{-}14$$

$$R_{PP} = r_{P\rightarrow PP} - r_{PP\rightarrow C5} - 2r_{PP\rightarrow PentylPP} + r_{PentylPP\rightarrow PP+C5} \quad 5\text{-}15$$

$$R_{PentylPP} = r_{PP\rightarrow PentylPP} - r_{PentylPP\rightarrow PP+C5} \quad 5\text{-}16$$

$$R_{C5} = r_{PP\rightarrow C5} + r_{PentylPP\rightarrow PP+C5} \quad 5\text{-}17$$

Table 5-5. Estimates for the activation energies and chemisorption heats along with their corresponding 95% confidence interval obtained from the non-isothermal liquid phase pyridine hydrodenitrogenation regression using the disproportionation mechanism. The simulated molar outlet flow rates were calculated from reactor model equation presented in chapter (Eq. 2-20) along with rate equations 5-10 to 5-13 and net rates of formation 5-14 to 5-17 and parameters from chapter 4 (Table 4-10) and Table 5-4.

Parameter	Symbol	Value
$K_{solvent}$	-ΔH	39.8 ± 8.8
$K_{n\text{-pentylpiperidine}}$	-ΔH	115.6 ± 11.0
$k_{PP\text{->}PentylPP}$	Ea	97.7 ± 17
$k_{PentylPP\text{->}Pa+PP}$	Ea	172.2 ± 10.0

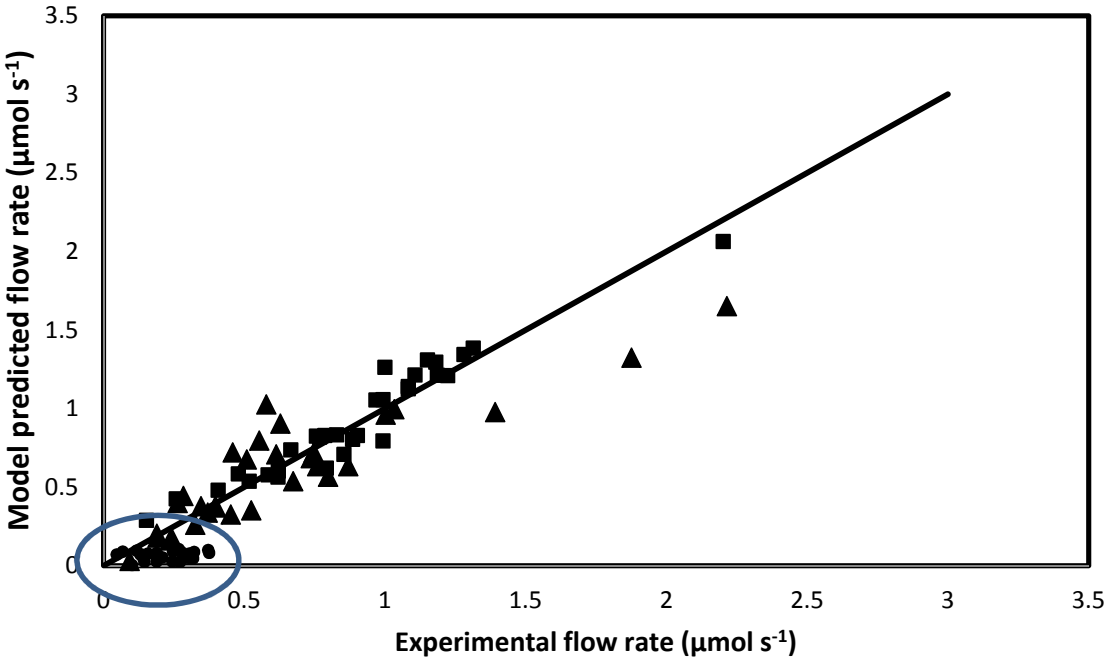

Figure 5-6. Product parity diagram for piperidine, pentane and *n*-pentylpiperidine for the liquid phase kinetics model for pyridine hydrodenitrogenation on a sulphided industrial NiMo/γ-Al_2O_3 catalyst. The simulated molar outlet flow rates were calculated from reactor model equation presented in chapter (Eq. 2-20) along with rate equations 5-10 to 5-13 and net rates of formation 5-14 to 5-17 and parameters from chapter 2, Tables 5-4 and 5-5.

The F value for the global significance of the regression of the disproportionation model amounted to 287. All model parameters could be estimated statistically significantly, see Table 5-5. Little quantitative information is available in the literature with respect to *n*-pentylpiperidine formation and its corresponding dealkylation to C_5 products as well as with respect to piperidine. Hence, the work by Sonnemans *et.al.* [25] on a CoO-MoO_3/Al_2O_3 catalyst is recurred to as reference point for assessing the present parameter estimates. The activation energy for *n*-pentylpiperidine dealkylation is in good agreement with that reported by Sonnemans *et al.* [25], the latter being about 20 kJ mol^{-1} lower than the one obtained in the present work, *i.e.*, 150 kJ mol^{-1} versus 170 kJ mol^{-1}, which can be attributed to the different catalyst used in both works. The piperidine disproportionation activation energy was estimated at approximately 100 kJ mol^{-1} in this work. The chemisorption heats were estimated significantly. While the solvent chemisorption heat is limited to about 40 kJ mol^{-1} indicating that the solvent only occupies a small fraction on the catalyst surface, that of *n*-pentylpiperidine amounts to 115kJ mol^{-1}. This latter chemisorption heat is similar to that of piperidine and,

hence, higher than expected because of the lower proton affinity of *n*-pentylpiperidine compared to piperidine. Moreover, steric hindrance due to the pentyl substituent is also expected to result in a comparatively lower heat of chemisorption for *n*-pentylpiperidine.

The agreement between experimental data and model simulations is shown in Figure 5-6. The simulated product outlet flow rates for piperidine and pentane appear to satisfactorily approach the experimentally observed values, except for pentane at high molar flow rates. Moreover, the model significantly under-predicts the *n*-pentylpiperidine outlet molar flow rates at all experimental conditions, see the encircled part of Figure 5-6. Also the residual figure for the molar pyridine outlet flow rates indicates a consistent over prediction.

5.4.4 Condensation between piperidine and pentylamine

The second mechanism, referred to as "piperidine pentylamine condensation" considers *n*-pentylpiperidine formation from a pentyl amine addition to piperidine with the release of ammonia as a condensation product, see Figure 5-7. Similar to the "piperidine disproportionation" mechanism, *n*-pentylpiperidine can decompose into piperidine and a C_5 hydrocarbon fragment via dealkylation. Accordingly model equations 5-18, 5-19, 5-20 along with equations 5-10 and 5-11 complete the set of kinetic equations for pyridine hydrodenitrogenation accounting for piperidine and pentyl amine condensation.

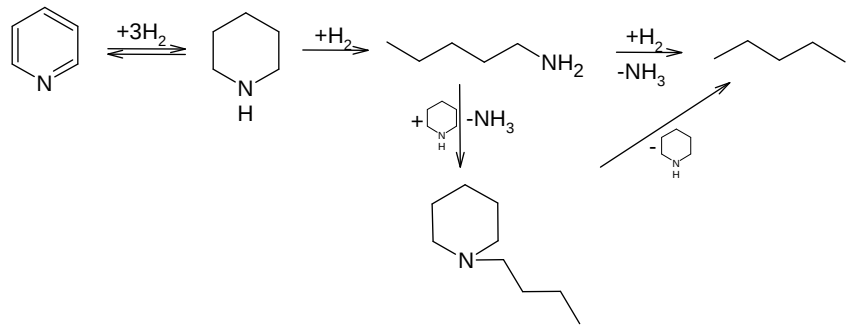

Figure 5-7. Piperidine pentylamine condensation reaction scheme

Pentylamine denitrogenation

$$r_{PA\rightarrow C5} = k_{PA}\, K_{PA-PAH}\, K_{PA}\, \mu\, f_{C_5H_{11}NH_2}\, C_*{}^2 \qquad 5\text{-}18$$

Piperidine and pentylamine condensation

$$r_{PA+PP\rightarrow PentylPP} = k_{PA+PP}\, K_{PP}\, K_{PA} \sqrt{\frac{\mu}{\delta}}\, f_{C_5H_{10}NH} f_{C_5H_{11}NH_2} C_*{}^2 \qquad 5\text{-}19$$

***n*-pentylpiperidine dealkylation**

$$r_{PentylPP\rightarrow PP+C5} = k_{PentylPP}\, K_{PentylPP-PentylPPH}\, K_{PentylPP}\, \mu\, f_{PentylPP}\, C_*{}^2 \qquad 5\text{-}20$$

It leads to the following net production rates for the various products according to the piperidine pentylamine condensation model:

$$R_P = -r_{P\rightarrow PP} \qquad 5\text{-}21$$

$$R_{PP} = r_{P\rightarrow PP} - r_{PP\rightarrow PA} - r_{PA+PP\rightarrow PentylPP} + r_{PentylPP\rightarrow PP+C5} \qquad 5\text{-}22$$

$$R_{PentylPP} = r_{PP+PA\rightarrow PentylPP} - r_{PentylPP\rightarrow PP+C5} \qquad 5\text{-}23$$

$$R_{C5} = r_{PA\rightarrow C5} + r_{PentylPP\rightarrow PP+C5} \qquad 5\text{-}24$$

As pentylamine has not been observed experimentally its rate of consumption is potentially much higher than its rate of formation. In the previously discussed disproportionation model, the pentylamine fugacity was, hence, not explicitly required. However, to calculate the condensation rate between piperidine and pentylamine, the fugacity of the latter, needs to be determined. Using the pseudo steady state approximation for pentylamine, its fugacity can be expressed as a function of the known piperidine fugacity, see equation 5-27.

$$r_{PP\rightarrow PA} = r_{PA\rightarrow C5} + r_{PA+PP\rightarrow PentylPP} \qquad 5\text{-}25$$

Replacing the reaction rates in equation 5-25 with equations 5-28 and 5-29 allows solving for the pentylamine fugacity.

$$k_{PP}{}^*\, \mu\, f_{C_5H_{10}NH}\, C_*{}^2 \qquad 5\text{-}26$$

$$= k_{PA}{}^*\, \mu\, f_{C_5H_{11}NH_2}\, C_*{}^2 + k_{PA+PP}{}^*\, f_{C_5H_{10}NH} f_{C_5H_{11}NH_2} \sqrt{\frac{\mu}{\delta}}\, C_*{}^2$$

$$f_{C_5H_{11}NH_2} = \frac{k_{PP}{}^*\, \mu\, f_{C_5H_{10}NH}}{k_{PA}{}^*\, \mu + k_{PA+PP}{}^*\, f_{C_5H_{10}NH} \sqrt{\frac{\mu}{\delta}}} \qquad 5\text{-}27$$

Thus an analytical expression for the right hand side terms in equation 5-25 can be derived starting from the rates of the individual reactions

$$r_{PA\rightarrow C5} = \frac{\frac{k_{PA}{}^*}{k_{PA+PP}{}^*}\, \mu}{\frac{k_{PA}{}^*}{k_{PA+PP}{}^*}\, \mu + f_{C_5H_{10}NH} \sqrt{\frac{\mu}{\delta}}}\, k_{PP}{}^* f_{C_5H_{10}NH}\, \mu\, C_*{}^2 \qquad 5\text{-}28$$

$$r_{PA+PP\rightarrow PentylPP} = \frac{f_{C_5H_{10}NH}\sqrt{\frac{\mu}{\delta}}}{\frac{k_{PA}^{*}}{k_{PA+PP}^{*}}\mu + f_{C_5H_{10}NH}\sqrt{\frac{\mu}{\delta}}} k_{PP}^{*} f_{C_5H_{10}NH}\,\mu\, C_{*}^{\,2} \qquad 5\text{-}29$$

Table 5-6. Estimates for the activation energies and chemisorption heats along with their corresponding 95% confidence interval obtained from the non-isothermal liquid phase pyridine hydrodenitrogenation regression using the condensation mechanism The simulated molar outlet flow rates were calculated from reactor model equation chapter (Eq. 2-20) along with rate equations 5-10 and 5-11 and 5-18 to 5-20 and net rates of formation 5-21 to 5-24 and parameters from chapter 4 (Table 4-10) and Table 5-4.

Parameter		Value
$K_{solvent}$	-ΔH	39.8 ± 3.0
$K_{n\text{-pentylpiperidine}}$	-ΔH	81.8 ± 3.6
k_{ratio}	E_a	100 ± 46
$k_{PentylPP->PP+C5}$	E_a	67.8 ± 16.2

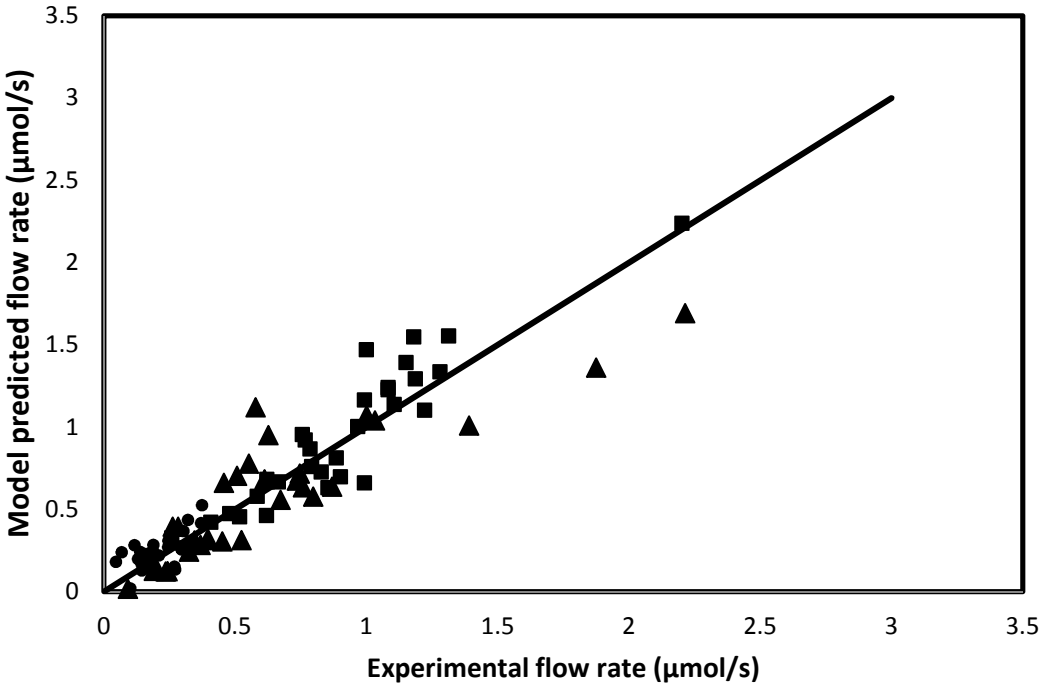

Figure 5-8. Product parity diagram piperidine, pentane and *n*-pentylpiperidine for the liquid phase kinetics model for pyridine hydrodenitrogenation on a sulphided industrial NiMo/γ-Al_2O_3 catalyst, The simulated molar outlet flow rates were calculated from reactor model equation presented in chapter (Eq. 2-20) along with rate equations 5-10 and 5-11 and 5-18 to 5-20 and net rates of formation 5-21 to 5-24 and parameters from chapter 2, Tables 5-4 and 5-6.

The F value for the global significance of the regression amounted to 355. It is determined from k_{ratio} that the activation energies for pentylamine denitrogenation and condensation with piperidine differ by about 100 kJ mol^{-1}. Sonnemans *et al.* [25] reported an activation energy in the range of 160-170 kJ mol^{-1} for pentylamine denitrogenation ($k_{PA,}$) and of 100 kJ mol^{-1} for condensation between pentylamine and piperidine. Hence, the differences in activation energies obtained in the present work are in agreement with those reported by Sonnemans *et al.* [25] accounting for, among others, the different catalyst used. The higher activation energy for pentylamine denitrogenation compared to its condensation with piperidine explains the experimentally observed promotion of C-N bond scission reactions at higher operating temperatures, *i.e.*, a selectivity towards C_5 hydrocarbons amounting to 0.45 at 583K compared to 0.34 in similar pyridine conversion range at 573 K, see Table 5-3. The activation energy estimated for dealkylation reaction is much lower than the value obtained by Sonnemans *et.al.* [25], but can be interpreted in terms of a compensation between this dealkylation activation energy and the *n*-pentylpiperidine chemisorption heat. Similar to the disproportionation model,

the solvent chemisorption heat in the condensation model is limited, indicating a limited impact of the solvent on the surface coverage. The *n*-pentylpiperidine chemisorption heat amounts to 82 kJ/mol, which is in line with the lower proton affinity of *n*-pentylpiperidine compared to piperidine as well as with some steric hindrance effects as discussed in the previous section
The F value for the global significance of the condensation model clearly exceeds that of the disproportionation model. Also the physical significance of the model parameters can be better rationalized, accounting for some compensation between the dealkylation activation energy and the *n*-pentylpiperidine chemisorption heat. Moreover, the condensation model is able to simulate the product molar outlet flow rates better, see Figure 5-8 compared to Figure 5-6 Additionally, the condensation model also outperforms the disproportionation model in simulating the reactant molar outlet flow rates and, hence, the conversion, see Figure 5-9. Hence, overall, the condensation mechanism between pentylamine and piperidine allows the best description of the experimental data and is selected as the most probable mechanism.

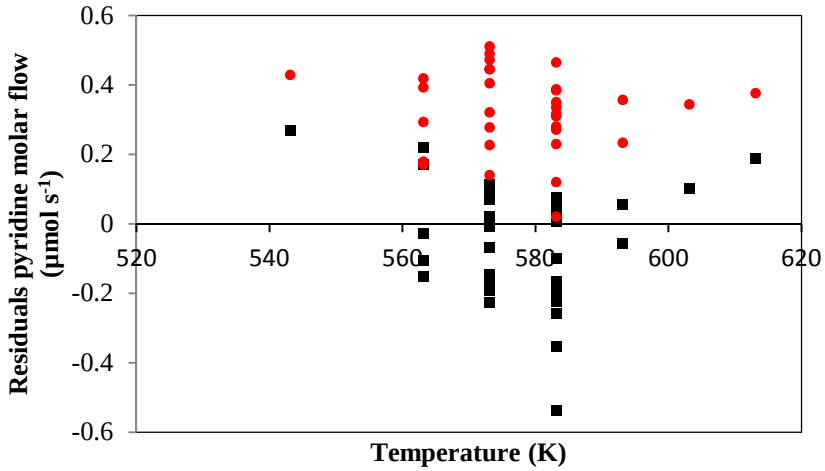

Figure 5-9. Comparison of residuals between the experimentally observed and simulated pyridine molar outlet flow rates in liquid phase pyridine hydrodenitrogenation on a sulphided NiMo/γ-Al_2O_3 catalyst according to the "piperidine disproportionation" model using reactor model equation presented in chapter (Eq. 2-20) along with rate equations 5-10 to 5-13 and net rates of formation 5-14 to 5-17 and parameters from chapter 4 (Table 4-10) , Tables 5-4 and 5-5 and the "piperidine-pentylamine condensation" model using reactor model equation presented in chapter (Eq. 2-20) along with rate equations 5-10, 5-11 and 5-18 to 5-20 and net rates of formation 5-21 to 5-24 and parameters from chapter 4 (Table 4-10) , Tables 5-4 and 5-6. Symbols ■ : piperidine-pentylamine condensation model, ●: piperidine disproportionation model.

5.4.5 Liquid phase kinetics model assessment

5.4.5.1 Gas phase kinetics simulation using the liquid phase kinetics model

In order to validate the applicability of the gas to liquid phase kinetics methodology, the extended kinetic model, as it was developed for adequately simulating the liquid phase experiments, was used to simulate the gas phase experimental results. The kinetic model and, hence, the methodology, can be claimed to be robust and accurate if, indeed, the extensions required to adequately simulate the liquid phase kinetics, *i.e.*, the *n*-pentylpiperidine formation, would appear to contribute only insignificantly at gas phase conditions. Figure 5-10 shows the results of simulation at the gas phase conditions and as can be observed visually, the performance curves are in good agreement with the experimental data [8]. The sufficiently low

yield, *i.e.*,. always below 2% towards the *n*-pentylpiperidine, even at higher pressures, can be explained by the differences in surface coverages obtained at the gas versus liquid phase conditions. Particularly the surface coverage by H_2S at gas phase conditions largely exceeds that at liquid phase conditions, whereas the surface coverage by piperidine is in the same range. As a result, at gas phase conditions the substitution rates are so high that bimolecular reactions between piperidine and pentylamine become very unlikely.

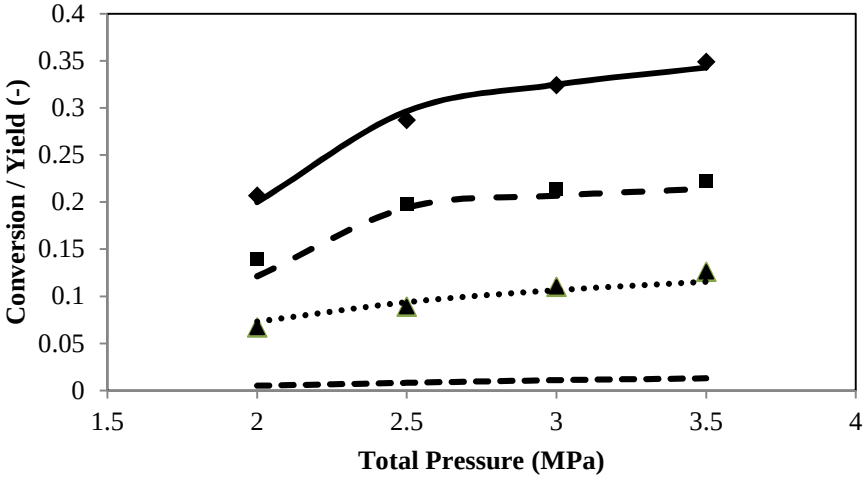

Figure 5-10. Pyridine conversion and product yields in gas phase pyridine hydrodenitrogenation over a commercial NiMo/γ-Al_2O_3. Operating conditions: Temperature = 573 K, space time = 1400 kg_{cat} s mol^{-1}, H_2/Pyridine = 620 and H_2S/Pyridine = 15. Solvent/pyridine = 40; Symbols: experimentally obtained values, ♦ : Pyridine, ■ : Piperidine, ▲: C_5 hydrocarbons; Lines: Calculated using model simulated outlet flow rates from reactor model equation provided in chapter (Eq. 2-20) along with rate equations 5-10, 5-11 and 5-18 to 5-20 and net rates of formation 5-21 to 5-24 and parameters from chapter 4 (Table 4-10) , Tables 5-4 and 5-6, —— : Pyridine, — — : Piperidine, - - : *n*-Pentylpiperidine, ••• : C_5 hydrocarbons.

5.4.5.2 Surface coverages

The pyridine conversion was already shown to significantly increase with the molar inlet H_2S to pyridine ratio due to enhanced C-N bond breaking in piperidine, see Section 5.3.4. The corresponding surface coverages are presented in Figure 5-11. At practically all conditions, except at the combination of high temperature and high molar inlet H_2S to pyridine ratio, piperidine was the most abundant surface species. At 563K 45% of the surface was covered by piperidine at a molar inlet H_2S to pyridine ratio of 0.04, while this was reduced to 35% at a molar inlet H_2S to pyridine ratio of 0.2. The enhancement of the piperidine C-N bond scission

by higher H_2S surface concentrations, *i.e.*, 0.31 at the highest compared to 0.1 at the lowest molar inlet H_2S to pyridine ratio logically explains the above described evolution in piperidine surface coverage.

Both at high and low molar inlet H_2S to pyridine ratios, the piperidine surface coverage decreases more rapidly compared to that of H_2S, while that of H_2 steadily increases. Whereas the contrasting trend between H_2S and H_2 can be explained by the lower chemisorption heat for H_2 compared to H_2S, the more pronounced decrease in piperidine surface coverage is a consequence of the high activation energy for C-N bond breaking and, hence, the significant enhancement of piperidine conversion at higher temperatures.

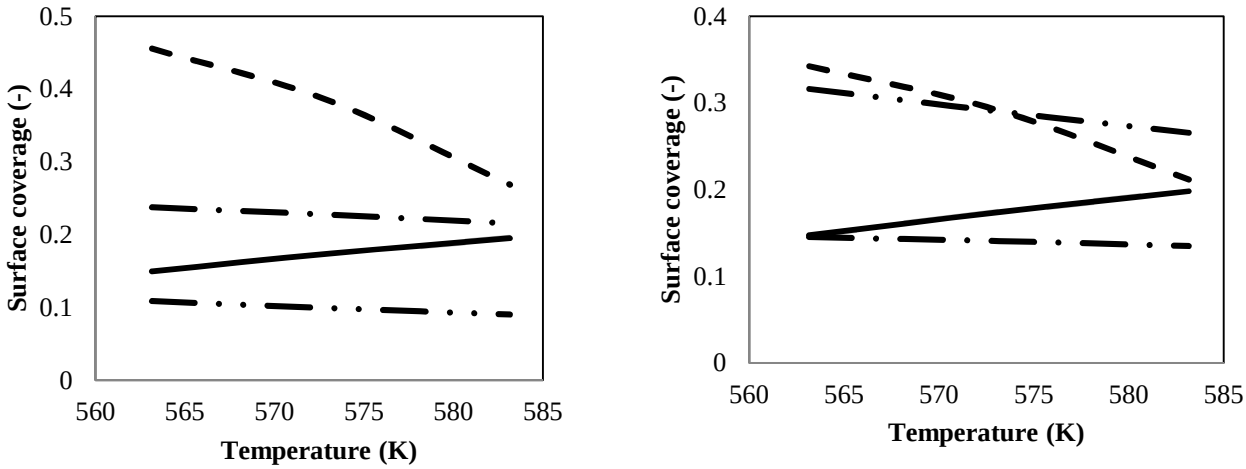

Figure 5-11. Simulated surface coverages as a function of the inlet molar H_2S to pyridine ratio for liquid phase pyridine hydrodenitrogenation using reactor model equation presented in chapter (Eq. 2-20) along with the rate equations 5-10, 5-11 and 5-18 to 5-20 along with corresponding net rates 5-21 and 5-24 and parameter values from chapter 2, Tables 5-4 and 5-6. Operating conditions: Pressure = 6.0 MPa, molar inlet solvent/pyridine = 40 (mol mol^{-1}), (Left) molar inlet H_2S/pyridine = 0.04 (mol mol^{-1}), spacetime = 790 kg s mol^{-1} (Right) = molar inlet H_2S/pyridine = 0.2 (mol mol^{-1}), space time = 439 kg s mol^{-1}. (——: pyridine, — —: piperidine, •••: *n*-pentylpiperidine, —— • : H_2, —— •• : H_2S).

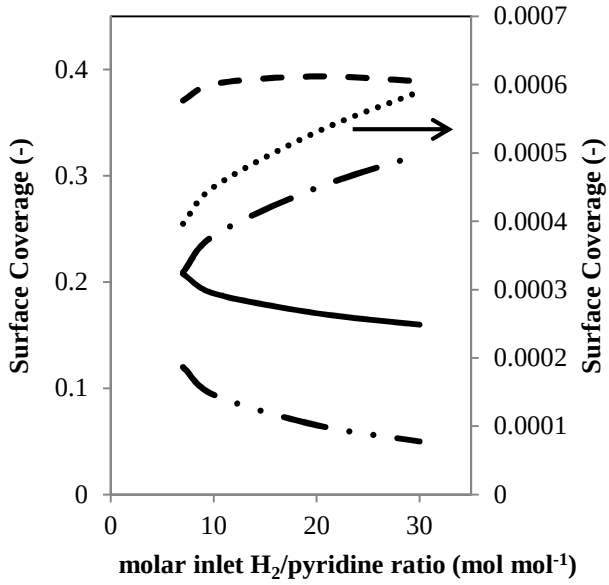

Figure 5-12. Simulated surface coverages as a function of the inlet molar H_2 to pyridine ratio for liquid phase pyridine hydrodenitrogenation using reactor model equation chapter (Eq. 2-20) along with the rate equations 5-18, 5-19 and 5-20 along with 5-10 and 5-11 and corresponding net rates 5-21 and 5-24 and parameter values from chapter 4 (Table 4-10) , Tables 5-4 and 5-6. Operating conditions: Pressure = 6.0 MPa, Temperature = 573K, Spacetime = 564 kg s mol^{-1}, molar inlet H_2S/pyridine = 0.04 (mol mol^{-1}); molar inlet solvent/pyridine = 40 (mol mol^{-1}) (——: Pyridine, — — : Piperidine, ••• : 1-Pentylpiperidine, —— • : H_2, —— •• : H_2S).

The model predicts a moderate increase in piperidine surface coverage from 0.35 to 0.37 with increasing inlet molar H_2 to pyridine ratios, while that by hydrogen increases more significantly from 0.21 to 0.32 over the entire range of investigated inlet molar H_2 to pyridine ratios, see Figure 5-12. The latter increase occurs at the expense of both pyridine and more importantly the hydrogen sulphide surface coverage, which decrease from 0.20 to 0.15 and from 0.12 to 0.05 respectively. The decrease in the hydrogen sulphide surface coverage results in lower C-N bond scission rates at higher inlet molar H_2 to pyridine ratios. Correspondingly, lower C_5 hydrocarbon and higher piperidine yields can be expected, due to the decrease in the rate of the substitution reactions in the C-N bond scission. This is indeed in agreement with the experimental observations, see Figure 5-4, where a negligible increase in the pyridine conversion is observed, but an increase in the piperidine yield from 0.24 to 0.31 and a corresponding decrease in the pentane yield from 0.08 to 0.06.

5.5 Conclusions

The ‘gas to liquid phase kinetics’ methodology has been successfully extended from acid towards metal (sulphide) catalysis with pyridine hydrodenitrogenation as example reaction. As part of a systematic approach, kinetic model construction and determination of the corresponding model parameters has been performed based on an extended set of gas phase kinetic data. This model can subsequently be applied in the assessment of a limited set of liquid phase data by accounting for the thermodynamic non-ideality, solvent adsorption and the potential occurrence of additional reactions due to the high density at liquid phase conditions. The differences in the operating conditions were quantitatively captured by a comprehensive pyridine hydrodenitrogenation model. The lower H_2S partial pressures and corresponding surface coverages at liquid phase conditions in comparison to the gas phase conditions resulted in lower C-N bond scission rates via substitution reactions. As a consequence of the reduced denitrogenation rates, alternative, bimolecular reactions between nitrogen surface species can became important at liquid phase conditions and lead to *n*-pentylpiperidine formation. The latter product was found to be formed via a condensation between piperidine and its ring opening product, pentylamine, rather than via disproportionation. A versatile methodology has been developed for the reliable extrapolation of gas phase laboratory kinetics data towards three phase industrial reactors.

5.6 References

1. Carrillo, J.A. and L.M. Corredor, **Fuel Processing Technology**, 2013. 109(0): p. 156-162.

2. Dukanovic, Z., S.B. Glisic, V.J. Cobanin, M. Niciforovic, C.A. Georgiou, and A.M. Orlovic, **Fuel Processing Technology**, 2013. 106: p. 160-165.

3. Kasztelan, S., T. des Courieres, and M. Breysse, **Catalysis Today**, 1991. 10(4): p. 433-445.

4. Guevara-Lara, A., R. Bacaud, and M. Vrinat, **Applied Catalysis A: General**, 2007. 328(2): p. 99-108.

5. Topsoe, H., **Applied Catalysis A: General**, 2007. 322: p. 3-8.

6. Raybaud, P., **Applied Catalysis A: General**, 2007. 322: p. 76-91.

7. Egorova, M. and R. Prins, **Journal of Catalysis**, 2006. 241(1): p. 162-172.

8. Pille, R. and G. Froment, **Hydrotreatment and Hydrocracking of Oil Fractions**, 1997. 106: p. 403-413.

9. Kopyscinski, J., J. Choi, and J.M. Hill, **Applied Catalysis A: General**, 2012. 445: p. 50-60.

10. Adam, F., F. Bertoncini, C. Dartiguelongue, K. Marchand, D. Thiebaut, and M.C. Hennion, **Fuel**, 2009. 88(5): p. 938-946.

11. Adam, F., F. Bertoncini, N. Brodusch, E. Durand, D. Thiebaut, D. Espinat, and M.C. Hennion, **Journal of Chromatography A**, 2007. 1148(1): p. 55-64.

12. Prins, R., M. Jian, and M. Flechsenhar, **Polyhedron**, 1997. 16(18): p. 3235-3246.

13. Prins, R., A. Egorova, A. Rothlisberger, Y. Zhao, N. Sivasankar, and P. Kukula, **Catalysis Today**, 2006. 111(1-2): p. 84-93.

14. Jian, M. and R. Prins, **Recent Advances in Basic and Applied Aspects of Industrial Catalysis**, 1998. 113: p. 111-123.

15. Jian, M. and R. Prins, **11th International Congress on Catalysis - 40th Anniversary, Pts A and B**, 1996. 101: p. 87-96.

16. Egorova, M., Y. Zhao, P. Kukula, and R. Prins, **Journal of Catalysis**, 2002. 206(2): p. 263-271.

17. Egorova, M. and R. Prins, **Journal of Catalysis**, 2004. 221(1): p. 11-19.

18. Wang, H. and R. Prins, **Catalysis Letters**, 2008. 126(1): p. 1-9.

19. Satterfield, C.N. and J.F. Cocchetto, **AIChE Journal**, 1975. 21(6): p. 1107-1111.

20. McIlvried, H.G., **Industrial & Engineering Chemistry Process Design and Development**, 1971. 10(1): p. 125-130.

21. Chu, Y., Z. Wei, S. Yang, C. Li, Q. Xin, and E. Min, **Applied Catalysis A: General**, 1999. 176(1): p. 17-26.

22. Sonneman, J. and P. Mars, **Journal of Catalysis**, 1973. 31(2): p. 209-219.

23. Sonneman, J., G.H. Van den Berg, and P. Mars, **Journal of Catalysis**, 1973. 31(2): p. 220-230.

24. Sonneman, J. and P. Mars, **Journal of Catalysis**, 1974. 34(2): p. 215-229.

25. Sonneman, J., W.J. Neyens, and P. Mars, **Journal of Catalysis**, 1974. 34(2): p. 230-241.

26. Thybaut, J.W., C.S. Laxmi Narasimhan, and G.B. Marin, **Catalysis Today**, 2006. 111(1-2): p. 94-102.

27. Berger, R.J., E.H. Stitt, G.B. Marin, F. Kapteijn, and J.A. Moulijn, **Cattech**, 2001. 5(1): p. 30-60.

28. Romero, C.M.C., J.W. Thybaut, and G.B. Marin, **Catalysis Today**, 2008. 130(1): p. 231-242.

29. Weisz, P.B. and C.D. Prater, *Interpretation of Measurements in Experimental Catalysis*, in *Advances in Catalysis*, V.I.K. W.G. Frankenburg and E.K. Rideal, Editors. 1954, Academic Press. p. 143-196.

30. Mears, D.E., **Journal of Catalysis**, 1971. 20(2): p. 127-131.

31. Madon, R.J. and E. Iglesia, **Journal of Molecular Catalysis A: Chemical**, 2000. 163(1-2): p. 189-204.

32. Poling, P., *The Properties of Gases and Liquids*. 2001, McGraw-Hill.

33. Moysan, J.M., H. Paradowski, and J. Vidal, **Chemical Engineering Science**, 1986. 41(8): p. 2069-2074.

34. Kopyscinski, J., J. Choi, L. Ding, S. Zhang, B. Ibeh, and J.M. Hill, **Catalysis Letters**, 2012. 142(7): p. 845-853.

35. Schwartz, V., V.T. da Silva, and S.T. Oyama, **Journal of Molecular Catalysis A: Chemical**, 2000. 163(1-2): p. 251-268.

36. Hanlon, R.T., **Energy & Fuels**, 1987. 1(5): p. 424-430.

37. Schwartz, V. and S.T. Oyama, **Journal of Molecular Catalysis A: Chemical**, 2000. 163(1-2): p. 269-282.

38. Hadjiloizou, G.C., J.B. Butt, and J.S. Dranoff, **Journal of Catalysis**, 1991. 131(2): p. 545-572.

39. Perot, G., P. Daraujo, L. Vivier, S. Kasztelan, and F.R. Ribeiro, **Abstracts of Papers of the American Chemical Society**, 1993. 206: p. 48-Petr.

40. Cattenot, M., J.L. Portefaix, J. Afonso, M. Breysse, M. Lacroix, and G. Perot, **Journal of Catalysis**, 1998. 173(2): p. 366-373.

41. Pille, R., *Sleutelcomponenten bij de hydrodenitrogenering en hydrodesulfurisering van aardoliefracties*. 1997, Universiteit Gent.

42. Kasztelan, S. and D. Guillaume, **Industrial & Engineering Chemistry Research**, 1994. 33(2): p. 203-210.

43. Vanrysselberghe, V., R. Le Gall, and G.F. Froment, **Industrial & Engineering Chemistry Research**, 1998. 37(4): p. 1235-1242.

44. Dumesic, D.A., D.F. Rudd, L.M. Aparicio, J.E. Kekoske, and A.A. Trevino, *The microkinetics of heterogeneous catalysis*. 1993, American Chemical Society: Washington, DC.

6 Pyridine hydrodenitrogenation chemistry and Reaction Network Generation with ReNGeP

In order to develop a comprehensive model for pyridine hydrodenitrogenation according to the Single-Event MicroKinetic, SEMK, methodology, an elementary steps based reaction network is required. Given the potential complexity of such reaction networks, dedicated software such as the Reaction Network Generation Program, ReNGeP, is typically employed. Compared to the already existing reaction families within ReNGeP, an extension will be required to cover all elementary steps relevant within hydrodenitrogenation. While the model component in the present work was pyridine, the extension within ReNGeP has been implemented such that reaction networks of other model components, such as quinoline, can be generated as well. Some of the important reactions occurring in pyridine hydrodenitrogenation, were already discussed in Chapter 4 and 5. Relevant details of the corresponding reaction mechanisms with respect to the extension of ReNGeP are further elaborated in the present chapter, which is divided into two parts. First the strategy that has been adopted to generate the pyridine hydrodenitrogenation reaction network is explained, followed by a section which goes into more detail about the actual reaction network generation program. Special attention is paid to the elementary reactions within hydrodenitrogenation in general and pyridine in particular. The program is briefly explained and references to the relevant publications are given. The subsequent chapter 7 employs the reaction network

generated with ReNGeP aiming at comprehensive model construction according the SEMK methodology.

6.1 Pyridine hydrodenitrogenation and reaction network generation strategy

A detailed understanding of the underlying pyridine hydrodenitrogenation chemistry is required to formulate the implementation of the corresponding reaction families within ReNGeP. Inspiration is taken from literature on hydrodenitrogenation of pyridine and other components [1-26]. It is evident from all possible sources that pyridine hydrodenitrogenation is a two-step reaction [7, 12, 27, 28]. First the pyridine hetero aromatic ring is hydrogenated into piperidine, followed by the actual denitrogenation of the latter, see also chapter 4. Literature on pyridine hydrodenitrogenation catalysed by various metal sulphides at different operating conditions is available [8, 11-14, 22, 28-40]. However, no truly microkinetic, elementary steps based models have been reported.

The first part of the SEMK model formulation involves the identification of the elementary reactions that need to be considered. In chapter 4 and 5 of this thesis various elementary reactions occurring during pyridine hydrodenitrogenation were discussed. The models were constructed based on the assumptions of different steps being rate determining, The selection of the best performing model was the result of a laborious task requiring the discrimination between a huge set of models. In addition to the earlier mentioned complexity, some reactions that were considered to be insignificant at the existing reaction conditions were not considered e.g., the elimination of nitrogen through Hoffmann elimination, see Chapter 4. However, for the model construction according to the SEMK methodology, all occurring reactions need to be considered, ensuring its versatility and applicability at all possible operating conditions. Through an in-depth literature survey nine types of elementary reactions i.e., hydrogenation of hetero-aromatic ring, protonation of amines, C-N bond scission via β-(H) elimination, C-N bond scission via (-SH) substitution, formation of heavier species via pentylamine condensation, formation of heavier species via piperidine condensation, acyclic (-SH) direct hydrogenolysis and finally alkene hydrogenation, have been identified as required to describe the complete conversion of pyridine to its products pentane and pentene [8, 11, 22, 26, 29-33, 37, 38, 40]. These elementary reaction types, which in some cases can be subdivided into exocyclic, endocyclic and the acyclic types are further classified into reaction families based on the reaction chemistry involved. Such a classification will allow the assumption of

identical enthalpy/energy effects induced by the elementary steps in this family during the actual modelling. In the following section, the elementary reactions are presented in detail along with the reaction mechanism.

6.1.1 Hydrogenation of hetero-aromatic ring

Pyridine, H_2 and H_2S molecules all chemisorb on the catalyst active sites. Pyridine chemisorption is considered to occur in different orientations, determining the corresponding activation energy required for hydrogen addition. DFT calculations have been instrumental in providing critical insight in pyridine chemisorption on promoted Mo in a sulphided phase. Sun et al. [41] reported that over a Ni promoted Mo catalyst, the most stable and optimal configuration for pyridine chemisorption is the end-on one in which the molecule orients itself perpendicularly to the chemisorption plane via a N-Ni interaction. Sun et al. [41] further add that such a configuration is the most stable due to the electronic configuration within the pyridine molecule. The chemisorption energy which is calculated as the difference between the energy of the optimised geometry and a clean surface and gas phase pyridine is reported to be about -125 kJ mol^{-1}. Such a chemisorption is equivalent with a strong bonding of the pyridine molecule as a pyridinium ion and facilitates the further addition of hydrogen as protons and hydride from neighbouring sites. In the formulation of the SEMK model it is assumed that such an end-on chemisorption on the surface and first hydrogen addition as a proton on the nitrogen occur. Once the proton has been added further saturation of the hetero-aromatic ring takes place with alternative additions of hydrides and protons, according to the scheme presented in chapter 4.

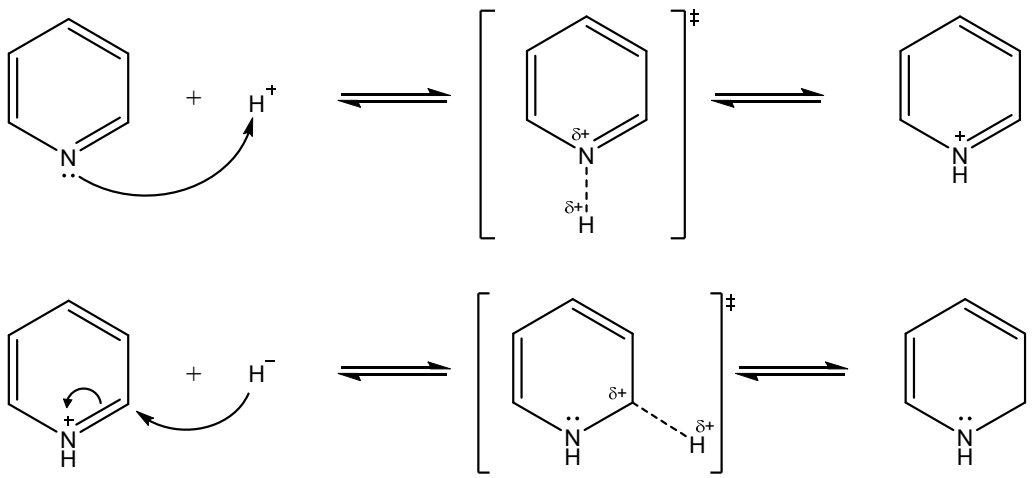

Figure 6-1. Pyridine hydrogenation mechanism via consecutive proton and hydride addition.

As opposed to the SEMK model for benzene, toluene and o-xylene hydrogenation over a Pt catalyst proposed by Bera et al. [42, 43] in which the aromatic ring saturation occurs via atomic hydrogen addition, on the sulphided catalyst considered as part of the present thesis a proton addition first mechanism is proposed in accordance with previous work from Romero et al. [44], see chapter 4. The first step is explained in Figure 6-1, i.e., the proton from a nearby sulphur anion site (S^{2-}) attacks the lone electron pair on the nitrogen atom resulting in N-monohydro-pyridine. In the next step, a hydride from a coordinatively unsaturated site (*) site is added to one of the other carbon atoms. No particular distinction is made between carbon atoms adjacent to the nitrogen atom and others. The hydride addition consecutive to a proton additions ensures the electronically neutral character of the produced intermediate. Subsequent, consecutive proton and hydride additions are included in the reaction network to ensure the complete saturation of the aromatic pyridine molecule, see Figure 6-2.

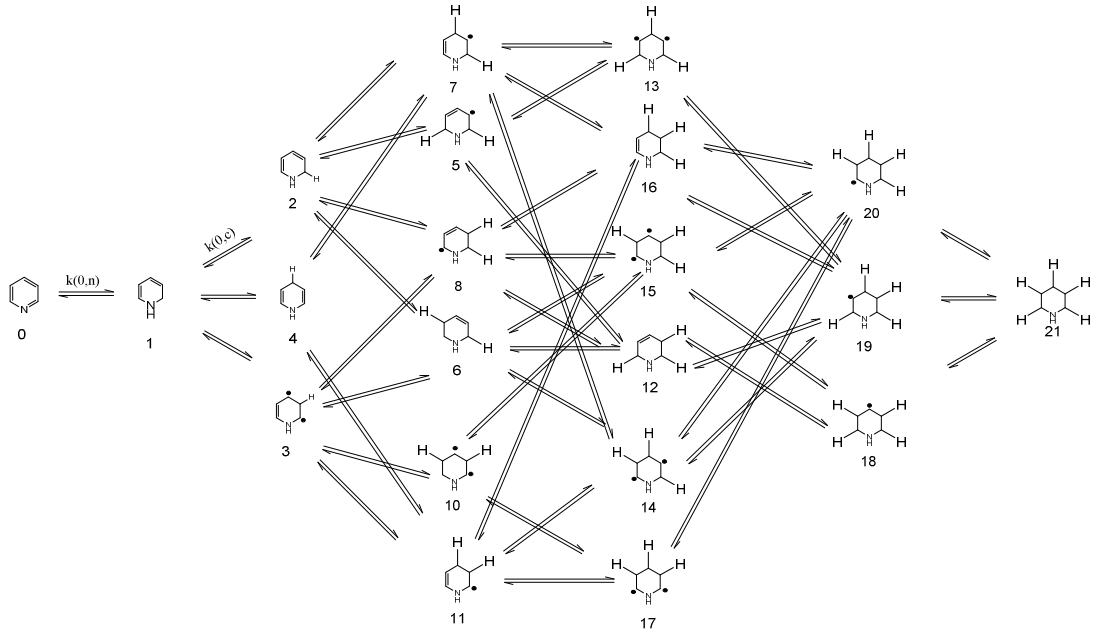

Figure 6-2. Hydrogenation reaction network as generated by ReNGeP for the complete saturation of pyridine to piperidine.

6.1.2 Protonation of amines

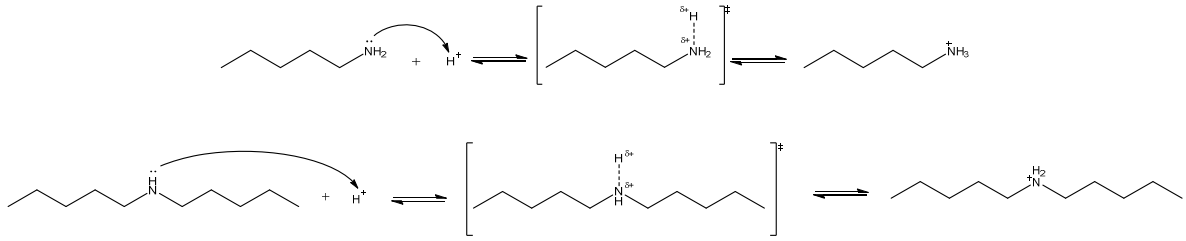

Figure 6-3. Mechanism of the amine protonation reaction encountered during the hydrodenitrogenation reactions.

Primary and secondary amines are formed during pyridine conversion. The resulting amines are susceptible to protonation reactions due to the presence of a free electron pair on the nitrogen atom. The primary or secondary nature of the latter depends on the elementary steps undergone by the considered nitrogen containing species. For the amine to become susceptible to C-N bond scission via β-(H) elimination, this nitrogen atom must be quaternised via protonation by a H^+ available from the neighbouring S^{2-} site, see Figure 6-3.

6.1.3 C-N bond scission via β-(H) elimination

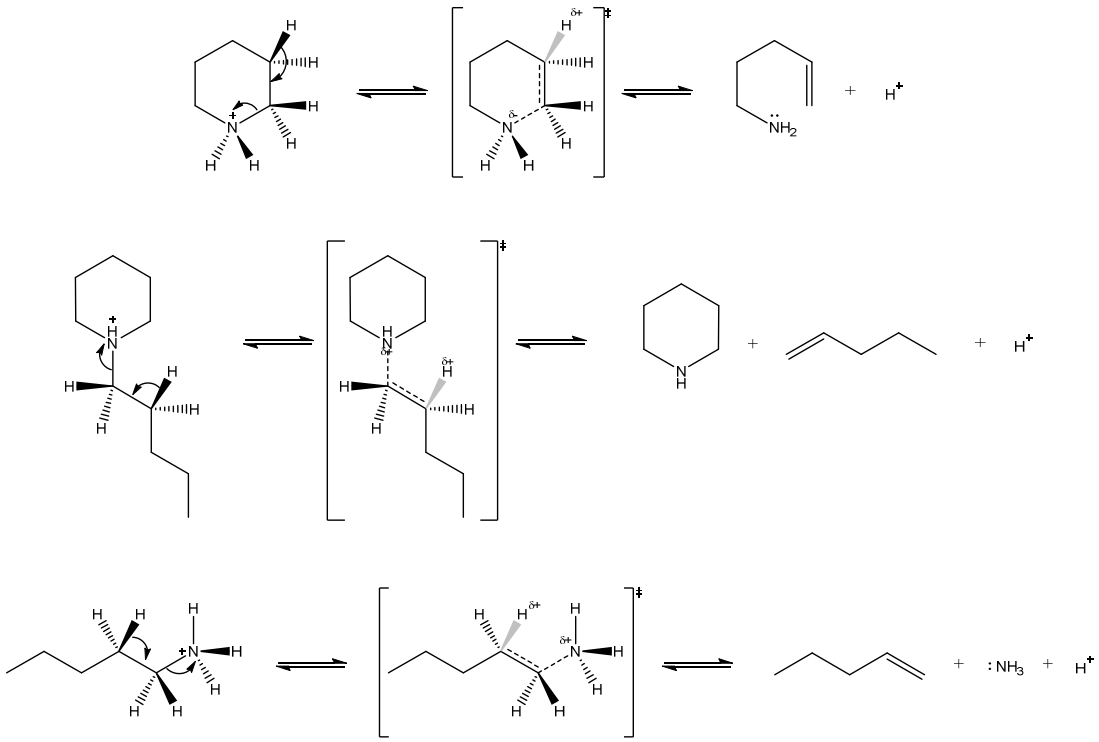

Figure 6-4. Mechanism of the β-(H) elimination reaction for C-N bond scission, endocyclic (top), exocyclic (middle) acyclic (bottom), starting from a protonated amine.

The intermediates in hydrodenitrogenation are subject to C-N bond scission reactions via β-(H)elimination reactions in an endocyclic, exocyclic or acyclic manner as illustrated in

Figure 6-4. The reaction mechanism involves the abstraction of a H^+ from the carbon atom in β-position of the nitrogen atom in a protonated species. which results in the stabilisation of the molecular structure. The electrons of the C-N bond are drawn towards the nitrogen atom, resulting in a neutral amine function with a lone electron pair and a primary, positively charged carbon atom. The unstable character of the latter results in a rapid deprotonation leading to a double bond between the carbon atoms that were originally in α and β-position with respect to the nitrogen atom. The endocyclic variety of this reaction family leads to an alkylamine, i.e., via ring opening, while the exocyclic one results in a heterocyclic amine and an alkyl fragment that was split off from the ring. Finally, the acyclic variety provokes the ultimate C-N bond scission releasing the nitrogen as NH_3 [8].

6.1.4 C-N bond scission via (–SH) substitution

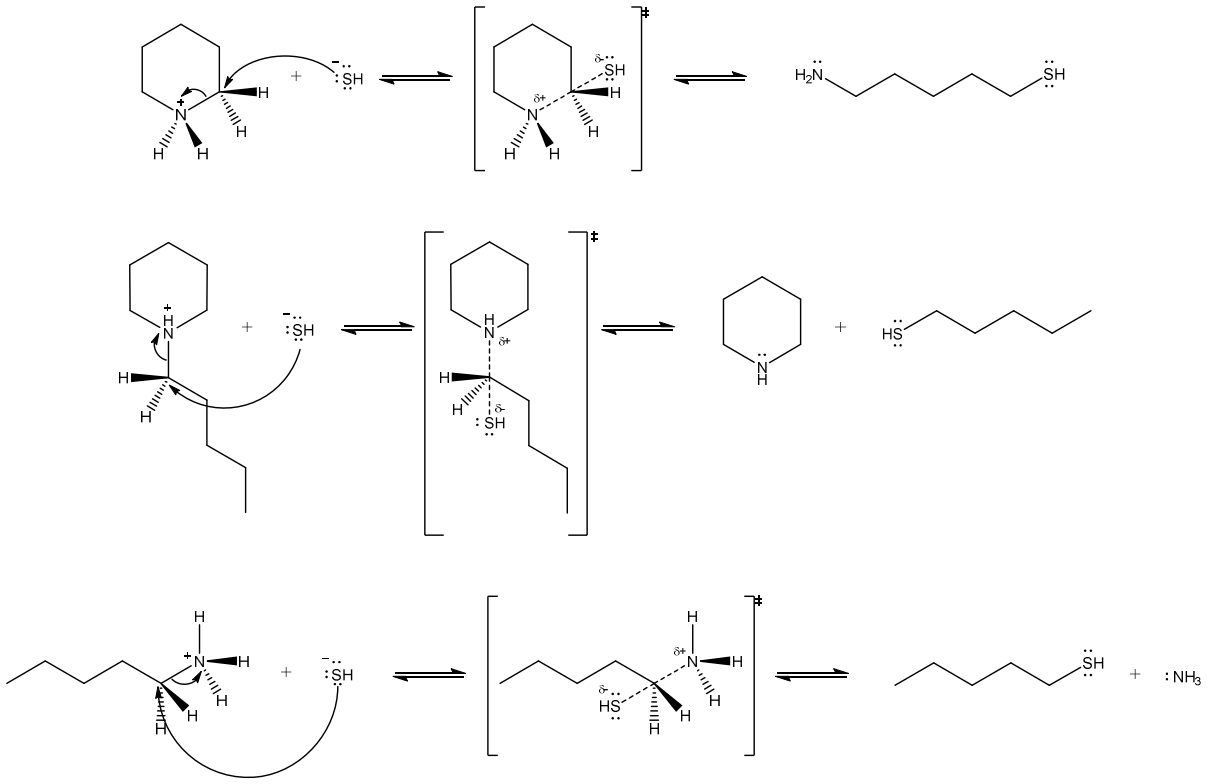

Figure 6-5. Mechanism of the –SH substitution reaction for C-N bond scission endocyclic (top), exocyclic (middle) acyclic (bottom), starting from a protonated amine.

Rather than via an elimination reaction, the C-N bond scission can also occur via a nucleophilic substitution reaction involving a sulphydril species ($-SH^-$). As proposed by Schwartz et al. [8] an electron pair of the SH^- group attacks the carbon present in the α position with respect to the nitrogen atom, which causes the C-N bond electron pair to relocate towards the nitrogen resulting in the bond scission, see Figure 6-5. The quaternised nitrogen atom in protonated pyridine is neutralized by this relocation of electrons and its lone electron pair is

restored. The endocyclic, exocyclic and acyclic variety follow similar reaction mechanisms, but result in the formation of different products as it was the case for the C-N bond scission via β-(H) elimination.

6.1.5 Formation of heavier species via pentylamine condensation

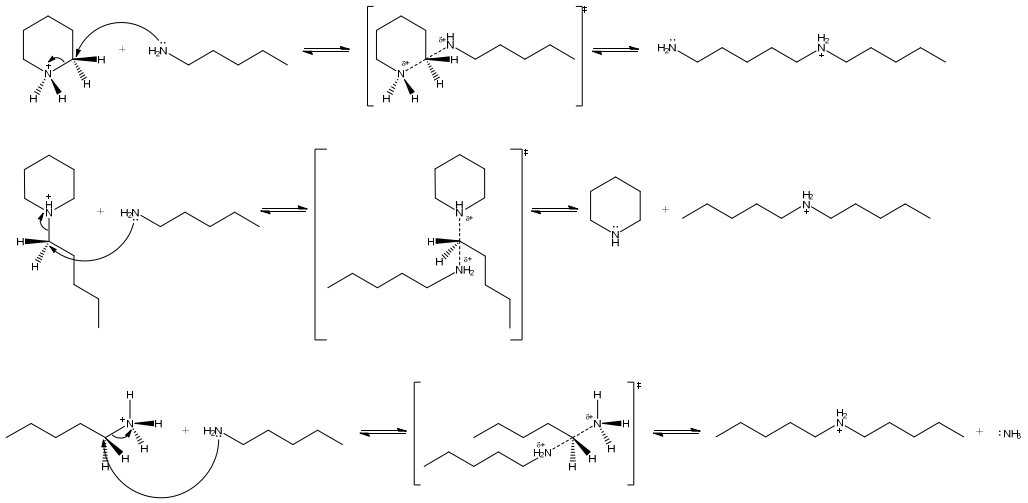

Figure 6-6. Pentylamine condensation reaction mechanism, endocyclic (top), exocyclic (middle) acyclic (bottom).

The *n*-pentylamine that is formed not only undergoes elimination and substitution reactions followed by nitrogen removal under the form of ammonia but it can also react with amines such as piperidine, *n*-pentylpiperidine and *n*-pentyl amine, see Figure 6-6. The lone electron pair on the reacting pentylamine nitrogen atom adds to the α carbon atom with respect to the (protonated) nitrogen atom of the other amine. As a result, the C-N bond electron pair relocates towards the nitrogen atom of this other amine. Depending on the C-N bond that is broken during pentylamine condensation, the endocyclic, exocyclic or acyclic variety is concerned. Apart from the substituting agent, this pentylamine condensation is mechanistically identical to the previously discussed C-N bond scission via (-SH) substitution, see also 6.1.4. Because of the difference in substituting agent and the potentially different fate of the reaction product, a separate reaction type is defined for this pentylamine condensation.

6.1.6 Formation of heavier species via piperidine condensation

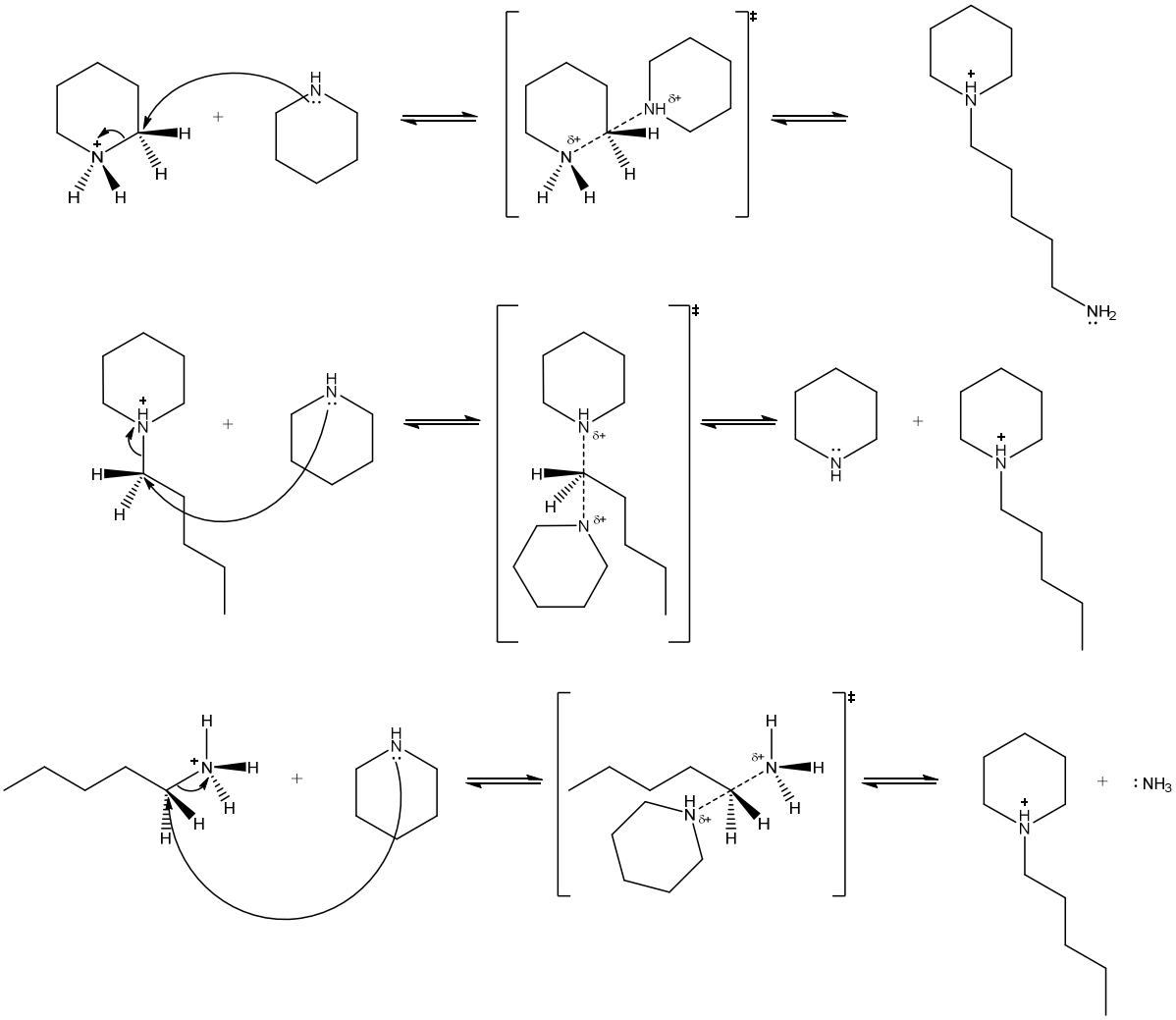

Figure 6-7. Piperidine condensation reaction mechanism, endocyclic (top), exocyclic (middle) acyclic (bottom).

Analogous to the *n*-pentylamine condensation also piperidine can be involved in condensation reactions as shown in Figure 6-7. Again endocyclic, exocyclic and acyclic varieties can be differentiated but the mechanism remains essentially the same as discussed above. *n*-Pentylpiperidine has effectively been observed in the experimental program performed at liquid phase conditions. In line with the conclusions drawn in Chapter 5, *n*-pentylpiperidine results from a reaction between a pentyl amine and piperidine, i.e., the acyclic variety included in Figure 6-7.

6.1.7 Acyclic (-SH) direct hydrogenolysis

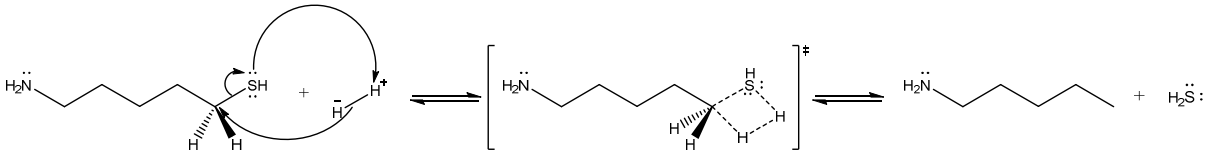

Figure 6-8. –SH direct hydrogenolysis reaction mechanism.

The thiol group at the end of a saturated hydrocarbon chain formed after C-N bond scission via (-SH) substitution is susceptible to a direct hydrogenolysis, i.e., C-S bond scission, as shown in Figure 6-8. The α carbon atom with respect to the sulphur atom reacts with the hydride from a * site and facilitates the C-S bond scission, since the –SH is a good leaving group. The proton from a S^{2-} site reacts with the SH- group in order to form the H_2S. Because the thiol end group is highly reactive these components are generally not observed experimentally. However, they form important intermediates through which the reaction proceeds and, hence, need to be accounted for during the network generation.

6.1.8 Alkene hydrogenation

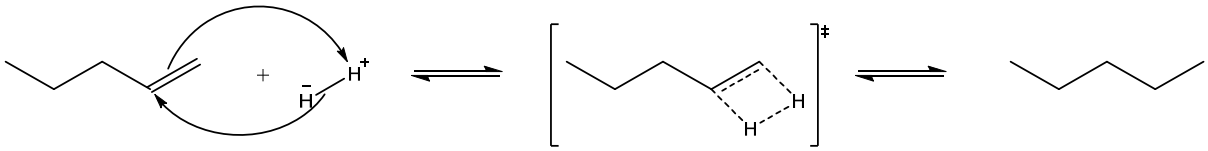

Figure 6-9. Double bond hydrogenation reaction mechanism.

Unsaturated hydrocarbons are formed by the direct removal of the end chain amine group through the β-(H) elimination reaction. However, due to the presence of very high amounts of H^+ and H^- on the catalyst surface, the double bonds in the unsaturated hydrocarbons are hydrogenated as shown in Figure 6-9. During the hydrogenation the hydride attacks one of the carbon atoms which results in the electron pair of the π-bond to relocate to form a bond with the proton.

6.2 Introduction to ReNGeP

As introduced in the previous sections, different reaction types occur during pyridine hydrodenitrogenation. Such a complex reaction network involves a multitude of elementary steps and various intermediates are formed. No energetic/enthalpic differences are considered

between the elementary steps of a single reaction family, however, entropic differences related to symmetry effects may exist and need to be adequately accounted for. The manual generation of such a gigantic reaction network as well as the assessment of the entropic effects would be tedious and error prone. Hence, computer algorithms are used for this purpose. The corresponding software needs to generate species and extract complete information about the reaction network, i.e., reactant to intermediate and product mapping, markers for elementary reactions and their corresponding reaction families, the entropic effects in terms of number of single events for each and every reaction pair. All this starts by applying the elementary chemistry rules to the starting component for the reaction.

Reaction network generation algorithms and programs have been proposed by various authors [45-53] and have been utilised already for various applications. One such automatic Reaction Network Generation Program, i.e., ReNGeP, has been developed at the Laboratory for Chemical Technology (LCT), Ghent University [54]. ReNGeP is a standalone program capable of generating an entire reaction network starting from the user-supplied feed and applying the chemistry rules of the selected (or default) reaction families.

ReNGeP was conceptualized and practically first implemented by Clymans and Froment in the early 1980's for thermal cracking [55, 56]. The concept was further extended to heterogeneously catalysed hydroisomerisation and hydrocracking by Baltanas and Froment [54, 57]. Feng et al. extended it to catalytic cracking [58] Martinis and Froment added several features to extend the same program to reforming [59]. Other contributions in order to incorporate different reactions were made by Toch et al. [60] for oligomerisation, by Kumar et al. for methanol to olefins conversion [61, 62] and by Bera et al. for aromatic saturation over metal catalyst [42, 43]. In addition to the above mentioned extensions to the ReNGeP, Lozano et al. [63-66] developed a separate version of the ReNGeP to account for the reactions occurring during the Fischer-Tropsch process and in particular for the bonds with the catalyst surface. While most of the aforementioned reactions relate to hydrocarbon and carbocation chemistry, hetero-components are explicitly considered for the first time. Utmost care has been taken in order to adhere to the structure of already considered reaction families when implementing new ones. The originally developed concept could be extended towards the reactions involving hetero-atoms such as nitrogen which helped to keep the program free from bugs and to guarantee its versatility.

ReNGeP can be compiled using standard commercially available compilers such as the ones by Compaq or Intel and the results can be analysed using standard programs such as Notepad or Microsoft Excel, providing total flexibility to the end user. ReNGeP comprises nine

sections including various subroutines, each with a specific purpose and performing specific steps in the code. A brief introduction to each of the sections is provided in section 6.4 of this chapter.

Reactions such as hydrocracking and thermal cracking potentially result in the formation of a huge number of intermediates and reaction products. In order to keep the number of considered species in the reaction network within limits, some restrictions were previously imposed in the network generation algorithm:

- For acyclic species, only methyl- and ethyl branches were considered, with a maximum branching degree of three. This is reasonable since tri-branched carbenium ions are susceptible to fast cracking reactions which are dominant over isomerization towards tetra-branched isomers.
- For cyclic species, the branched side chains only contain methyl branches. The number of primary carbon atoms is restricted to four, which corresponds to one tribranched side chain, two mono-branched side chains, one mono-branched side chain and two unbranched side chains or four unbranched side chains.
- The number of rings for cyclic components is limited to four, and the formation of pericondensed and biphenylic components is excluded
- Interaction with the catalyst surface is not considered during the generation of the reaction network while the number of single events are considered based on the loss of entropy that molecules undergo after ad/chemisorption. However, in the ReNGeP version developed for Fischer-Tropsch process [63-66], the hydrocarbon chain was assumed to grow over the metal catalyst. This was done by the corresponding consideration of the interaction between the metal catalyst and the reactants.

In addition to the above rules for reaction network generation some specific constraints were required in the present thesis with respect to the inclusion of nitrogen as hetero-atom:

- A maximum of two hetero atoms is considered in each molecule at any time in the network generation procedure. This facilitates the processing components that are generated through specific reactions, such as, e.g., endocyclic piperidine condensation within the ReNGeP.

6.3 Labelling and handling of hydrocarbon species

A key aspect in the implementation of an automatic reaction network generation, apart from the chemistry and the chemical transformation, is the representation and handling of the hydrocarbon species in the network. Two important features need to be dealt with:

- The representation of each and every species loaded or generated in ReNGeP should be unique, i.e., they must be different and identifiable by the user and the program likewise
- The characterization must also allow a relatively simple implementation of the elementary reaction steps and must be in a position to provide markers for identifying reaction families and provide the relevant information on the transformations between reactants and intermediates.

The above mentioned features have been identified to be highly unlikely to be compatible with one another, resulting in two types of representation for the hydrocarbon species during the network generation:

- Vectors for the input, storage and the output, for the involved species
- Boolean relation matrices for the implementation of the elementary reaction steps and providing information about the reactions.

6.3.1 Vectorial or label representation

For the input, storage and output of the hydrocarbon species, a vector representation has been implemented in ReNGeP. This representation has two important advantages:

a) Each hydrocarbon is represented by a unique vector or label, by using unique numbering, including prioritization, for the different atoms present in the hydrocarbon feedstock and all the processed molecules
b) This representation is very compact in terms of memory usage and saves simulation time while reading and writing species on standard documents.

For a given hydrocarbon species, the vector (or label) contains 41 elements, when a feed molecule of maximum 20 carbon (or hetero) atoms is considered. The size of the array can, however, be changed if the number of maximum allowed carbon/hetero atoms in the feedstock or the reaction network has to be increased to a larger value, by changing a few lines of code.

This vector is represented as a sequence of 3 rows:

- The first row contains only a single element, which indicates the position of the charge, if any. Its value is set to 0 if no charge is present in the molecule.

- The second row contains 20 elements which represent the branching degree of the carbon/hetero atoms in the hydrocarbon:

  1 = primary carbon/hetero atom

  2 = secondary carbon/hetero atom

  3 = tertiary carbon/hetero atom

  4 = quaternary carbon/hetero atom

- The third row also contains 20 elements, which describe the type of the carbon/hetero atoms in the hydrocarbon [67]. Table 6-1, provides an overview of the codes for atoms utilized in the third row of the vector. Figure 6-10 shows two examples with the atoms numbered according to . These codes are assigned based on priority, i.e., the atom type of the highest priority having the lowest number.

a b

Figure 6-10. Example of the representation of various atoms of different components in ReNGeP.

The uniqueness of this labelling method can be shown by the following examples, see Figure 6-11: simple components such as benzene and pyridine followed by a more complex component.

For acyclic molecules and positively charged ions, the numbering always starts at a primary carbon/hetero atom. The first carbon/hetero atom has to be chosen in such way that it yields a main chain of maximal length. The numbering of the main chain is started at the primary carbon/hetero atom which yields the lowest rank number for the charged carbon/hetero atom, if any. If a neutral, hetero-atom containing species is concerned the numbering starts at the primary carbon atom which yields the lowest rank number for the hetero atom. If the species is neutral and only consists of carbon and hydrogen atoms, but is unsaturated, the unsaturated carbon atoms must have the lowest rank number. For saturated pure hydrocarbon species, the numbering has to yield the lowest rank number for the carbon atom bearing the first branch. If

this numbering is not yet unique, which is only possible if there is more than one branch, the second branch must have the lowest rank number.

Table 6-1. Unique numbers allocated for different types of atoms encountered in the generation of the reaction network using ReNGeP [67].

1	bridge head aromatic biphenyl carbon atom	16	aromatic carbon atom
2	bridge head unsaturated naphthenic biphenyl carbon atom	17	naphthenic sulphur atom
3	bridge head saturated naphthenic biphenyl carbon atom	18	naphthenic nitrogen atom
4	aromatic pericondensed carbon atom	19	naphthenic oxygen atom
5	unsaturated naphthenic pericondensed carbon atom	20	unsaturated naphthenic carbon atom
6	saturated naphthenic pericondensed carbon atom	21	saturated carbon atom
7	bridge head aromatic pericondensed carbon atom	22	acyclic sulphur atom
8	bridge head unsaturated naphthenic pericondensed carbon atom	23	acyclic nitrogen atom
9	bridge head saturated naphthenic pericondensed carbon atom	24	acyclic oxygen atom
10	bridge head aromatic carbon atom	25	alcoholic oxygen atom*
11	bridge head unsaturated naphthenic carbon atom	26	unsaturated heptamethylbenzenium ion atom*
12	bridge head saturated naphthenic carbon atom	27	saturated heptamethylbenzenium ion atom*
13	aromatic sulphur atom	28	unsaturated acyclic carbon atom
14	aromatic nitrogen atom	29	saturated acyclic carbon atom
15	aromatic oxygen atom	*	These were added earlier for other research

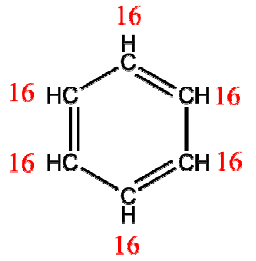

0

2 2 2 2 2 2 ... N_{Lab}

16 16 16 16 16 16 ... N_{Lab}

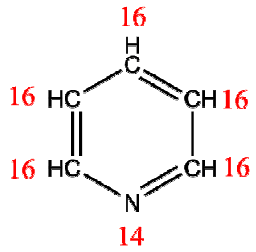

0

2 2 2 2 2 2 ... N_{Lab}

14 16 16 16 16 16 ... N_{Lab}

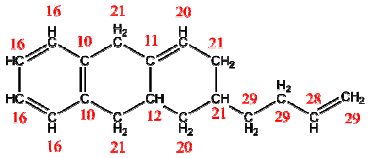

0

3 2 3 2 2 3 2 3 2 3 2 2 2 2 2 2 2 1

10 21 11 20 21 21 21 12 21 10 16 16 16 16 29 29 28 29

Figure 6-11. Label representation of benzene (above), pyridine (middle) and a naphtheno aromatic component (below).

For cyclic components, the numbering always starts at a ring carbon atom. If a ring carbon/hetero atom is charged, it obtains rank number 1. If a carbon/hetero atom in a side chain is charged, the numbering must yield the lowest number for that particular atom. If a neutral species is concerned, the priority of the carbon/hetero atoms follows the numbering of the types of the carbon atoms as presented in Figure 6-11 (below): a biphenyl bridge head aromatic carbon atom (type = 1) has the highest priority, a biphenyl bridge head unsaturated naphthenic carbon atom (type = 2) has the second highest priority. The numbering has to be such that it minimizes the rank numbers of the carbon/hetero atoms with the highest priority, starting at the ring carbon/hetero atom with the highest priority. In the example of the naphtheno-aromatic component, which is an anthracene derivative i.e., 2-(but-3-en-1-yl)-1,2,3,9,9a,10-hexahydroanthracene, see Figure 6-11 (below), the numbering is started at the bridge head aromatic carbon atom (rank number 1) which yields the lowest rank number for the bridge head unsaturated naphthenic carbon atom (rank number 3). If the numbering is started at the other bridge head aromatic carbon atom, the lowest possible rank number is 4 for the second bridge head aromatic carbon atom.

6.3.2 Boolean relationship matrix

The vectorial representation offers less flexibility in terms of operations on the molecules for the actual generation of the reactions. Therefore, these vectors are converted into Boolean relation matrices before the various functions relating to specific reaction families are applied. An element (i, j) of a Boolean relation matrix equals 1 if there is a bond between the atoms i and j. Otherwise, the element (i, j) is equal to 0. For the naphtheno-aromatic component, i.e. 2-(but-3-en-1-yl)-1,2,3,9,9a,10-hexahydroanthracene, see Figure 6-11 (below), the Boolean relation matrix is given by:

	1	**2**	**3**	**4**	**5**	**6**	**7**	**8**	**9**	**10**	**11**	**12**	**13**	**14**	**15**	**16**	**17**	**18**	**19**	**20**
1	0	1	0	0	0	0	0	0	0	1	0	0	0	1	0	0	0	0	0	0
2	1	0	1	0	0	0	0	0	0	0	0	0	0	0	0	0	0	0	0	0
3	0	1	0	1	0	0	0	1	0	0	0	0	0	0	0	0	0	0	0	0
4	0	0	1	0	1	0	0	0	0	0	0	0	0	0	0	0	0	0	0	0
5	0	0	0	1	0	1	0	0	0	0	0	0	0	0	0	0	0	0	0	0
6	0	0	0	0	1	0	1	0	0	0	0	0	0	0	1	0	0	0	0	0
7	0	0	0	0	0	1	0	1	0	0	0	0	0	0	0	0	0	0	0	0
8	0	0	1	0	0	0	1	0	1	0	0	0	0	0	0	0	0	0	0	0
9	0	0	0	0	0	0	0	1	0	1	0	0	0	0	0	0	0	0	0	0
10	1	0	0	0	0	0	0	0	1	0	1	0	0	0	0	0	0	0	0	0
11	0	0	0	0	0	0	0	0	0	1	0	1	0	0	0	0	0	0	0	0
12	0	0	0	0	0	0	0	0	0	0	1	0	1	0	0	0	0	0	0	0
13	0	0	0	0	0	0	0	0	0	0	0	1	0	1	0	0	0	0	0	0
14	1	0	0	0	0	0	0	0	0	0	0	0	1	0	0	0	0	0	0	0
15	0	0	0	0	0	1	0	0	0	0	0	0	0	0	0	1	0	0	0	0
16	0	0	0	0	0	0	0	0	0	0	0	0	0	0	1	0	1	0	0	0
17	0	0	0	0	0	0	0	0	0	0	0	0	0	0	0	1	0	1	0	0
18	0	0	0	0	0	0	0	0	0	0	0	0	0	0	0	0	1	0	0	0
19	0	0	0	0	0	0	0	0	0	0	0	0	0	0	0	0	0	0	0	0
20	0	0	0	0	0	0	0	0	0	0	0	0	0	0	0	0	0	0	0	0

These Boolean relation matrices are very well suited for the implementation of elementary steps and determining reaction possibilities, i.e., the identification of neighbour and, more particularly, next-nearest neighbour atoms is quite straightforward. However, It has to be noted that the Boolean relation matrix does not constitute a unique representation of the molecular structure. Additional vectors for indicating double bonds and hetero-atoms are required, rendering the them more complex. Given the excessive computer memory that such

matrices require compared to the vectorial representation, it is obvious that such Boolean relation matrices are not suited for the storage of hydrocarbon species.

6.4 Reaction network Generation

Over the years ReNGeP has been extended to include a variety of reactions ranging from acid catalysed cracking to metal catalysed hydrogenation, see also section 6.2. The inclusion of these reactions was done by subsequent addition of relevant reaction families. Two main versions of the ReNGeP were developed i.e., one for acid and metal catalyzed reactions in which the catalyst is not explicitly accounted for in the species representation and the reaction network generation[42, 43, 60, 63, 64, 66, 68, 69] and a second one for Fischer Tropsch synthesis developed by Lozano et al. [63-66] in which the interaction between the growing chain and the metal catalyst was explicitly included. Given the closer relation between the hydrodenitrogenation reaction investigated in the present thesis and the reactions considered in the first described ReNGeP version, the latter is focused on in what follows.

The main program is divided into various sections which contain the subroutines pertaining to the particular section. An overview of the sections present in the network generation program is given below and more details are given in the next paragraphs.

Section I Main program: the program is controlled from within the main program, by calling the suitable functions available in the other sections.

Section II Input/output and storage section.

Section III This section creates the Boolean relation matrix of a hydrocarbon specified by label, and groups specific operations, such as construction of ring, main hydrocarbon chain etc. starting from the input label.

Section IV Special tasks section, searches characteristic information, such as calculation of number of carbon and hetero atoms in the ring, verifying the positive charge on the hydrocarbon component etc. based on the Boolean relation matrix.

Section V This section performs the standardization, i.e., the conversion of Boolean relation matrix (including auxiliary information array to label representation of a hydrocarbon.

Section VI This section generates the reactions occurring on the metal sites.

Section VII This section performs the reaction steps for hydrocracking occurring on the acid sites.

Section VIII This section performs the hetero atom removal reactions.

Section IX This section performs the calculation of the symmetry number and the chirality.

Metal and acid site reactions are not treated differently, the reaction proceeds according to the specified chemistry and a complete list of the participating components is generated along with the number of single-events for each of the reactions.

6.4.1 Description of the main program

In the main program, variables are defined for each type of hydrocarbon species to store the labels of the generated products. For each hydrocarbon type, two counters are initialized: at each moment during the network generation, the first counter indicates the number of species belonging to that hydrocarbon type, while the second counter indicates the number of species belonging to that hydrocarbon type that have already been processed.

Finally, various output files, which still may contain data from a previous run, are emptied and the feed input file is opened. The names of these files can be chosen arbitrarily, and those names are passed to the main program as arguments upon calling the generation program.

6.4.2 Input of feed molecules

The feed file ‘a1’ contains a number of feedstock molecules, grouped per hydrocarbon type. For each of the hydrocarbon types that can be found in a heavy hydrocarbon feedstock, i.e., paraffins, olefins, mono- to tetracyclic olefins, mono- to tetra-naphthenes, mono- to tetra-aromatics, di-olefins, mono- to tetra-cyclic di-olefins, and hetero-aromatic components the number and the vectors of the characteristic feedstock molecules of that group are read. These vectors are written to the corresponding hydrocarbon arrays and the corresponding product counters are set.

A second file ‘a2’ contains the list of reaction families that can be selected for reaction network generation. In the case of HDN a new default value can be read which automatically applies all the reaction families that are included in ReNGeP.

6.4.3 Network generation loop

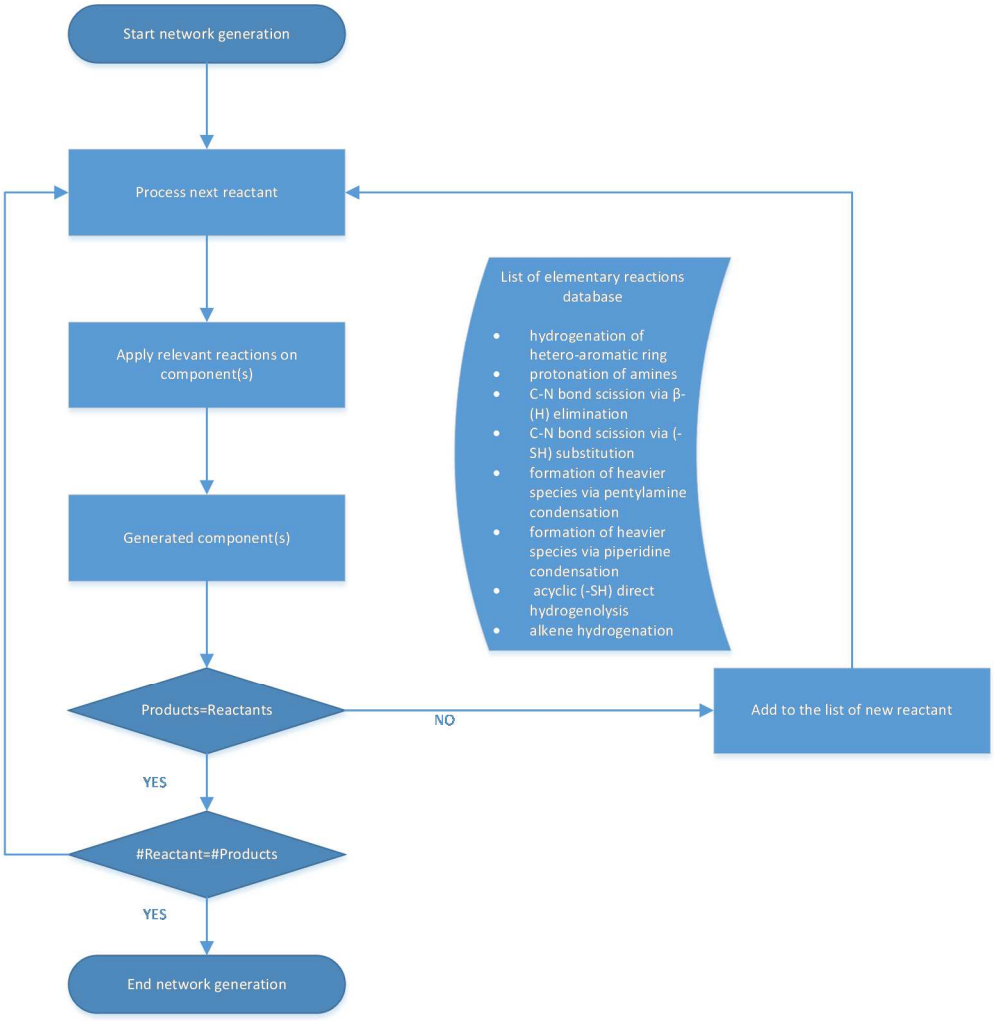

Figure 6-12. Overview of the iterative generation of the network.

Once the feed molecules are read from the input file ‘a1’, in this case pyridine, the generation loop is started. After the reactant molecule(s) is/are read by the program and the counters are initialized, the reaction families that were enabled in file ‘a2’ take over the program and call in various subroutines to generate the intermediates and calculate the corresponding symmetry numbers. The network generation loop continues as long as not all the products, fed or generated, have been processed. The program compares the two species counters for each hydrocarbon type. If, for a certain hydrocarbon type, a molecule is found which has not yet been processed, the specific reactions for this group are generated. These reactions are then written to their respective output files and the generated products are stored in their respective hydrocarbon type arrays. Note that a lot of the changes to the ReNGeP code are located in the subroutines that perform the calculations for the number of single-events based on symmetry operations on molecules

6.4.4 Output of the network generation program

Finally, when all products have been processed, the statistics of the generated network are written to the file ‘a3’. In this overview, the number of species for each hydrocarbon type as well as the number of reactions generated for each reaction family is written. Additionally, various files containing the information with respect to each of the generated reactions are written. These files can then be directly exported to the simulation and parameter estimation program and used in the determination of the model parameters according to the SEMK methodology.

6.5 Modifications towards inclusion of nitrogen components

To maintain continuity with the previous version of ReNGeP, the feed file ‘a1’ is used as the feedstock input file. This file contains the feedstock hydrocarbons, grouped per hydrocarbon type, for which the reaction network is to be generated. For each of the hydrocarbon types that are found in a heavy hydrocarbon feedstock, the number and the labels of the feed hydrocarbons of that type are read. These labels are written to the corresponding hydrocarbon arrays and the corresponding product counters are changed accordingly. In the present work, modifications were made to ReNGeP to include the possibility of processing a variety of nitrogen components. Different classes of nitrogen components were defined, requiring a distinction in the feed file ‘a1’. Aromatic, naphthenic and acyclic nitrogen components can be read from this file. In order to accommodate the different types of nitrogen components that need to be read from file ‘a1’ new arrays such as ‘mono_arom_n’, mono_naph_n and acyc_n were added to the program. They are named intuitively, i.e., mono_naph_n corresponds to a naphthenic component consisting of a single ring with nitrogen as the hetero component. These arrays typically correspond to the size of the label defined in the program. This distinction between various component types provides the program with the necessary flexibility, e.g., to adjust the reaction families that can operate on the various component types. File ‘a2’ is used for the selection of the individual reaction families or the group of reaction families that need to be applied to the feed component(s). The user can manually enable/disable each of the reaction families or group of reaction families separately. During the extension of ReNGeP towards accounting for nitrogen, a similar approach was followed and a default set of reactions, e.g., all reactions corresponding to pyridine

hydrodenitrogenation, was implemented. Once the program is modified critical testing allowed to finalise upon a stable version of the program.

In the earlier ReNGeP versions hydrogenation and dehydrogenation reactions occur by molecular H_2-addition. In the context of hydrocracking or thermal cracking or any other reaction this might have served the purpose but steps towards the inclusion of stepwise atomic hydrogen additions to simulate aromatic hydrogenation have been presented in the meantime by Bera et al. [42, 43]. Quantum chemical calculations for pyridine hydrogenation suggest that an elementary step mechanism comprises H addition via hydride species or protons [41]. The earlier ReNGeP versions are incapable of handling aromatic structures that are partially hydrogenated and these new components cannot be classified into one of the existing hydrocarbon classes.

Hence, a new hydrocarbon type was defined in which all the partially hydrogenated hydrocarbons are stored. The heterocyclic alkanes, heterocyclic alkenes, heterocyclic dienes and hetero-aromatics are stored as well in this same new hydrocarbon type. This type is denoted as ‘mono_arom_ns’ in the program and contains all the species for the hydrogenation of hetero-aromatics wherein nitrogen is the hetero atom. This can easily be extended to components in which the hetero atom is sulphur or oxygen. Incorporating all these components in a single new class ensures a compact output, facilitating in turn the reading in the output files for the modelling. All H addition and subtraction reactions are now listed two reaction files only, i.e., ‘a351’ and ‘a352’. Apart from this, a more fundamental reason for incorporating a new type is that it would be artificial to store the ‘mono_arom_ns’ in different hydrocarbon classes since quantum chemical calculations reveal that the different species of the first part of the network (hydrogenation) cannot be distinguished based on mutual resemblance. No distinct features between several chemisorption states of ‘mono_arom_ns’ can be drawn. Similarly, it would be artificial to classify the H addition reactions into different reaction families, which would be the case if the four original hydrocarbon types would be preserved. In that case, two different H addition files would be reported for the H addition reactions of the hetero-aromatics and the H addition reactions of the heterocyclic di-olefins.

Similarly, for the denitrogenation step, two new hydrocarbon types ‘mono_naph_ns’ and ‘acyc_ns’ were implemented, containing saturated ring nitrogen components and acyclic nitrogen components, respectively. Note that, as a result of the considered elementary reactions, components containing both sulphur and nitrogen are formed. These components are also stored in the ‘acyc_ns’ class because all these species are acyclic. Thiols are also formed in the considered reaction network and are stored together with the resulting paraffins in the

'paraffins' type for the ease of processing. As explained earlier in section 6.1, one reaction family can lead to products belonging to different hydrocarbon types, depending on which atoms of the compound undergo the elementary step, as well as depending on which component is used as reactant. In order to make the correct differentiation between the formed products and between the ways in which a reaction family can occur, e.g., endocyclic, exocyclic or acyclic, more output files are necessary. One output file is considered for each of the cases. This resulted in a rather long, but absolutely necessary list of output files, provided in Appendix C.

6.6 References

1. Yang, S.H. and C.N. Satterfield, **Industrial & Engineering Chemistry Process Design and Development**, 1984. 23(1): p. 20-25.

2. Yang, S.H. and C.N. Satterfield, **Journal of Catalysis**, 1983. 81(1): p. 168-178.

3. Yang, S.H. and C.N. Satterfield, **Journal of Catalysis**, 1983. 81(1): p. 168-178.

4. Vivier, L., V. Dominguez, G. Perot, and S. Kasztelan, **Journal of Molecular Catalysis**, 1991. 67(2): p. 267-275.

5. Vivier, L., P. Daraujo, G. Perot, and S. Kasztelan, **Abstracts of Papers of the American Chemical Society**, 1992. 203: p. 35-Petr.

6. Uzkan, U.S., L.P. Zhang, S.Y. Ni, and E. Moctezuma, **Journal of Catalysis**, 1994. 148(1): p. 181-193.

7. Schwartz, V. and S.T. Oyama, **Journal of Molecular Catalysis a-Chemical**, 2000. 163(1-2): p. 269-282.

8. Schwartz, V., V.T. da Silva, and S.T. Oyama, **Journal of Molecular Catalysis A: Chemical**, 2000. 163(1-2): p. 251-268.

9. Satterfield, C.N. and S.H. Yang, **Industrial & Engineering Chemistry Process Design and Development**, 1984. 23(1): p. 11-19.

10. Satterfield, C.N. and S.H. Yang, **Journal of Catalysis**, 1983. 81(2): p. 335-346.

11. Satterfield, C.N. and J.F. Cocchetto, **AIChE Journal**, 1975. 21(6): p. 1107-1111.

12. Raghuveer, C.S., J.W. Thybaut, R. De Bruycker, K. Metaxas, T. Bera, and G.B. Marin, **Fuel**, 2014. 125(0): p. 206-218.

13. Kopyscinski, J., J. Choi, and J.M. Hill, **Applied Catalysis A: General**, 2012. 445: p. 50-60.

14. Kopyscinski, J., J. Choi, L. Ding, S. Zhang, B. Ibeh, and J.M. Hill, **Catalysis Letters**, 2012. 142(7): p. 845-853.

15. Kasztelan, S., T. des Courieres, and M. Breysse, **Catalysis Today**, 1991. 10(4): p. 433-445.

16. Jian, M. and R. Prins, **Journal of Catalysis**, 1998. 179(1): p. 18-27.

17. Jian, M. and R. Prins, **Catalysis Letters**, 1995. 35(3-4): p. 193-203.

18. Hadjiloizou, G.C., J.B. Butt, and J.S. Dranoff, **Journal of Catalysis**, 1991. 131(2): p. 545-572.

19. Egorova, M. and R. Prins, **Journal of Catalysis**, 2006. 241(1): p. 162-172.

20. Egorova, M. and R. Prins, **Journal of Catalysis**, 2004. 221(1): p. 11-19.

21. Ding, L.H., Y. Zheng, Z.S. Zhang, Z. Ring, and J.W. Chen, **Applied Catalysis A: General**, 2007. 319: p. 25-37.

22. Chu, Y.J., Z.B. Wei, S.W. Yang, C. Li, Q. Xin, and E.Z. Min, **Applied Catalysis a-General**, 1999. 176(1): p. 17-26.

23. Cattenot, M., J.L. Portefaix, J. Afonso, M. Breysse, M. Lacroix, and G. Perot, **Journal of Catalysis**, 1998. 173(2): p. 366-373.

24. Cattenot, M., E. Peeters, C. Geantet, E. Devers, and J. Zotin, **Catalysis Letters**, 2005. 99(3-4): p. 171-176.

25. Bunch, A., L. Zhang, G. Karakas, and U.S. Ozkan, **Applied Catalysis A: General**, 2000. 190(1-2): p. 51-60.

26. Pille, R. and G.F. Froment, **Hydrotreatment and Hydrocracking of Oil Fractions**, 1997. 106: p. 403-413.

27. Sonnemans, J., G.H. Van Den Berg, and P. Mars, **Journal of Catalysis**, 1973. 31(2): p. 220-230.

28. Pille, R., G. Froment, B.D. G.F. Froment, and P. Grange, *Kinetic study of the hydrodenitrogenation of pyridine and piperidine on A NiMo catalyst*, in *Studies in Surface Science and Catalysis*. 1997, Elsevier. p. 403-413.

29. Sonneman, J., G.H. Van den Berg, and P. Mars, **Journal of Catalysis**, 1973. 31(2): p. 220-230.

30. Sonneman, J., W.J. Neyens, and P. Mars, **Journal of Catalysis**, 1974. 34(2): p. 230-241.

31. Sonneman, J. and P. Mars, **Journal of Catalysis**, 1974. 34(2): p. 215-229.

32. Sonneman, J. and P. Mars, **Journal of Catalysis**, 1973. 31(2): p. 209-219.

33. Schwartz, V. and S.T. Oyama, **Journal of Molecular Catalysis A: Chemical**, 2000. 163(1-2): p. 269-282.

34. Park, Y.-C., E.-S. Oh, and H.-K. Rhee, **Industrial & Engineering Chemistry Research**, 1997. 36(12): p. 5083-5089.

35. Park, Y.C. and H.K. Rhee, **Korean Journal of Chemical Engineering**, 1998. 15(4): p. 411-416.

36. McIlvried, H.G., **Industrial & Engineering Chemistry Process Design and Development**, 1971. 10(1): p. 125-130.

37. Machida, M., Y. Sakao, and S. Ono, **Applied Catalysis a-General**, 2000. 201(1): p. 115-120.

38. Joo, H.S. and J.A. Guin, **Fuel Processing Technology**, 1996. 49(1-3): p. 137-155.

39. Jian, M., J.L.R. Cerda, and R. Prins, **Bulletin Des Societes Chimiques Belges**, 1995. 104(4-5): p. 225-230.

40. Al-Megren, H.A., S.L. González-Cortés, T. Xiao, and M.L.H. Green, **Applied Catalysis A: General**, 2007. 329: p. 36-45.

41. Sun, M.Y., A.E. Nelson, and J. Adjaye, **Journal of Catalysis**, 2005. 231(1): p. 223-231.

42. Bera, T., J.W. Thybaut, and G.B. Marin, **ACS Catalysis**, 2012. 2(7): p. 1305-1318.

43. Bera, T., J.W. Thybaut, and G.B. Marin, **Industrial & Engineering Chemistry Research**, 2011. 50(23): p. 12933-12945.

44. Romero, C.M.C., J.W. Thybaut, and G.B. Marin, **Catalysis Today**, 2008. 130(1): p. 231-242.

45. Broadbelt, L.J., S.M. Stark, and M.T. Klein, **Industrial & Engineering Chemistry Research**, 1994. 33(4): p. 790-799.

46. Broadbelt, L.J., S.M. Stark, and M.T. Klein, **Chemical Engineering Science**, 1994. 49(24b): p. 4991-5010.

47. Yoneda, Y., **Bulletin of the Chemical Society of Japan**, 1979. 52(1): p. 8-14.

48. Yoneda, Y., **Bulletin of the Chemical Society of Japan**, 1979. 52(5): p. 1297-1314.

49. Rangarajan, S., A. Bhan, and P. Daoutidis, **Computers & Chemical Engineering**, 2012. 46: p. 141-152.

50. Rangarajan, S., A. Bhan, and P. Daoutidis, **Computers & Chemical Engineering**, 2012. 45: p. 114-123.

51. Rangarajan, S., T. Kaminski, E. Van Wyk, A. Bhan, and P. Daoutidis, **Computers & Chemical Engineering**, 2014. 64: p. 124-137.

52. Van Geem, K.M., M.F. Reyniers, G.B. Marin, J. Song, W.H. Green, and D.M. Matheu, **AIChE Journal**, 2006. 52(2): p. 718-730.

53. Vandewiele, N.M., K.M. Van Geem, M.F. Reyniers, and G.B. Marin, **Chemical Engineering Journal**, 2012. 207: p. 526-538.

54. Baltanas, M.A. and G.F. Froment, **Computers & Chemical Engineering**, 1985. 9(1): p. 71-81.

55. Clymans, P.J. and G.F. Froment, **Computers & Chemical Engineering**, 1984. 8(2): p. 137-142.

56. Clymans, P.J., G.F. Froment, M. Berthelin, and P. Trambouze, **AIChE Journal**, 1984. 30(6): p. 904-915.

57. Baltanas, M.A., K.K. Vanraemdonck, G.F. Froment, and S.R. Mohedas, **Industrial & Engineering Chemistry Research**, 1989. 28(7): p. 899-910.

58. Feng, W., E. Vynckier, and G.F. Froment, **Industrial & Engineering Chemistry Research**, 1993. 32(12): p. 2997-3005.

59. Martinis, J.M. and G.F. Froment, **Industrial & Engineering Chemistry Research**, 2006. 45(3): p. 954-967.

60. Toch, K., J.W. Thybaut, B.D. Vandegehuchte, C.S.L. Narasimhan, L. Domokos, and G.B. Marin, **Applied Catalysis A: General**, 2012. 425: p. 130-144.

61. Kumar, P., J.W. Thybaut, S. Svelle, U. Olsbye, and G.B. Marin, **Industrial & Engineering Chemistry Research**, 2013. 52(4): p. 1491-1507.

62. Kumar, P., J.W. Thybaut, S. Teketel, S. Svelle, P. Beato, U. Olsbye, and G.B. Marin, **Catalysis Today**, 2013. 215: p. 224-232.

63. Lozano-Blanco, G., K. Surla, J.W. Thybaut, and G.B. Marin, **Oil & Gas Science and Technology-Revue D Ifp Energies Nouvelles**, 2011. 66(3): p. 423-435.

64. Lozano-Blanco, G., J.W. Thybaut, K. Surla, P. Galtier, and G.B. Marin, **AIChE Journal**, 2009. 55(8): p. 2159-2170.

65. Lozano-Blanco, G., J.W. Thybaut, K. Surla, P. Galtier, and G.B. Marin, **Industrial & Engineering Chemistry Research**, 2008. 47(16): p. 5879-5891.

66. Lozano-Blanco, G., J.W. Thybaut, K. Surla, P. Galtier, and G.B. Marin, **Oil & Gas Science and Technology-Revue D Ifp Energies Nouvelles**, 2006. 61(4): p. 489-496.

67. Vynckier, E., *Kinetische modellering van de katalytische hydrokraking*. 1997, Ghent University

68. Thybaut, J.W., C.S.L. Narasimhan, G.B. Marin, J.F.M. Denayer, G.V. Baron, P.A. Jacobs, and J.A. Martens, **Catalysis Letters**, 2004. 94(1-2): p. 81-88.

69. Thybaut, J.W., C.S.L. Narasimhan, and G.B. Marin, **Catalysis Today**, 2006. 111(1-2): p. 94-102.

7 Single-Event Microkinetics of pyridine hydrodenitrogenation over NiMo/γ-Al_2O_3

A proof of principle for the extension of the Single-Event Microkinetic (SEMK) methodology towards hetero atom containing components is presented with pyridine hydrodenitrogenation as example. An exhaustive gas phase pyridine hydrodenitrogenation data set over a commercial, sulphided NiMo/γ-Al_2O_3 catalyst that has previously been acquired in a Berty type Continuous Stirred Tank Reactor (CSTR), was used for this purpose [1, 2]. Temperatures and total pressures were varied from 573 to 633 K and from 1.5 to 4.0 MPa in a space time range from 350 to 1800 kg_{cat} s $mol^{-1}{}_P$. A detailed reaction network comprising all potentially relevant intermediates and elementary steps occurring during pyridine hydrodenitrogenation was generated using the in-house software tool 'ReNGeP'. Pyridine conversion into piperidine and C_5 hydrocarbons was found to involve a total of 33 intermediates. In total, 19 partially hydrogenated hetero naphthenic species were generated during pyridine hydrogenation and 14 intermediates occurred in the conversion of piperidine to pentane and ammonia. 70 elementary reactions were identified between these intermediates and were classified in 9 reaction families. Despite all efforts to reduce the number of parameters a priori, 48 kinetic and catalyst descriptors needed to be determined. By a) fixing catalyst descriptors to previously determined values and b) proposing reasonable pre-exponential factor values for the rate coefficients based on assumptions with respect to variations in surface mobility of the species involved, the number of parameters to be fine-tuned during the simulation was reduced to 9. It resulted in a model that could satisfactorily reproduce the experimental data. A surface coverage analysis at typical operating conditions revealed the SH^- as the most abundant surface species on the coordinatively unsaturated sites, followed by H^- ,

pyridine NH_3, piperidine and C_5, while the H^+ coverage on the sulphur anion sites (S^{2-}) amounted to about 70%.

7.1 Introduction

The SEMK methodology constitutes a fundamental approach to kinetic model construction. It accounts for all elementary steps in the reaction mechanism, both for homogeneous, bulk phase reactions as well as for heterogeneously catalysed surface reactions [3-25]. Commonly used modelling techniques and reaction schemes such as those by Langmuir-Hinshelwood or Eley-Rideal typically propose a limited number of elementary steps. Rival rate equations are derived based on considering different elementary steps as rate determining. A final model selection is made based on the statistical and physical significance of the model parameter estimates. The SEMK methodology aims to relate the experimentally observed data with the underlying kinetic phenomena by means of a mathematical model that considers finite rates for all the elementary steps in the reaction mechanism. It does so by making use of rules and hypotheses proposed after a critical evaluation of self-acquired and literature reported data as well as ab-initio based results [25-27].

Models constructed according to the SEMK methodology result in the elegant linking of the experimental data to elementary reactions. This is achieved by means of reaction families which can be established by grouping similar elementary steps in the conversion of complex feeds to the corresponding products [27]. This classification of elementary steps into reaction families is a convenient way of accounting for a comprehensive network while keeping the number of parameters in the model within tractable limits. Since the SEMK model is constructed based on the fundamental phenomena occurring during reaction, another advantage of SEMK modelling is situated in the ability of adequately simulating the behaviour of alternative feeds and operating conditions.

SEMK models are independent of the feed composition, since they rely on *kinetic descriptors* for *reaction families* rather than *rate coefficients* for *each individual reaction*. This requires the need for identifying these reaction families and assigning one or more appropriate identifiers. A unique single-event rate coefficient is then obtained for each reaction family. As indicated above, the identification of the elementary steps which can be considered comparable, if not 'identical', not only experimental kinetics investigations but also density functional theory based calculations are often used [19, 21, 26].

SEMK models are accurate owing to their fundamental nature, *i.e.,* they are not based on a predetermined reaction mechanism or, in other words, a dominant reaction path. Instead the

contributions of various alternative paths becoming relevant at different operating conditions are considered [19, 21]. Hence, slow reactions that seem unimportant at first sight may become important when surface concentrations of the corresponding reactants become high. This methodology accounts for the reactions that could have a significant effect on the overall kinetics at a different operating conditions. The pursued SEMK model potentially results in a large number of components and, hence, an even higher number of elementary steps interconverting these species, in the reaction network. The varying reaction rates of the various elementary steps at different operating conditions need to be accounted for. These reaction rates depend on the reactant surface concentrations as well as on the kinetic descriptor of the reaction family involved. These reaction rates are required for the net production rates in the equations constituting the mass balances for the encountered components. The corresponding sets of equations may become quite challenging to solve numerically and potentially require, among others, a dedicated mathematical solver, good initial guesses for the model parameters as well as for the component surface concentrations [27, 28].

The general reaction scheme for pyridine hydrodenitrogenation has already been discussed in chapter 1 and further elaborated in chapters 4 and 5. Two important global steps are involved, *i.e.*, the initial saturation of the hetero-aromatic ring structure and the further denitrogenation to C_5 hydrocarbons. With pyridine as model component, the objective of this chapter is to extend the SEMK methodology towards components containing hetero atoms on the one hand and towards reactions occurring on sulphided catalysts on the other hand. In chapter 6, the elementary reactions occurring in pyridine hydrodenitrogenation were presented and a methodology for reaction network generation was discussed. The reactions were classified in reaction families and the corresponding number of single events between conversion of intermediates were calculated automatically. In this chapter, the construction of the actual rate equations and corresponding modelling results are further discussed.

7.2 Procedures

7.2.1 Gas phase pyridine hydrodenitrogenation data

The data that were used for pyridine hydrodenitrogenation modelling according to the SEMK methodology have been presented in more detail in Chapter 4. More information about the experimental programme is provided by Pille [1]. The data treatment and the mass balance equations for the reactor balance are similar to the ones presented in Chapter 2.

7.2.2 Transition state theory

The SEMK methodology is inspired by and based on Transition State Theory (TST), as originally presented by Henry Eyring [29] and Evans and Polanyi [30] in 1935. These separate works had the sole aim of better explaining the kinetics of elementary reactions. This was efficiently done by assuming the transition states to be in "quasi equilibrium" with the corresponding reactants. This assumption is important in the context of explaining kinetics, since the rate of formation of the various products can be related to the reactant via the rate coefficients of the reactions and measurable reactant concentrations. The development and application of TST have been very well documented by Laidler and King [31] and Truhlar et al. [32] through their contributions in the special issue of the journal of physical chemistry dedicated to Henry Eyring in 1983. Eq. 7-1, represents the famous formula for the rate coefficient proposed by Eyring in terms of the entropic and the enthalpy differences between the reactants and the transition state species [29, 33]:

$$k = \frac{k_B T}{h} exp\left(\frac{\Delta S^{o,\neq}}{R}\right) exp\left(-\frac{\Delta H^{o,\neq}}{RT}\right) \qquad 7\text{-}1$$

With k_B the Boltzmann constant, 1.083 x10^{-23} J K^{-1}, h the Planck constant, 6.62 x10^{-34} J s, T the absolute temperature in K and $\Delta H^{o,\neq}$ and $\Delta S^{o,\neq}$ the standard enthalpy and standard entropy of activation.

7.2.3 Single-event concept

The rate coefficients in the single-event methodology are related on a one-to-one basis with the considered reaction families. This aims, in the first place, at describing similar elementary steps with identical parameter values, c.q., activation energies or reaction enthalpies. E.g., during the construction of a comprehensive model for hydrocracking, the kinetically relevant acid-catalysed elementary steps occurring were classified in the following three reaction types, *i.e.*, alkyl shift isomerization, protonated cyclopropane branching, and β-scission [34, 35]. Each of these reaction types comprises 4 reaction families to allow differentiation between the reactant and product carbenium ion types, *i.e.*, secondary or tertiary.

In Figure 7-1, an isomerisation reaction between two substituted carbenium ions is shown. Considering only a similar, c.q., identical, energetic effect of the forward and the backward reaction, the rate of the forward and the backward reaction would be the same. However, since for the forward reaction two candidate methyl groups are available for shifting while for the backward reaction only a single methyl group is present, at equal concentrations of both carbenium ions, the forward reaction can reasonably be expected to occur at a rate

amounting to the double of the backward rate. These entropic effects are captured by the so called number of single events. The motion of one methyl group can be considered as a single event with which a single-event rate coefficient can be associated. Differences in reaction rates between elementary steps belonging to the same reaction family can, hence, be interpreted in terms of differences in the number of these single events.

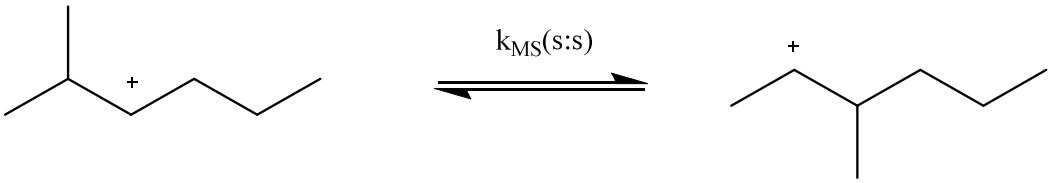

Figure 7-1. Isomerization between the 2 methylhept-3-yl and the 3 methyl hept-2-yl ion via a secondary–secondary methyl-shift reaction.

The mathematical derivation of the SEMK concept is presented starting from Eq. 7-1. The standard entropy consists of translational, vibrational and rotational contributions:

$$S^o = S^o_{trans} + S^o_{vibr} + S^o_{rot} \qquad 7\text{-}2$$

The rotational entropy comprises an internal and an external contribution, both containing a single-event entropy term S^o and a symmetry number σ:

$$S^o_{rot,ext} = \tilde{S}^o_{rot,ext} - R \ln \sigma_{ext} \qquad 7\text{-}3$$

$$S^o_{rot,int} = \tilde{S}^o_{rot,int} - R \ln \sigma_{int} \qquad 7\text{-}4$$

The symmetry numbers may vary from reaction to reaction and are calculated based on the number of possible rotations of the molecule resulting in an identical molecule. Apart from the external and internal symmetry numbers, the number of chiral centres n in the molecule needs to be accounted for as well. Altogether, this leads to the global symmetry number:

$$\sigma_{glob} = \frac{\sigma_{ext}\sigma_{int}}{2^n} \qquad 7\text{-}5$$

As a result, the symmetry dependent contribution to the entire standard entropy of activation can be isolated and expression for the rate coefficient can be rewritten as:

$$k(m,n) = \frac{\sigma^r_{glob}}{\sigma^{\neq}_{glob}} \frac{k_B T}{h} exp\left(\frac{\Delta \tilde{S}^{o,\neq}}{R}\right) exp\left(-\frac{\Delta H^{o,\neq}}{RT}\right) = n_e . \tilde{k}(m,n) \qquad 7\text{-}6$$

With n_e the number of single events, *i.e.*, the ratio of the global symmetry number of the reactant to that of the activated complex:

$$n_e = \frac{\sigma^r_{glob}}{\sigma^{\neq}_{glob}} \qquad 7\text{-}7$$

7.2.4 Model assumptions

Along with the theoretical concepts discussed in the present section with respect to the single-event methodology, some additional assumptions and constraints are required to actually construct the corresponding rate equations and perform the model simulations:

- A two site model is proposed for the construction of the comprehensive SEMK for pyridine hydrodenitrogenation over a sulphided NiMo/γ-Al_2O_3. This is consistent with previous work performed at the Laboratory for Chemical Technology (LCT) [36], and with what is reported in Chapters 4 and 5. Accordingly molecular chemisorption of the hydrocarbons is assumed to occur on the coordinatively unsaturated sites (*) and dissociative chemisorption of the H_2 and H_2S is assumed to occur on the sulphur anion sites (S^{2-}) and the coordinatively unsaturated sites (*), see Table 7-1. A more detailed description is given in Chapters 4 and 5.
- The values for the chemisorption enthalpies and the pre-exponential factors for the chemisorption coefficients of piperidine, ammonia, H_2 and H_2S for the same catalyst were determined previously, see Chapter 4. These values are used without further modification during the SEMK modelling. Pre-exponential factors for the chemisorption coefficients of the remaining components *i.e.*, pyridine and C_5 are calculated considering a minimum and maximum loss of translation degrees of freedom, see chapter 4. This is one of the strategies used for the reduction of the number of model parameters and is further discussed in section 7.4.2.

Table 7-1. Chemisorption equilibria accounted for in the SEMK model for pyridine hydrodenitrogenation.

Chemisorption equilibria	Chemisorption coefficient
Coordinatively unsaturated sites (*)	
$C_5H_5N + * \rightleftharpoons * - C_5H_5N$	K_P
$C_5H_{11}N + * \rightleftharpoons * - C_5H_{11}N$	K_{PP}
$C_5H_{12} + * \rightleftharpoons * - C_5H_{12}$	K_{PA}
$NH_3 + * \rightleftharpoons * - NH_3$	K_{NH3}
Sulphur anion sites (S^{2-})	
$H_2 + * + S^{2-} \rightleftharpoons * - H^- + S^{2-} - H^+$	K_{H2}
$H_2S + * + S^{2-} \rightleftharpoons * - SH^- + S^{2-} - H^+$	K_{H2S}

- According to the SEMK methodology no rate-determining step is considered during the derivation of the model equations. All the steps and corresponding reactants, intermediates and products are explicitly accounted for during the model equation derivation. As presented in Chapter 6, each of the steps encountered during the network

generation is saved along with the corresponding identifiers for the type of reaction along with the reactant and product.

- Based on the reaction network constructed and discussed in Chapter 6, a total of 9 reaction types are identified and summarised in Table 7-2. While some of the reaction types may require further classification into reaction families according to the endocyclic, exocyclic and acyclic nature of the reaction, at present no distinction was made to limit the model complexity. Accordingly, in the present chapter, each reaction type is considered as an independent reaction family and is associated with a unique rate coefficient. However, control levers have been included in the code that can be employed to differentiate between these rate coefficients in the SEMK model, if required.
- Two additional identifiers $\boldsymbol{i_1}$ and $\boldsymbol{i_2}$ have been included to allow future distinctions between elementary steps that are, at present, classified into the same family. E.g., for the hydrogenation of the aromatic carbon atoms these identifiers can be used to distinguish between hydrogenation at carbon atoms with a different branching degree and/or number of saturated neighbouring carbon atoms within the unsaturated ring as proposed by Bera et al. [21] for aromatic hydrogenation over a metal catalyst. For the other reactions, as mentioned in the previous item, these identifiers can be used to distinguish exocyclic, endocyclic, acyclic reactions from each other, see Table 7-2.

Table 7-2. Overview of the single-event rate coefficients and the associated reaction families used in the pyridine hydrodenitrogenation model.

Symbolic notation	Description
$\tilde{k}_{n,hyd}(i_1, i_2)$	Aromatic nitrogen hydrogenation
$\tilde{k}_{c,hyd}(i_1, i_2)$	Aromatic carbon hydrogenation[x]
$\tilde{k}_{prot}(i_1, i_2)$	Protonation of amines
$\tilde{k}_{\beta-(H)elim}(i_1, i_2)$	C-N bond scission via β-(H) elimination[#]
$\tilde{k}_{(-SH)sub}(i_1, i_2)$	C-N bond scission via (SH^-) substitution[#]
$\tilde{k}_{PA,cond}(i_1, i_2)$	Formation of heavier species via pentylamine condensation [#]
$\tilde{k}_{PP,cond}(i_1, i_2)$	Formation of heavier species via piperidine condensation[#]
$\tilde{k}_{(-SH)hydrogenolysis}(i_1, i_2)$	Acyclic (SH^-) direct hydrogenolysis
$\tilde{k}_{alk\ hyd}(i_1, i_2)$	Alkene hydrogenation

[x] this reaction family can be further distinguished depending on the degree of branching of the involved carbon and degree of saturation of the neighbouring carbon . [#] these reaction families can be sub-divided into endocyclic/exocyclic/acyclic types.

- The pseudo steady state approximation is applied to all surface intermediates, for the calculation of their concentrations and their corresponding rates of formation and rates of consumption, see section 7.3.

7.3 Single-Event MicroKinetic Model

Following the theoretical discussions along with the model assumptions and constraints described in sections 7.2.2 to 7.2.4, the present section further elaborates on the translation of all those considerations into the corresponding rate equations. Along with the reaction family and rate coefficient definition, these equations are necessary for the calculation of the surface species concentrations. They are solved simultaneously with the reactor mass balance equations for the responses, *i.e.*, piperidine and C_5. These equations are similar to the ones provided in Chapter 2.

7.3.1 Site balances and surface species

Surface species concentrations need to be determined for the calculation of the reaction rates of all elementary steps considered in the network. Adequate site balances are required in this respect. Given the particular character of sulphided NiMo catalysts impacting on the definition of the active sites, the elaboration of the corresponding balances is presented in more detail in Appendix B. As mentioned in Section 7.2.4, a two site assumption, *i.e.*, Coordinatively

Unsaturated Sites (*) and Sulphur Anion Sites (S^{2-}), similar to that proposed by Kasztelan and Guillaume [37] for toluene hydrogenation over unpromoted MoS_2/Al_2O_3 catalyst and by Romero et al. [36] for naphthalene hydrogenation over Ni promoted MoS_2/Al_2O_3 has been used.

The site balance for the S^{2-} is identical to the one proposed by Romero et al. [36] and is presented in Appendix B, however, the site balance for the * is slightly different because of the surface hydrocarbon species that have been considered, see Table 7-1. The chemisorption enthalpy for the C_5 hydrocarbons was not explicitly considered during the simulation of these data according to the Langmuir-Hinshelwood methodology used in Chapter 4. The more comprehensive character of the model discussed in the present chapter makes that it is included now. Additionally, the hydride (H^-) and the sulphydril (SH^-) species which are formed during the dissociative H_2 and H_2S chemisorption are also present on the * sites. Equation 7-8 shows the total site balance for the * site.

$$C_{t,*} = C_* + C_{*-P} + \sum_{i}^{19} C_{*-arom,i} + \sum_{i}^{3} C_{*-naph,i} + \sum_{i}^{10} C_{*-acyc,i} + C_{*-olef} + C_{*-PP} + C_{*-C5} + C_{*-NH_3} + C_{*-H^-} + C_{*-SH^-} \quad 7\text{-}8$$

7.3.2 Net production rates

The net production rate, R_n, for an intermediate *n* is calculated from equation 7-9. A total number of 33 intermediates are encountered during the generation of the SEMK network, out of which 19 are partially hydrogenated pyridine components while 14 are involved in the denitrogenation reactions. The rates of all the 70 reactions occurring between these intermediates need to be calculated.

$$R_n = \sum_{n_{react}=1}^{70} (\vec{r}_{n_{react},m\to n} - \overleftarrow{r}_{n_{react},n\to m}) \quad (n = 1 \dots 33) \quad 7\text{-}9$$

In Eq. 7-9, $\vec{r}_{m\to n}$ refers to the production rate of component *n* from *m* in the forward direction and $\overleftarrow{r}_{n\to m}$ the consumption rate of component *n* to *m* in the reverse direction.

$$\vec{r}_{n_{react},m\to n} = n_{e_{n_{react},m\to n}} \tilde{k}_{n_{react},m\to n}(i_1, i_2) C_{m-*} C_{H^- - *} \quad 7\text{-}10$$

With $\vec{r}_{n_{react},m\to n}$ the forward reaction rate of elementary reaction, e.g., hydrogenation of the component with a hydride, $n_{e_{n_{react},m\to n}}$ the number of single events for the forward reaction, n_{react}, and $\tilde{k}_{n_{react},m\to n}(i_1, i_2)$ the unique single-event rate coefficient for the reaction family with identifiers i_1 and i_2. The concentrations of the surface intermediates are determined by

the application of the pseudo-steady state approximation, *i.e.*, their net rate of formation is set equal to zero.

Because of the assumed quasi equilibration of the product chemisorption, the net production rate of the gas phase hydrogenation product is identical to the net production rate of the corresponding, chemisorbed one. For the calculation of the latter, all surface intermediate concentrations are required and are obtained by applying the above mentioned pseudo-steady state approximation.

As mentioned earlier in section 7.1, in order to calculate the net production rate of the chemisorbed products, *i.e.*, piperidine and C_5 hydrocarbon, the algebraic equations constructed for all the intermediates according to the pseudo steady-state hypothesis had to be solved simultaneously along with the reactor mass balance equations, see also Chapter 2. This results in a complex set of equations that needs to be solved by a capable and reliable numerical solver and requires good initial guesses for the surface concentrations.

Table 7-3. Overview of the elementary reactions and reaction families considered during SEMK modelling of pyridine hydrodenitrogenation over a commercial NiMo/γ-Al_2O_3 catalyst.

Reaction	Reaction step	Single-Event rate coefficient	Equilibrium coefficient
Aromatic nitrogen hydrogenation	$* - C_5H_5N + S^{2-} - H^+ \rightleftharpoons * - C_5H_5NH^+ + S^{2-}$	$\tilde{k}_{n,hyd}(i_1, i_2)$	$\tilde{K}_{n,hyd}(i_1, i_2)$
Aromatic carbon hydrogenation[*]	$* - C_5H_5NH^+ + * - H^- \rightleftharpoons * - C_5H_6NH + *$	$\tilde{k}_{c,hyd}(i_1, i_2)$	$\tilde{K}_{c,hyd}(i_1, i_2)$
Protonation of amines	$* - RNH_2 + S^{2-} - H^+ \rightleftharpoons * - RNH_3{}^+ + S^{2-}$	$\tilde{k}_{prot}(i_1, i_2)$	$\tilde{K}_{prot}(i_1, i_2)$
C-N bond scission via β-(H) elimination	$* - RNH_3{}^+ + * + S^{2-} \rightleftharpoons * - NH_3 + * - R^= + S^{2-} - H^+$	$\tilde{k}_{\beta-(H)elim}(i_1, i_2)$	$\tilde{K}_{\beta-(H)elim}(i_1, i_2)$
C-N bond scission via (SH^-) substitution	$* - RNH_3{}^+ + * - SH^- \rightleftharpoons * - NH_3 + * - RSH$	$\tilde{k}_{(-SH)sub}(i_1, i_2)$	$\tilde{K}_{(-SH)sub}(i_1, i_2)$
Formation of heavier species via pentylamine condensation	$* - RNH_3{}^+ + * - RNH_2 \rightleftharpoons * - NH_3 + * - RNH_2R^+$	$\tilde{k}_{PA,cond}(i_1, i_2)$	$\tilde{K}_{PA,cond}(i_1, i_2)$
Formation of heavier species via piperidine condensation	$* - RNH_3{}^+ + * - R_2NH \rightleftharpoons * - NH_3 + * - R_2NHR^+$	$\tilde{k}_{PP,dispro}(i_1, i_2)$	$\tilde{K}_{PP,dispro}(i_1, i_2)$
Acyclic (SH^-) direct hydrogenolysis[#]	$* - RSH + * - H^- \rightleftharpoons * - R + * - SH^-$	$\tilde{k}_{(-SH)hydrogenolysis}(i_1, i_2)$	$\tilde{K}_{(-SH)hydrogenolysis}(i_1, i_2)$
Alkene hydrogenation[#]	$* - R^= + * - H^- \rightleftharpoons * - R + * + S^{2-}$	$\tilde{k}_{alk\ hyd}(i_1, i_2)$	$\tilde{K}_{alk\ hyd}(i_1, i_2)$

[#] The subsequent proton addition from the S2- is considered to occur as a single step.

7.4 SEMK model assessment against gas phase data

7.4.1 Adjustable parameters

In addition to the rate coefficients related to the surface reactions discussed in Section 7.2.4, see Table 7-4, chemisorption coefficients for the hetero aromatic reactant pyridine, the hydrogenated intermediate product piperidine, completely denitrogenated final product C_5 along with the gas phase reactants hydrogen and hydrogen sulphide and gas phase product ammonia need to be accounted for. In total six chemisorption coefficients are required, see Table 7-4.

For the complete pyridine hydrodenitrogenation network, as explained in section 7.2.4 and presented in Table 7-2, nine reaction families are considered. Hence, the Single-Event Micro Kinetic model for the hydrodenitrogenation of pyridine employs 24 coefficients, *i.e.*,6 chemisorption equilibrium coefficients, 9 single-event rate coefficients for the forward reactions and 9 single-event equilibrium coefficients. The backward single-event rate coefficient can be calculated from the forward one and the corresponding single-event equilibrium coefficient as follows:

$$\tilde{k}_{c,hyd,reverse}(i_1, i_2) = \frac{\tilde{k}_{c,hyd,forward}(i_1, i_2)}{\tilde{K}_{c,hyd}(i_1, i_2)} \qquad 7\text{-}11$$

Accounting for the temperature dependence of each of these parameters doubles the number of adjustable parameters to 48. The accurate estimation of such a number of adjustable parameters from 148 experiments in which two responses were measured, *i.e.,* the outlet flow rate of piperdine and C_5, is quite challenging, not to say impossible. Hence, statistical thermodynamics and previously determined parameter values were used to reduce this number of adjustable parameters.

7.4.2 Model simulation and refinement

In order to present a proof of principle for the extension of the SEMK methodology towards hetero atom chemistry over sulphided catalysts, preliminary model simulations have been performed to acquire a better understanding of the model behaviour. The adjustable model parameters are fine-tuned during this part of the procedure, starting from literature reported values and guaranteeing an adequate physical meaning of the parameters. Such a procedure is important to find a suitable starting point for the model regression which will be the future step in the model validation. In the following subsections all the parameters are discussed in detail

along with the relevant references and an attempt is made to address any potential discrepancies in the parameter values.

7.4.2.1 Chemisorption coefficients

In Chapter 4, chemisorption entropies and enthalpies for NH_3, piperidine, H_2 and H_2S were calculated or estimated. These values were used without further modifications in the present chapter. A similar strategy *i.e.*, considering a minimum and maximum loss of translation entropy, for pyridine and C_5 was adopted. The assessment of the gas phase entropy of the components was done using the equation as derived by Sackur and Tetrode, see Eq. 7-12. Accordingly, values of the chemisorption entropies and enthalpies that resulted in the best simulation are reported Table 7-4.

$$S^{o}_{trans} = Rln\left(\frac{RT}{P^{0}N_A}\left(\frac{2\pi\left({M_W}/{N_A}\right)k_BT}{h^2}\right)^{3/2}\right) + \frac{5}{2}R \qquad 7\text{-}12$$

Table 7-4. Parameter values for the chemisorption coefficients in the SEMK modeling of pyridine hydrodenitrogenation.

Chemisorption	Equilibrium coefficient	Chemisorption entropy (J mol K^{-1})	Chemisorption enthalpy (kJ.mol^{-1})
Pyridine	$K_{P,*}$	-162	-115.0
Piperidine	$K_{PP,*}$	-158*	-117.0
C_5	$K_{C5,*}$	-98	-40.0
NH_3	$K_{NH3,*}$	-98*	-76.0
H_2	$K_{H2,*,S^{2-}}$	-187*	-104.0
H_2S	$K_{H2S,*,S^{2-}}$	-190*	-129.0

*Values obtained from chapter 4

The C_5 chemisorption enthalpy is expected to be less negative than that of the basic components namely ammonia, pyridine and piperidine. A range between -50 and -40 kJ mol^{-1} is chosen as the initial guess. The temperature dependence of the pyridine chemisorption enthalpy could not be estimated making use of Langmuir-Hinshelwood kinetics, see Chapter 4. It is expected in the present chapter that a well-defined model will be able to better accommodate the observed experimental variations. Hence, the pyridine chemisorption enthalpy is also accounted for during the modelling procedure. It has been well established in our previous work that the basicity of the these nitrogen compounds can be correlated to their chemisorption coefficient. Following the guidelines proposed by LaVopa and Satterfield [38], a slightly higher pyridine chemisorption enthalpy compared to that of piperidine is assumed, see Table 7-4.

7.4.2.2 Rate coefficients

Proposed ranges for the pre-exponential factor of the single-event rate coefficients, surface reaction equilibrium coefficients have been determined based on transition state theory and statistical thermodynamics, as described by Dumesic et al. [39] and used by Bera et al. [21]. A value in the range of 10^8 to 10^{16} s^{-1} is calculated for the pre-exponential factor of the surface reaction rate coefficient by assuming the chemisorbed reactants and the corresponding transition state as either fully mobile and/or completely immobile. A value in the range of 10^{-5} and 1 is proposed for the surface reaction equilibrium coefficients. The 9 single-event rate coefficients used during the model simulation are listed in Table 7-5. Based on the mobility of the surface species involved the pre-exponential factors for the surface reactions are proposed and kept fixed during regression, see Table 7-5 for the corresponding values.

The initiation of the ring saturation proceeds through hydrogenation of the nitrogen within the ring, *i.e.*,a surface proton species reacts with the chemisorbed pyridine. The end-on chemisorption as proposed by Sun et al. [40] will assist the relatively stronger binding of the pyridine molecule on the surface thereby reducing its mobility. The subsequent ring saturation steps proceed with the alternating addition of H^- and H^+ to the unsaturated carbon atoms. Consecutive additions of a H^+ and a H^- are necessary in order to balance the pyridine charge, in accordance with the reaction mechanism discussed in Chapter 4. Ranges for pre-exponential values for the rate coefficients are proposed by Dumesic et al. [39] by considering different scenarios for the surface mobility of the species involved as reactants and in the transition state. An intermediate value of 10^{14} s^{-1} has been adopted corresponding with a slight gain in mobility of the transition state species compared to the reactants. Identical considerations are made for hydrogenation at the nitrogen and the carbon atom in the ring. The initial guess for the hydrogenation activation energies are made in the range of 60-65 kJ mol^{-1}. These values are in agreement with those proposed by Thybaut et al. [41] and Bera et al. [21] for aromatics hydrogenation over metal catalysts. The hydrogenation of the aromatic nitrogen atom in the first step may proceed with a slightly lower activation energy compared to the subsequent hydrogenation of the carbon atoms, since the free electron pair on the aromatic-nitrogen is readily available for the H^+ addition.

As discussed in Chapter 6, protonation of the amine function is an important elementary step in nitrogen removal from an acyclic, aromatic or cyclic hydrocarbon component. The protonation of the amine function results in a quaternised amine species which is a necessary step for the removal of the amine species through substitution and/or elimination reactions. No activation energy for amine protonation, β-(H) elimination or SH^- substitution reaction is

available in the literature over sulphided catalysts. Inspiration for initial guesses, or at least, for the relative order in the initial guesses, has been obtained from parameter values as reported by Quintana-Solorzano [42] for catalytic cracking, e.g., a protonation is regarded as a facile reaction requiring a limited activation energy only, while a β-scission is way more demanding. Quintana-Solorzano [42] proposed a protonation activation energy between 94 and 114 kJ mol-^{1}, and an activation energy between 160 and 243 kJ mol^{-1} for β-scission depending on the type of carbenium ion involved. Identical values have been adopted in the present work as a first approximation. The initial guess for the SH^- substitution activation energy is assumed identical to that of the protonation reaction.

In Chapter 5 activation energies for the condensation and disproportionation reaction occurring during liquid phase hydrodenitrogenation were estimated [43]. The activation energies for these specific reactions were also in agreement with those published by Sonnemans et al. [44] for an unpromoted MoO_3 catalyst. The reaction occurs between two surface piperidine species or between a piperidine species and a pentylamine species. An initial guess value for this activation energy amounting to 100 kJ mol^{-1} , which is in line with the previously estimated parameter values, see Chapter 5, was used.

The activation energy for the sulphydril assisted denitrogenation was estimated at gas phase conditions, see Chapter 4, and amounted to 185 kJ mol^{-1}. The same value was used for the SH^- hydrogenolysis activation energy.

The double bond hydrogenation is a reaction encountered during the saturation of the C_5 alkene produced during the reaction of pentyl amine through elimination. The pentene selectivity at the operating conditions used was very low in comparison to pentane, *i.e.*,below 5%. The kinetic relevance of this reaction family at the operating conditions used is, hence, only minimal. In agreement with the conclusions reached by Thybaut et al [41] the activation energy for hydrogen addition to an olefinic carbon atom is taken identical to that of hydrogen additions to an aromatic carbon atom.

The above discussed initial guesses are inspired by earlier work and data available from the literature [19, 42, 43, 45]. While it is believed that these initial guesses would suffice to reach a decent agreement between model simulations and experimental observations, subtle differences in the parameter values may still enhance the model performance. As a result, rather than a full fledge regression, some manual fine tuning of these initial guesses has been performed in order to achieve an even better agreement between the model simulation and experimental results. Accordingly, the parameter values that resulted in the best model simulations are reported in Table 7-5.

Table 7-5. Parameter values used for the rate coefficients and the reaction equilibrium coefficients during the simulation of the SEMK model for pyridine hydrodenitrogenation.

Rate coefficient	Pre-exponential factor (s^{-1})	Activation energy ($kJ.mol^{-1}$)
$\tilde{k}_{n,hyd}(i_1, i_2)$	1 x10^{14}	61.3
$\tilde{k}_{c,hyd}(i_1, i_2)$	1 x10^{14}	64.0
$\tilde{k}_{prot}(i_1, i_2)$	1 x10^{16}	94.8
$\tilde{k}_{\beta-(H)elim}(i_1, i_2)$	1 x10^{16}	132.0
$\tilde{k}_{(-SH)sub}(i_1, i_2)$	1 x10^{16}	92.3
$\tilde{k}_{PA\ cond}(i_1, i_2)$	1 x10^{16}	88.5
$\tilde{k}_{PP,cond}(i_1, i_2)$	1 x10^{16}	88.5
$\tilde{k}_{(-SH)hydrogenolysis}(i_1, i_2)$	1 x10^{13}	157.3
$(\tilde{k}_{alk\ hyd} i_1, i_2)$	1 x10^{13}	52.9

7.5 Model performance and evaluation

Figure 7-2 shows the space time effect on the overall pyridine conversion and the product yields is shown. Increasing space times and, hence, pyridine conversions, resulted in an enhanced C_5 yield while that of piperidine correspondingly decreased. As mentioned in Chapter 4, these results are in agreement with the primary nature of the latter and the secondary one of the former. The simulations nicely follow the trend exhibited by the experimental observations, albeit a bit less pronounced.

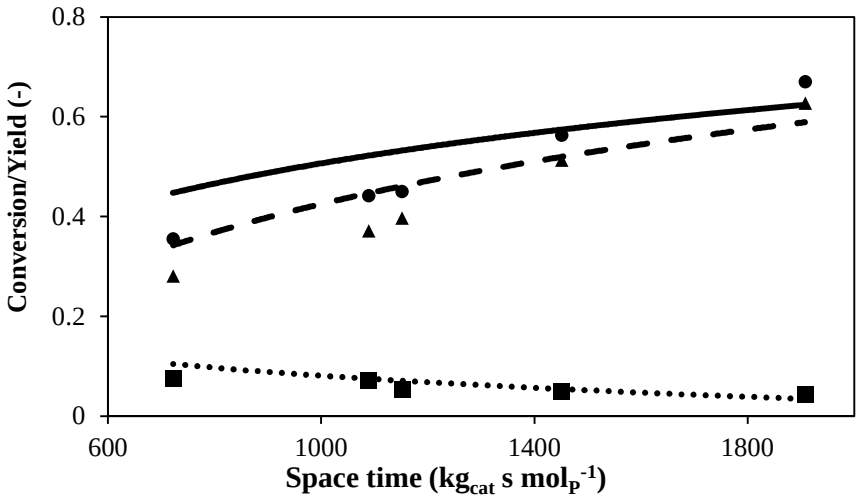

Figure 7-2. Pyridine conversion and product yields as a function of the space time. Operating conditions: T = 599 K, p = 3.0 MPa, H_2/Pyridine (mol mol^{-1}) = 500, H_2S/Pyridine(mol mol^{-1}) = 7.5. Symbols: ● pyridine conversion; ■ yield-piperidine; ▲yield-C5. Lines: --- pyridine conversion; … yield-piperidine; - - - yield-C_5 model simulated values obtained by solving reactor model equations provided in chapter 2 and rate of production of piperidine and C_5 hydrocarbons from equation 7-9 corresponding to an SEMK model over an industrial NiMo/ γ-Al_2O_3 catalyst, along with the set of parameter values of kinetic and catalyst descriptors reported in Tables 7-4 and 7-5.

The temperature effect is shown in Figure 7-3. As could be expected, a higher pyridine conversion was observed at higher temperatures, see also chapter 4. Similarly to the space time effect discussed above, the C_5 yield increases with temperature and a slight decrease is obtained for the piperidine yield. The model is able to reproduce these trends. Particularly, the increase in the conversion and the C_5 yield are simulated to be slightly more pronounced compared to what was observed experimentally.

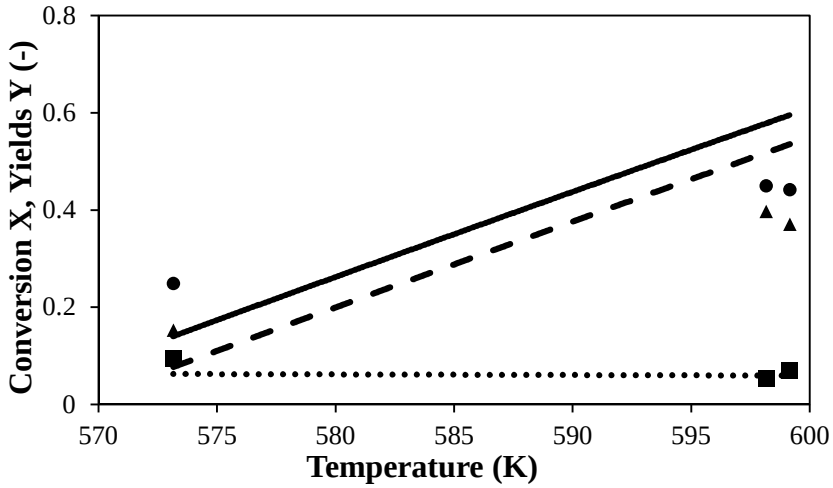

Figure 7-3. Pyridine conversion and product yields as a function of the temperature. Operating conditions: p_t = 3.0 MPa, W_{cat}/F_p = 1100 kg_{cat} s mol^{-1}, H_2S/Pyridine (mol mol^{-1}) = 7.5, H_2/Pyridine(mol mol^{-1}) = 500. Symbols: ● pyridine conversion; ■ yield-piperidine; ▲yield-C5. Lines: --- pyridine conversion; … yield-piperidine; - - - yield-C_5 model simulated values obtained by solving reactor model equations provided in chapter 2 and rate of production of piperidine and C_5 hydrocarbons from equation 7-9 corresponding to an SEMK model over an industrial NiMo/γ-Al_2O_3 catalyst, along with the set of parameter values of kinetic and catalyst descriptors reported in Tables 7-4 and 7-5.

The evolution of the species surface coverages on the coordinatively unsaturated sites (*) as a function of the space time has been visualised in Figure 7-4. These surface coverages provide strategic insight in which, at least according to the SEMK model simulations, are the most relevant species on the surface and, hence, allows acquiring unprecedented insight in the reaction mechanism. Moreover, these surface coverages constitute the basis for a critical analysis of the physical significance of the proposed mechanism, *i.e.*,does this mechanism, together with the employed model parameter values form an adequate, physical representation of the experimental observations?

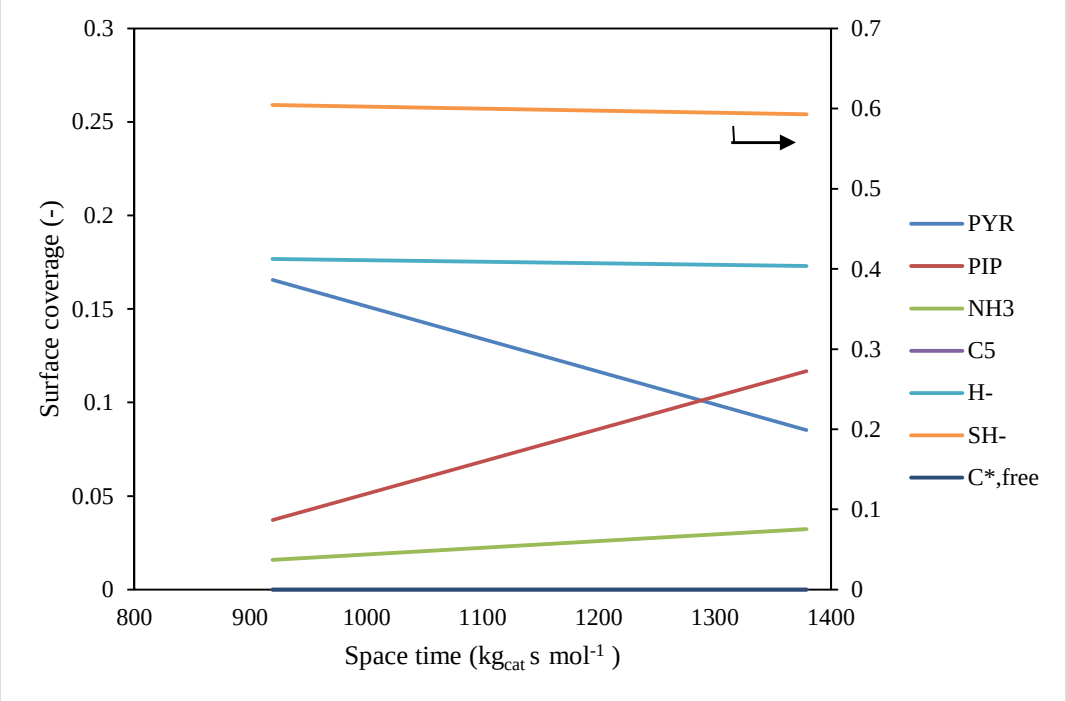

Figure 7-4. Simulated surface coverage at the * site as a function of space time. Operating conditions: T = 573 K, p_t = 4.0 MPa, H_2/Pyridine (mol mol^{-1}) = 500, H_2S/Pyridine (mol mol^{-1}) = 15. Model simulated values are obtained by solving reactor model equations provided in chapter 2 and rate of production of piperidine and C_5 hydrocarbons from equation 7-9 corresponding to an SEMK model over an industrial NiMo/γ-Al_2O_3 catalyst, along with the set of parameter values of kinetic and catalyst descriptors reported in Tables 7-4 and 7-5.

At typical operating conditions used, only a negligible amount of free coordinatively unsaturated sites were observed. About 60 % of these sites were occupied by the SH^- species, which is in line with the values obtained with the Langmuir-Hinshelwood model, see Chapter 4. Such a high surface coverage of SH^- species is due to the rather high inlet molar H_2S/Pyridine ratio *i.e.*,7.5 mol mol^{-1} and a pronounced H_2S chemisorption as evident from the highly negative chemisorption enthalpy of the H_2S, see below. The presence of SH^- species as most abundant surface species promotes the denitrogenation reaction via the sulphur assisted pathway Surface H^- species are also important for both the aromatic and the olefin hydrogenation reactions. About 20 % of the surface is covered by these species. This is result of the very high molar inlet H_2/Pyridine ratios amounting to 500 mol mol^{-1} which is maintained during the experimentation combined with the H_2 chemisorption coefficient being comparatively lower than that of H_2S, *i.e.*,0.02 MPa^{-1} versus the 2.1 MPa^{-1}.

The 50% decrease in the pyridine surface coverage with increasing space time stems from the conversion effect. Correspondingly, particularly the piperidine and the NH_3 products surface coverage increase with the hydrodenitrogenation conversion.

The sulphur anion sites (S^{2-}) are covered for 70 % by H^+ species. This is a result of the heterolytically chemisorbing H_2 and H_2S on the catalyst surface. Such high values of the H^+ coverages stem from the high molar inlet H_2/Pyridine and H_2S/Pyridine ratios i.e. 500 and 7.5 mol mol^{-1} respectively and are necessary for the hydrogenation and protonation reactions to occur at a sufficiently high rate.

Overall, the SEMK model developed for pyridine hydrodenitrogenation over an industrial sulphided catalyst resulted in a complex model that was mathematically challenging to solve. The model was able to capture the effects of the experimental variables over the pyridine conversion and the product selectivity. The number of adjustable parameters in the SEMK model can be further reduced by introducing lumps of similar components rather than defining reaction families for a particular species. This can potentially results in a 'less-complex' mathematical model but can inherently account for the level of detail required to represent all the reactions.

7.6 Conclusions and future work

Single-Event MicroKinetic model simulations have been performed for pyridine hydrodenitrogenation in a CSTR over a NiMo/γ-Al_2O_3 catalyst. A total of 33 intermediates and the corresponding 70 elementary reactions occurring between these intermediates were considered during the SEMK model construction. Kinetic descriptors available from literature were used along with previously determined catalyst descriptors *i.e.*, based on LHHW kinetics, see chapter 4 and 5. After some minor fine tuning of the model parameters, simulations allowed reproducing experimentally observed conversion and yields trends as a function of the space time and the temperature. 60% of the coordinatively unsaturated sites was found to be covered by SH^- species, which is required for promoting the actual C-N bond scission in the hydrodenitrogenation reaction via the sulphydril assisted pathway.

The present simulations constitute a proof of concept for the SEMK methodology extension to hetero atom containing components. While a comprehensive SEMK model was constructed based on elementary chemistry rules and theoretical understanding of the reaction, the number of parameters in the model remained on the high side. It results in sets of model equations which are mathematically quite challenging to solve. Further reducing the number

of adjustable parameters, e.g., by including more elementary steps in a single reaction family potentially allows addressing this issue. The desired level of detail in the SEMK model should be preserved, however. The present SEMK model can also easily be extended to multi ring hetero components containing nitrogen, since the corresponding reaction mechanism can be expressed in terms of the same reaction families.

7.7 References

1. Pille, R., *Sleutelcomponenten bij de hydrodenitrogenering en hydrodesulfurisering van aardoliefracties*. 1997, Universiteit Gent.

2. Pille, R. and G.F. Froment, **Hydrotreatment and Hydrocracking of Oil Fractions**, 1997. 106: p. 403-413.

3. Froment, G.F., **Catalysis Today**, 1999. 52(2-3): p. 153-163.

4. Martens, G.G. and G.B. Marin, **AIChE Journal**, 2001. 47(7): p. 1607-1622.

5. Dewachtere, N.V., F. Santaella, and G.F. Froment, **Chemical Engineering Science**, 1999. 54(15-16): p. 3653-3660.

6. Martens, G.G., G.B. Marin, J.A. Martens, P.A. Jacobs, and G.V. Baroni, **Journal of Catalysis**, 2000. 195(2): p. 253-267.

7. Froment, G.F., **Chemical Engineering Science**, 1992. 47(9-11): p. 2163-2177.

8. Clymans, P.J. and G.F. Froment, **Computers & Chemical Engineering**, 1984. 8(2): p. 137-142.

9. Froment, G.F., **Chemical Engineering Science**, 1981. 36(8): p. 1271-1282.

10. Lozano-Blanco, G., J.W. Thybaut, K. Surla, P. Galtier, and G.B. Marin, **AIChE Journal**, 2009. 55(8): p. 2159-2170.

11. Lozano-Blanco, G., J.W. Thybaut, K. Surla, P. Galtier, and G.B. Marin, **Industrial & Engineering Chemistry Research**, 2008. 47(16): p. 5879-5891.

12. Lozano-Blanco, G., K. Surla, J.W. Thybaut, and G.B. Marin, **Oil & Gas Science and Technology-Revue D Ifp Energies Nouvelles**, 2011. 66(3): p. 423-435.

13. Lozano-Blanco, G., J.W. Thybaut, K. Surla, P. Galtier, and G.B. Marin, **Oil & Gas Science and Technology-Revue D Ifp Energies Nouvelles**, 2006. 61(4): p. 489-496.

14. Clymans, P.J., G.F. Froment, M. Berthelin, and P. Trambouze, **AIChE Journal**, 1984. 30(6): p. 904-915.

15. Froment, G.F., B.O. Vandesteene, P.S. Vandamme, S. Narayanan, and A.G. Goossens, **Industrial & Engineering Chemistry Process Design and Development**, 1976. 15(4): p. 495-504.

16. Toch, K., J.W. Thybaut, B.D. Vandegehuchte, C.S.L. Narasimhan, L. Domokos, and G.B. Marin, **Applied Catalysis A: General**, 2012. 425: p. 130-144.

17. Kumar, P., J.W. Thybaut, S. Teketel, S. Svelle, P. Beato, U. Olsbye, and G.B. Marin, **Catalysis Today**, 2013. 215: p. 224-232.

18. Kumar, P., J.W. Thybaut, S. Svelle, U. Olsbye, and G.B. Marin, **Industrial & Engineering Chemistry Research**, 2013. 52(4): p. 1491-1507.

19. Bera, T., J.W. Thybaut, and G.B. Marin, **ACS Catalysis**, 2012. 2(7): p. 1305-1318.

20. Choudhury, I.R., K. Hayasaka, J.W. Thybaut, C.S.L. Narasimhan, J.F. Denayer, J.A. Martens, and G.B. Marin, **Journal of Catalysis**, 2012. 290: p. 165-176.

21. Bera, T., J.W. Thybaut, and G.B. Marin, **Industrial & Engineering Chemistry Research**, 2011. 50(23): p. 12933-12945.

22. Narasimhan, C.S.L., J.W. Thybaut, J.A. Martens, P.A. Jacobs, J.F. Denayer, and G.B. Marin, **Journal of Physical Chemistry B**, 2006. 110(13): p. 6750-6758.

23. Thybaut, J.W., C.S.L. Narasimhan, and G.B. Marin, **Catalysis Today**, 2006. 111(1-2): p. 94-102.

24. Thybaut, J.W., *Production of low-aromate fuels: kinetics and industrial application of hydrocracking*. 2003, Universiteit Gent.

25. Martens, G.G., J.W. Thybaut, and G.B. Marin, **Industrial & Engineering Chemistry Research**, 2001. 40(8): p. 1832-1844.

26. Bera, T., *Hydrogenation of aromatics: single-event microkinetic (SEMK) methodology and scale-up*, in *Laboratory for Chemical Technology*. 2012, Ghent University: Ghent.

27. Thybaut, J.W. and G.B. Marin, **Journal of Catalysis**, 2013. 308: p. 352-362.

28. Vandegehuchte, B.D., J.W. Thybaut, C. Detavernier, D. Deduytsche, J. Dendooven, J.A. Martens, S.P. Sree, T.I. Koranyi, and G.B. Marin, **Journal of Catalysis**, 2014. 311: p. 433-446.

29. Eyring, H., **The Journal of Chemical Physics**, 1935. 3(2): p. 107-115.

30. Evans, M.G. and M. Polanyi, **Transactions of the Faraday Society**, 1935. 31(0): p. 875-894.

31. Laidler, K.J. and M.C. King, **The Journal of Physical Chemistry**, 1983. 87(15): p. 2657-2664.

32. Truhlar, D.G., W.L. Hase, and J.T. Hynes, **The Journal of Physical Chemistry**, 1983. 87(15): p. 2664-2682.

33. Wynne-Jones, W.F.K. and H. Eyring, **The Journal of Chemical Physics**, 1935. 3(8): p. 492-502.

34. Narasimhan, C.S.L., J.W. Thybaut, G.B. Marin, J.F. Denayer, G.V. Baron, J.A. Martens, and P.A. Jacobs, **Chemical Engineering Science**, 2004. 59(22-23): p. 4765-4772.

35. Narasimhan, C.S.L., J.W. Thybaut, G.B. Marin, P.A. Jacobs, J.A. Martens, J.F. Denayer, and G.V. Baron, **Journal of Catalysis**, 2003. 220(2): p. 399-413.

36. Romero, C.M.C., J.W. Thybaut, and G.B. Marin, **Catalysis Today**, 2008. 130(1): p. 231-242.

37. Kasztelan, S. and D. Guillaume, **Industrial & Engineering Chemistry Research**, 1994. 33(2): p. 203-210.

38. LaVopa, V. and C.N. Satterfield, **Journal of Catalysis**, 1988. 110(2): p. 375-387.

39. Dumesic, D.A., D.F. Rudd, L.M. Aparicio, J.E. Kekoske, and A.A. Trevino, *The microkinetics of heterogeneous catalysis*. 1993, American Chemical Society: Washington, DC.

40. Sun, M.Y., A.E. Nelson, and J. Adjaye, **Journal of Catalysis**, 2005. 231(1): p. 223-231.

41. Thybaut, J.W., M. Saeys, and G.B. Marin, **Chemical Engineering Journal**, 2002. 90(1-2): p. 117-129.

42. Quintana-Solorzano, R., J.W. Thybaut, and G.B. Marin, **Chemical Engineering Science**, 2007. 62(18-20): p. 5033-5038.

43. Raghuveer, C.S., J.W. Thybaut, R. De Bruycker, K. Metaxas, T. Bera, and G.B. Marin, **Fuel**, 2014. 125(0): p. 206-218.

44. Sonnemans, J. and P. Mars, **Journal of Catalysis**, 1974. 34(2): p. 215-229.

45. Saeys, M., J.W. Thybaut, M. Neurock, and G.B. Marin, **Molecular Physics**, 2004. 102(3): p. 267-272.

8 Conclusions and future work

Hydrodenitrogenation remains one of the most important processes in crude oil refining. Environmental concerns and governmental regulations are pushing engineers and technology developers to come up with better techniques and catalysts for the removal of harmful sulphur and nitrogen compounds. Apart from the main theme of this thesis, which was the investigation of various *reaction* aspects of pyridine hydrodenitrogenation, also the performance of a commercial three-phase bench-scale Robinson-Mahoney *reactor* was studied in great detail.

The Robinson-Mahoney three-phase reactor set-up was identified as a powerful tool for kinetic analysis and catalyst testing of hydrotreating reactions. The volumetric gas-liquid mass transfer coefficient, k_La, and gas and liquid phase hold-up, $\varepsilon_G/\varepsilon_L$ in the reactor were experimentally investigated at industrially relevant conditions and were found to be qualitatively in line with the results obtained with a H_2 - gas-oil/water mixture at room temperature and atmospheric pressures. The k_La, was observed to depend on the agitator rotation speed, $N_{agitator}$, according to $k_La = 2.29\ 10^{-8} * N_{agitator}{}^{4.03} + 1.24\ 10^{-2}$, which was proven to be sufficiently high to have a negligible impact of mass transfer effects on the chemical kinetics. Experimental investigations to assess the liquid hold-up at both industrially relevant and ambient conditions using step and an impulse input of a tracer, respectively, were performed. While a minimal effect on the ε_L was observed with varying temperature and pressure, volumetric inlet gas-liquid ratio exerted a considerable decrease in the ε_L. The ε_L varied between 1 and 0.5 at volumetric inlet gas-liquid ratios of 5 and 250 $m^3\ m^{-3}$ with a H_2-Halpasol™ mixture at industrially relevant conditions, 0 and 580 $m^3\ m^{-3}$ with H_2-water mixture at ambient conditions. The reactor consisted of a continuous liquid phase while the gas phase was dispersed one.

In agreement with the previously acquired gas phase data, it was found that pyridine hydrodenitrogenation occurs as a two-step reaction over an industrial NiMo/γ-Al_2O_3 catalyst. The first step is the hydrogenation of the aromatic ring to form piperidine which subsequently undergoes denitrogenation to release ammonia and yield C_5 hydrocarbons. Heterolytically

chemisorbing H_2 and H_2S are sources for proton, hydride and sulphydril species which are participating in the occurring surface reactions. Rival models were constructed by assuming different rate-determining steps for hydrogenation and denitrogenation. A stepwise hydrogenation with proton addition first to the basic N atom and the third hydrogen addition being rate determining was found to best describe the experimental data. Due to the high H_2S/pyridine molar inlet ratios used, nitrogen was predominantly eliminated *via* a H_2S enhanced substitution mechanism. An a priori calculation of the chemisorption entropies allowed a significant estimation of all remaining model parameters, except for the pyridine chemisorption enthalpy. The C-N bond scission was observed to have a more pronounced temperature dependence than the hydrogenation. A higher activation energy was quantified for the former in comparison to the latter, *i.e.*, 185 versus 41 kJ mol^{-1}.

The gas to liquid phase kinetics methodology previously developed for hydrocracking and hydrogenation reactions was successfully extended to hydrodenitrogenation. As part of a systematic approach, gas phase data were used for the kinetic model construction and determination of the corresponding model parameters. This model was, subsequently, applied in the assessment of a limited set of liquid phase data by accounting for the thermodynamic non-ideality, solvent adsorption and the potential occurrence of additional reactions due to the high density at liquid phase conditions. The lower H_2S partial pressures and corresponding surface coverages at liquid phase conditions resulted in reduced denitrogenation rates leading to alternative bimolecular reactions between nitrogen surface species. As a consequence *n*-pentylpiperidine formation was observed at liquid phase conditions. Based on model discrimination between two rival models it was found that *n*-pentylpiperidine was formed via a condensation between piperidine and its ring opening product, pentylamine, rather than via disproportionation. The validity of the methodology was evident from the negligible *n*-pentylpiperidine yields simulated at gas phase conditions.

Finally, a proof of concept for the extension of the Single-Event MicroKinetic methodology for hetero atom containing components has been presented. Nine reaction families for hydrodenitrogenation, i.e., aromatic nitrogen hydrogenation, aromatic carbon hydrogenation, amine protonation, C-N bond scission via β-(H) elimination, C-N bond scission via (SH^-) substitution, formation of heavier species via pentylamine condensation, formation of heavier species via piperidine condensation, acyclic (SH^-) direct hydrogenolysis and alkene hydrogenation, have been incorporated in the in-house reaction network generation program 'ReNGeP'. The pyridine hydrodenitrogenation reaction network comprises 33 intermediates involved in a total number of 70 reactions. SEMK model simulation indicated the capability of

the methodology to reproduce conversion and selectivity trends as a function of the space time and the temperature. Further fine tuning of the model aiming at a reduction of the number of parameters, while preserving the model's level of detail, should enhance its performance.

The work discussed in this thesis lays a strong foundation for the extension of the knowledge towards other research projects. Some recommendations for future work are summarised below.

- The experiments conducted with realistic feedstocks at industrially relevant conditions give a good estimation of the liquid hold-up within the reactor. The liquid components had very low vapour pressures at the investigated operating conditions and, hence, their presence in the vapour phase could be considered negligible. It would be interesting to investigate the reactor behaviour with liquids exhibiting high vapour pressures, such that their composition as a function of the liquid hold-up can be assessed. Experiments at industrially relevant conditions with the same liquid phase, i.e., Halpasol™ but with a lighter tracer such as pentane or hexane could be performed to assess the latter mentioned effect.
- Construction of gas phase models based on elementary reaction steps have provided insights in reactions and kinetics. Further extension of these models to liquid phase conditions have provided a robust, yet convenient methodology towards using thermodynamics in kinetics. While an example for the extension of the methodology towards to sulphided catalysts from acid catalyst was provided in this work, the components used remained non-polar hydrocarbons in both cases. This methodology could be extended to polar components which are of interest to a lot of chemical and process industries. Significant challenges with respect to the choice of the equation of state and the actual implementation of the model will have to be overcome in order to prove the methodology.
- The SEMK methodology aims at reduction in the model complexity by using reaction families and, hence, lesser model parameters. While it was done with reasonable accuracy for the case of pyridine hydrodenitrogenation, the model was rather complex owing to a high number of reaction families. This however could be advantageous when different types of nitrogen compounds are being processed simultaneously. It would be interesting to assess the applicability of the already proposed model for a components having multi rings and nitrogen as the hetero atom.

This page intentionally left blank

Appendix A

Calibration factors and GC layout.

A.1 Calibration factors of components used during the liquid phase pyridine hydrodenitrogenation experiments

Component	$CF_{i,FID}$
Pentane	0.89
Pentene	0.89
Pyridine	1.06
Piperidine	1.33
n-Pentylpiperidine	1.33
n-C_9	1
n-C_{10}	1.04
n-C_{11}	1.04
n-C_{12}	1.04
n-C_{13}	1.04
n-C_{14}	1.04

A.2 GC-layout

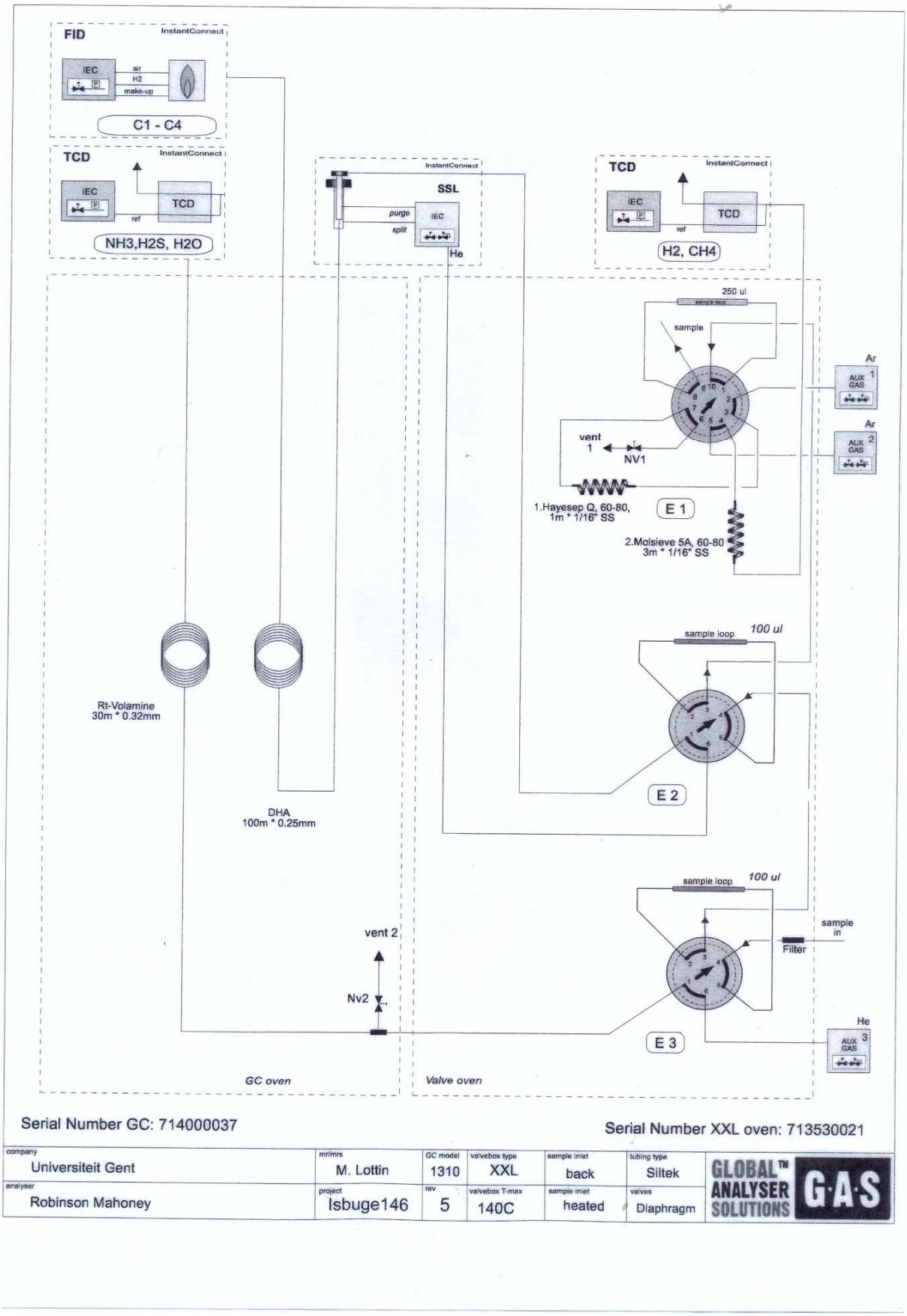
FID
InstantConnect
IEC
air
H2
make-up
C1 - C4
TCD
InstantConnect
IEC
TCD
ref
NH3,H2S, H2O
InstantConnect
SSL
purge
split
IEC
He
TCD
InstantConnect
IEC
TCD
ref
H2, CH4
250 ul
sample loop
sample
Ar
AUX GAS 1
Ar
AUX GAS 2
vent 1
NV1
1.Hayesep Q, 60-80, 1m * 1/16" SS
E 1
2.Molsieve 5A, 60-80 3m * 1/16" SS
sample loop
100 ul
E 2
Rt-Volamine 30m * 0.32mm
DHA 100m * 0.25mm
sample loop
100 ul
sample in
Filter
vent 2
Nv2
He
AUX GAS 3
E 3
GC oven
Valve oven
Serial Number GC: 714000037
Serial Number XXL oven: 713530021
company
Universiteit Gent
mr/mrs
M. Lottin
GC model
1310
valvebox type
XXL
sample inlet
back
tubing type
Siltek
analyser
Robinson Mahoney
project
Isbuge146
rev
5
valvebox T-max
140C
sample inlet
heated
valves
Diaphragm
GLOBAL™ ANALYSER SOLUTIONS
G·A·S

Appendix B

Site balance on sulphided catalysts

B.1. Site balances on promoted sulphided catalysts

The site balances used during the modelling performed in chapters 4, 5 and 7 are based on the available literature of sulphided catalysts by Kasztelan and Guillaume [1] for studying toluene hydrogenation over a unpromoted MoS_2/Al_2O_3 catalyst and by Romero et al. [2] for naphthalene hydrogenation over Ni promoted MoS_2/Al_2O_3.

The promoted MoS_2/Al_2O_3 which are assumed to have two sites, i.e., Coordinatively unsaturated sites (*) and the Sulphur Anion (S^{2-}). The hydrocarbon species are assumed to chemisorb on the * sites, which can be related to the corresponding chemisorption equilibria. The hydrocarbon intermediates that are formed during the reaction are also present on the *. Additionally, the hydride (H^-) and the sulphydril (SH^-) species which are formed during the dissociative H_2 and H_2S chemisorption are also present on the * sites. Equation 1 shows the total site balance for the * site.

$$C_{t,*} = C_* + \sum_i^n Reactants_i + \sum_i^m Intermediates_i + \sum_i^o Products_i + \sum Solvent^{\#} + C_{*-H^-} + C_{*-SH^-} \quad (1)$$

\# Used for liquid phase reactions

Similar to the * sites a site balance S^{2-} needs to be made, see equation 2. These sites are occupied only by the surface proton species that are produced due to the dissociative chemisorption of the H_2 and H_2S.

$$C_{t,S^{2-}} = C_{S^{2-}} + C_{S^{2-}-H^+} \quad (2)$$

According to assumptions proposed Romero et al. [2], the most favourable interactions occur between the reactant and products with the catalyst surface rather than between the

reaction intermediates and the catalyst surface. This assumption allows simplifying equation 1 into 3.

$$C_{t,*} = C_* + \sum_i^n Reactants + \sum_i^o Products + C_{*-H^-} + C_{*-SH^-} \quad 3$$

In order to determine the surface concentrations of the species involved in terms of the component partial pressures, the Langmuir hypothesis is used. Accordingly, the reactant i.e., pyridine (P), H_2 and H_2S and product i.e., piperidine (PP), pentane (PA) and ammonia (NH_3) species surface concentrations can be expressed in terms of the chemisorption equilibrium coefficient, partial pressures and the free * sites, see equations 4 to 6.

$$C_{*-P} = K_P\, p_P\, C_* \quad 4$$

$$C_{*-H^-} = K_{H_2}\, p_{H_2}\, C_* \frac{C_{S^{2-}}}{C_{S^{2-}-H^+}} \quad 5$$

$$C_{*-SH^-} = K_{H_2S}\, p_{H_2S}\, C_* \frac{C_{SA}}{C_{S^{2-}-H^+}} \quad 6$$

The site balance presented in equation 3 can be written in terms of chemisorption coefficients and partial pressures as shown in 7.

$$C_{t,*} = C_* \left(1 + K_P\, p_P + K_{PP}\, p_{PP} + K_{PA}\, p_{PA} + K_{NH_3}\, p_{NH_3} + \left(K_{H_2}\, p_{H_2} + K_{H_2S}\, p_{H_2S}\right)\frac{C_{S^{2-}}}{C_{S^{2-}-H^+}}\right) \quad 7$$

This summation can be noted in short when grouping the species adsorbing on the * sites only and the species adsorbing on both the * and the S^{2-} sites as shown in equations 8 and 9.

$$\delta = 1 + K_P\, p_P + K_{PP}\, p_{PP} + K_{PA}\, p_{PA} + K_{NH_3}\, p_{NH_3} \quad 8$$

$$\mu = K_{H_2}\, p_{H_2} + K_{H_2S}\, p_{H_2S} \quad 9$$

Equation 10 shows a modified form of equation 7.

$$C_{t,*} = C_* \left(\delta + \mu \frac{C_{S^{2-}}}{C_{S^{2-}-H^+}}\right) \quad 10$$

In order to express $\frac{C_{S^{2-}}}{C_{S^{2-}-H^+}}$ in terms of known concentrations, it is assumed that the total concentration of * sites equals that of the S^{2-}, see equation 11. This is valid for the sulphided NiMo catalysts since the saturation of one site would lead to the suppression of the H_2 and H_2S chemisorption.

$$C_{t,*} = C_{t,S^{2-}} \quad 11$$

A direct relationship for the proton surface concentration on the S^{2-} can be established based on the chemisorption stoichiometry of H_2S dissociation.

$$C_{S^{2-}-H^+} = C_{*-H^-} + C_{*-SH^-} \quad 12$$

By substitution of Eqs. 10 and a combination of 2 and 12 in 11, a relationship between the concentration of free * and S^{2-} can be established.

$$C_* \left(\delta + \frac{C_{S^{2-}}}{C_{S^{2-}-H^+}}\right) = C_{*,tot} = C_{S^{2-},tot} = C^*_{S^{2-}} + C_{H^+} = C^*_{S^{2-}} + C_{H^-} + C_{SH^-} \quad 13$$

The hydride and the sulphydril concentrations are expressed using 5 and 6

$$C_* \left(\delta + \frac{C_{S^{2-}}}{C_{S^{2-}-H^+}}\right) = C_{S^{2-}} + C_* \left(\mu \frac{C_{S^{2-}}}{C_{S^{2-}-H^+}}\right) \quad 14$$

Which gives a relationship between the free * and the S^{2-} sites.

$$\delta\, C_* = C_{S^{2-}} \quad 15$$

From Eqs. 13 and 15, an expression for the total proton concentration on the S^{2-} can be established see 17 via 16.

$$C_* \left(\delta + \mu \frac{\delta\, C_*}{C_{S^{2-}-H^+}}\right) = \delta\, C_* + C_{S^{2-}-H^+} \quad 16$$

$$C_{S^{2-}-H^+} = \sqrt{\mu\, \delta}\; C_* \quad 17$$

An expression for the number of free active sites free on the * will be required for the development of the rate expressions. This is done by combining equations 15 and 17 in 10. Equation 19 gives a relationship that can be used directly in the rate equations.

$$C_{t,*} = C_* \left(\delta + \mu \frac{\delta\, C_*}{\sqrt{\mu\, \delta}\; C_*}\right) = C_* \left(\delta + \sqrt{\mu\, \delta}\right) \quad 18$$

$$C_* = \frac{C_{t,*}}{\delta + \sqrt{\mu\, \delta}} \quad 19$$

The surface area of the present catalyst was reported to be 1.9 10^5 m^2 $kg^{-1,}$ see also chapter 2, but the site density of the present catalyst was unavailable. However, Choi et al. [3] propose a site density of 0.31 10^{19} m^{-2} for a molybdenum carbide catalyst. Considering a similar site density for sulphided catalyst, a total number of active sites both * and S^{2-} together was calculated and amounted to 0.97 mol kg_{cat}^{-1}.

References

1. Kasztelan, S. and D. Guillaume, **Industrial & Engineering Chemistry Research**, 1994. 33(2): p. 203-210.

2. Romero, C.M.C., J.W. Thybaut, and G.B. Marin, **Catalysis Today**, 2008. 130(1): p. 231-242.

3. Choi, J.S., V. Schwartz, E. Santillan-Jimenez, M. Crocker, S.A. Lewis, M.J. Lance, H.M. Meyer, and K.L. More, **Catalysts**, 2015. 5(1): p. 406-423.

Appendix C

Information related to ReNGeP

C.1 . Example variables in the ReNGeP for processing reactants and intermediates for pyridine hydrodenitrogenation.

nmono_arom_n_H_addition, nmono_arom_n_H_subtraction,	// Mono aromatic H addition // Mono aromatic H subtraction
mono_arom_n[NLAB], mono_naph_n[NLAB], acyc_n[NLAB],	// Labels
nmono_arom_n = 0, nmono_naph_n = 0, nacyc_n = 0,	// Number of each compound
imono_arom_n = 0, imono_naph_n = 0, iacyc_n = 0,	// Counter on each compound
mono_arom_ns[NHYC+1][NLAB], mono_naph_ns[NHYC+1][NLAB], acyc_ns[NHYC+1][NLAB],	// Matrix for each compound type
iprocess_mono_arom_n = 0, iprocess_mono_naph_n = 0, iprocessacyc_n = 0,	// Counters for reaction compounds
imono_arom_n_H_addition, imono_arom_n_H_subtract,	// Counter for monoaromatic surface adds and subs

C.2 Example reaction families implemented for pyridine hydrodenitrogenation.

Example 1: Hydrogen addition and subtraction.

```
H_addition_n (reactant, products, ne)
H_subtraction_n (reactant, products, ne)
```

‘H_addition_n’ adds a charge bearing hydrogen atom to each unsaturated carbon and stores each of the corresponding products in a new row of products. ‘H_subtraction_n’ works the opposite way.

REMARKS:

- Applies to:
  - Arom_ns
- Product(s):
  - Arom_ns
- Constraints:
  - Ring nitrogen atoms must be saturated first.
- Identifiers:
  - Number of unsaturated carbon neighbors.
  - Number of branches on carbon atom.
- Other:
  - Transition state symmetry and chirality is calculated by temporarily adding a hydroxyl group. Take care when oxygen is already present.
  - A routine is present to write fully saturated product to the naphthenics file.

Example 2: Acyclic SH substitution.

`Acyclic_SH_substitution_n (reactant, products1, products2, ne, ne2)`

`Acyclic_SH_substitution_n` performs an acyclic SH^- substitution to each saturated carbon neighbor of nitrogen and adds a sulfhydryl group to this neighbor which causes the bond with nitrogen to break. Also performs the backward reaction.

REMARKS:

- Applies to:
  - Acyc_ns
- Products:
  - Acyc_ns
  - Paraffins
- Constraints:
  - Sulfur atoms must be removed first.
  - Unsaturation's must be removed first.
  - If another acyclic nitrogen is in the branch, the branch product is still written to paraffins instead of acyclic nitrogen.
- Identifiers:
  - Unknown.
- Other:
  - Transition state symmetry and chirality is calculated by temporarily adding a hydroxyl group. Take care when oxygen is already present.
  - Transition state calculations are essentially equal to the product. This does not cause problems for this thesis. If problems do occur in future work, adapt like in exo/acyc pentylamine condensation.
  - Symmetry and chirality of product is calculated as the product of both.

C.3 Output of ReNGeP for pyridine hydrodenitrogenation..

Compounds

20 mono aromatic nitrogen compounds
4 mono naphthenic nitrogen compounds
10 acyclic nitrogen compounds
1 olefins
3 paraffins (including sulfides)

Reactions of mono aromatic nitrogen compounds

42 atomic H additions
42 atomic H subtractions

Reactions of mono naphthenic nitrogen compounds

2 protonations
2 deprotonations
2 endocyclic beta elimination
2 reverse endocyclic beta elimination
1 exocyclic beta elimination
1 reverse exocyclic beta elimination
2 endocyclic -SH substitution
2 reverse endocyclic -SH substitution
1 exocyclic -SH substitution
1 reverse exocyclic -SH substitution
0 endocyclic condensation with pentylamine
0 reverse endocyclic condensation with pentylamine
1 exocyclic condensation with pentylamine
1 reverse exocyclic condensation with pentylamine
0 endocyclic condensation with piperidine
0 reverse endocyclic condensation with piperidine
1 exocyclic condensation with piperidine
1 reverse exocyclic condensation with piperidine

Reactions of acyclic nitrogen compounds

3 protonations
3 deprotonations
2 beta elimination
2 reverse beta elimination
2 -SH substitution
2 reverse -SH substitution
2 -SH direct hydrogenolysis
2 reverse -SH direct hydrogenolysis
2 condensation with pentylamine
2 reverse condensation with pentylamine
2 condensation with piperidine
2 reverse condensation with piperidine
2 hydrogenation of double bonds.
2 dehydrogenation of double bonds.

Reactions of olefins

1 hydrogenation

Reactions of paraffins (including sulphides)

1 dehydrogenation
1 -SH direct hydrogenolysis
1 reverse -SH direct hydrogenolysis